Contents

Abstract

With increasing concern for the security and environmental sustainability of the UK energy supply, the penetration of low carbon technologies on the grid has increased significantly. As the installed capacity of residential rooftop PV systems increases in the UK, the likelihood that LV networks will experience unacceptably high voltages and line utilizations increases also. Furthermore, an increased penetration of ASHP systems increases the likelihood of unacceptably low voltages and ampacity violations during winter periods.

Such network stresses are typically managed via reconductoring or redesign, but effective control of behind-the-meter BESSs may allow distribution network operator DNOs to delay traditional reinforcement. However, there is little consideration for the technical and economic barriers to BESS based violation management in current literature.

In this thesis, a series of mixed-integer quadratically constrained programming (MIQCP) formulations that determine optimal customer BESS takeover for violation control at various PV & ASHP penetrations are designed, a multi-period mixed integer linear programming (MILP) BESS placement and sizing model that optimally locates 3rd party owned BESSs systems is formulated, and a real time dispatch algorithm based on a 2-stage convex linear programming (LP) heuristic is developed.

These algorithms are applied to 6 networks located in the northwest of England to examine the technical feasibility of BESS control under varying PV penetrations, and BESS based control of ASHP demand on urban and suburban feeders is examined. The feasibility of BESS control for violation management in both the customer owned and DNO owned case are considered.

It is found that the costs associated with deploying behind-the-meter BESSs for the purpose of violation control greatly exceed those of reconductoring In the DNO-owned BESS case, and that significant technical barriers to the use of BESSs for violation control exist in the customer owned BESS case when violations are controlled using BESSs alone.

Acknowledgements

I would like to thank my supervisor, Professor Martin Mayfield for his continued academic support and constructive feedback throughout this process, and for his understanding during periods in which academic work could not be my priority – without this support the project simply could not have been completed.

Thank you to Professor Stephen Beck, my secondary supervisor, for his advice on general engineering modelling practices and academic writing, and to the RISE group for their continued feedback on my projects.

Thanks to the Sheffield ESA CDT students for offering their technical advice and knowledge in areas where mine was lacking, and for being great fun to be around on a day to day basis - you've been a pleasure to work with! Special thanks to Sharon Brown, the ESA CDT manager, for accepting me on the program and giving me the opportunity to work toward this PhD, despite my non-engineering background.

Than you to my family for supporting my decision to leave my job and pursue this PhD in the first place, and for the good times we've had throughout this period. Most importantly, I would like to thank my wife, Emma, who has supported me all day every day, throughout the entire process, even during stressful times in which I have not been the most positive or attentive character. Thank you for all your support and understanding, love you more than anything.

List of Publications

The work carried out during the course of this PhD has led to the following publications:

1. R. C. Johnson, M. Mayfield, and S. B. M. Beck, "Optimal placement, sizing, and dispatch of multiple BES systems on UK low voltage residential networks," J. Energy Storage, vol. 17, pp. 272–286, 2018.

2. R. C. Johnson, M. Mayfield, and S. B. M. Beck, "Utilization of stochastically located customer owned battery energy storage systems for violation management on UK LV residential feeders with varying renewables penetrations," J. Energy Storage, vol. 19, pp. 52–66, 2018.

3. R. C. Johnson, M. Mayfield, and S. B. M. Beck, "Battery energy storage for management of LV network operational violations: a multi-feeder analysis". (Unpublished, Accepted for publication in Energy Procedia on September 13th 2018).

Nomenclature

General Mathematical

$\otimes$	Tensor product
$\oslash$	Elementwise division of vectors
$\circ$	Elementwise multiplication of vectors
$\boldsymbol{J}_{i,k}$	$i \times k$ vector of 1's
$\boldsymbol{0}_{i,k}$	$i \times k$ vector of 0's

General Variables

B_{ik}	Susceptance between bus i and bus k (Ω^{-1})
G_{ik}	Conductance between bus i and bus k (Ω^{-1})
R_{ik}	Resistance between bus i and bus k (Ω)
X_{ik}	Reactance between bus i and bus k (Ω)
$\boldsymbol{V}_i$	Voltage at bus i (complex, V)
$\boldsymbol{V}_{ik}$	Voltage difference between bus i and bus k (complex, V)
$\boldsymbol{I}_{inj,i}$	Current inject at bus i (complex, A)
$\boldsymbol{S}$	Complex Power
$\boldsymbol{Y}_{ik}$	Admittance between bus i and bus k (Ω^{-1})
$\boldsymbol{Z}_{ik}$	Impedance between bus i and bus k (Ω)
θ_i	Admittance angle between bus i and bus k (associated with an admittance magnitude) (degrees)
$\emptyset_{ik}$	Voltage angle at bus i (associated with a voltage magnitude) (degrees)

Thesis Specific Variables

$A_{\boldsymbol{ch,i,t}}$	Import cost for BESS i (£)
$\boldsymbol{A}_{\boldsymbol{ch,t}}$	$n_l \times 1$ vector of $A_{\boldsymbol{ch,i,t}}$ values
$\boldsymbol{A}_{\boldsymbol{deg,t}}$	$n_l \times 1$ vector of $A_{\boldsymbol{deg,i,t}}$ values
$A_{GenDem,i,}$	Cost penalty for import/export of real power by BESS i at time t
$\boldsymbol{A}_{\boldsymbol{GenDem,t}}$	$n_l \times 1$ vector of $A_{\boldsymbol{GenDem,i,t}}$ values

$\boldsymbol{A_{LL,P,t}}$, $\boldsymbol{A_{LL,Q,t}}$	$n_{\emptyset} n_c \times 1$ vectors of line loss costs for all major line segments on all phases (£) caused by real and reactive power transfer respectively
$\boldsymbol{A_{m,t}}$	$n_l \times 1$ vector of max trajectory penalties for each BESS (£)
$\boldsymbol{A_{PF,t}}$	$n_{\emptyset} \times 1$ total excessive reactive power cost penalty for each phase at the feeder head (£)
$\boldsymbol{A_{Q,t}}$	$n_l \times 1$ penalty for reactive demand/export from BESS inverters at each residential site at time t (£)
$\boldsymbol{A_{SL,t}}$	$n_l \times 1$ vector of BESS i η losses at time t (£)
$\boldsymbol{B_{HP}}, \boldsymbol{B_{HQ}}$	Sensitivity matrices that describe the change in real and reactive power flow across each phase of the feeder head with change in real and reactive power inject/demand at each residence.
$\boldsymbol{B_{LP}}, \boldsymbol{B_{LQ}}$	Sensitivity matrices that describe the change in real and reactive power flow across each major line segment with change in real and reactive power inject/demand at each residence.
$\boldsymbol{B_{VP}}, \boldsymbol{B_{VQ}}$	Sensitivity matrices that describe the change in voltage at each monitor point with change in real and reactive power inject/demand at each residence.
$\boldsymbol{B_{Recon}}$	Sensitivity matrix that describes the change in voltage at each monitor point with reconductoring of each major line segment
$c_{deg,i,t}$	Predicted cost of BESS i capacity loss per change in power setting (£/ΔkW)
c_{DEG}	Cost per kWh of BESS degradation (£/kWh)
c_E	Cost per unit of BESS energy capacity (£/kWh)
c_{Inc}	Incentive in £ paid to customers for BESS takeover (£/BESS)
$c_{kWh,d,i,t}$	Per kWh energy import costs for customer i at time t (£/kWh)
$\boldsymbol{c}_{kWh,d,t}$	$n_l \times 1$ vector of $c_{kWh,d,i,t}$ values (£/kWh)
$\boldsymbol{c}_{kWh,ex}$	$n_l \times 1$ vector of per kWh Penalty for export of power – all elements equal (£/kWh)
$c_{LL,P}$	Per kWh penalty for line losses related to real power transfer (£/kWh)
$c_{LL,Q}$	Per kWh penalty for line losses related to reactive power transfer (£/kWh)
c_m	Per kWh penalty for breach of the maximum SOC trajectory (£/kWh)
c_{PF}	Per kvar penalty for excessive reactive power consumption (£/kvar)

c_S	Cost per unit inverter power capacity (£/kW)
$\boldsymbol{c}_{X^{Recon}}$	$n_c \times 1$ vector of conductor segment reinforcement costs
$c_{sys,i}$	Cost of BESS i (£)
c_X	Cost of installation per BESS (£/Installation)
$\boldsymbol{c}_{x_{Head}^{Recon,P}}$	Cost of reconductoring the feeder head line segment in parallel (£)
ΔC_{SC}	Cost of self-consumption reduction if changing from the SC algorithm to the FIL algorithm (£)
ΔC_{DEG}	Cost of degradation increase if changing from the SC algorithm to the FIL algorithm (£)
D_{FIL}	BESS degradation associated with operating in the FIL or ASHP demand limiting mode for the duration of either period (kWh)
D_{SC}	BESS degradation associated with operating in the self-consumption mode for the duration of either period (kWh)
$DNS_{total,i}$	Predicted demand that will not be served by either PV generation or the BESS at residence i
ΔD_i	Change in daily capacity loss with increase in SOC by 1 kWh
$E_{i,t}^{Remain}$	Amount of energy remaining above the FIL for PV array i at time t for any given day. Remaining energy is predicted conservatively, and based on the 99th percentile for the given month (kWh)
E_i^S	Energy capacity of BESS i (kWh)
$\boldsymbol{E}^S$	$n_l \times 1$ vector of BESS energy capacities (kWh)
EOL	Remaining fraction of initial BESS capacity at which BESS is considered to be at the end of its life (0 to 1).
$\boldsymbol{I}_{max}$	$n_\emptyset n_c \times 1$ per phase line segment ampacity limits (A)
$\boldsymbol{I}^{Head}$	$n_\emptyset \times 1$ Per phase feeder head ampacities (A)
$\boldsymbol{I}_{max}^{Head}$	$n_\emptyset \times 1$ Per phase feeder head maximum acceptable ampacities (A)
$\Delta \boldsymbol{I}^{\boldsymbol{Recon}}$	$n_l n_\emptyset \times 1$ vector of changes in line ampacity with existence of conductor replacement (A)
$\Delta \boldsymbol{I}_{Head}^{Recon,P}$	$n_l n_\emptyset \times 1$ sparse vector of changes in line ampacity with existence of feeder head line segment reconductoring (A)
n_a	Number of ampacity monitor points

n_c	Total number of major line segments
n_E	Number of voltage monitoring Points
η_{eff}	BESS charging/discharging efficiency
n_l	Total number of residences
n_t	Number of time points in time series analysis
$n_{S,ASHP}$	Number of BESSs taken over to solve a particular ASHP configuration
$n_{S,PV}$	Number of BESSs taken over to solve a particular PV configuration
PF	Power factor
$\boldsymbol{P}_t^{Head}$	$n_\emptyset \times 1$ vector of real power flows across each phase of the feeder head (kW)
$\boldsymbol{P}_t^{Line}$	$n_\emptyset n_c \times 1$ vector of real power transfers across each phase of each ampacity monitor (centralized algorithm) or major line segment (all other uses) (kW)
$\boldsymbol{P}_{i,t-1}^{d}$	$n_l \times 1$ vector of real power demand on network by load i at time $t-1$ (kW)
$P_{i,t}^{d}$	Real power demand on network by load i at time t (Used in SC and FIL algorithm explanations only) (kW)
$\boldsymbol{P}_t^{d}$	$n_l \times 1$ vector of predicted load demand values at each residence (used in prediction stage of OPF model only) (kW)
$P_{i,t}^{d+P2P}$	Sum of PV array owners demand and peer demands
$P_{i,MAX}^{g}$	The power rating of array i (kW)
$\boldsymbol{P}_{MAX}^{g}$	$n_l \times 1$ vector of $P_{i,MAX}^{g}$ values (kW)
$\boldsymbol{P}_{i,t-1}^{g}$	$n_l \times 1$ vector of real power inject by generator i at time $t-1$ (kW)
$P_{i,t}^{g}$	Real power inject by generator i at time t (Used in SC and FIL algorithm explanations only) (kW)
$\boldsymbol{P}_t^{g}$	$n_l \times 1$ vector of predicted generation values at each residence (used in prediction stage of OPF model only)
$\boldsymbol{P}^{HP}$	$n_\emptyset n_c \times 1$ vector of real power on each phase across each major line segment under ASHP operation, (used in the PV & ASHP reconductoring models only) (kW)
$P_{i,t-1}^{S}$	Real power discharged onto network by BESS i at time $t-1$ (negative charging) (kW)
$\boldsymbol{P}_{t-1}^{S}$	$n_l \times 1$ vector of $P_{i,t-1}^{S}$ values (kW)

$P_{i,t}^{S}$	Real power discharged onto network by BESS i at time t (negative denotes charging) (kW)
$\boldsymbol{P}_{t}^{S}$	$n_l \times 1$ vector of $P_{i,t}^{S}$ values (kW)
$\boldsymbol{P}_{lim}^{S}$	Maximum allowed BESS real discharge power (ASHP demand limiting operational mode only) (kW)
$P_{i,t}^{S,Ch}$	Real power charged by BESS i at time t (kW)
$P_{i,t}^{S,Disch}$	Real power discharged by BESS i at time t (kW)
$P_{i,t}^{S,FIL}$	Real power discharged by BESS i at time t (negative charging), specifically in the FIL operation mode (kW)
$P_{i,t}^{S,SC}$	Real power discharged by BESS i at time t (negative charging), specifically in the self-consumption operation mode (kW)
$\boldsymbol{P}^{PV}$	$n_{\emptyset} n_c \times 1$ vector of real power on each phase across each major line segment under PV generation, (used only in reconductoring models) (kW)
$\Delta P_{i,t}^{S}$	Change in real power discharged onto network by BESS i at time t (negative towards charging) (kW)
$\Delta \boldsymbol{P}_{t}^{S}$	$n_l \times 1$ vector of $\Delta P_{i,t}^{S}$ values (kW)
$\boldsymbol{P}_{MAX}$	$n_{\emptyset} n_c \times 1$ vector of maximum observed real power flow across each phase of each major line segment
$\boldsymbol{Q}_{t}^{Head}$	$n_{\emptyset} \times 1$ vector of reactive power flow across each phase of the feeder head (kvar)
$\boldsymbol{Q}_{t}^{Line}$	$n_{\emptyset} n_c \times 1$ vector of reactive power transfers across each phase of each ampacity monitor (centralized algorithm) or line segment (all other uses) (kvar)
$\boldsymbol{Q}^{HP}$	$n_{\emptyset} n_c \times 1$ vector of reactive power transfers across each phase of each major line segment, specifically in the ASHP simulation case (kvar)
$\boldsymbol{Q}_{t-1}^{S}$	$n_l \times 1$ vector of leading reactive powers injected onto network by each BESS at time $t-1$ (negative lagging) (kvar)
$Q_{i,t}^{S}$	Leading reactive power injected onto network by BESS i at time t (negative lagging) (kvar)
$\boldsymbol{Q}_{t}^{S}$	$n_l \times 1$ vector of $Q_{i,t}^{S}$ values (kvar)

$\boldsymbol{Q}^{PV}$	$n_\emptyset n_c \times 1$ vector of reactive power transfers across each phase of each major line segment, specifically in the PV simulation case (kvar)
$\Delta \boldsymbol{Q}_t^S$	$n_l \times 1$ vector of changes in leading reactive powers injected onto network by each BESS at time t (negative towards lagging) (kvar)
$\boldsymbol{Q}_{MAX}$	$n_\emptyset n_c \times 1$ vector of maximum observed reactive power flow across each phase of each major line segment
$\boldsymbol{R}$	$n_\emptyset n_c \times 1$ vector of impedance of each phase of each major line segment
S_i^{inv}	Total apparent power capacity of BESS inverter i (kVA)
$\boldsymbol{S}^{inv}$	$n_l \times 1$ vector of S_i^{inv} values (kVA)
$SOC_{i,t}$	State of charge of BESS i at time t (kWh)
$SOC_{DA,i}$	Maximum allowed SOC at the beginning of the next day for BESS i (kWh)
SOC_{max}	Maximum allowed State of charge of a BESS (kWh)
t^{mag}	The magnitude of the timestep used in time series calculations (min)
$Traj_{i,t}^{max}$	Maximum trajectory; the maximum allowed SOC of BESS i at time t (kWh)
$\boldsymbol{V}_{avg}$	$n_\emptyset n_c \times 1$ vector of average voltages on each phase of each major line segment (v)
$\boldsymbol{V}_t^{Amp}$	$n_\emptyset n_a \times 1$ vector of voltages at each ampacity monitoring point at time t (V)
$\boldsymbol{V}_t^{Head}$	$n_\emptyset \times 1$ vector of voltage reciprocals at each ampacity monitoring point at time t (V)
$\boldsymbol{V}_t^{End}$	$n_\emptyset n_e \times 1$ vector of voltages recorded on each phase of each endpoint monitor at time t (V)
$\boldsymbol{V}^{HP}$	$n_\emptyset n_E \times 1$ vector of voltage magnitude values for each phase of each major line segment under ASHP operation, (used in the PV & ASHP reconductoring model only) (V)
$\boldsymbol{V}_{min}$	Vector of Minimum allowable steady state voltage – 216.2 V ESQCR, with column length equal the number of monitoring points (V)
$\boldsymbol{V}_{max}$	$n_\emptyset n_c \times 1$ vector of Maximum allowable steady state voltage – 253 V ESQCR, with column length equal the number of monitoring points (V)
$\boldsymbol{V}^{PV}$	$n_\emptyset n_E \times 1$ vector of voltage magnitude values for each phase of each major line segment under PV generation, (used in the reconductoring models only) (V)

$\boldsymbol{X}^{Recon}$	$n_c \times 1$ vector of binary variables representing the existence of reinforcement of major line segments (Binary)
$X_{Head}^{Recon,P}$	Binary existence variable for parallel reconductoring along the feeder head line segment (Binary)
$\boldsymbol{X}^{HP}$	n_l×1 Vector of Binary ASHP existence variables (Binary)
$\boldsymbol{X}^{S}$	$n_l \times 1$ vector of binary variables for the existence of each BESS (Binary)

Common Abbreviations

ARIMA	Autoregressive integrated moving average
ASHP	Air Source Heat Pump
BESS	Battery Energy Storage System
CAES	Compressed Air Energy Storage
CHP	Combined Heat and Power
DNO	Distribution Network Operator
DOD	Depth of Discharge
E7	Economy 7
EES	Electrical Energy Storage
EESs	Electrical Energy Stores
EFR	Enhanced Frequency Response
ENWL	Electricity North West Limited
ESQCR	Electricity Safety, Quality, and Continuity Regulations
FA	Firefly Algorithm
FIL	Feed-In Limit
GA	Genetic Algorithm
GSHP	Ground Source Heat Pump
IRENA	The International Renewable Energy Agency
LV	Low Voltage
MILP	Mixed Integer Linear Programming
MIQCP	Mixed integer Quadratically Constrained Programming
OLTC	On-Load Tap Changer
OPF	Optimal Power Flow
PHS	Pumped Hydroelectric Storage
PV	Photovoltaic
ROCOF	Rate of Change of Frequency
RPC	Reactive Power Control
RT	Real Time
SA	Simulated Annealing

SC	Self-Consumption
SCADA	Supervisory Control and Data Acquisition
SMES	Superconducting Magnetic Energy Storage
SOC	State of Charge
SOH	State of Health
SOS	Special Ordered Set
SSS	Secondary Substation
STOR	Short Term Operating Reserve
UOM	University of Manchester
UOS	University of Sheffield
VPP	Virtual Power Plant

1 Introduction

Since the impact of traditional fossil fuel generation on the environment and on the security and sustainability of supply has become a concern, the penetration of renewable and low carbon technologies in the UK energy mix has continuously increased. Current estimates suggest a total installed capacity of 12.7 GW solar photovoltaic (PV) (Dept. of BEIS, 2017) and 17.9 GW wind (RenewableUK, 2018), combined heat and power (CHP systems) make up 560 MW of electrical power capacity and 2.3 GW heat capacity (Dept. of BEIS, 2016), and interest in poly-generation and microgrid systems and their operation is growing in literature (Guan, Vasquez and Guerrero, 2016; Somma *et al.*, 2018).

The rate of rooftop PV uptake in the UK has somewhat slowed since a significant reduction in feed in tariff, with plans to remove the tariff entirely by April 2019 (figure 1.1) (Ofgem, 2018). However, sources still predict a potential for increase in penetration to between 18% - 25% total installed capacity by 2035 (National Grid, 2017), which is attributed to the emergence of peer to peer (P2P) energy trading schemes (National Grid, 2017; Butcher, 2018; Reed, 2018), simultaneous roof replacement and PV installation (Ardani *et al.*, 2018), and general system and supply chain cost reductions (International Energy Agency, 2014; REA, 2015). The reasons for reductions in system costs can be further analysed; The International Renewable Energy Agency (IRENA) show that the costs of PV modules have fallen by 80% over the last 8 years due to efficiency improvements and general economy of scale (IRENA, 2017b), and it is predicted that panel costs could fall by a further 59%, which is in some part due to projected improvements in affordability of state of-the-art technologies such as concentrated silicon solar cells (Xing *et al.*, 2015) and multi-junction solar cells, which have been shown to achieve efficiencies of 27.5% and 42% respectively (Jana, Gangopadhyay and Das, 2013). An increase in number of PV systems has the potential to stress the UK grid in the following ways:

- Provide sufficient power generation to cut into UK baseline generation;
- Reduce system inertia via displacement of traditional generation methods;
- Cause ampacity and voltage violations on low voltage (LV) networks;
- Reduce the predictability of dispatchable generation requirements.

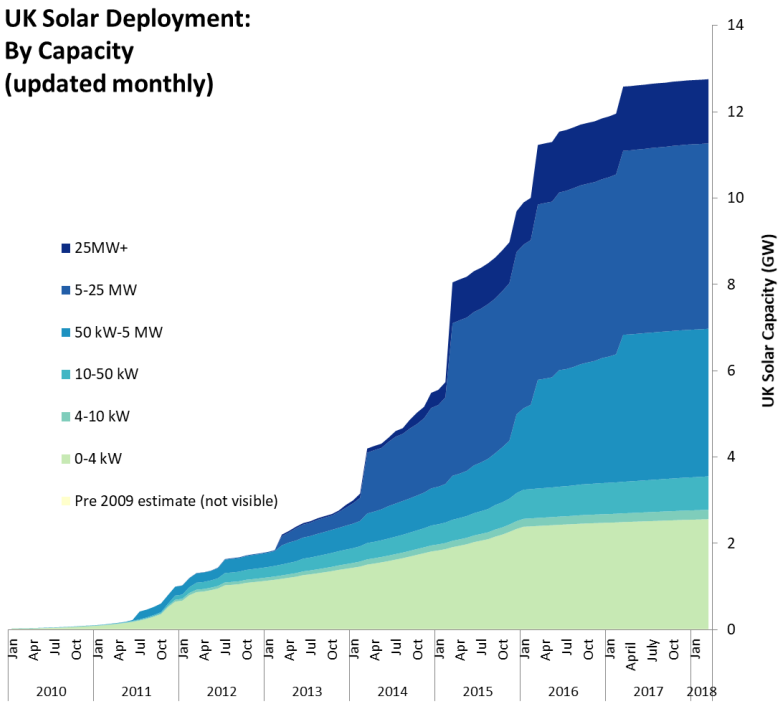

Fig. 1.1 - Installed capacity of PV vs time. Installation rate has somewhat slowed, though it is clear from the plot that current install rate cannot confidently predict future installed capacity (Dept. of BEIS, 2017).

Furthermore, interest in electrified heating technologies, such as air source heat pumps (ASHPs), is beginning to increase, with some sources predicting a possible penetration of 1 million residential ASHP systems by the year 2030. Despite this, little concern is given to whether power networks can handle the localized demand increases associated with uptake of this technology, though some studies do predict that distribution network violations are likely to occur (Navarro-Espinosa and Ochoa, 2016).

Various network management strategies may be used to reduce or eliminate the aforementioned stresses, such as curtailment of generation, reconductoring, and energy storage. Battery energy storage system (BESS) costs have been decreasing over recent years, and are projected to fall further over the following decades; some sources suggest a per kilowatt cost decrease to £80 - £160 by 2030 (IRENA, 2017a; Olinsky-paul and Mullendore, 2018).

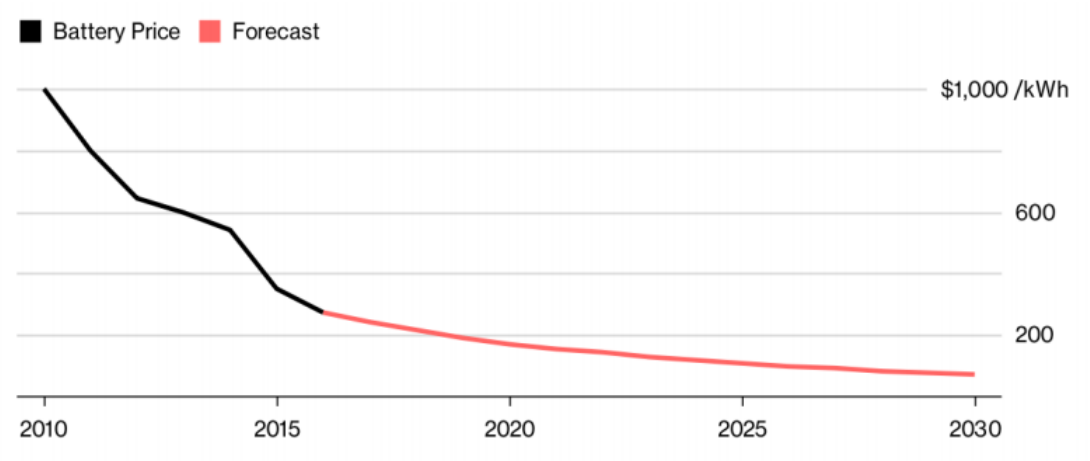

Fig. 1.2 – Shows projected reduction in per kilowatt li-ion battery costs. Costs are predicted to fall below £80/kWh by 2030 by some sources (Olinsky-paul and Mullendore, 2018).

As a result of falling costs, the use of energy storage to limit voltage and ampacity violations (and thus delay reconductoring works) on LV networks is being investigated in literature, though the technical and economic feasibility of such control and placement strategies under realistic dispatch and ownership regimes is not yet clear. The work presented in this thesis focusses on LV network management via control of BESSs. The work performed in, and major contributions of this thesis are as follows:

1. A novel BESS placement algorithm, which optimally sizes and locates BESS systems for voltage and ampacity control on any input LV feeder with any PV & ASHP ownership pattern is developed. The algorithm is able to take into account whether BESSs will be operated via a central controller or via a feed-in-limiting type algorithm.
2. Novel BESS control algorithms of varying complexity for management of PV & ASHP caused voltage and ampacity violations.
3. A preliminary analysis of the costs associated with the use of residentially located behind-the-meter BESSs for the purpose of violation control, from both a DNO/3rd party owned perspective and a customer owned perspective.
4. An examination of the technical feasibility of violation control using BESSs, when non-ideal BESS ownership and availability patterns occur. The feasibility is analysed across multiple feeder topologies and technology penetration levels, and compared to reconductoring.
5. A comparison of the effectiveness of simple, decentralized BESS control methods (that require very little data to function) to centralized control strategies (that

require substantial data communications and processing to operate), for the provision of voltage and thermal constraint management.

And these contributions are developed to address the research questions:

1. Are the costs associated with deploying behind-the-meter BESSs for the purpose of violation control enough to the cost of reconductoring, such that BESS control could be considered as a means to delay reconductoring if necessary (chapters 5, 6 & 7)? How does cost vary when switching between a DNO/3rd party owned perspective (chapter 5) and a customer owned perspective (chapters 6 & 7)?
2. Are there technical barriers to the use of BESSs for violation control, when ideal and non-ideal BESS ownership and availability patterns occur (chapters 5, 6 & 7)?
3. Is increased self-consumption a potential additional revenue in the instance that BESSs are controlling for violation control (chapter 5)?
4. Are BESS systems technically and economically suited to control of violations caused by ASHP systems (chapter 6)?
5. How does technical and economic feasibility of BESS based violation control vary with feeder topology (chapter 7)?
6. Does control algorithm complexity affect the technical suitability of BESSs to management of voltage and thermal violations on LV feeders (Chapters 6 & 7)?

The relationship between contributions, research questions, publications, and thesis chapters is summarized in figure 1.3.

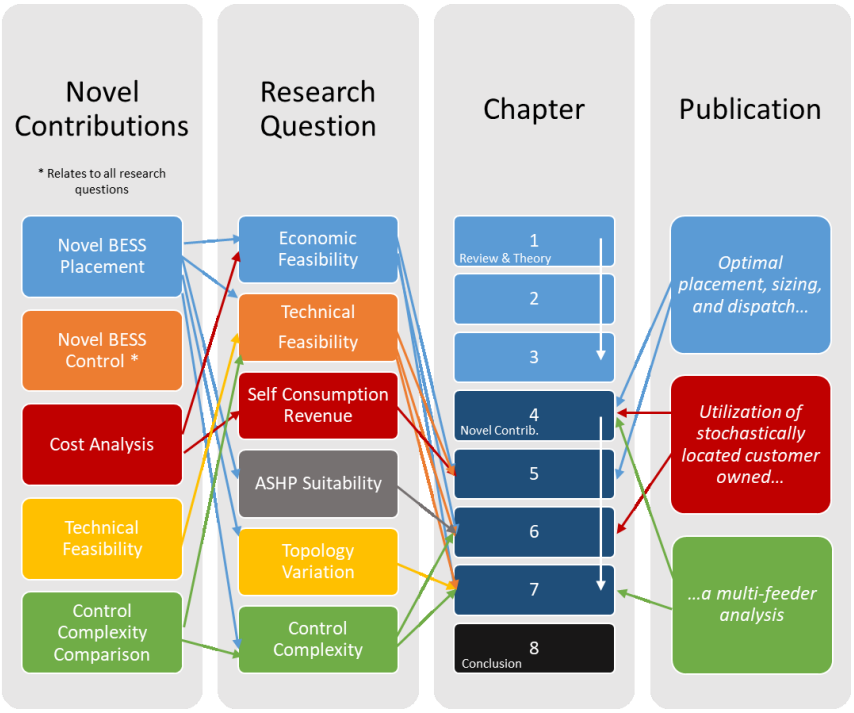

Figure 1.3 – Shows the relationship between research questions, the chapters in which they are addressed, and the publications that these chapters have resulted in.

2 Literature Review

The following literature review will discuss the history and state of the art of energy storage technologies, their applications in power network management, current academic and industrial investigations into the use of EES for voltage and thermal management of distribution networks, and alternative technologies that may be used to provide the same service.

2.1 Background

2.1.1 History of energy storage

Whilst it is not possible to determine the date upon which energy storage utilization first occurred, medieval precursors to modern energy storage systems are accounted for in literature. For example, the flywheel can be traced back as far as 1070, in which the Russian architect Theophilus implemented such devices into pottery wheels as a means of speed regulation (White, 1975). However, the first direct attempt at EES was probably Volta's primary (non-rechargeable) zinc-copper electrochemical cell with brine electrolyte (1800). A 2 electrolyte equivalent of this cell was developed by Daniel in 1836, and a zinc-Carbon electrolyte equivalent was developed by Leclanche in 1866 (Whittingham, 2012). The discovery of the cell was followed by the first known pumped hydro system, which was commissioned in 1909 in Switzerland, with a rated power of 1 MW (Whittingham, 2012). The the invention of redox-flow battery followed in 1954. The first supercapacitors were developed by SOHIO in 1961, and development of superconducting magnetic energy storage (SMES) systems began development in the 1970s throughout the western world, and the first successfully integrated system was connected to the Moscow power grid, with 0.29 Wh/ 300 kWh capacity (Danila, 2010). In 1978, the first compressed air energy storage (CAES) was built in Huntorf, Germany using a salt dome for storage of the compressed air, though only a handful of these systems exist worldwide today (IRENA, 2017b). The underlying chemistry behind the modern lithium Ion battery was discovered between 1974 and 1976 by Besenhard (Besenhard and Eichinger, 1976), and the theory was used to develop working cells with CoO_2 cathodes by Godshall in 1979 (Godshall and Huggins, 1980), and Goodenough and Mizushima the next year (Mizushima *et al.*, 1980). The $LiFePO_4$ cell was discovered by the Goodenough group in 1996 (Padhi and Goodenough, 1997), and numerous variations on the secondary Li ion cell have been developed since.

The modern history of energy storage largely concerns new applications of existing technologies. Whilst pumped hydro systems have been integrated into power grids for over a century, many other energy storage technologies have become of interest to electrical grid operators, as they may be technically and economically viable providers of various ancillary services. This consideration has led to many recent grid trials. For example, coupling of modern flywheel systems to transmission systems for frequency regulation purposes, such as the connection of a 500 kW/10 kWh flywheel to the UK national grid (as a device for frequency regulation), and installation of various large grid coupled battery systems across the world (Whittingham, 2012). In recent years, home battery systems have become available (Mercedes, 2014; Lin, 2015; Tesla, 2016), and the opportunity to investigate the use such BESSs for grid management at lower voltages has therefore emerged.

2.1.2 Electrical energy storage technologies and their characteristics

Electrical energy storage technologies come in numerous forms with significantly different characteristics. Here, the characteristics energy and power density, geographic constraint, self-discharge, round trip efficiency, renewable credentials, and cost, are discusses.

2.1.2.1 Energy and power characteristics

Two of the most important criteria that energy storage systems are judged on are their power and energy characteristics (Akhil *et al.*, 2015). These are generally measured in W/Kg or Wh/kg (specific power density and specific energy respectively), or particularly in the case of battery technologies, W/l or Wh/l (power density and energy density). This data may be displayed on a Ragone plot (figure 2.1) (Ghoniem, 2011). Values for energy and power characteristics of a given technology are often specific to a certain system design (Akhil *et al.*, 2015), and thus vary from source to source (Eckroad, 2007; MacKay, 2008; Chen *et al.*, 2009; Tester, 2012; Baqari and Vahidi, 2013; Shibata *et al.*, 2013; Akhil *et al.*, 2015; Lin, 2015). A set of reasonable estimates for electrical energy and power characteristics have been compiled from various sources (Eckroad, 2007; MacKay, 2008; Chen *et al.*, 2009; Tester, 2012; Baqari and Vahidi, 2013; Shibata *et al.*, 2013; Akhil *et al.*, 2015; Lin, 2015), and are shown in table 2.1. Technologies with higher power densities are lower energy densities generally well suited to applications such as enhanced frequency response (EFR), management of transient high power demands (e.g. capacitors to smooth transient demands on electric vehicle batteries (Zhang *et al.*, 2016)), or protection from transient grid events (e.g. SMES systems for protection of sensitive machinery from transient voltage dips (Ali *et al.*, 2010)). High energy density, low power density technologies are often better suited to

applications that require sustained operation for several minutes to hours, such as steady state voltage control, self-consumption of on-site generation, and short-term operating reserve (STOR) (National Grid, 2018).

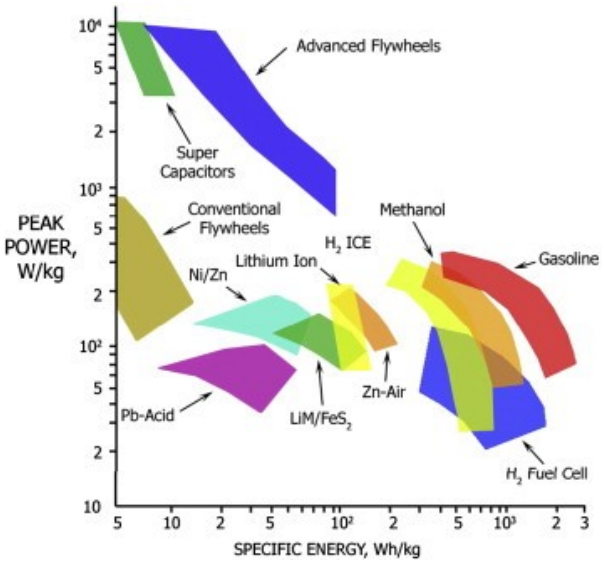

Figure 2.1 - A Ragone plot of specific power vs specific energy (Ghoniem, 2011)

A noteworthy property of Li-ion cells is the near independency of available energy capacity on discharge rate at any feasible C rate (Figure 2.2); many other electrochemical storage technologies experience a temporary reduction in energy capacity when operated at higher powers, and this is particularly true of lead acid systems (Omar *et al.*, 2013).

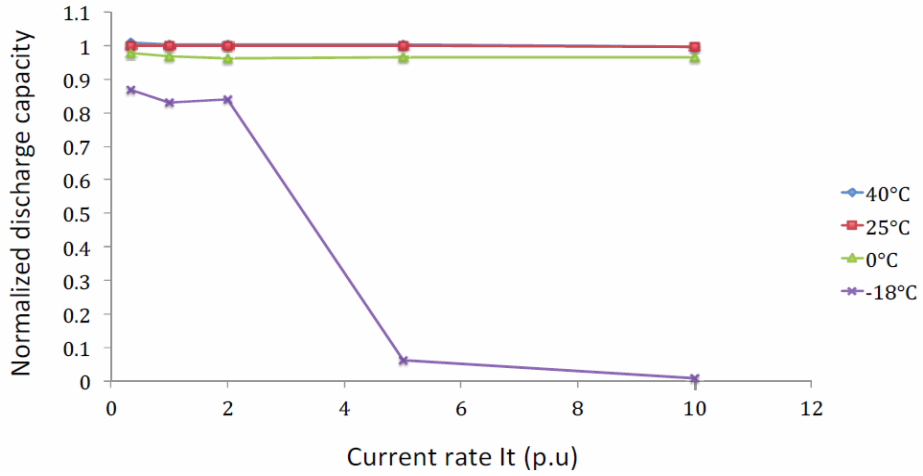

Figure 2.2 - Shows the discharge capacity (relative to rated capacity) of an LFP cell at different C rates and temperatures. Clearly the cell can perform at near rated capacity at

any C rate and temperature that would be realistically experienced by a load levelling store in most climates (Omar *et al.*, 2013).

2.1.2.2 Self-discharge and round trip efficiency

Round trip efficiency is the ratio of energy put into a storage device to the energy received from it (i.e. the product of charging and discharging efficiency). Round trip efficiency in EES devices may be reduced by heat evolution, friction and drag (electromechanical only), internal electrical resistance, and switching and resistive losses associated with the required power electronics. Additionally all EES systems exhibit some degree of self-discharge. The literature around self-discharge and round trip efficiency values are typically consistent across sources (Eckroad, 2007; MacKay, 2008; Chen *et al.*, 2009; Tester, 2012; Baqari and Vahidi, 2013; Shibata *et al.*, 2013; Akhil *et al.*, 2015; Lin, 2015). Self-discharge values from (Chen *et al.*, 2009) and round trip efficiency values compiled from (Eckroad, 2007; MacKay, 2008; Chen *et al.*, 2009; Tester, 2012; Baqari and Vahidi, 2013; Shibata *et al.*, 2013; Akhil *et al.*, 2015; Lin, 2015) are shown in Table 2. High self-discharge rates and low efficiency are generally undesirable properties.

Systems	Power rating	Discharge time	Self-discharge per day	Round Trip efficiency	£/kW	£/kWh
PHS	100–5000 MW	1–24 h+	<0.1%	70-83%	480–1600	5–80
CAES	5–300 MW	1–24 h+	<0.1%	68-75%	320–640 (640-1600)	2–40
Lead-acid	0–20 MW	s - h	0.1–0.3%	70-90%	240–480 (1360-4640)	160–320
NiCd	0–40 MW	s - h	0.2–0.6%	60-70%	400–1200	700–1200
NaS	50 kW–8 MW	s - h	~20%	75-90%	800–2400 (2400-3200)	250–400
ZEBRA	0–300 kW	s - h	~15%	85-90%	120–240	80–160
Li-ion	0–100 kW	m - h	0.1–0.3%	80-97%	960–3200 (960-3600)	480–2000
Li-ion (residential)	0 - 5 kW	ms–h's	0.1–0.3%	80-97%	≈600	≈400
Fuel cells	0–50 MW	s–24 h+	<0.1%	20-45%	4000-8000	4800–16000
VRB	30 kW–3 MW	s–10 h	<0.1%	68-75%	480–1200	120–800
ZnBr	50 kW–2 MW	s–10 h	<0.1%	65-70%	560–2000	120–800
PSB	1–15 MW	s–10 h	<0.1%	-	560–2000	120–800
SMES	100 kW–10 MW	ms–8 s	10–15%	95%	160–240	800–8000
Flywheel	0–250 kW	ms –15 m	100%	85-95%	200–300	800–4000
Capacitor	0–50 kW	m - s	40%	-	160–320	400–800
Super-capacitor	0–300 kW	ms –60 m	20–40%	99%	80–240 (160-320)	240–1600

Table 2.1 – Various characteristics of different electrical energy storage technologies.

2.1.2.3 Cost and geographic constraints

EES technology costs vary greatly between sources – and a summary of these ranges is presented in table 2.1. Where there is a discrepancy between sources, an alternative range is given in brackets – this range is determined from data published in the electrical energy storage handbook, and relates to installed capital cost (Akhil *et al.*, 2015). There has been a significant decrease in the cost of Li ion storage for home battery system applications in recent years, and therefore the typical cost for this application is shown separately to general Li-ion costs.

Geographic constraints are of paramount importance in determining the suitability of an EES technology. The most obviously geographically constrained systems are CAES and pumped

hydroelectric storage (PHS); the former requiring suitable local geology (i.e. the ground geology must be appropriate for the construction of an adequate cavern) and the latter requiring lower and upper natural reservoirs in close proximity (it is considered technically possible to construct artificial reservoirs, but costs and construction times are likely to be much more significant (MacKay, 2008). Conversely, commercialization of battery systems (e.g. Tesla Powerwall 2), have made it possible to locate li-ion systems virtually anywhere.

2.1.3 Current and potential uses of energy storage

The following section outlines the various functions that electrical energy storage systems may perform in future energy systems, and the technological and economic aspects that may affect the implementation and sustainability of such deployments.

2.1.3.1 Management of grid frequency and grid inertia

Although the UK daily power demand profile can be, and is predicted with reasonable accuracy on the half hourly time scale (National Grid, 2014), it is not currently possible to predict the small, short term demand fluctuations that occur from second to second (Denholm *et al.*, 2010), and the result is an imbalance between power supply and demand. When generation > demand, frequency increases at a rate proportional to the imbalance and inversely proportional to the overall system inertia (Delille *et al.*, 2012), and a decrease in frequency when demand < generation. There is also some concern as to the effect of renewables on frequency control; PV and wind generators exhibit no and very little inertial response respectively, and Tielens (2009) suggests that the rate of change of frequency (ROCOF) on a power system will greatly increase with an increase in the ratio of renewable to dispatchable generation capacity (Tielens and van Hertem, 2012).

To mitigate frequency changes, some dispatchable generators operate in frequency response mode; such generators increase their output if frequency is falling and decrease their output when frequency is increasing. Specifically, such generators may be contracted to provide primary response (deliver rated power within 10 seconds of a low frequency event for at least 30 seconds), secondary response (deliver rated power within 30 seconds of a low frequency event for at least 30 minutes), and high frequency response (reduce power by a contractually agreed amount within 10 seconds of a high frequency event indefinitely) (Greenwood *et al.*, 2017).

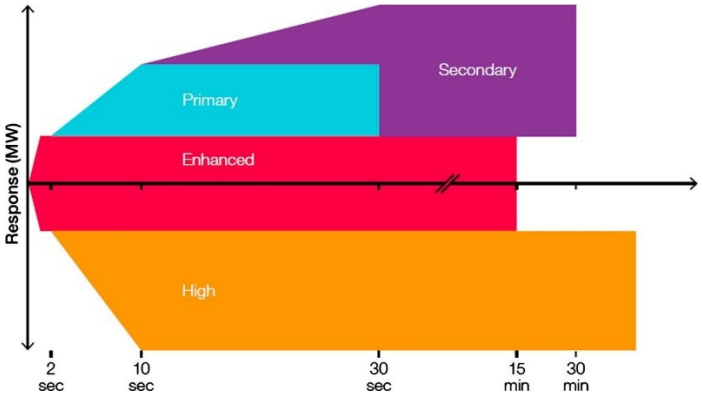

Figure 2.3 - Shows frequency service requirements as a function of time (Greenwood *et al.*, 2017).

As a result of the rapid response capabilities of EES technologies, the UK national grid has introduced enhanced frequency response (EFR), which is a frequency response mode exclusively available to EES owners (Greenwood *et al.*, 2017). ESSs are required to operate within a power envelope that varies on grid frequency (see figure 2.4), must respond to grid frequency changes within 1 second, and be capable of maintaining rated output for a minimum 15 minute duration. Furthermore, ramping rate is limited to prevent system instability that may result from rapid frequency changes caused by the EES technologies themselves; this limit is determined by the ROCOF within the envelope, and the rated power of the EES when operating outside of the envelope. Additionally, some researchers have begun to examine the possibility of using ESSs to provide synthetic inertia (Delille *et al.*, 2012; Gonzalez-longatt, 2016). This is somewhat different to EFR; synthetic inertia control uses the ROCOF to determine an appropriate rate of change of power output (i.e. differential control), whereas EFR is predominantly concerned with absolute power provision at specific frequencies. Francisco-Longatt et al. (Gonzalez-longatt, 2016) observed a significant dampening of frequency oscillations on a simulated 100 MW power system with the addition of 17 MW of BESS capacity, and Dellille et al (Delille *et al.*, 2012) showed that BESSs operating under synthetic inertia control could be used to reduce blackout occurrences in instances of renewable disconnection resulting from frequency transients on the Guadeloupean grid.

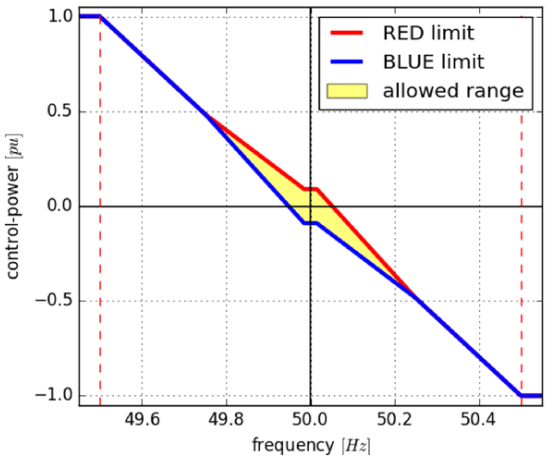

Figure 2.4 – Shows the operating envelope for EES operating for EFR, in terms of rated power vs. grid frequency (narrow service) (Hell, no date).

There are no fixed tariffs for provision of EFR, however the 2016 tender process resulted in contract agreements with 8 BESS owners, with tariffs between £7 and £11.97 per MW per hour (National Grid, 2016b).

2.1.3.2 Management of demand variation

At present, the UK power grid can accommodate the relatively small quantity of renewable generation in the supply mix (approximately 10.1 GW PV (DECC, 2016) and 13.6 GW wind (EWEA, 2016)). This is because flexible generators, such as gas peaking plants, provide a significant amount of power to the grid at any given time (an average generation of 11.7 GW, with variations of ±10 GW (National Grid, 2016a)), so an unpredicted increase in renewable generation can be almost instantaneously met with a decrease in output from flexible generators (a GE FlexEfficency 50 type CCGT plant can achieve ramp rates of 51 MW/min, or 10 % rated power/min (General Electric, 2011)), and vice versa (Hay and Macwhinnie, 2015). However, at higher penetration levels the power supplied by renewable generation will begin to cut into the baseload (the constant baseline power supplied by inflexible generators such as nuclear plants and some coal fired power stations) (Denholm *et al.*, 2010), and studies performed using data from grids around the developed world suggest that significant curtailment will begin to be required when renewable penetration reaches between 20-30%, regardless of the baseload level (with little or no curtailment required below this range, dependent baseload level) (Denholm *et al.*, 2010; Enernex, 2010; Grünewald, McKenna and Thomson, 2015). In addition, forecasting operational strategies for dispatchable generators will become more challenging at higher renewables penetrations, due to difficult-to-predict

fluctuations in PV and wind generation, and flexible generation capacity may need to be increased due to deal with larger discrepancies in scheduled and actual demand requirements. At current renewables penetration levels this is not an issue, as renewables are only displacing demand that would be supplied by flexible generation, though problems may arise if renewables become abundant enough to displace inflexible generation (GE Energy, 2008; Denholm *et al.*, 2010).

The national grid future energy scenarios predict that up to 6.3 million residences may be served exclusively by ASHPs by 2035 (National Grid, 2015). This will significantly increase peak daily demand and add a much more pronounced seasonal variation to electricity demand, which may be further exacerbated by a change in primary fuel mix toward less flexible supply; installed capacity of nuclear is predicted to double under some future scenarios, resulting in a higher inflexible baseload (National Grid, 2015).

EES may be operated in the following ways to alleviate such problems:

1. Feed-in smoothing - feed-in smoothing (de la Parra *et al.*, 2015) relates to the use of storage to reduce the magnitude and rate of changes of renewable generation system output. This reduces the rate at which dispatchable generation must to react to a perceived decrease in demand resulting from increased renewable generation, and may reduce the magnitude and frequency of changes, allowing less flexible generation to react effectively. General predictions suggest that smoothing wind and solar output to 10% rated capacity/minute would be sufficient to eradicate frequency and generator flexibility issues resulting from their presence (Jabir *et al.*, 2017). This operation mode requires a store to have a power capacity much larger than its energy capacity (Remund *et al.*, 2015), though required power capacity can be significantly reduced by locating a store such that it can serve multiple, significantly spatially separated (10's km scale) renewable generation sites (Jamieson, 2011; de la Parra *et al.*, 2015; Remund *et al.*, 2015), due to the smoothing effect resulting from weather differences at the separated sites (de la Parra *et al.*, 2015). Specifically, De la Parra *et al.* (2015) calculated that aggregation of 6 - 7 spatially separated sites would reduce power capacity requirements by a factor of 2, and 20 PV sites should reduce required capacity by a factor of 4. Flywheel systems are suitable for this task, and have been shown to effectively smooth wind power variations (Gayathri, Senroy and Kar, 2016).

2. Peak shaving and valley filling - refers to the practice of charging an EES during periods of net low demand, and discharging at high demand to flatten the daily demand profile of a load, thus allowing: (a) potential evasion of cutting into the baseload generation (Denholm *et al.*, 2010), (b) the creation of grid headroom for the connection of more loads, allowing us to better utilize the capacity that is available (Tielens and van Hertem, 2012). These services were provided on the transmission scale by EES in the UK via by pumped hydro storage plants such as Dinorwig and Ffestiniog (*Dinorwig*, no date), but these plants are typically used for short term operating reserve STOR purposes. Peak shaving and valley filling at the distribution level were examined by Hilton (2015); a half hourly demand profile for 4 days in October 2013 for 55 residences was modified with the generation profile expected for 60 kW of solar PV capacity, and results suggested that a 100 kWh EES would be required to bring daily minimum demand back to that expected for the time of year in question (Hilton, 2015). This suggests that levelling tasks at the distribution level may not be optimum, as only considering demand at the secondary substation ignores larger scale smoothing resulting from demand and generation diversity effects.
3. Short term operating reserve – refers to the use of EES for provision of real power for short periods of time to mitigate the effects of demand misprediction or unexpected loss of generation (National Grid, 2009). Pumped hydro plants such as Dinorwig are currently used for this purpose (*Dinorwig*, no date). Providers of this service are paid two tariffs; a rate based on the fraction of a month in which the unit is available to provide the STOR service (availability payment), and a per unit delivered/expected rate (utilization payment) (National Grid, 2009).

There is no obvious way to mitigate renewables generation unpredictability issues using EES; this problem is likely to be reliant on improvements on renewables generation forecasting.

2.1.3.3 Contingency reserve and black start

Contingency reserve concerns the process of discharging a local battery in the event that the area served by the store becomes isolated from the wider grid due to faults or unscheduled outages. Reserves may also be used to compensate for interruptions in power supply due to unexpected generation loss, and may be classified as spinning (less than 15 min response time) or non-spinning (greater than 15 min response time). This is a questionable, as the store will be underutilized if used for this purpose alone, so contingency would probably

need to be stacked along with other ancillary services. Black start refers to the process of discharging an electrical store to provide the power and reference frequency required to allow other generators to restart (Lott and Kim, 2014).

2.1.3.4 Voltage control

The injection of real power onto a distribution power system will always result in a voltage magnitude rise, the size of which is dependent on the quantity of power injected and the network impedance between generation and consumption points. It therefore follows that the requirement for voltage control on LV networks increases with renewables penetration (a greater power inject results in greater voltage rises), remote positioning of renewables [1].

ESQCR statute dictates that the steady state voltage on UK LV networks must remain within the range 230 V +10%/-6% (HSE, 2003), and a substantial number of studies have shown that LV urban feeders can be vulnerable to falling outside of this range in the presence on PV and other low carbon technologies (Crossland, Jones and Wade, 2014; Marra *et al.*, 2014; Navarro-Espinosa and Mancarella, 2014; Fortenbacher, Andersson and Mathieu, 2015; Giannitrapani *et al.*, 2016; Navarro-Espinosa and Ochoa, 2016; S. Alnaser and Ochoa, 2016; Lamberti *et al.*, 2017). One solution to this problem is to place BESSs close to generation sources and charge on PV export, which effectively limits the real power inject from generators and consequently also the voltage rise (Marra *et al.*, 2013, 2014). This approach has been shown to be technically feasible in various specific test cases (Marra *et al.*, 2014; Hilton, 2015; Santos-Martin *et al.*, 2015; Ranaweera and Midtgard, 2016; S. W. Alnaser and Ochoa, 2016; Fortenbacher, Mathieu and Andersson, 2017). Control strategies range from simple feed-in-limiting heuristics (Marra *et al.*, 2014; Hilton, 2015; Lamberti *et al.*, 2015, 2017) to much more complex optimization algorithms (Fortenbacher, Mathieu and Andersson, 2017; Giannitrapani *et al.*, 2017). There is currently no incentive or tariff for provision of such services in the UK, but the value of the technique may lie in it simply being cheaper than alternative voltage violation control methods (e.g. reconductoring). However, no studies have yet considered cost comparisons in detail; Crossland et al. compared BESS costs to reconductoring, though considered only reconductoring of the entire network (therefore biasing against reconductoring) (Crossland, Jones and Wade, 2014), and some

[1] PV connected at the end of a feeder creates greater voltage rises due to generally greater impedance between the generation and the 11 kV network connection point (Broderick, 2013)) and the length of the network (urban networks tend to be much shorter than rural ones so have lower impedance between generation/demand and 11 kV connection points (Tonkoski, Turcotte and El-Fouly, 2012).

authors have examined the BESS costs without comparison the alternatives (L. Wang *et al.*, 2015; Fortenbacher, Mathieu and Andersson, 2017)

2.1.3.5 Ampacity control

In addition to voltage violations, injection of power from renewable generators can cause cable ampacity violations, provided that enough generating capacity is present to exceed the cable ampacity rating (Procopiou and Ochoa, 2017). In recent studies, this has been found to be most common in feeders with high residence to feeder head ampacity ratios (Navarro-Espinosa and Ochoa, 2016), though may also occur on feeder branches with lower ampacities.

By limiting generator export using BESSs, the magnitude of feeder current can in some cases be reduced to within acceptable limits. Again, there is no incentive or tariff for such services, though a comparison to traditional reconductoring may show it to be the more cost effective option.

2.1.3.6 Customer self-consumption

Self-consumption control concerns the addition of EES to a residence for the purpose of storing excess generation from the residences renewables. The stored energy can then be used when required by the residence, thus increasing consumption of on-site generation. The general algorithm involves charging the EES whenever PV generation exceeds demand, and discharging when demand exceeds generation, and is investigated at single load scale in (Yang, Lu and Zhou, 2007), and on the LV feeder scale in (Hilton, Cruden and Kent, 2017). Whilst such control was seen to cause no meaningful reduction in network voltage and ampacity violations, customer self-consumption was increased by up to 50%. With high enough renewables penetration and a large enough energy store, it is theoretically possible to attain 100% security of supply (i.e. total independence from the electricity grid).

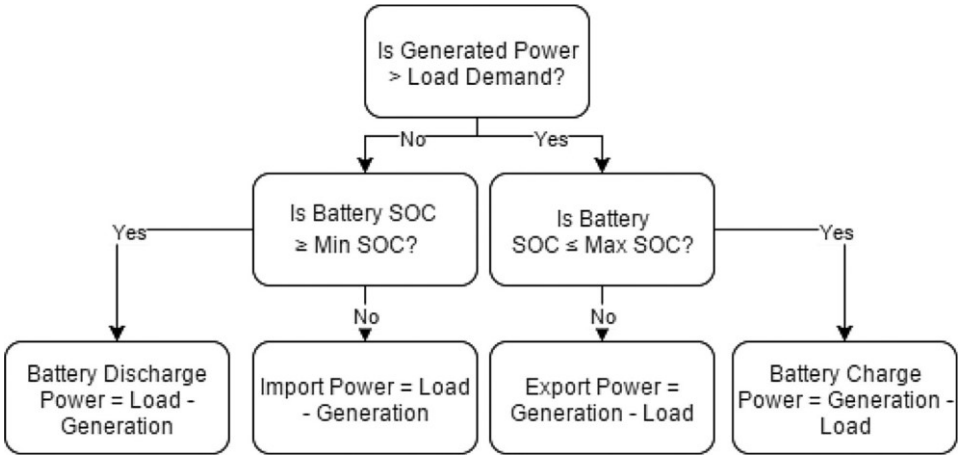

Figure 2.5 – Flow chart representation of a typical self-consumption algorithm (Hilton, Cruden and Kent, 2017).

2.1.4 Literature Review Scope

Whilst there are many potential uses of EES on UK transmission and distribution networks, the focus of this thesis is voltage and ampacity control on LV distribution networks at high PV & ASHP penetrations. This is because:

1. There is sufficient feeder topology, irradiance, and demand input data available to perform studies considering this type of control.
2. Interest and investigation in this area is notable (Liu *et al.*, 2012; Crossland, Jones and Wade, 2014; L. Wang *et al.*, 2015; Fortenbacher, Mathieu and Andersson, 2017; Giannitrapani *et al.*, 2017; Moixa, 2017a), but studies are lacking and potentially overestimate the viability of this type of network control, as discussed in section 2.3.4.
3. The technical and economic barriers to this type of control are not intuitively obvious e.g. the ability of EESs to perform the task has many dependencies (EES location, network topology, PV penetration) whose importance are not well understood.

The remainder of the literature review will therefore focus on studies related to voltage and ampacity fluctuations resulting from renewables penetration, and on work concerning BESS placement and control for control of such violations.

2.2 Impacts of renewable energy technologies, and BESS placement and control

Proposed BESS control schemes vary significantly in their placement methodology, dispatch logic, and BESS ownership assumptions. This section is split into a review of methodologies that rely on decentralized control, and those which rely on centralized control.

2.2.1 Renewables Impact Studies

The following subsection concerns studies that do not attempt to solve, but rather highlight the potential voltage and thermal constraints caused by increasing PV penetration (Ochoa, Dent and Harrison, 2010; Ruben *et al.*, 2011; Tonkoski, Turcotte and El-Fouly, 2012; Santos-Martin *et al.*, 2015; Ballanti and Ochoa, 2016; Navarro-Espinosa and Ochoa, 2016), and ASHPs (Navarro-Espinosa and Mancarella, 2014; Navarro-Espinosa and Ochoa, 2016). It should be noted that whilst this section summarises the most important PV impact studies, the two ASHP impact studies are the only applicable studies available at the time of writing.

Earlier impact analysis studies performed by Tonkosi et al (2012) examined the effect of PV penetration of rural and urban LV networks using power flow methods, and concluded that PV penetrations as high as 6.25 kW per household could be achieved in urban networks with feeders up to ≈300 meters long without voltage violations, and longer networks with feeders up to 400 m long could accommodate 2.5 kW PV per residence before the occurrence of voltage violations (Tonkoski, Turcotte and El-Fouly, 2012). However PV arrays were distributed homogenously amongst residences – this assumption excludes any voltage rise effects that may be emerge from more realistic deployment patterns (e.g. if half of all residents owned a 5 kW array, and most of these were located towards the end of the feeder, a greater voltage rise would be expected than in the examined 2.5 kW case).

More recent studies have analysed such phenomena with fewer placement assumptions. Navarro-Espinosa et al. (Navarro-Espinosa and Mancarella, 2014) Used real UK demand profiles from the microCHP project (The Carbon Trust, 2011), together with the corresponding heat consumption profiles to determine the likely maximum ASHP penetration on an LV test network. Heat profiles for a relatively cool UK day (average 7^{o}C) were converted to ASHP and ground source heat pump (GSHP) electricity consumption profiles using a novel methodology, and 100 simulations (each investigating different ASHP placement configurations) were performed at each ASHP penetration between 0 and 100%

at 10% increments, and the distribution of results were analysed in terms of feeder head utilization % and % of customers experiencing voltage violations by EN 50160 standards. It was noted that aggregation of the ASHP electrical demand profiles resulted in network demand spikes in the morning, and during the late evening, as a result of higher building occupancy (see figure 2.6). The study did not, however, consider the effects of very cold UK winter days on network operation.

Line ampacity violations were observed on the feeder heat at 40% ASHP penetration and 50% GSHP penetration, whilst voltage violations were not observed until 60% ASHP and 80% GSHP (see figure 2.6).

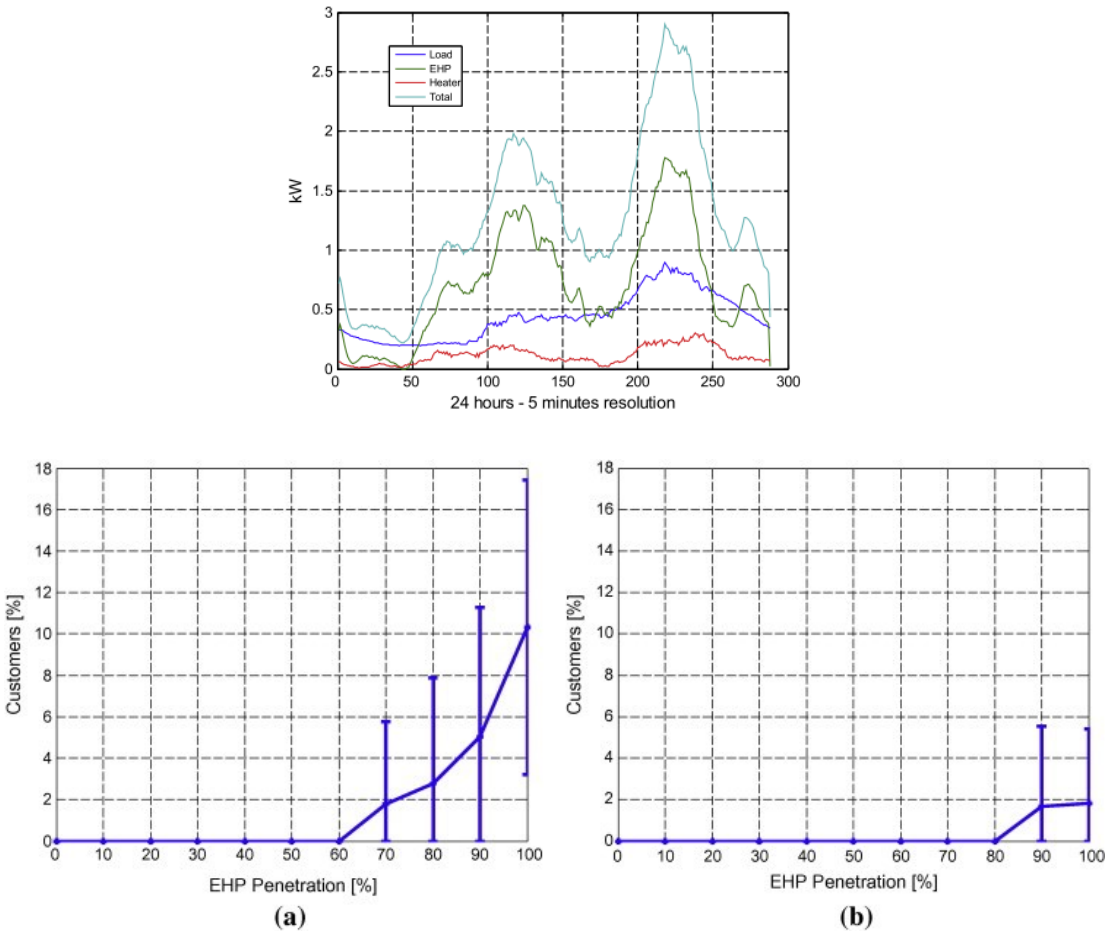

Figure 2.6 – Shows (top) the typical aggregated electrical demand profile for ASHPs on a cool UK day, and (bottom) the % of customers experiencing voltage violation vs. different (a) ASHP and (b) GSHP penetrations from the study presented in (Navarro-Espinosa and Mancarella, 2014). *In this case, electric heat pump (EHP) referes to ASHPs.*

This study was expanded in (Navarro-Espinosa and Ochoa, 2016), in which the authors examined the effect of varying the penetration of residence owned PV, ASHPs, and microCHP on LV feeders located in the northwest of England on the frequency of voltage and cable ampacity violations. Simulations were performed on 128 feeders at renewables penetrations between 0 and 100% at 10% increments (where penetration is defined as the percentage of residents who own and operate a particular renewable), and Monte Carlo methods were used to vary the location and kW sizing of technologies; 100 simulations were performed on each network for each technology and each % penetration. Feeders were considered to have problems if more than 1% of properties experienced voltage violations (by EN 50160 standards) or if the feeder head experienced a thermal violation in any of the simulations performed on them. Additionally, a sensitivity analysis was performed to examine the effect of relaxing rules to allow violations in up to 5% of simulations. The authors found that 46% of feeders experienced problems in the base case (0% of simulations were permitted to show violations, if they were to be considered violation free), and that 37% experienced problems In the 5% case. In the ASHPs case, 48% of feeders experienced problems in both the base and 5% case.

Similar studies have been performed in countries with very similar distribution networks, with similar observations. Notably, Santos-Martin et al. performed similar work to Navarro et al., examining voltage violation on New Zealand LV networks under varying PV penetrations (Santos-Martin *et al.*, 2015). The group examined over 10,000 LV feeders, applying maximum power inject from generators and diversified maximum midday summer demands to all residences on feeders. When allowing a maximum voltage of 253V (equal to the UK allowable steady state max) violations began at 30% PV penetration, and affected 10% of urban LV networks at 56% penetration.

MV network studies were performed by Ruben *et al* (2011) to determine the limiting factors for distributed generation on an urban network; 11 kV primary feeder loops were modelled with different levels of utilization, distributed generation, and generator positioning, and results suggested that generation was limited by line and primary substation power capacity, not voltage violation, under all tested circumstances (Ruben *et al.*, 2011). A similar study by Ochoa *et al* (2010) (Ochoa, Dent and Harrison, 2010), employed similar techniques to investigate the effects of the addition of distributed generation on the simplified EHV1 network from the UK generic distribution system. Temporal demand variation was modelled

using demand and generation data from central Scotland, and modelling results showed that thermal limits of lines and transformers are met before unacceptable voltage rises occur. Similarly, Ballanti et al. determined the threshold for PV-caused voltage and thermal violation on an 11 kV UK network (Ballanti and Ochoa, 2016). Demand profiles for each phase of each secondary substation were generated with the CREST model, which was also used to develop spatially resolved PV generation profiles for different substations. It was found that a homogenous PV penetration of 60 % across all secondary substations was required to induce voltage violations on the MV network, whilst thermal violation began at 70 %.

2.2.2 Active Violation Management Technologies (Non BESS)

Many studies also note that voltage violations can be managed in many alternative ways that may be easier to control, and practically easier and cheaper than BESSs. These studies most frequently consider absorption of reactive power by PV inverters (known as reactive power control (RPC)), reduction of tap changer set points, or the use of on load tap changers (OLTCs) at secondary substations (SSSs).

RPC has been shown to provide little effect when used on LV feeders without any other form of active management; Santos-Martin et al. showed that for any noticeable voltage control effect to be gained from RPC alone, all PV inverters on a network must operate at PF = 0.8 lagging (Santos-Martin *et al.*, 2015), which negatively affects network PF, and still only offers an improvement of a few percent (see figure 2.7). Regardless, some studies consider the combination of RPC and other network management strategies (L. Wang *et al.*, 2015; Fortenbacher, Mathieu and Andersson, 2017).

Threshold, percentage of networks with overvoltage problems	Maximum allowable PV penetration level, %	Increase in PV penetration over base case, %
1% urban	13	3
5% urban	20	4
10% urban	23	5

Figure 2.7 – Shows the increase in PV hosting capacity of 10,000 urban LV feeders when PV inverters operate at PF = 0.8, from (Santos-Martin *et al.*, 2015).

OLTC control has proven more effective than RPC for voltage management. Procopiou et al. (2014), modelled a 351 residence LV network with 6 feeders (between 0.78 – 2.32 km in length) in the north of England at varying % PV penetrations, and found that modification of

the SSS with a ±8% on-load tap changer with remote monitoring (voltage monitors at the extremes of each feeder branch) and automatic control allowed 80% PV penetration with no voltage violation on any feeder, and 100% penetration with only a small number of customers suffering voltage violations (Procopiou, Long and Ochoa, 2014). Without the addition of an OLTC, all feeders were able to reach ≈50% PV penetration before any occurrence of voltage violations (figure 2.8). Long et al. performed a similar analysis on 6 LV feeders, and concluded that OLTC with remote monitoring was sufficient to achieve EN 50160 compliance for 98.4% of customers across all feeders (Long, Ochoa and Member, 2016). However, the inability of OLTCs to address thermal contstraints is not considered in this work, and so the benefits of network management using OLTCs are likely overestimated.

	PV Penetrations Level (%)						
Feeder ID	**10-40**	**50**	**60**	**70**	**80**	**90**	**100**
1	100	100	100	100	100	100	100
2		100	100	100	100	100	100
3		100	100	100	100	100	100
4		100	100	100	100	94	92
5		100	100	100	100	98.5	97.1
6		100	100	100	100	100	98.8
Number of tap changes	0	6	6	4	4	4	4

Figure 2.8 - The % of residences experiencing no voltage violations at varying % PV penetrations after installation of an OLTC.

A later study by the same author considered the scope for reducing the complexity of the monitoring system by estimating branch end voltages based on feeder head voltage and power transfers (Procopiou and Ochoa, 2017). Average estimation errors were typically below 1%, and the effectiveness of control (based on frequency of voltage violations) was barely affected by the removal of remote monitoring, suggesting that OLTC based control could be applied to a feeder using only and OLTC, a single monitor, and a remote terminal unit. Again, despite the clear effectiveness of OLTCs for voltage control, OLTCs cannot be used to manage ampacity violations, and this is not addressed.

2.2.3 Active Network Control – Enabling Technologies

The traditional way to limit the potential for ampacity and voltage violations at the LV level is to ensure the conductors are sufficiently sized. It therefore follows that reconductoring a feeder or network that is experiencing violations with larger diameter conductors may provide a passive solution to voltage and ampacity problems, and this is considered in

(Crossland, Jones and Wade, 2014). However active management techniques are being explored, and technological developments are beginning to make these techniques possible.

Studies often concern the active management of operational violation on distribution networks using on-load tap changers (OLTCs) at secondary substations (SSSs) (Procopiou and Ochoa, 2017), reactive power compensation using PV inverters (Fortenbacher, Mathieu and Andersson, 2017), Curtailment of generation (Haque, Nguyen and Kling, 2014), and control of distributed battery energy storage systems (BESSs) (Fortenbacher, Mathieu and Andersson, 2017). Availability of affordable residential BESS systems with large enough capacities to handle feed in limiting tasks across multiple hours, such as the Tesla Powerwall 2 (13.2 kWh, 5kW max continuous) (Tesla, 2016) and the Mercedes-Benz Energiespeicher (2.3 - 18 kWh, 1.25 - 4.6 kW max continuous) (Mercedes, 2014), have made violation control via BESS charging a potential solution. Furthermore, modern BESS inverters often have the capability to operate at non-unity power factors, such as those produced by Fronius (Tesla, 2016; CCL, 2017), and SunnyBoy (SMA, no date). Research and development of inverters able to make operational decisions based on remote grid signals is ongoing; for example, Ippolito et al. (Ippolito *et al.*, 2013) developed an inverter capable of determining the (SMA, no date) appropriate operation under frequency control, voltage control, load shifting, load prioritising under islanded conditions, and harmonics compensation, based on signals from the wider grid. SCADA based control systems have been developed to coordinate control of multiple battery sets (Isono *et al.*, 2013) for frequency control, and this has made centralized BESS control for violation management a technical possibility. Control infrastructure and logic for the automatic adjustment of OLTC tap positions has been proposed (Long, Ochoa and Member, 2016), and such strategies are already applied at many primary substations in the UK for 11/6.6 kV network management (Lamberti and Calderaro, 2013). PV curtailment may also be an option at the LV network level as a result of export limiting devices such as the SolarEdge (SolarEdge, 2017). Certain active management methods require user power export and import data, but with the increased rollout of smart monitoring equipment, the proposition of utilizing an operational scheme that requires spatially and temporally resolute power and voltage data is becoming more feasible.

2.2.4 Active Violation Management Technologies (BESS based)

Studies that concern the management of steady state network violations using BESSs typically fall into 3 categories;

- Sizing and Placement – concerns the design and testing of algorithms that determine the optimal size, number, and location of BESS systems on LV networks, such that the set of BESSs are able to act to manage violations.
- Decentralized Control – concerns the design and testing of an operational strategy that dictates how individual BESSs should operate based on information available solely to them i.e. BESSs are not controlled as an ensemble. For example, feed in-limiting (FIL) requires only a knowledge of the power export at the residence a BESS is associated with, and no knowledge of the state of the rest of the feeder, or how other BESSs are operating, and therefore would be considered a decentralized control algorithm. Such control strategies require very little/no data communication infrastructure, and voltage and ampacity control is often an indirect side effect of power inject limiting.
- Centralized Control - concerns the design and testing of an operational strategy that dictates how BESSs should operate as an ensemble, based on the state of the network i.e. a decision is made by a centralized controller as to how best operate each BESS on the network to control a factor that is not necessarily local to each store. For example, such a control strategy may seek to limit the voltage at the end of a feeder using as little total charging power as is possible across all network stores, and require a central controller to receive and process all network voltage information, then send BESS operation set points. Consequently, such operational strategies will require data communication infrastructure.

The discussion of BESS based active violation management strategies is split to cover these 3 distinct types of studies.

2.2.4.1 Sizing and Placement

Wong et al. attempted to find the minimum size required for a feeder connected BESS to mitigate voltage rise on a 69 bus LV test feeder, which resulted from placement of a 3.66 MW PV array, to acceptable levels (0.95 - 1.05 p.u. in this instance). The authors employ a 2-stage firefly algorithm (FA) to iteratively approach the set of per hour BESS real power outputs that minimize voltage violations (step 1), and minimizes full state of charge (SOC)

events (step 2), across a 2184 h (91 day) period. The algorithm is effective in reducing the number of hourly voltage violations from 297 to 78. However, the FA is global search algorithm and is not guaranteed to find (or even approach) the true optimum, and does not solve rapidly enough to be used in a monte-carlo simulation. This is important, as it is typically necessary to consider the variation in sizing across uncertainty in operation.

Shaaban et al. optimized the placement and sizing of BESSs on a 123 bus test network with residential and commercial loads and a 30% penetration of PV using a novel genetic algorithm (Petinrin and Shaaban, 2016). The fitness function concerned minimization of high or low voltage violations, and reduction in network losses, though did not consider the cost of purchase and installation of the BESS systems, and again is relatively slow, and does not guarantee an optimum result.

Crossland et al. proposed a novel hybrid genetic algorithm/simulated annealing (GA/SA) model to minimize the placement costs of residential and feeder-located BESSs on an LV (400V) network, whilst preventing voltage rise (Crossland, 2014). In the first stage, BESSs were added sequentially from the most to least voltage sensitive nodes on the network, stopping when voltage issues were solved, and this was considered the initial population of BESSs. A population of 500 was generated from the initial population via random changes to BESS sizes, and these new populations were tested to see whether they were able to control voltage. If not, a cost of reconductoring was added. Each population was then ranked in order of fitness (power capacity, installation, energy capacity, and reconductoring cost were considered in this). Random changes were then made to the populations which were accepted if they resulted in fitness increase, and accepted probabilistically if they did not. This probability decreased with each run of the algorithm (thus contributing the simulated annealing aspect of the formulation). Mating and crossover processes were then applied (contributing the GA aspect), and the ranking, SA, and GA processes were repeated until convergence. The algorithm was applied to a 281 bus network serving 406 residences with varying PV penetration and PV array placements, and it was shown that BESSs located at the residence were able to provide the same benefits as feeder-located BESSs, and required smaller energy and power capacities to do so (fig 2.9). Results also suggested that storage may provide a cheaper alternative to reconductoring the network at PV penetrations below 40 %. However, the study only considers full network reconductoring (partial reconductoring

would be possible in practice), and uses a slow global search algorithm that does not guarantee an optimal result.

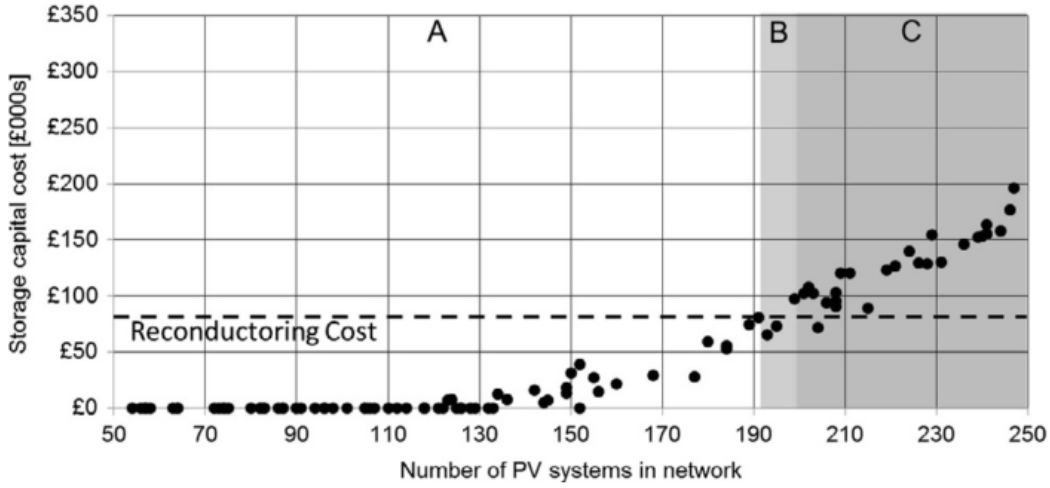

Figure 2.9 - Shows BESS cost vs number of PV systems for the study performed by Crossland (Crossland, Jones and Wade, 2014)*. The cost equality point (between BESS and reconductoring methods) at 200 PV systems translates to a PV penetration of 50%.*

Recent work has explored heuristics for simplification of BESS placement and sizing, so that near optimal placement may be achieved with lower computational costs on relatively large networks. Giannitrapani et al. explored the spatial resolution required to optimally site BESSs on LV networks. In this instance the solution to the integer aspect of the BESS placement problem (i.e. the installation cost) is approximated using a novel clustering algorithm; a 17 bus Italian LV network (figure 2.10) is split into clusters, with each automatically assigned a one BESS (if any of the nodes in the cluster experience a voltage violation) or zero BESSs (if no nodes in the cluster experience violations). The BESS energy capacity algorithm is run for every possible number of clusters (where the maximum cluster number is equal to the number of residences), and it was found that cost reached an unchanging minimum at 8 clusters (approx. ½ of the 26 residences). The authors did not investigate how this varies with PV penetration, nor how effective the algorithm might be for larger networks with much greater bus numbers (the network examined had only 26 loads) (Giannitrapani *et al.*, 2015). Furthermore, the algorithm was limited in that the number of BESSs to place had to be predetermined i.e. the algorithm could not determine the optimal number, placement, and size automatiocally.

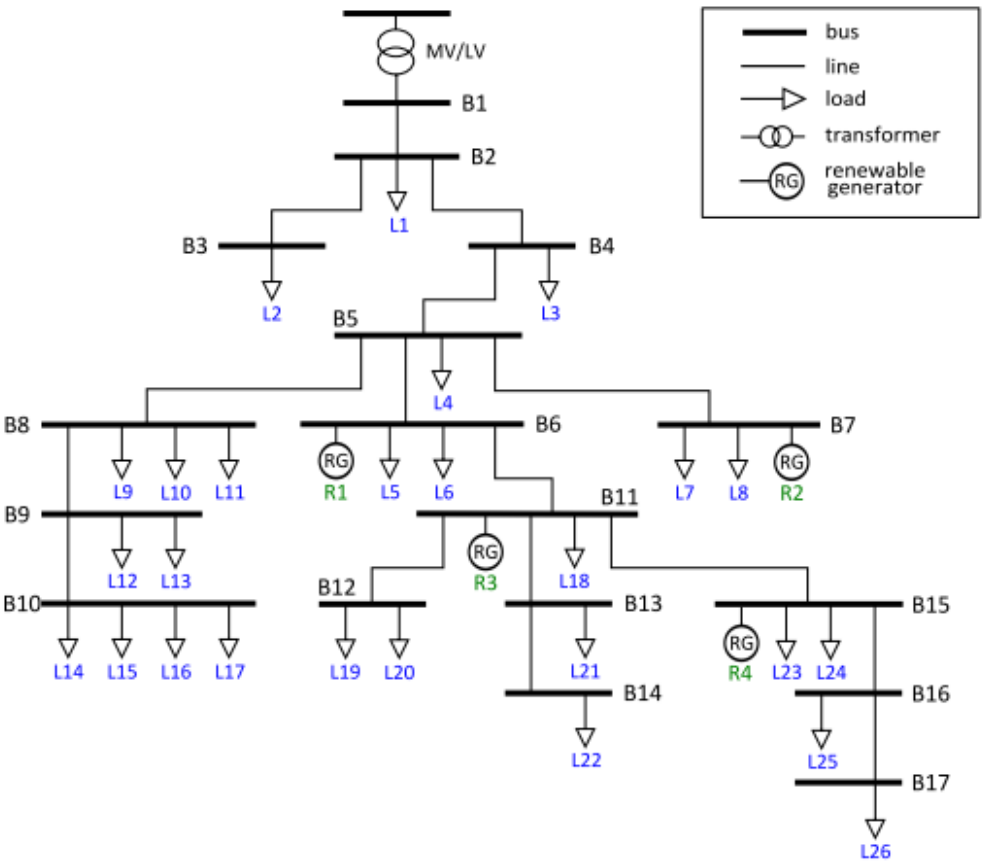

Figure 2.10 – The 17 bus, 26 load test feeder used in (Giannitrapani *et al.*, 2015).

Bucciarelli et al. applied this algorithm on 4 days of varying sky clearness, and found total installed capacity requirements varied between 1 kWh, and 26.43 kWh across scenarios, though this analysis was only applied to the same 17 bus LV network. (Bucciarelli *et al.*, 2016).

Giannitrapani applied the algorithm to 200 randomly generated networks, assuming 2 BESSs on the network (scenario 1) or 3 BESSs (Scenario 2). Results were compared to the true optimum (from a non-convex mixed integer AC optimal power flow (OPF) formulation), and the authors found the results were optimal in 45% and 57% of cases for scenarios 1 and 2 respectively (Giannitrapani *et al.*, 2016). This method did, however, require strict constraints on BESS count.

2.2.4.2 Decentralized control methods

Marra et al. (Marra *et al.*, 2014) proposed a decentralized feed in limiting based BESS control heuristic for customer owned BESSs. The exact feed in limit to be applied to each BESS was determined using a linear programming heuristic, and it was determined that adequate

voltage control could be achieved by limiting export to 70% of PV rated power. After sunset, BESSs were instructed to discharge. Applying these rules to a network of 33 residences, 9 PV arrays and 9 BESS, the authors found that each PV system requires a minimum capacity of 5.4 kWh/2 KW. If the penetration were increased to 18 PV arrays (≈50% of all residences), the required BESS capacity increased to 28 kWh/6 kW (if still only 9 BESSs were used), or 14 kWh/ 3 kW (if every PV owner owns a BESS). The study did not however consider multiple placements and sizes of BESSs, and assumes location of BESSs at all/exactly half of residences with PV arrays.

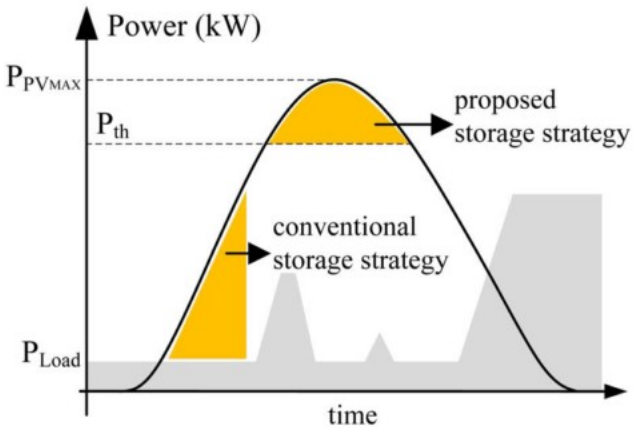

Figure 2.11 – A diagram explaining the difference between the typical self-consumption (conventional storage) algorithm and the typical FIL algorithm which is used in (Marra *et al.*, 2014)*. In each case, the yellow regions denote the energy from clear sky generation that is stored in the BESS. As shown, the BESS has often fully charged before peak generation time. P_{th} represents the PV generation threshold above which the BESS begins to change in the FIL case, P_{load} represents load demand, and P_{PVmax} is the maximum possible generation from the PV system in question.*

Lamberti et al. proposed 2 control heuristics for the reduction of voltage violations and increase in self-consumption on a LV Italian distribution network (Lamberti *et al.*, 2017). Location and rating of PV arrays and rating of BESSs are assigned randomly and multiple network configurations are solved during summer and winter months to determine the statistical likelihood of violation under different PV penetration and BESS control scenarios. As suggested in (Marra *et al.*, 2014), it was determined that feed in limiting was more effective for voltage control than the simple self-consumption strategy, and resulted in only a very small reduction in self-consumption across all penetration levels. The study assumed

that all PV is co-located with BESSs, so is likely to overestimate the effectiveness of BESSs based violation management on real networks.

Von Appen et al. compared the effect of 5 decentralized BESS dispatch algorithms on the voltage profile of a 34 residence German network, and analysed the cost/benefit of changes in grid import and export in each case (Von Appen *et al.*, 2014). It is assumed that each property owns a BESS, and all BESS systems were equal sizes (i.e variation of location and sizing of BESSs was not considered). It was found that self-consumption based algorithms, and those that incorporated both self-consumption and PV curtailment, resulted in 10% greater customer savings than FIL based counterparts, and that the control algorithm chosen had little effect on the number of voltage violations observed by EN 50160 standards. Although the study considers different control algorithms, it is performed of a very short (34 residence) feeder, and the algorithms are all relatively similar and simple i.e. the study does not consider the difference in control effectiveness between a simple feed-in limiting algorithm and a complex centralized algorithm.

Hilton et al. (Hilton, Cruden and Kent, 2017), Marra et al. (Marra *et al.*, 2014), and Lamberti et al. (Lamberti *et al.*, 2017), however, all observed ineffective voltage control from self-consumption (SC) algorithms due to premature BESS filling before the occurrence of voltage rise events on clear summer days.

2.2.4.3 Centralized Control

Wang et al (Z. Wang *et al.*, 2015) propose a BESS operation heuristic in which behind the meter BESSs are time-shared between DNOs (for voltage and utilization management during periods of pressure) and residents (for increased self-consumption) . Whilst potential cost savings are proposed, these are not fully analysed with regards to system install costs and alternative means of reinforcement. Ranaweera and Midtgard (Ranaweera and Midtgard, 2016) proposes a more elaborate method using optimal operation forecasting to allow self-consumption and violation control operation to occur simultaneously. They then compare this to a simple self-consumption only heuristic via application of each dispatch scheme to an IEEE European low voltage test feeder. It is found that a centralized control scheme is required to ensure sufficient network control is maintained, though the degree of self-consumption is independent of complexity of the control scheme. Again, the economic feasibility of such an approach is not considered, and it is assumed that all residences have identical BESSs + PV arrays. Anusha considered a very similar DNO coordinated BESS

approach, and observe similar results (Anusha, 2015). Fortenbacher et al. constructed a centralized MILP optimal power flow (OPF) control algorithm for residential BESSs to minimize network losses, storage losses, and BESS degradation whilst satisfying network constraints (Fortenbacher, Mathieu and Andersson, 2017). The formulation adds a predictive method to determine a suitable SOC trajectory for the BESS set over the course of a day, which prevents premature filling before all voltage control tasks have been completed. BESS inverters were also permitted to provide reactive power control by operating at non-unity power factors. The study is limited to only one PV and BESS placement (all houses have the same size PV array and same size BESSs) didn't consider the comparative costs of such a system, assumes balanced operation, and is applied to a very small test network of 18 buses. Furthermore, the very large 10 kVA/20 kWh systems assumed in this study are much larger than even the largest available home battery systems (Mercedes, 2014; Tesla, 2016), and so it is difficult to say how easily such systems could be obtained and installed.

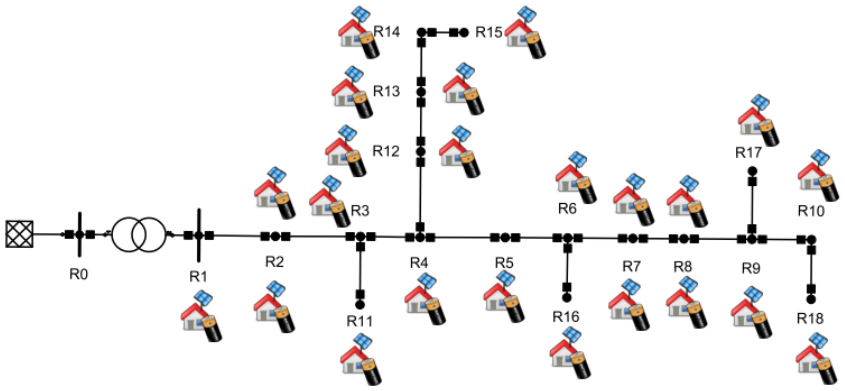

Figure 2.12 – The CIGRE test network used in the study performed by Fortenbacher et al. (Fortenbacher, Mathieu and Andersson, 2017).

Liu et al combined OLTC operation with BESS charging to examine the systems suitability to control of voltage rises, reduction of demand peaks, and reduction of transformer stress. The OLTC was used primarily to manage feeder voltage, whilst the BESS was charged to prevent reverse power flow, and discharged during peak demand hours. The algorithm was applied to a GE 240 V test feeder with one 22 kWh BESS and varying PV penetration levels of 10%, 30%, and 50%, and simulations using an experimental setup in a smart grid lab showed 15% peak reductions, reduced OLTC operation, and a very slow degradation of the BESS (provided that depth of discharge (DOD) was limited to 20%). However, the network model is again

much smaller than the typical UK LV feeder, and only considers using one BESS on a larger network (Liu *et al.*, 2012).

Some proposed control algorithms that rely on communications do not require centralized processing. Mokhtari et al. proposed a consensus algorithm for control of multiple BESSs without a centralized processor (Mokhtari *et al.*, 2013). The algorithm relies on communication between BESSs upon detection of a voltage violation at any node. When a violation is detected, a signal to control for voltage violation is passed between BESSs; the magnitude of the power output request sent to each BESSs is dependent on the magnitude of the voltage violation, the power capacity of the BESS, and a BESS specific weighting factor (though in this paper all weighting factors are set equal so all units output the same proportion of their maximum real power). The algorithm was shown to effectively and rapidly stop violations, and the communications structure ensured that the system was more robust to communications errors than algorithms relying on one central controller. However, the test network was composed of only 12 customers with no branching. A very similar study was performed on models of Australian LV feeders by Alam et al. (Alam, Muttaqi and Sutanto, 2012). BESSs were operated on the same principle, though centralized data processing and communication was assumed.

Occasional studies consider BESS placement at higher voltage levels. Alnaser and Ochoa examined wind curtailment reduction on a real UK 33 kV distribution network via OLTC, BESS, and RPC operations. The authors implemented a storage sizing algorithm (with the objective of minimising BESS energy and power capacities whilst remaining within voltage and ampacity ranges), then a 2 stage quadratic programming control algorithm that maintained curtailment below a chosen level (stage 1) with minimum possible BESS charging/maximum possible discharging (stage 2). It was shown that the violations arising from 6 MW of wind generation could be effectively mitigated using BESS, OLTC and RPC control, and that a curtailment reduction from 42% to 5% could be achieved for between £5.5M – £7.5M, which is potentially lower than the value of the curtailed energy over the lifetime of the BESS (figure 2.13).

Storage PF and Curtailment	Additional Flexibility	5% Desired Curtailment						0% Desired Curtailment					
		Storage size per bus			Total MVA/MWh	Total Unit Cost	Time (min)	Storage size per bus			Total MVA/MWh	Total Unit Cost	Time (min)
		201	205	210				201	205	210			
Unity PF	-	1.5/13.4	3.3/15.2	-	4.8/28.6	31.8	45	1.9/20.5	5.8/42.1	0.6/1.7	8.3/64.3	69.9	16
0.975PFc	-	1.8/6.3	3.1/13.5	-	4.9/19.8	23.1	52	2.0/24.6	3.8/26.7	1.1/4.8	6.9/56.1	60.7	19
0.95PFc	-	1.6/6.9	3.4/9.4	-	5.0/16.3	19.6	51	2.3/25.9	3.2/22.1	1.3/5.8	6.8/53.8	58.4	21
Unity PF	OLTC	1.5/6.8	-	-	1.5/6.8	7.6	49	2.8/30.6	-	1.8/9.9	4.6/40.5	43.6	16
0.975PFc	OLTC	1.5/6.5	-	-	1.5/6.5	7.5	53	2.9/30.0	-	1.9/9.8	4.8/39.8	43.0	18
0.95PFc	OLTC	1.5/6.4	-	-	1.5/6.4	7.4	58	2.9/29.9	-	1.9/9.7	4.8/39.6	42.8	19
Unity PF	OLTC + DG PF	1.1/4.9	-	-	1.1/4.9	5.6	58	2.8/28.5	-	1.8/9.4	4.6/37.9	41.0	18
0.975PFc	OLTC + DG PF	1.1/4.8	-	-	1.1/4.8	5.5	59	2.8//28.3	-	1.8/9.4	4.6/37.7	40.8	18
0.95PFc	OLTC + DG PF	1.2/4.7	-	-	1.2/4.7	5.5	60	2.8/28.3	-	1.8/9.4	4.6/37.7	40.8	18

Figure 2.13 – Shows required BESS sizes and costs for the simulations performed by Alnaser et al. It can be seen that the cost of BESS capacity may fall below the benefit of curtailment reduction in the instance that an OLTC is present at the primary substation (S. W. Alnaser and Ochoa, 2016).

Wang et al modelled a UK 11 kV network and LV network simultaneously to investigate the effectiveness of coordinated OLTC, BESS, and RPC control on unwanted voltage rises and phase imbalances (Wang *et al.*, 2014). 3Ø BESSs were placed at a 5 MW windfarm, and by cluster of rooftop PV systems on an LV network (where penetration across phases was uneven). Control via optimization for lowest operation cost of BESSs, RPC, and OLTC was implemented, and testing via IPSA 2 models and 'network in the loop' simulations suggested that the approach was sufficient to reduce voltages to within statutory limits on both MV and LV networks, and mitigate the unbalance factor on the LV portion of the network. Although costs were considered in the optimization problem, system costs were not specifically stated or analysed.

Kashem et al. designed the control logic for a BESS inverter and demonstrated its effectiveness in controlling voltage on an 11 kV Australian feeder. Considering a peak feeder load demand of ≈700 kVA, it was shown that between 22 and 575 kWh of BESS capacity was required to ensure voltage remained within acceptable limits (depending on the definition of acceptable limits), though the BESS inverter was able to operate at any power factor (Kashem and Ledwich, 2007).

2.2.5 Summary

The effects of rooftop PV generator installation on network overvoltage and thermal overload (assuming not network management) are already well understood in literature, and therefore little benefit could be attained from repeating these studies. However, there is relatively little work on the impact of ASHPs on network undervoltage and thermal overload, and that which has been performed does not address the possibility of low diversity on very cold winter days.

Literature studies concerning active management strategies other than BESS management (OLTCs and RPC) are lacking in some aspect; RPC is ineffective on LV networks due to relatively low cable inductance, and OLTCs are unable to manage thermal violations. Traditional reconductoring, as either a complementary or standalone strategy for network violation management, is not examined at all.

Current placement and sizing algorithms rely largely on global search algorithms which are slow and only sometimes produce a globally optimum results, and often involve undesirable pre-allocation, such a predefinition of the number of BESSs to place, or the quantity of the network to reconductor.

Whilst decentralized control algorithms are demonstrated as a effective in some controlled instances, assumptions such as 100% BESS availability, very short networks, and limited consideration of possible PV placements limit the validity of results in all cases. Furthermore, there are no studies that consider the suitability of BESS control to ASHP caused violation management.

Whilst it is interesting that BESSs may be economically feasible at the 33 kV level, technical and economic feasibility at the LV level are rarely examined in an appropriate manner in centralized control studies i.e. realistic BESS ownership and availability patterns are usually not considered if random PV array ownership is assumed, and the costs compared to other reinforcement strategies are usually ignored.

2.3 Modelling trends

2.3.1 Modelling generation and demand

In many steady state studies, particularly those concerning only placement and sizing, the authors do not use or model PV generation profiles at all, and simply size BESSs for maximum possible array output (Crossland, Jones and Wade, 2014; Santos-Martin *et al.*, 2015; Giannitrapani *et al.*, 2016). Some studies make use of available generation-time series data recorded from real PV arrays (Lamberti *et al.*, 2015, 2017), and others use irradiance readings from local weather stations in conjunction with regressive power-to-irradiance models, or just assume a fixed irradiance to power conversion efficiency (Navarro-Espinosa and Ochoa, 2016). LV studies usually consider a small area (<0.4 x 0.4 km), and temporal resolution between 1 min and 15 min. At such temporal resolutions, it has been demonstrated that the correlation between rooftop array generation profiles exceeds 95% (Lave, 2011; Elsinga and Sark, 2014). Consequently, all such studies approximate the generation profiles at each array to be identical. Where larger areas are covered, spatial variation in irradiance must be considered, and Ballanti et al. solved this issue by generating spatially correlated irradiance profiles for each SSS area on a primary substation feeder using the CREST model (Ballanti and Ochoa, 2016; McKenna and Thomson, 2016). Furthermore, recent studies have suggested that PV generation can be modelled more accurately using satellite derived irradiance data for the area in question than by using ground derived data from observatories located several km away from the area (Ruf *et al.*, 2016).

Sizing and placement models generally use fixed after diversity max demand (ADMD) values for residence demands (Crossland, Jones and Wade, 2014; Santos-Martin *et al.*, 2015), but sometimes use low temporal resolution profiles with a multiperiod optimization problem so as not to lose the effects of changing demand on sizing requirements (Fortenbacher, Andersson and Mathieu, 2015; Giannitrapani *et al.*, 2015, 2017; Bucciarelli *et al.*, 2016; Fortenbacher, Zellner and Andersson, 2016; Fortenbacher, Mathieu and Andersson, 2017). Papers that consider planning of operational method occasionally use ADMD values in initial parameter optimization, then fine tune these values via time series simulations that utilize real demand profiles (Marra *et al.*, 2014). Studies using residential demand time series may use real data if available (Marra *et al.*, 2014; Navarro-Espinosa and Mancarella, 2014; L. Wang *et al.*, 2015), though it is often the case that authors must resort to using modelled demand data to handle the large quantity of different profiles that are required to model an entire

LV network/feeder. A common source of modelled demand profiles is the CREST model (Richardson and Thomson, 2009; McKenna and Thomson, 2016), which generates profiles statistically based on appliance ownership, day of the year, and occupancy number (figure 2.14). The model is used extensively in literature (Procopiou, Long and Ochoa, 2014; Ballanti, 2015; Lamberti *et al.*, 2015, 2017; Ballanti and Ochoa, 2016; Long, Ochoa and Member, 2016; Navarro-Espinosa and Ochoa, 2016; Procopiou, Quiros-Tortos and Ochoa, 2017), as a result of its ability to simulate realistic demand over long time periods, and with realistic enough variation between residences to build up acceptable substation demand profiles (ENWL, 2014). None of the studies reviewed used demand data recorded at the residences modelled. Where commercial demand was considered, they were modelled using half hourly elexon profiles were used (Ballanti, 2015; Rigoni *et al.*, 2016), however, these studies considered MV (11 kV+) networks, and such low resolution demand profiles may not be appropriate at the LV level.

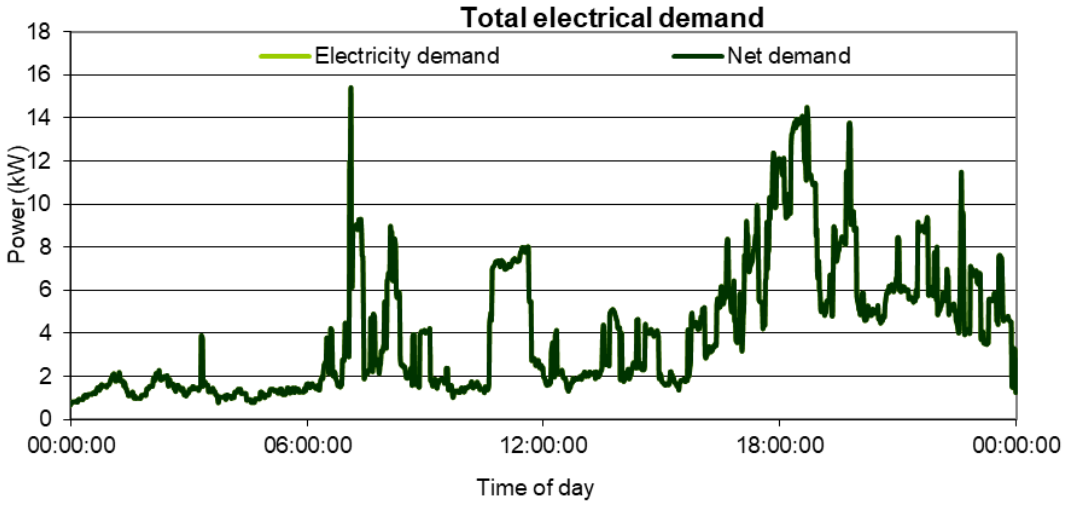

Figure 2.14 – Example electrical demand profile output from the CREST model.

Whilst it is possible to predict point irradiance with reasonable accuracy using the ARIMA method (Reikard, 2009) (figure 2.15), and persistence may be used to provide a fair estimator of daily demand (Veit *et al.*, 2014), forecasting decisions seem to absent from all studies in this research area, with most opting to assume perfect prediction where required.

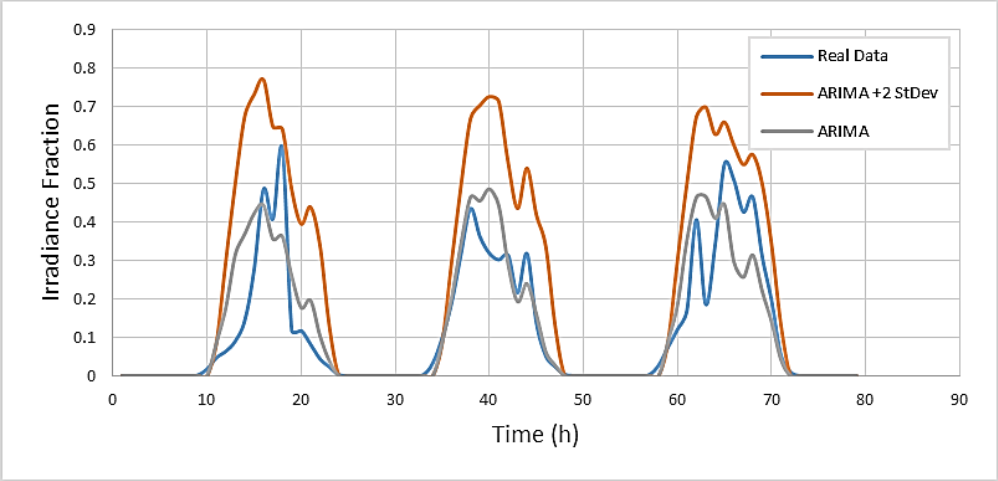

Figure 2.15 – Shows the effectiveness of the ARIMA (1,0,0)(1,1,0) modelling in the context of irradiance prediction. Whilst reasonably effective, there are some significant irradiance mispredictions, and therefore the use of perfect prediction is questionable.

2.3.2 Store Degradation

Battery degradation models are typically either empirically determined or theoretically formulated. Theoretical models consider battery process at the molecular level, are very specific to particular cell geometries and sizes, and require very detailed input data (Xu, Oudalov and Ulbig, 2016). Conversely, empirical models are usually broadly applicable to their given chemistry and require only simple inputs, such as SOC profiles and temperature (Lam and Bauer, 2013; Barcellona *et al.*, 2015; Xu, Oudalov and Ulbig, 2016), and are therefore more commonly used in network scale studies (Barcellona *et al.*, 2015; L. Wang *et al.*, 2015; Karagiannopoulos *et al.*, 2016). Empirically models may employ rainflow counting methods to account for the irregular cycling behaviour that may be observed in a practical setting. Rainflow counting involves the separation of a complex stress vs time spectra into a series of simple stress cycles (Nieslony, 2010) (figure 2.16), and is typically used in analysis of structural component fatigue in civil and mechanical engineering (Marsh *et al.*, 2016). Rainflow analysis is also applicable to the simplification of irregular BESS cycling profiles, as the electrodes used in Lead Acid and Li ion BESSs are subjected to similar mechanical stresses during cycling (Xu, Oudalov and Ulbig, 2016). After the rainflow process has been carried out, the component fatigue associated with each of the resulting simple stress cycles can be estimated as a function of the cycle's properties – for batteries, component fatigue represents capacity fading, and this is usually represented as a function of cycle depth and

average SOC during the cycle (Millner, 2010; Lam and Bauer, 2013; Xu, Oudalov and Ulbig, 2016).

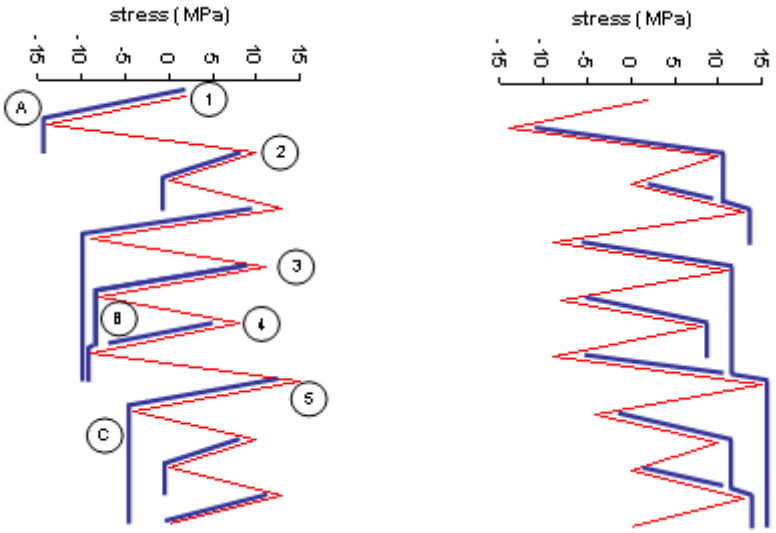

Figure 2.16 – Shows the process used to split complex loading cycles into simple half cycles. We imagine rain flowing from pagoda roofs (shown in blue), and consider the flow originating at both peaks (left) and troughs (right) (*Rainflow-Counting Algorithm*, no date). *The magnitude of each flow is approximated as single half cycle (e.g. 1 – A is assigned a magnitude of 15 MPa), and a flow terminates when it reaches the end of the graph (e.g. flow 1), merges with an earlier flow (e.g. flow 2), or merges with a later flow that starts from a more higher peak or lower trough (e.g. flow 2). The separate half cycles can then be analysed individually. For BESSs, MPa is replaced with SOC.*

A theoretical battery degradation model regarding energy capacity fade as function of SOC and cycle depth in Li ion cells was developed by Millner (Millner, 2010), and was validated using an $LiCoO_2$ cell. Lam and Bauer developed an empirical model to predict the cycling fade of an $LiFePO_4$ cell as a function of ambient temperature, average SOC, and depth of discharge. This empirical model was further expanded by Xu et al. (Xu, Oudalov and Ulbig, 2016), whom added a temperature and time dependent component to account for calendar aging, and applied this model in conjunction with a rainflow counting algorithm to estimate the capacity fade of a grid tied BESS providing EFR services. Wang et al. applied a rainflow counting algorithm to the SOC cycles of each BESS in (L. Wang *et al.*, 2015), then determined the degradation associated with each constituent cycle using a double exponential relationship suitable for the lead-acid batteries modelled.

To the author's knowledge, no optimal dispatch studies have incorporated rainflow analysis based degradation estimations into their objective functions, and optimal dispatch studies that consider degradation at all are uncommon (Y. Wang *et al.*, 2015; Fortenbacher, Mathieu and Andersson, 2017). Megel et al. considered provision of primary frequency control using a BESS connected to a typical Swiss LV network (Mégel, Mathieu and Andersson, 2015). Whilst BESS degradation was considered, this was via a fixed degradation penalty payable if an operation was expected to cause a BESS to reach an extreme SOC i.e. no attempt at determining degradation cost as a function of actual predicted degradation is made. Fortenbacher et al. (Fortenbacher, Andersson and Mathieu, 2015; Fortenbacher, Zellner and Andersson, 2016; Fortenbacher, Mathieu and Andersson, 2017) considered the cost of degradation during optimal operation for voltage and ampacity control, and in this instance the rate of degradation is approximated as a convex piecewise function of both BESS operating power and BESS SoC. However, because the capacity fade of Li ion cells is near independent of charge/discharge rate at realistic operating C-rates (Lam and Bauer, 2013; Xu, Oudalov and Ulbig, 2016), and heavily dependent on cycle depth (Millner, 2010; Lam and Bauer, 2013; Xu, Oudalov and Ulbig, 2016), that this type of degradation model would not be suited to studies concerning Li ion based BESSs.

2.3.3 Reactive Power Provision

As previously noted, the injection of lagging reactive power whilst a PV generator is exporting real power can reduce the voltage rise effect. As BESS and PV inverters with reactive power capabilities are becoming commercially available (Mercedes, 2014; Ranaweera and Midtgard, 2016; Tesla, 2016; CCL, 2017), the joint provision of real and reactive power for LV network violation management has become a sensible consideration in modelling studies. Whilst many studies did not consider the potential of RPC (Alam, Muttaqi and Sutanto, 2012; Liu *et al.*, 2012; Marra, Fawzy and Bulo, 2012; Bucher, Betcke and Andersson, 2013; Marra *et al.*, 2014; Bennett, Stewart and Lu, 2015; Lamberti *et al.*, 2015, 2017; Poulios, 2015; Petinrin and Shaaban, 2016), some also considered the provision of RPC using BESS inverters (K. H. Chua *et al.*, 2012; Fortenbacher, Andersson and Mathieu, 2015; L. Wang *et al.*, 2015; Fortenbacher, Zellner and Andersson, 2016; Fortenbacher, Mathieu and Andersson, 2017), PV inverters (Meghasai *et al.*, 2015), or both simultaneously (S. W. Alnaser and Ochoa, 2016). Reactive power provision was modelled either as entirely variable within a power factor range suitable for the inverter (Kein Huat Chua *et al.*, 2012; Fortenbacher, Andersson and Mathieu, 2015; Giannitrapani *et al.*, 2015; L. Wang *et al.*, 2015; Bucciarelli *et al.*, 2016;

Fortenbacher, Zellner and Andersson, 2016; Ranaweera and Midtgard, 2016; S. Alnaser and Ochoa, 2016; Fortenbacher, Mathieu and Andersson, 2017) (figure 2.17, bottom), or as a function of voltage at the inverter-grid coupling point (terminal voltage control) (Von Appen *et al.*, 2014; Santos-Martin *et al.*, 2015) (figure 2.17, top).

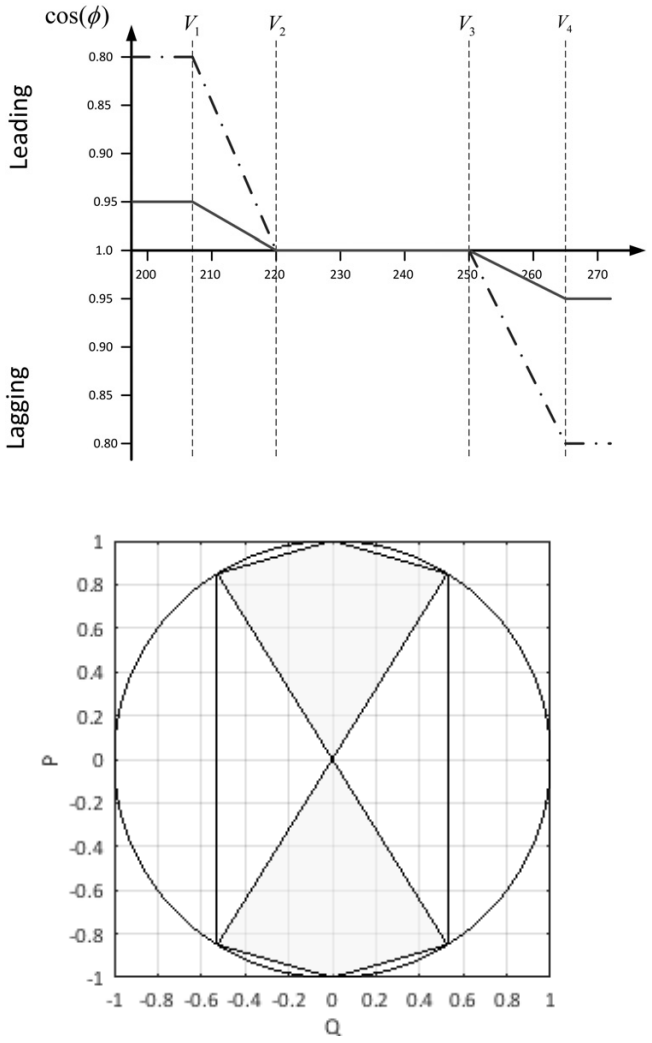

Figure 2.17 - (top) shows how inverter power factor may be varied with grid voltage in a terminal voltage control scheme for an inverter with minimum PF=0.95 (solid line) and minimum PF=0.80 (dashed line) (Santos-Martin *et al.*, 2015)*. (bottom) grey shaded area shows the allowed operating range for an inverter of rated power 1 KVA and minimum PF= 0.85 in variable reactive power mode.*

LV studies incorporating RPC into BESS schemes have noted slight increases in PV hosting capacity when compared to BESS active power only schemes (Von Appen *et al.*, 2014; Santos-

Martin *et al.*, 2015), though the effect is negligible if PF is limited to ≥0.95. Higher voltage studies have reported significant reductions in BESS active power and OLTC reliance with RPC incorporation (S. Alnaser and Ochoa, 2016); this is because the R/X ratio is much lower at higher voltages, and thus the sensitivity of voltage magnitude to reactive power injection is comparable to, or even greater than, the same measure for active power.

2.3.4 Storage Efficiency Losses

Storage placement and dispatch studies overwhelmingly favour the assumption of a fixed BESS efficiency (Weniger, Tjaden and Quaschning, 2013; Mokhtari, Nourbakhsh and Gosh, 2013; Crossland, Jones and Wade, 2014; Daud *et al.*, 2014; Lu *et al.*, 2014; Alam, Muttaqi and Sutanto, 2015; Foggia *et al.*, 2015; L. Wang *et al.*, 2015; S. Alnaser and Ochoa, 2016; Navarro-Espinosa and Ochoa, 2016; Petinrin and Shaaban, 2016; Procopiou, 2017), though sometimes this is unmentioned/ignored (Kashem and Ledwich, 2007; Ranaweera and Midtgard, 2016; Lamberti *et al.*, 2017), and occasionally variable efficiency (as a function of BESS power output) is considered (Von Appen *et al.*, 2014; Fortenbacher, Mathieu and Andersson, 2017). The strong favourability of fixed BESS efficiency is most likely a result of,

- There is never more than 1.5% difference between the variable and fixed model losses at any given system output power (where losses are considered as a proportion of the inverter rated output (figure 2.18)).
- The minimal improvements seen when switching to the variable model are accompanied by a significant increase in modelling complexity, with efficiency loss curves requiring computationally expensive special ordered set (SOS) type 2 mixed integer linear programming (MILP) piecewise approximations for integration into optimal dispatch problems (Fortenbacher, Andersson and Mathieu, 2015). The size of the network that can be examined is therefore limited due to the computational complexity of such constraints.

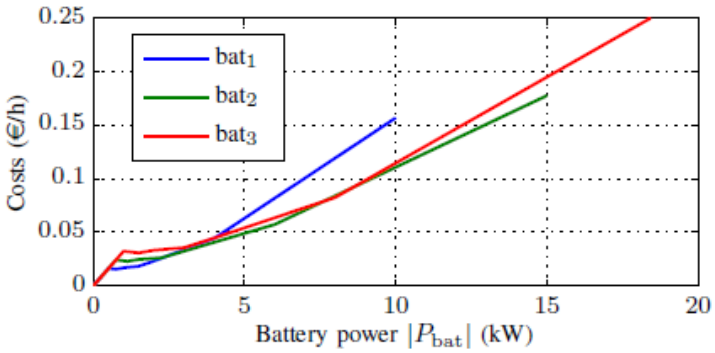

Figure 2.18 – cost of energy losses vs. battery charging/discharging power for 3 typical battery sets (Fortenbacher, Andersson and Mathieu, 2015).

2.3.5 Line Losses

Line losses are often neglected in renewables impact and BESS placement and control studies, as they are eclipsed by the importance of violation control. However, where they are considered in optimization formulations, losses relating to reactive power are often neglected (Giannitrapani *et al.*, 2015, 2016; Bucciarelli *et al.*, 2016), and when losses associated with transfer of both power types are considered their quadratic nature is linearly approximated (Fortenbacher, Andersson and Mathieu, 2015; Fortenbacher, Zellner and Andersson, 2016; Fortenbacher, Mathieu and Andersson, 2017). If the losses associated with a control strategy simply need to be monitored (i.e. not controlled), then actual losses can be determined from output of the power flow.

2.3.6 General considerations

Distribution network studies often do not specify the BESS chemistry, and instead opt for a general simplified BESS model (Crossland, 2014; Bennett, Stewart and Lu, 2015; Giannitrapani *et al.*, 2015; Lamberti *et al.*, 2015, 2017; Poulios, 2015; Bucciarelli *et al.*, 2016; Petinrin and Shaaban, 2016). However, those that do specify a chemistry always model either a general li ion system (Bucher, Betcke and Andersson, 2013; Von Appen *et al.*, 2014; Fortenbacher, Andersson and Mathieu, 2015; Fortenbacher, Zellner and Andersson, 2016; Fortenbacher, Mathieu and Andersson, 2017), or typical lead acid systems (K. H. Chua *et al.*, 2012; Alam, Muttaqi and Sutanto, 2015; L. Wang *et al.*, 2015). This is for reasons of low cost (L. Wang *et al.*, 2015) and ease of availability in the Lead Acid case, and high commercial availability, falling cost, long cycle life, and high efficiency in the case of li ion (Bucher, 2014; Santos-Martin *et al.*, 2015; Fortenbacher, Zellner and Andersson, 2016). Power and energy capacity limits are explained and justified in (Crossland, 2014; L. Wang *et al.*, 2015;

Procopiou, 2017), but more often there is no particular practical reason stated for chosen BESS energy capacity or inverter power limits in LV network studies. Aside from in (Lamberti *et al.*, 2015, 2017), it is assumed that BESS are located at all properties with PV arrays. Monte carlo simulation to overcome the problem of varying PV placement was considered only in (Lamberti *et al.*, 2017; Procopiou, 2017), and only one BESS study considered multiple networks (Giannitrapani *et al.*, 2016). There is therefore scope to develop models that consider practical and pragmatic BESS ownership, availability, and sizing constraints, so that the realistic potential for BESS based network management can be evaluated.

2.3.7 Power Flow methods

Power flow simulation engines are used in network impact and BESS placement, sizing and dispatch studies to calculate (at least) bus voltages and voltage angles from real and reactive power injects, where inject at a given bus is dependant residence demand, PV generation, and BESS inverter operation. Whilst authors may write simple power flow models for the above stated reason (Alam, Muttaqi and Sutanto, 2015; Bucciarelli *et al.*, 2016; Giannitrapani *et al.*, 2016; Fortenbacher, Mathieu and Andersson, 2017), it is becoming increasingly common to use commercially available models. Of the studies that used these, the majority used openDSS (Crossland, Jones and Wade, 2014; Hilton, 2015; L. Wang *et al.*, 2015; Lamberti *et al.*, 2015, 2017; Meghasai *et al.*, 2015; Long, Ochoa and Member, 2016; S. W. Alnaser and Ochoa, 2016). This is popular due to being open source, free to use, easy to interface, and capable of unbalanced power flow simulations.

2.3.8 Placement, sizing, and dispatch optimization methods

The non-convex placement and sizing problem is sometimes approached using global search algorithms (Ai *et al.*, 2014; Crossland, Jones and Wade, 2014; Petinrin and Shaaban, 2016), and otherwise approached with convex simplifications of the problem (Giannitrapani *et al.*, 2015, 2016; Bucciarelli *et al.*, 2016; Ranaweera and Midtgard, 2016), non-linear programming heuristics (S. W. Alnaser and Ochoa, 2016). Multiperiod optimization methods are often employed, such that the energy capacities of stores can be more accurately estimated (Bucciarelli *et al.*, 2016; Fortenbacher, Zellner and Andersson, 2016; Giannitrapani *et al.*, 2016; S. W. Alnaser and Ochoa, 2016). Otherwise, the location and sizing of BESSs is preassigned.

Most studies consider control and dispatch using simple algorithms e.g. (Alam, Muttaqi and Sutanto, 2012; Von Appen *et al.*, 2014; Bennett, Stewart and Lu, 2015; Lamberti *et al.*, 2015,

2017; Santos-Martin *et al.*, 2015). However optimal centralized control algorithms are considered by some authors (Ranaweera and Midtgard, 2016; S. W. Alnaser and Ochoa, 2016; Fortenbacher, Mathieu and Andersson, 2017), and use specialist optimization tools such as IBM CPLEX (Fortenbacher, Andersson and Mathieu, 2015; Fortenbacher, Mathieu and Andersson, 2017), CONOPT (S. W. Alnaser and Ochoa, 2016), IPOPT (Fortenbacher, 2016), and YALMIP (Fortenbacher, Mathieu and Andersson, 2017) to formulate and run the presented problems. Some studies that placement or real time optimization simplify the nonconvex non-linear AC OPF problem of calculating node voltages by approximating linear sensitivities of voltage to real and reactive power injects (Marra *et al.*, 2013, 2014; Bucher, 2014; Giannitrapani *et al.*, 2016; Ranaweera and Midtgard, 2016), and it is noted that this method can adequately approximate voltage changes regardless of the many influencing factors; this is because the phenomena is near linear within the voltage range that an LV network is typically operating within. This approach is suited to high temporal resolution, long term time series simulations as a result of the fast efficient optimization algorithms associated with LP solvers, and low failure rates.

2.3.9 Summary

The majority of network studies ignore BESS degradation, or use degradation models that do not reflect the actual degradation mechanisms of li ion cells, Efficiency is usually fixed, rather than variable with output power of the BESS, though the variable efficiency curve barely deviates from that which would be expected of a fixed (95%) efficiency system. Line losses are often considered, but are usually simplified to account fro only those arising from real power flow, if they are considered in an optimization formulation. Studies rarely consider 3Ø 4 wire unbalanced networks; LV networks are usually simplified to appear balanced, but this is not appropriate when considering such a small scale simulations.

2.4 Research gaps and aims

The research gaps identified from the available studies (and addressed in this thesis) are as follows:

- There is substantial scope to perform BESS studies on realistically sized LV feeders, as most studies consider networks of no greater than ≈30 residences, whilst the load count on a real UK feeder can exceed this by as much as 10 times (Navarro-Espinosa, no date).
- From the perspective that customers own the BESSs, there are no studies (known to the author) that examine situations in which less than 100% of PV array owners also own BESSs (excluding studies that examine one very specific technology placement configuration). In reality, if we were to take control of customer owned BESSs, we may need to consider the fact that not all PV owning customers will have a BESS, and therefore current studies are not sufficient in describing the technical feasibility of BESS control for violation management.
- From the perspective that DNOs/3rd parties own and operate the behind-the-meter BESSs, there has been little work to examine the value of improved customer self-consumption as a revenue stream that DNOs/3rd parties may recoup to offset initial capital investment. This should be examined, as it may be significant enough to ensure the economic feasibility of BESS based violation management.
- A direct comparison of BESS based active management costs to traditional reconductoring costs remains to be performed at the 230V network level from either of the ownership perspectives. This comparison was considered in one study (Crossland, Jones and Wade, 2014), but the varying reconductoring requirement with PV penetration level was not considered, creating a bias towards favouring BESS control at lower renewables penetrations. It is important that this assumption is eliminated to create a fair comparison between the costs of each reinforcement strategy.
- There is no previous work that quantifies the reliance of technical and economic feasibility of BESS based management for PV-caused violation control on network topology. Without this knowledge, it is impossible for the DNO/3rd party to determine the instances in which BESS based violation management may be feasible.

- The use of BESSs for the control of ASHP-caused ampacity and voltage violations has never (as far as the author is aware) been examined. It is possible that such management is useful and cost effective, and so should be examined.
- No previous work compares the technical and economic aspects of decentralized and centralized dispatch strategies.
- No previous work has combined realistic 3Ø 4 wire unbalanced network models with realistic BESS degradation considerations and full consideration of line losses. This is necessary as the discrepancies created by ignoring these factors could be significant enough to change the technical and economic feasibility of BESS based violation management.

The work in this thesis therefore aims to address all of these research gaps by answering the following research questions,

1. Are the costs associated with deploying behind-the-meter BESSs for the purpose of violation control comparable enough to the cost of reconductoring, such that BESS control could be considered as a means to delay reconductoring if necessary (chapters 5, 6 & 7)? How does cost vary when switching between a DNO/3rd party owned perspective (chapter 5) and a customer owned perspective (chapters 6 & 7)?
2. Are there technical barriers to the use of BESSs for violation control, when non-ideal BESS ownership and availability patterns occur (chapters 5 & 6)?
3. Is increased self-consumption a potential additional revenue in the instance that BESSs are controlling for violation control (chapter 5)?
4. Are BESS systems technically and economically suited to control of violations caused by ASHP systems (chapter 6)?
5. How does technical and economic feasibility of BESS based violation control vary with feeder topology (chapter 7)?
6. Does control algorithm complexity affect the technical suitability of BESSs to management of voltage and thermal violations on LV feeders (Chapters 6 & 7)?

3 Theory

The basic theory behind network voltage rise and power flow is summarized to allow the reader to appreciate the causes of steady state violations and the ways in which management strategies mitigate these problems.

3.1 Voltage rise with power inject

Any Injection of current onto a power network must be accompanied by a voltage rise, without which current cannot flow. Assuming a current, I_{inj}, is injected by a generator at node 2, and an equal current is consumed by a load at node 1, that the wire between nodes, is purely resistive with resistance R_{12}, and currents have no imaginary part, the voltage at node 2 may be calculated exactly as:

$$V_2 = I_{inj}R_{12} + V_1 \tag{3.1}$$

Where V_1 is the voltage at node 1.

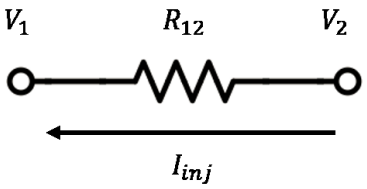

Figure 3.1 – Shows the cable represented in equation 3.1.

In reality, wires are both reactive and resistive, and therefore must be represented as complex impedances, $\boldsymbol{Z}_{12}$. Furthermore, residential loads are rarely purely resistive, and generators do not always inject at unity power factors, and so complex current injects, demands and flows must be considered. It follows that voltages must also be represented as complex quantities. Equation (3.2) therefore becomes,

$$\boldsymbol{V}_2 = \boldsymbol{I}_{inj}\boldsymbol{Z}_{12} + \boldsymbol{V}_1 \tag{3.2}$$

Where $\boldsymbol{Z}_{12}$ is the complex impedance of the wire between nodes 1 and 2, $\boldsymbol{I}_{inj}$ is the complex current flow, and $\boldsymbol{V}_1$ and $\boldsymbol{V}_2$ are the complex voltages at nodes 1 and 2 respectively.

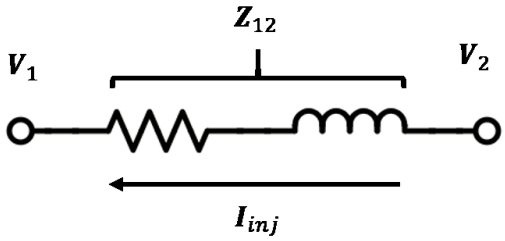

Figure 3.2 – Shows the wire represented in equation 3.2. The wire's resistance and inductive reactance are coupled in to one term, $\boldsymbol{Z}_{12}$.

As $\boldsymbol{V}_1$ is a complex number, the magnitude of the voltage (which is the actual voltage seen by any load at node 2), is simply the second order norm of $\boldsymbol{V}_1$,

$$|\boldsymbol{V}_1|_2 = \sqrt{Re(\boldsymbol{V}_1)^2 + Im(\boldsymbol{V}_1)^2} \tag{3.3}$$

Furthermore, if $\boldsymbol{V}_1$ and $\boldsymbol{V}_2$, are plotted on the complex coordinate plane, then the angle between the resulting vectors is the voltage phase difference between the buses, $\emptyset_{12}$.

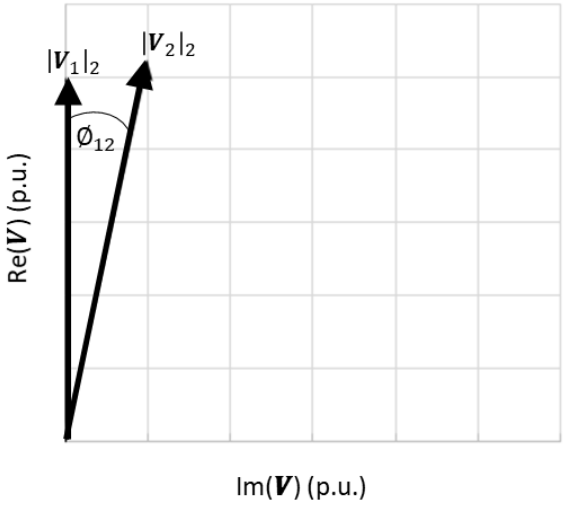

Figure 3.3 - The voltage magnitude, and the voltage angle between buses.

Complex power transfer from node 2 to node 1 is expressed as,

$$\boldsymbol{S} = \boldsymbol{V}_2 \boldsymbol{I}_{inj}{}^{*} \tag{3.4}$$

Where,

$$\boldsymbol{S} = P + jQ \tag{3.5}$$

Therefore, power inject must be accompanied with a voltage change, as to allow any flow of power to actually occur. With an increasing penetration of distributed PV generation on UK networks, it becomes increasingly likely that LV (230 V 1Ø, 400 V 3Ø) networks will experience voltage conditions that violate statutory regulations (Navarro-Espinosa and Ochoa, 2016). It is therefore important to consider the methods that may be used to limit LV network violations to within acceptable levels.

3.2 Determination of voltage at multiple nodes, and power flow studies

The above theory is useful only in the case of power flow between 2 buses via a single conductor. In reality, problems usually concern several buses, and the voltage rise at each node is usually considered with respect to the power inject at each node. The power inject at bus 1 (which is calculated as the discrepancy between the powers flowing into and out of the node) can be calculated exactly as function of all voltages on the network, and the admittances (reciprocals of impedances) between each other bus and bus 1

$$P - jQ = \boldsymbol{Y}_{11}\boldsymbol{V}_1\boldsymbol{V}_1{}^* + \boldsymbol{Y}_{12}\boldsymbol{V}_2\boldsymbol{V}_1{}^* + \cdots + \boldsymbol{Y}_{1n}\boldsymbol{V}_n\boldsymbol{V}_1{}^* \tag{3.6}$$

Which may be abbreviated to,

$$P - jQ = \sum_{k=1}^{n} \boldsymbol{Y}_{ik}\boldsymbol{V}_k\boldsymbol{V}_i{}^* \tag{3.7}$$

Where $\boldsymbol{Y}_{ik}$ is the admittances between buses i and k if $i \neq k$, and the sum of all admittances out of node i if $i = k$.

The same equation is very often expressed in polar form as,

$$P - jQ = |\boldsymbol{V}_i| \sum_{k=1}^{n} |\boldsymbol{Y}_{ik}||\boldsymbol{V}_k| \angle(\theta_{ik} + \emptyset_k - \emptyset_i) \tag{3.8}$$

And real and reactive power components can be extracted using,

$$P_i = |\boldsymbol{V}_i| \sum_{k=1}^{n} |\boldsymbol{Y}_{ik}||\boldsymbol{V}_k| \angle \cos(\theta_{ik} + \emptyset_k - \emptyset_i) \tag{3.9}$$

$$Q_i = |\boldsymbol{V}_i| \sum_{k=1}^{n} |\boldsymbol{Y}_{ik}||\boldsymbol{V}_k| \angle \sin(\theta_{ik} + \emptyset_k - \emptyset_i) \tag{3.10}$$

The equations are non-linear, and are often solved iteratively. This may be done for a balanced 3 phase system by (sensibly) guessing the voltages and voltage angles at each bus. Once a guess has been made, the mismatch between the true real and reactive power injects (P_i and Q_i, known quantities) and those calculated using the guess can be made using,

$$\Delta P_i = -P_i + |\boldsymbol{V}_i| \sum_{k=1}^{n} |\boldsymbol{Y}_{ik}||\boldsymbol{V}_k| \angle \cos(\theta_{ik} + \emptyset_k - \emptyset_i) \tag{3.11}$$

$$\Delta Q_i = -Q_i + |\boldsymbol{V}_i| \sum_{k=1}^{n} |\boldsymbol{Y}_{ik}||\boldsymbol{V}_k| \angle \sin(\theta_{ik} + \emptyset_k - \emptyset_i) \tag{3.12}$$

The partial differentials of mismatch at any given bus with respect to changes in voltage magnitudes and angles at all buses are then calculated. It is assumed that these differentials are independent of the network state i.e. they represent a linear approximation of equations (3.11) and (3.12). The linear approximation of the system may now be solved to calculate a

new set of bus voltage magnitudes and angles which cancel out power mismatches. The matrix representation of the linearized problem is,

$$-\begin{bmatrix} \Delta P_1 \\ \vdots \\ \Delta P_N \\ \Delta Q_1 \\ \vdots \\ \Delta Q_N \end{bmatrix} = \begin{bmatrix} \frac{\delta \Delta P_1}{\delta \emptyset_1} & \cdots & \frac{\delta \Delta P_1}{\delta \emptyset_N} & \frac{\delta \Delta P_1}{\delta |\boldsymbol{V}_1|} & \cdots & \frac{\delta \Delta P_1}{\delta |\boldsymbol{V}_N|} \\ \vdots & \ddots & \vdots & \vdots & \ddots & \vdots \\ \frac{\delta \Delta P_N}{\delta \emptyset_1} & \cdots & \frac{\delta \Delta P_N}{\delta \emptyset_N} & \frac{\delta \Delta P_N}{\delta |\boldsymbol{V}_1|} & \cdots & \frac{\delta \Delta P_N}{\delta |\boldsymbol{V}_N|} \\ \frac{\Delta Q_1}{\delta \emptyset_1} & \cdots & \frac{\Delta Q_N}{\delta \emptyset_N} & \frac{\Delta Q_1}{\delta |\boldsymbol{V}_1|} & \cdots & \frac{\mathrm{Q} P_N}{\delta |\boldsymbol{V}_N|} \\ \vdots & \ddots & \vdots & \vdots & \ddots & \vdots \\ \frac{\Delta Q_N}{\delta \emptyset_1} & \cdots & \frac{\Delta Q_N}{\delta \emptyset_N} & \frac{\Delta Q_N}{\delta |\boldsymbol{V}_1|} & \cdots & \frac{\mathrm{Q} P_N}{\delta |\boldsymbol{V}_N|} \end{bmatrix} \begin{bmatrix} \Delta \emptyset_1 \\ \vdots \\ \Delta \emptyset_N \\ \Delta |\boldsymbol{V}_1| \\ \vdots \\ \Delta |\boldsymbol{V}_N| \end{bmatrix} \tag{3.13}$$

Where $\Delta|\boldsymbol{V}_i|$ represents the required change in voltage at node I to ensure all ΔP values equal zero for the linearized system, $\Delta \emptyset_i$ represents the same for voltage angles, $\frac{\delta \Delta P_i}{\delta |\boldsymbol{V}_i|}$ is the linearized change in the power mismatch at node i with change in voltage at node i, and $\frac{\delta \Delta Q_i}{\delta |\boldsymbol{V}_i|}$, $\frac{\delta \Delta P_i}{\delta \emptyset_i}$, and $\frac{\delta \Delta Q_i}{\delta \emptyset_i}$ are similar partial differentials for reactive power and voltage angles.

The calculated magnitudes and angles may be used as the input 'guess' for the next iteration. Iterations continue until mismatches meet some convergence criteria, and at this point voltage magnitudes and angles considered solved.

In the case of unbalanced 3-phase power flow, the above methodology must be expanded upon to allow consideration of between-phase effects. There are multiple ways to solve unbalanced power flow problems. The specific method used in this thesis is implemented via the openDSS software operating in normal power flow mode.

3.3 OpenDSS unbalanced power flow method

The following section outlines the power flow method used by openDSS to solve unbalanced networks.

The current injection (sum of current flowing through/from loads/generators) at each bus is determined by dividing the required power injection by voltage (which is set to nominal voltage on the first iteration). Using the desired current injections and the admittance matrix (describing admittance between all non-power conversion elements) the node voltages for the solution/next iteration are determined by solving:

$$\begin{bmatrix} \boldsymbol{I}_{inj,1} \\ \vdots \\ \boldsymbol{I}_{inj,N} \end{bmatrix} = \begin{bmatrix} \boldsymbol{Y}_{11} & \cdots & \boldsymbol{Y}_{1N} \\ \vdots & \boldsymbol{Y}_{ik} & \vdots \\ \boldsymbol{Y}_{n_b 1} & \cdots & \boldsymbol{Y}_{NN} \end{bmatrix} \begin{bmatrix} \boldsymbol{V}_1 \\ \vdots \\ \boldsymbol{V}_N \end{bmatrix} \tag{3.14}$$

However, the change in voltage results in a change in current requirements for constant power injection at each node, and so the injection current is adjusted and the calculation repeats. This is repeated iteratively until voltage convergence of 0.0001 p.u. is achieved (Dugan, 2012). The overall process varies slightly for constant impedance (power demand at each iteration is adjusted for voltage, or the load is included in the admittance matrix) and constant current loads (current injection is not updated with voltage changes).

It should be noted that because the solver considers 3-phase unbalanced power flow, the voltage, current, and admittance entries in the above system are actually vectors and matrices that represent the values for each phase:

$$\boldsymbol{I}_{inj,i} = \begin{bmatrix} \boldsymbol{I}_{inj,i,1} \\ \vdots \\ \boldsymbol{I}_{inj,i,n_\emptyset} \end{bmatrix} \quad \boldsymbol{V}_i = \begin{bmatrix} \boldsymbol{V}_{i,1} \\ \vdots \\ \boldsymbol{V}_{i,n_\emptyset} \end{bmatrix} \quad \boldsymbol{Y}_{ik} = \begin{bmatrix} \boldsymbol{Y}_{ik,11} & \cdots & \boldsymbol{Y}_{ik,1n_\emptyset} \\ \vdots & \ddots & \vdots \\ \boldsymbol{Y}_{ik,n_\emptyset 1} & \cdots & \boldsymbol{Y}_{n_\emptyset n_\emptyset} \end{bmatrix} \tag{3.15}$$

Where diagonal elements of $\boldsymbol{Y}_{ik}$ represent mutual admittance between the same phases of buses i and k, and off diagonal elements represent admittance between non identical phases of buses i and k, which may be present as a result of inductive effects or neutral voltage changes. Furthermore, openDSS considers line elements using the pi-model, so that shunt capacitance to ground, and between phases is added to any value in the Y matrix that represents a self-admittance (i.e. all diagonal elements in 3.14). Because all values are complex, the solver takes advantage of the relationship,

$$\begin{bmatrix} re(\boldsymbol{C}) \\ im(\boldsymbol{C}) \end{bmatrix} = \begin{bmatrix} re(\boldsymbol{A}) & -im(\boldsymbol{A}) \\ im(\boldsymbol{A}) & re(\boldsymbol{A}) \end{bmatrix} \begin{bmatrix} re(\boldsymbol{B}) \\ im(\boldsymbol{B}) \end{bmatrix}, \quad \boldsymbol{A}, \boldsymbol{B}, \boldsymbol{C} \in \mathbb{C} \tag{3.16}$$

So that the system to be solved may be represented as,

$$\begin{bmatrix} re(\boldsymbol{I}_{inj,1}) \\ \vdots \\ re(\boldsymbol{I}_{inj,N}) \\ im(\boldsymbol{I}_{inj,1}) \\ \vdots \\ im(\boldsymbol{I}_{inj,N}) \end{bmatrix} = \begin{bmatrix} \boldsymbol{G}_{11} & \dots & \boldsymbol{G}_{1N} & -\boldsymbol{B}_{11} & \dots & -\boldsymbol{B}_{1N} \\ \vdots & \boldsymbol{G}_{ik} & \vdots & \vdots & -\boldsymbol{B}_{ik} & \vdots \\ \boldsymbol{G}_{N1} & \dots & \boldsymbol{G}_{NN} & -\boldsymbol{B}_{N1} & \dots & -\boldsymbol{B}_{NN} \\ \boldsymbol{B}_{11} & \dots & \boldsymbol{B}_{1N} & \boldsymbol{G}_{11} & \dots & \boldsymbol{G}_{1N} \\ \vdots & \boldsymbol{B}_{ik} & \vdots & \vdots & \boldsymbol{G}_{ik} & \vdots \\ \boldsymbol{B}_{N1} & \dots & \boldsymbol{B}_{NN} & \boldsymbol{G}_{N1} & \dots & \boldsymbol{G}_{NN} \end{bmatrix} \begin{bmatrix} re(\boldsymbol{V}_1) \\ \vdots \\ re(\boldsymbol{V}_N) \\ im(\boldsymbol{V}_1) \\ \vdots \\ im(\boldsymbol{V}_N) \end{bmatrix} \tag{3.17}$$

Whilst OpenDSS can model each power conversion element as a hybrid of a constant admittance and a varying current source, power flow studies ignore this admittance and consider only the current source injection (Dugan, 2012). Other constraints would be required for generators operating in P-V mode, however all rooftop arrays in this work are modelled as P-Q generators.

3.4 Network ampacity

The current magnitude at a given point on a cable can be calculated exactly from the total apparent power and the voltage magnitude at that point on the cable,

$$|\boldsymbol{I}| = \frac{|\boldsymbol{S}|}{|\boldsymbol{V}^*|} \tag{3.18}$$

Power cables are assigned a maximum operating ampacity, above which it becomes possible to raise the temperature to a level that causes the conductor and sheathing to degrade. This limit may vary seasonally (as the ability of the cable to dissipate heat to its surrounds is somewhat dependent on ambient temperature) and on location (a cable in free air is typically able to carry a higher current than the same cable located in an underground duct (AEI, 2014)).

3.5 Effects of network management strategies on violations

Considering the aforementioned theory, management strategies can be used to mitigate violations in the following ways.

- Reconductoring: Larger diameter cables may have larger ampacities and lower impedances, and so networks can handle greater generated currents without congestion, and transmit power with lower associated voltage rises i.e. if network impedances half, voltage rises associated with power transfer will approximately half also.

- BESS systems: BESSs can absorb power to prevent currents from ever being transmitted along the network conductors, therefore decreasing voltage rises and congestion associated with transmitting excessive currents. BESSs can discharge at high demand to reduce voltage drops on the network.
- OLTCs: OLTCs installed on an SSS allow automatic adjustment of the voltage on the entire network, so whilst voltage changes between buses on the secondary network may be almost the same at any OLTC setting, the absolute voltages may be reduced/raised so that the full network falls within acceptable limits. OLTCs are of very little use for ampacity management, although operating at higher tap positions will result in slightly lower currents.
- Curtailment: Inject of current is directly avoided, and subsequently so is any violation associated with current inject.
- RPC: Increasing reactive power demand at a given node reduces the node voltage magnitude, so can be used (to some extent) to counteract voltage rise due to real power inject. This operation slightly increases the total magnitude of total apparent power demand at the node in question and thus also the current magnitude, thus slightly increasing the maximum ampacity the network must handle.

4 Applied modelling practices

Whilst each of the presented studies involve the use of unique methods, the general modelling practices used throughout this work do not change. These general modelling practices are summarized in section 4.1. The novel placement, sizing and control algorithms are presented in section 4.2.

4.1 Choice of established practices

4.1.1 Generation and demand modelling

In this work, whenever generation time series data is required, 1 min resolution satellite derived irradiance data is converted to generation data. This methodology is chosen because:

- Satellite derived irradiance data can be obtained at a temporal resolution of 1 min over very long time periods (>1 year), and can be obtained for the location in question. This allows determination of long term economic benefits that cannot be inferred from single day/week simulations. The most temporally granular real data set accessible and permitted for use in this work contains data recorded at 2 min resolution, which is slightly below the minimum desirable resolution (about 1 min for steady state simulations according to (Lave, Reno and Broderick, 2015)).
- Recent studies have shown that satellite derived data, determined at the geographical point of the simulation, provides a better representation of irradiance than ground recorded data measured a short distance (≈10 km) away (Ruf *et al.*, 2016). Though a perfect representation of the actual irradiance is not essential in such long term steady state studies, it is good practice to use the most accurate data possible.

The studied feeders and networks cover small areas, and so the assumption that all rooftop PV systems experience exactly the same irradiance profiles is made. Whilst a few of the feeders studied in chapter 7 are technically large enough to be better represented by multiple irradiance profiles, these are only considered on clear sky days, and so all generation profiles are equal to maximum. Irradiance is converted to generation power using a simple regression model (King, Kratochvil and Boyson, 2004).

Where required, demand profiles are generated using the CREST model (McKenna and Thomson, 2016), because:

- A comparison of monitored feeder consumption to CREST predicted consumption showed a typical demand over prediction of 7 - 10%. This was determined by researchers at the University of Manchester, who, using feeder models (identical to those used in this thesis) and monitoring data, showed that the use of CREST profiles in the place of real demand data did not significantly affect the voltage and power profiles of the feeders in question. Therefore, the CREST model is considered acceptable for the set of feeder models used in this thesis.
- The model is able to generate data at 1 min resolution, which is essential to this thesis.
- The functionality of the model allows generation of demand profiles with annual duration.

Specific strategies used to apply the CREST model to each study are detailed in chapters 5, 6 and 7.

4.1.2 Reactive power control modelling

Reactive power provision from BESS inverters is modelled as entirely variable within an allowed power factor range where centralized control is concerned. This is because

- Although previous work suggests that RPC on LV networks is relatively ineffective for voltage control, the variable RPC model is very easy to implement in the centralized scheme, and modern BESS inverters used with commercially available BESSs are technically able to provide reactive power in this way (Tesla, 2016).
- The reactive power capabilities can be used to minimize line losses associated with the current magnitude increases associated with reactive power distribution.

4.1.3 Store efficiency and line loss modelling

Each BESS is modelled with a fixed charging and discharging efficiency of 0.95. This choice is made to avoid the significant increase in computational intensity that results from modelling the non-convex efficiency profiles, considering how little difference this makes to the accuracy of the modelling methodology (see section 2.3.4).

Whilst line losses are not a focus of this work, a consideration of such losses is included in the dispatch optimization problem to prevent any set of BESS inverters from operating in

ways that create more line losses than necessary; without this consideration it was found that inverters at neighbouring properties connected to the same service cables may trade equal and opposite amounts of reactive power for no reason, and random reactive power operation was occasionally seen at times of acceptable voltage. The piecewise linear approximations of real and reactive power transmission losses (presented in (Fortenbacher, Mathieu and Andersson, 2017)) were used (more details in section 4.2.4.3.2.4), as these were relatively easy to implement and solve, and resulted in the required effect. For post-simulation analysis of line losses, the real values were extracted from openDSS.

4.1.4 Optimization methods

IBM CPLEX is used to solve all optimization problems because:

- It is able to solve MILP problems, and MIQCP, allowing effective placement and sizing algorithms that consider integer placement costs and non-linear ampacity constraints to be developed.
- It is able to interface with MATLAB through a COM interface. MATLAB can therefore be used to handle central logic and communicate information between openDSS and the optimizer. Whilst the same was true with other optimizers, it was found that CPLEXs COM interface exhibited greater stability than most others.
- It exhibits an extremely high solve rate when compared to alternative options (typical LP problems were found to solve 3x faster with CPLEX than in any other readily available optimizer, and 10x faster than in any MATLAB solver). This allows thorough Monte Carlo simulations, and extensive time series simulations to be performed throughout the work.

4.1.5 Power flow solutions

openDSS is used to solve power flow problems because

- It is much more convenient than programming a solver manually.
- It is able to operate using 1 min resolution, which is the simulation time step for all dispatch algorithms.
- The iterative injection current based method the solver employs to solve power flow problems is extremely fast (typically <0.005s per solve) in time series simulations, as it is able to use the solution of the previous time step as a starting point for the next time step. The solver therefore allows longer time series to run without excessive computation time.

- The solver is able to deal with unbalanced power flow problems.
- It can interface with MATLAB through a COM interface, allowing the user to write code that flexibly assigns/removes network elements. Therefore, the user may rapidly assign different technology ownership patterns to networks, or switch networks altogether.

4.1.6 Other modelling considerations

All electrical energy stores (EESs) are modelled as Li-ion BESSs. In Chapter 5, these BESSs are modelled with degradation properties and reactive power capabilities expected for typical home battery systems such as the Tesla Powerwall 2 (but variable power and energy capacity), and in later chapters all BESSs are modelled with exact energy capacity, power capacity, reactive power capability, and degradation properties of Tesla systems. These choices are made because:

- Home BESS systems are the only type of EESs that could be deployed at residences immediately and in great quantities.
- They have cycle lives that suit them to perform tasks for many years without replacement, and have predictable and reliable available capacity-discharge rate behaviour (i.e. Peukerts law does not need to be considered for Li-ion systems).
- BESS systems have suitable energy to power capacity ratios for steady state voltage and ampacity control, and are not geographically constrained.
- In chapter 5, DNO/3rd party BESS ownership is assumed, and therefore some freedom in BESS sizing decisions is expected.
- In later chapters, resident ownership is assumed, and therefore the system capacity is restricted to that of easily available home BESS systems. Tesla Powerwall 2 capacity is assumed, because Tesla systems are becoming increasingly popular and are readily available to the consumer.

In all studies, residences are only be assigned/own a BESS if they also own a PV array, this is because,

- In chapter 5, self-consumption is investigated as a revenue stream in the DNO/3rd party owned case, and installation of BESSs at sites without generators interferes with this investigation.
- In customer owned BESS studies (in chapters 6 and 7) there is no practical sense in a residence purchasing and installing a BESS without a generator to interact with, as

no residential level revenue streams, other than increased self-consumption of generation, exist in the UK yet.

For all the studies presented, instead of choosing fixed BESS, ASHP and PV array placements, results are obtained for multiple placements using Monte-Carlo methodology (specific details of Monte Carlo methodologies for each study are found in their respective chapters), where the number of placements examined is equal to that required to ensure convergence. Therefore, outputs often take the form of statistical distributions or probabilities, and it is believed that this is appropriate for the work performed, as:

- The specific placement and power rating of a set of PV systems heavily effects the resulting voltage profile (fig 4.1), and thus the amount of BESS capacity required to mitigate rises. As no-one knows exactly which customers will install BESS/ASHP/PV technologies, simulating just one/a few placements does not necessarily tell us what is likely to happen under different technology penetrations. It is more appropriate to simulate multiple placements and determine quantities such as average and standard deviation of required BESS costs, and likelihood that the violations caused by a randomly selected placement configuration can be controlled using BESSs.
- It is not possible to simulate every possible technology placement at every penetration level (there are 5.16×10^{18} ways to assign equally sized rooftop PV arrays to a feeder serving 75 residences with a PV penetration of 70%, and this ignores the variation in PV array size and availability of customer owned BESSs that are also often considered in this thesis). However, preliminary work showed that in most scenarios results converge after simulation of < 30 random placements and always converge within < 50.

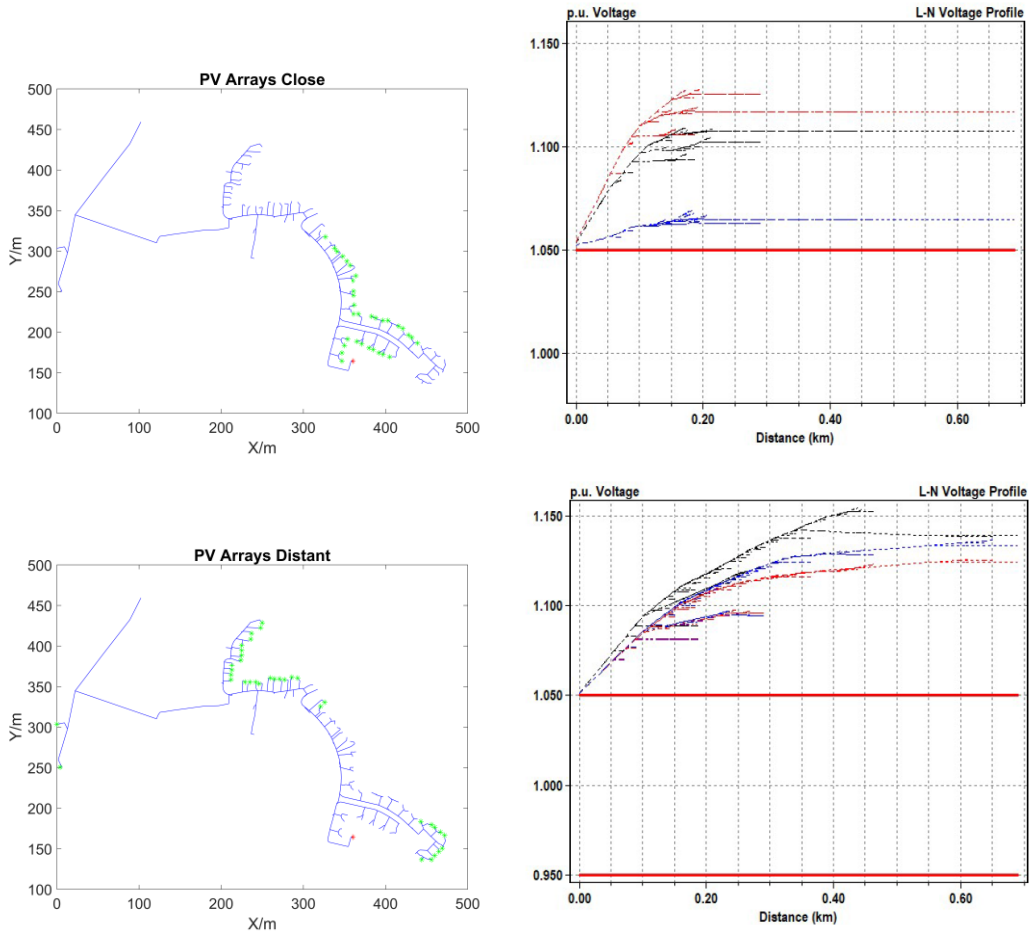

Figure 4.1 – The topology of a feeder serving 75 residences with a PV penetration of 45%, where the location of each of the PV arrays is marked with a green star. The top and bottom figures show the same feeder but with different PV locations, and each topology map is accompanied by the voltage profile produced if all PV arrays generate at rated capacity. Distance refers to distance from the SSS.

4.2 Applied optimization formulations and control algorithms

The studies described in this thesis utilize a series of novel optimal BESS placement and operation algorithms, and optimal reconductoring formulations, to calculate the minimum cost solutions to voltage and ampacity violations on LV feeders under different generation and demand scenarios. These optimization formulations can be split into 4 distinct categories:

- DNO/3rd party owned BESS placement and sizing
- Customer owned BESS takeover
- Reconductoring
- BESS operational algorithms

The categories, and the algorithms they encompass, are explained herein.

4.2.1 DNO/3rd party owned BESS placement and sizing

This category concerns formulations that are used to determine the minimum cost to a DNO/3rd party of purchasing and installing BESSs behind-the-meter at customer properties, whilst ensuring enough capacity is present to prevent any possible voltage or ampacity violations that would otherwise be caused by PV generation. The category concerns only one algorithm.

BESSs are placed using a multi-period mixed-integer linear programming (MILP) formulation. This aims to minimize the total cost of system installation, where the total cost is determined by multiplying the total number of BESSs placed $\boldsymbol{J}_{n_l,1}^T \boldsymbol{X^s}$ by the unit installation cost c_X, the total installed energy capacity $\boldsymbol{J}_{n_l,1}^T \boldsymbol{E^s}$ by the per kWh cost c_E, and the total installed inverter power capacity $\boldsymbol{J}_{n_l,1}^T \boldsymbol{S^{inv}}$ by the per kW cost c_S, then summating the results. The MILP formulation is applied to a 14 hour clear sky summer generation profile at 1 hour intervals, and therefore the charging power of any given BESS can take multiple different values throughout the day.

$$\min_{(\boldsymbol{X^s},\boldsymbol{S^{inv}},\boldsymbol{E^s})\in\mathbb{R}^{n_l,1}} c_X \boldsymbol{J}_{n_l,1}^T \boldsymbol{X^s} + c_S \boldsymbol{J}_{n_l,1}^T \boldsymbol{S^{inv}} + c_E \boldsymbol{J}_{n_l,1}^T \boldsymbol{E^s} \tag{4.1}$$

This allows determination of the best case placement scenario, and thus determine whether further work considering non-optimal ownership and availability patterns may be of value.

The formulation is subject to various constraints – constraint (4.2) predicts the change in end of line voltages for each phase of every monitored end point as a function of real power charging and reactive power injections by BESSs, $\boldsymbol{B_{VP}P_t^S} + \boldsymbol{B_{VQ}Q_t^S}$, and ensures that the predicted change is at least as negative as that required to bring voltage below the maximum limit (253 V), $\boldsymbol{V_{max}} - \boldsymbol{V_t^{End}}$. For example, voltage is monitored at the end of 4 feeder branches ($n_E = 4$) for the feeder shown in shown in fig. 4.2, as this is found to be the minimum required to ensure voltage control at all other customer nodes. It should be noted that whilst all customer voltages are considered in the results, control is based on readings at monitoring points only.

$$\boldsymbol{B_{VP}P_t^S} + \boldsymbol{B_{VQ}Q_t^S} \leq \boldsymbol{V_{max}} - \boldsymbol{V_t^{End}} \tag{4.2}$$

Where,

$$\boldsymbol{B_{VP}} = \begin{bmatrix} \frac{\partial V_{1,1}}{\partial P_1^S} & \cdots & \frac{\partial V_{1,1}}{\partial P_{n_l}^S} \\ \vdots & \ddots & \vdots \\ \frac{\partial V_{n_E,3}}{\partial P_1^S} & \cdots & \frac{\partial V_{n_E,3}}{\partial P_{n_l}^S} \end{bmatrix} \quad , \quad \boldsymbol{B_{VQ}} = \begin{bmatrix} \frac{\partial V_{1,1}}{\partial Q_1^S} & \cdots & \frac{\partial V_{1,1}}{\partial Q_{n_l}^S} \\ \vdots & \ddots & \vdots \\ \frac{\partial V_{n_E,3}}{\partial Q_1^S} & \cdots & \frac{\partial V_{n_E,3}}{\partial Q_{n_l}^S} \end{bmatrix}$$

The constraint uses linearized sensitivities of voltage to real and reactive power injects to predict end of line voltage changes with BESS operation, and these are stored in the sensitivity matrices $\boldsymbol{B_{VP}}$ and $\boldsymbol{B_{VQ}}$. Constructing the sensitivity matrices for specific network states is time consuming, and the actual element values of the sensitivity matrices vary only slightly across the range of network states encountered during modelling (not more than 5%), so values are determined at zero generation and apply this matrix in all circumstances. The maximum error observed between predicted and actual voltages from one iteration of the MILP formulation with the sensitivity matrix method was 1.3 V. To further reduce the sizing and placement errors resulting from the linear approximations, the model iterates until convergence of network maximum voltage and feeder head utilizations. This typically requires 2-3 iterations. The constraint must be satisfied at each hourly interval, and therefore $\boldsymbol{V_t^{End}}$, varies with time.

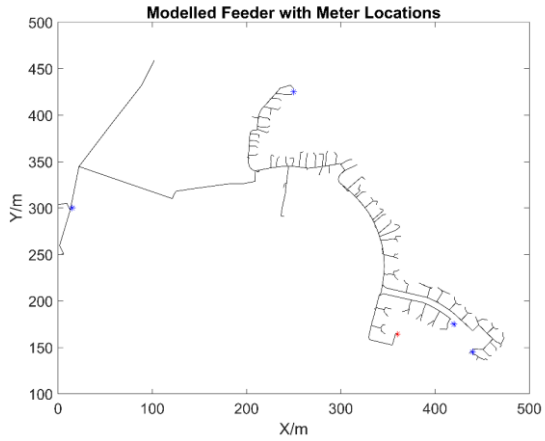

Figure 4.2 – Shows an example of a 75 residence feeder model, with the location of the feeder head monitor shown in red, and the voltage monitors shown in blue.

Constraints (4.3 - 4.8) are a hexagonal representation of the inverter capacity limit constraint $\sqrt{P_i^{s2} + Q_i^{s2}} \leq S_i^{inv}$ (see fig. 4.3), and ensure that all BESS inverters are assigned a total apparent power capacity $\boldsymbol{S}^{inv}$ great enough to accommodate the real and reactive power demands, $\boldsymbol{P}_t^s$ and $\boldsymbol{Q}_t^s$, of their respective BESSs at all hourly time intervals. As in (Fortenbacher, Mathieu and Andersson, 2017), this linear representation is used to avoid the introduction of difficult to solve quadratic constraints that barely affect the result of the formulation (system cost difference was always ≈0% where quadratic constraints were replaced with linear alternatives). The numbers 0.285 and 0.527 are empirically determined factors that allow construction of hexagonal constraints suitable for an inverter that may operate at power factors between 0.85 and 1, which is typical of modern home BESS inverters (Tesla, 2016; CCL, 2017). Constraint (4.9) limits the inverter to this power factor range.

$$\boldsymbol{P}_t^s + 0.285\boldsymbol{Q}_t^s \leq \boldsymbol{S}^{inv} \quad , \quad \boldsymbol{P}_t^s - 0.285\boldsymbol{Q}_t^s \leq \boldsymbol{S}^{inv} \quad , \quad -\boldsymbol{P}_t^s + 0.285\boldsymbol{Q}_t^s \leq \boldsymbol{S}^{inv}$$
$$-\boldsymbol{P}_t^s - 0.285\boldsymbol{Q}_t^s \leq \boldsymbol{S}^{inv} \quad , \quad \boldsymbol{Q}_t^s \leq 0.527\boldsymbol{S}_i^{inv} \quad , \quad -\boldsymbol{Q}_t^s \leq 0.527\boldsymbol{S}^{inv} \qquad (4.3 - 4.8)$$
$$|\boldsymbol{Q}_t^s| \leq \gamma|\boldsymbol{P}_t^s| \qquad (4.9)$$

Where,

$\gamma = \sqrt{1 - 0.85^2}$

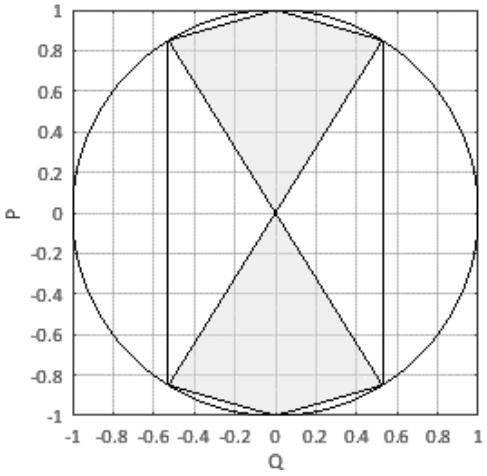

Figure 4.3 – Shows the allowed operating region (shaded grey) of an inverter capable of the PF range 0.85 - 1. The hexagonal constraints (4.3-4.8) represent the hexagon within the $\sqrt{{P_{i,t}^s}^2 + {Q_{i,t}^s}^2} \leq S_i^{inv}$ *circle, and the diagonal lines represent the PF constraint (4.9).*

The MILP formulation utilizes an octagonal representation of the feeder head ampacity limit constraint $\boldsymbol{I}^{Head} \leq \boldsymbol{I}_{max}^{Head}$ which states that the current magnitude across any phase measured at the feeder head must remain within the ampacity limit of that phase. For any given phase, this is achieved by taking the sum of all real power contributions (real power transfer at the feeder head on the chosen phase, plus any BESS operation) and the sum of all reactive power contributions, dividing each by the feeder head voltage to obtain $re(I)_{h,\emptyset}$ and $im(I)_{h,\emptyset}$, and ensuring the coordinate described by this pair of values does not fall outside of the area described by the octagonal constraints (see fig. 4.4). The equations representing an octagonal approximation of feeder head ampacity limit are,

$$-\alpha \boldsymbol{V}_t^{Head} \boldsymbol{B}_{HP} \boldsymbol{P}_t^s + \boldsymbol{V}_t^{Head} \boldsymbol{B}_{HQ} \boldsymbol{Q}_t^s \leq \alpha \boldsymbol{V}_t^{Head} \circ \boldsymbol{P}_t^{Head} - \boldsymbol{V}_t^{Head} \circ \boldsymbol{Q}_t^{Head} + \boldsymbol{I}_{max}^{Head}$$

$$\alpha \boldsymbol{V}_t^{Head} \boldsymbol{B}_{HP} \boldsymbol{P}_t^s + \boldsymbol{V}_t^{Head} \boldsymbol{B}_{HQ} \boldsymbol{Q}_t^s \leq -\alpha \boldsymbol{V}_t^{Head} \circ \boldsymbol{P}_t^{Head} - \boldsymbol{V}_t^{Head} \circ \boldsymbol{Q}_t^{Head} + \boldsymbol{I}_{max}^{Head}$$

$$-\alpha \boldsymbol{V}_t^{Head} \boldsymbol{B}_{HP} \boldsymbol{P}_t^s + \boldsymbol{V}_t^{Head} \boldsymbol{B}_{HQ} \boldsymbol{Q}_t^s \geq \alpha \boldsymbol{V}_t^{Head} \circ \boldsymbol{P}_t^{Head} - \boldsymbol{V}_t^{Head} \circ \boldsymbol{Q}_t^{Head} - \boldsymbol{I}_{max}^{Head}$$

$$\alpha \boldsymbol{V}_t^{Head} \boldsymbol{B}_{HP} \boldsymbol{P}_t^s + \boldsymbol{V}_t^{Head} \boldsymbol{B}_{HQ} \boldsymbol{Q}_t^s \geq -\alpha \boldsymbol{V}_t^{Head} \circ \boldsymbol{P}_t^{Head} - \boldsymbol{V}_t^{Head} \circ \boldsymbol{Q}_t^{Head} - \boldsymbol{I}_{max}^{Head}$$

$$-\beta \boldsymbol{V}_t^{Head} \boldsymbol{B}_{HP} \boldsymbol{P}_t^s + \boldsymbol{V}_t^{Head} \boldsymbol{B}_{HQ} \boldsymbol{Q}_t^s \leq \beta \boldsymbol{V}_t^{Head} \circ \boldsymbol{P}_t^{Head} - \boldsymbol{V}_t^{Head} \circ \boldsymbol{Q}_t^{Head} + \beta \boldsymbol{I}_{max}^{Head}$$

$$\beta \boldsymbol{V}_t^{Head} \boldsymbol{B}_{HP} \boldsymbol{P}_t^s + \boldsymbol{V}_t^{Head} \boldsymbol{B}_{HQ} \boldsymbol{Q}_t^s \leq -\beta \boldsymbol{V}_t^{Head} \circ \boldsymbol{P}_t^{Head} - \boldsymbol{V}_t^{Head} \circ \boldsymbol{Q}_t^{Head} + \beta \boldsymbol{I}_{max}^{Head}$$

$$-\beta \boldsymbol{V}_t^{Head} \boldsymbol{B}_{HP} \boldsymbol{P}_t^s + \boldsymbol{V}_t^{Head} \boldsymbol{B}_{HQ} \boldsymbol{Q}_t^s \geq \beta \boldsymbol{V}_t^{Head} \circ \boldsymbol{P}_t^{Head} - \boldsymbol{V}_t^{Head} \circ \boldsymbol{Q}_t^{Head} - \beta \boldsymbol{I}_{max}^{Head}$$

$$\beta \boldsymbol{V}_t^{Head} \boldsymbol{B}_{HP} \boldsymbol{P}_t^s + \boldsymbol{V}_t^{Head} \boldsymbol{B}_{HQ} \boldsymbol{Q}_t^s \geq -\beta \boldsymbol{V}_t^{Head} \circ \boldsymbol{P}_t^{Head} - \boldsymbol{V}_t^{Head} \circ \boldsymbol{Q}_t^{Head} - \beta \boldsymbol{I}_{max}^{Head} \qquad (4.10 - 4.17)$$

Where,

$$\alpha = \frac{1-\cos\frac{\pi}{4}}{\cos\frac{\pi}{4}} \quad , \quad \beta = \frac{\cos\frac{\pi}{4}}{1-\cos\frac{\pi}{4}}$$

$$\boldsymbol{B}_{HP} = \begin{bmatrix} \frac{\partial P_1^{Head}}{\partial P_1^S} & \cdots & \frac{\partial P_1^{Head}}{\partial P_{n_l}^S} \\ \vdots & \ddots & \vdots \\ \frac{\partial P_{n_\emptyset}^{Head}}{\partial P_1^S} & \cdots & \frac{\partial P_{n_\emptyset}^{Head}}{\partial P_{n_l}^S} \end{bmatrix} \quad , \quad \boldsymbol{B}_{HQ} = \begin{bmatrix} \frac{\partial Q_1^{Head}}{\partial Q_1^S} & \cdots & \frac{\partial Q_1^{Head}}{\partial Q_{n_l}^S} \\ \vdots & \ddots & \vdots \\ \frac{\partial Q_{n_\emptyset}^{Head}}{\partial Q_1^S} & \cdots & \frac{\partial Q_{n_\emptyset}^{Head}}{\partial Q_{n_l}^S} \end{bmatrix}$$

Where element i, j of the matrices $\boldsymbol{B}_{HP}$ and $\boldsymbol{B}_{HQ}$ equal 1 if P_j^S is downstram from P_i^{Head} (i.e. the BESS is coupled to phase j). In the case that a feeder is particularly thermally congested, the octagonal representation can be replaced with a true ampacity constraint, though this is significantly slower, as doing requires the use an MIQCP solver. Furthermore, similar constraints can easily be added to represent branch ampacity limits, if it is found that congestion issues occur at locations other than the feeder head.

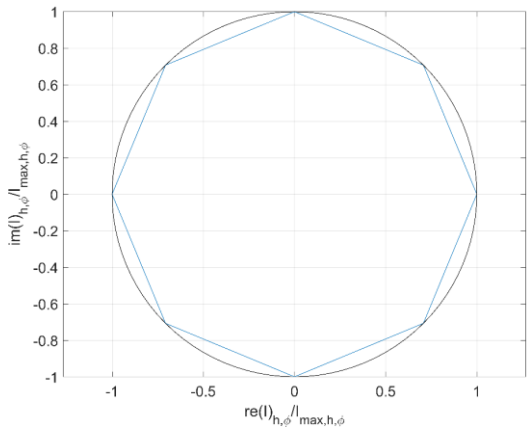

Figure. 4.4 – Shows the actual ampacity constraint on a power line with ampacity limit 1 A, and how the octagonal constraints are used to approximate this limit. $re(I)_{h,\emptyset}$ Represents the component of current that is in phase with voltage, and $im(I)_{h,\emptyset}$ represents the 90° out of phase component.

Each element of the vector that describes the required usable energy capacity of each BESS, $\boldsymbol{E^S}$, is equal to the sum of all charging events during the day for a given BESS e.g. element 1 of $\boldsymbol{E^S}$ is equal to the sum of charging events at residence 1, corrected for a charging efficiency $\eta_{eff} = 0.95$ (see section 4.1.3. for justification).

BESS inverter capacities may not exceed the power capacities of the PV arrays that are located at the same residence. This is necessary to prevent BESSs from being assigned to residences that do not own a PV array, and to ensure that BESSs do not import power from the grid (i.e. they only limit the power export from the PV array they are associated with). The energy/power capacity ratio is restricted to 2 to 1 (i.e. the BESS must have an energy capacity at least 2 times greater than its inverter power capacity), so that the BESS never operates above 0.5 C, which is in line with typical modern residential BESSs with Li-ion chemistries (Mercedes, 2014; Tesla, 2016). Furthermore, BESSs are limited to charging only (because only voltage reduction is considered, and the generation profile is symmetrical, meaning that no opportunities to discharge will arise between charging events).

The BESS existence variables for each residence, stored in $\boldsymbol{X^S}$, are declared as binary, and vector elements equal 1 on existence of any power or energy capacity e.g. if any BESSs capacity exists at residence '1', then element 1 of $\boldsymbol{X^S}$, changes from 0 to 1.

A realistic typical minimum load demand of 0.160 kW (the typical diversified minimum summer demand produced by the CREST model) is applied to all residences during use of this model.

4.2.2 Customer owned BESS takeover

This category concerns formulations that are used to determine the minimum cost to a DNO/3rd party of taking control of BESSs that are already owned by customers, whilst ensuring enough capacity is present to prevent any possible voltage or ampacity violations that would otherwise be caused by PV generation (and in one case, violations caused by ASHP demand). In this thesis, a 'takeover' is an event in which the DNO/3rd party pays a resident a set fee to use their BESS for network constraint management.

4.2.2.1 Centralized dispatch based BESS takeover

BESSs are taken over under the assumption that feeder end voltages, line utilizations, and customer BESS operation can be remotely monitored by a central controller, and the optimum set points for utilization and voltage control may then be calculated and communicated by the controller (using a control algorithm such as that presented in section 4.2.4.3). This method requires monitoring and communication infrastructure that would not be required in a decentralized control scheme (e.g. Feed In-Limiting), but it is important to consider whether such a method could reduce the quantity of BESSs required for network management (in comparison to the FIL method), and increase the range of scenarios in which

BESSs could provide adequate network control. Furthermore, the reliance on voltage as an input variable may affect the scalability of the scheme, as control of BESSs on different SSS's may somewhat affect voltage conditions on the current network, resulting in oscillatory behaviour, and customer's BESSs do not necessarily experience the same operational pattern, resulting in variable self-consumption and BESS degradation.

The algorithm takes the form of a multiperiod mixed-integer quadratically constrained programming (MIQCP) problem with the objective of minimising the number of customer BESSs that the DNO/3rd party must take control of,

$$\min_{(\boldsymbol{X}^S)\in\mathbb{R}^{n_l,1}} \boldsymbol{J}_{n_l,1}^T \boldsymbol{X}^S \tag{4.18}$$

The minimization is subject to numerous network and BESS constraints. Constraint (4.19) ensures voltage remains below the 253 V limit. The term $\boldsymbol{B}_{VP}\boldsymbol{P}_t^S + \boldsymbol{B}_{VQ}\boldsymbol{Q}_t^S$ calculates the change in voltage at each feeder end point with change in BESS real and reactive powers, and $\boldsymbol{V_{max}} - \boldsymbol{V_t^{End}}$ is voltage change required to bring the network voltage below the upper statutory limit. As in section 4.2.1, the linearized sensitivities of voltage magnitude to real and reactive power injects are used to predict end of line voltage changes with BESS operation, and are stored in the sensitivity matrices $\boldsymbol{B}_{VP}$ and $\boldsymbol{B}_{VQ}$.

$$\boldsymbol{B}_{VP}\boldsymbol{P}_t^S + \boldsymbol{B}_{VQ}\boldsymbol{Q}_t^S \leq \boldsymbol{V_{max}} - \boldsymbol{V_t^{End}} \tag{4.19}$$

Constraint (4.20) prevents line ampacity from exceeding the limit at monitored points, which are chosen based on potential for congestion. The term $\boldsymbol{P_t^{Line}} \oslash \boldsymbol{V_t^{Amp}} + (\boldsymbol{B}_{LP}\boldsymbol{P}_t^S) \oslash \boldsymbol{V_t^{Amp}}$

$$\sqrt{\left(\boldsymbol{P_t^{Line}} \oslash \boldsymbol{V_t^{Amp}} + (\boldsymbol{B}_{LP}\boldsymbol{P}_t^S) \oslash \boldsymbol{V_t^{Amp}}\right)^2 + \left(\boldsymbol{Q_t^{Line}} \oslash \boldsymbol{V_t^{Amp}} + (\boldsymbol{B}_{LQ}\boldsymbol{Q}_t^S) \oslash \boldsymbol{V_t^{Amp}}\right)^2} \leq \boldsymbol{I_{max}} \tag{4.20}$$

sums the contribution of generation, demand and BESS systems to the current at each monitoring point, where the matrix $\boldsymbol{B}_{LP}$ maps BESSs to upstream monitoring points.

where,

$$\boldsymbol{B}_{LP} = \begin{bmatrix} \frac{\partial P_{1,1}}{\partial P_1^S} & \cdots & \frac{\partial P_{1,1}}{\partial P_i^S} & \cdots & \frac{\partial P_{1,1}}{\partial P_{n_l}^S} \\ \vdots & \ddots & \vdots & & \vdots \\ \frac{\partial P_{L,\emptyset}}{\partial P_1^S} & & \frac{\partial P_{L,\emptyset}}{\partial P_i^S} & & \frac{\partial P_{L,\emptyset}}{\partial P_{n_l}^S} \\ \vdots & & \vdots & \ddots & \vdots \\ \frac{\partial P_{n_a,n_\emptyset}}{\partial P_1^S} & \cdots & \frac{\partial P_{n_a,n_\emptyset}}{\partial P_i^S} & \cdots & \frac{\partial P_{n_a,n_\emptyset}}{\partial P_{n_l}^S} \end{bmatrix} \quad \boldsymbol{B}_{LQ} = \begin{bmatrix} \frac{\partial Q_{1,1}}{\partial Q_1^S} & \cdots & \frac{\partial Q_{1,1}}{\partial Q_i^S} & \cdots & \frac{\partial Q_{1,1}}{\partial Q_{n_l}^S} \\ \vdots & \ddots & \vdots & & \vdots \\ \frac{\partial Q_{L,\emptyset}}{\partial Q_1^S} & & \frac{\partial Q_{L,\emptyset}}{\partial Q_i^S} & & \frac{\partial Q_{L,\emptyset}}{\partial Q_{n_l}^S} \\ \vdots & & \vdots & \ddots & \vdots \\ \frac{\partial Q_{n_a,n_\emptyset}}{\partial Q_1^S} & \cdots & \frac{\partial Q_{n_a,n_\emptyset}}{\partial Q_i^S} & \cdots & \frac{\partial Q_{n_a,n_\emptyset}}{\partial Q_{n_l}^S} \end{bmatrix}$$

It should be noted that this formulation uses voltages and ampacity recorded at monitor points, whereas all other formulations use values for every major line segment (see section 4.2.3) i.e. a greater number of points. This is because the centralized control algorithm relies on remote measurements during operation, whereas for all others we need only to ensure that voltages can be held within limits during the placement stage. Therefore, as many monitoring points as desired may be used with no concern as to whether these monitors would actually need to exist.

Each BESS inverter is constrained to a maximum total apparent power (constraints (4.3 - 4.8)), and a minimum power factor (constraint (4.9)). Furthermore, BESS takeover may only occur where a BESS is already owned by a customer, is in suitable working condition, and the customer agrees to the takeover. Wherever this model is used, this availability is predetermined randomly by forcing some elements of $\boldsymbol{X^s}$ to take the value 0, where the number of zero elements depends on the chosen BESS availability for the given simulation (e.g. 25% of PV array owners will have a forced zero BESS availability when BESS availability = 75%). Equality constraints are included to ensure that the SOC at each BESS at each time step is equal to the sum of charging events up to that point, and to prevent the SOC from falling below 0, or exceeding $\boldsymbol{SOC_{max}}$ during any time period. As in section 4.2.1, the MILP formulation is applied to a 14 hour clear sky summer generation profile at 1 hourly intervals.

4.2.2.2 FIL based BESS takeover

BESSs are taken over under the assumption that there is no data communication between residences and centralized controllers, and BESSs primarily prevent the output of their associated PV array from exporting at more than half their rated power. This scheme has the advantages of avoiding communication and monitoring infrastructure costs, being independent of voltage i.e. stable to voltage changes on the wider grid, and treating customer's BESSs consistently and proportionally to their PV array size.

$$\min_{(\boldsymbol{X^s})\in\mathbb{R}^{n_{l,1}}} \boldsymbol{J}_{n_l,1}^T \boldsymbol{X^s} \tag{4.21}$$

The formulation is subject to the same voltage, ampacity, and control takeover constraints as the centralized scheme discussed in section 4.2.2.1. However, BESS inverters do not provide reactive power, and charging is limited to inverter capacity by constraint (4.22), to half of maximum PV generation (4.23), and to inverter capacity. Furthermore, neither energy constraints nor multiple time periods are considered, as the assumed BESS has sufficient energy capacity to satisfy the FIL scheme on a clear sky summer day (see section 4.2.4.2).

$$|\boldsymbol{P}_t^s| \leq \boldsymbol{S}^{inv} \tag{4.22}$$

$$-\frac{\mathbf{1}}{\mathbf{2}}\boldsymbol{P}_{\boldsymbol{max}}^{g} \leq \boldsymbol{P}^{\boldsymbol{s}} \leq \mathbf{0}_{n_l,1} \tag{4.23}$$

As before, if any charging is requested of a BESS, the relevant element of the takeover requirement vector $\boldsymbol{X}^S$ is set to 1, and BESS availability is randomly predetermined.

4.2.2.3 ASHP demand limiting BESS takeover

Available ASHP physical modelling data (Good, 2015), developed using the methodology presented in (Good *et al.*, 2013), was made available by the University of Manchester's Electrical Energy and Power Systems Group. The modelling assumes a cold, but not excessively cold UK winter day (min temp 0°C). From examination of this data it can be shown that, even for feeders with very high load counts (for which greater diversity would be expected), the ASHP load diversity factor approaches 1. The takeover model therefore aims to procure enough BESSs to handle utilization or voltage violations during periods in which all ASHPs operate at nominal power.

The ASHP uses BESS's to limit the maximum demand of the pump under normal operation (i.e. without consideration of auxiliary heater operation), by discharging when the pump is operational. The formulation uses the objective function represented in equation (4.13). Constraint (4.24) ensures that a feasible solution has enough BESS capacity to ensure voltage can always be held above V_{min} (216.2 V), where $-(\boldsymbol{V}^{HP} - \boldsymbol{V}_{min})$ is the voltage increase required to bring voltages at the end of each major line segment to within statutory limits, and $\boldsymbol{B}_{VP}\boldsymbol{P}^S$ represents the voltage change as a result of BESS operation

$$-(\boldsymbol{V}^{HP} - \boldsymbol{V}_{min}) \leq \boldsymbol{B}_{VP}\boldsymbol{P}^S \tag{4.24}$$

Constraint (4.25) limits BESSs to discharge at a rates no higher than those noted in $\boldsymbol{P}_{lim}^{S}$**;** this is equal to the bought capacity of the BESS in kWh (70% of total capacity in this study, chosen as compromise between energy capacity and degradation rate, which was seen to increase significantly when operating the BESS outside of this range) divided by the highest number of on hours observed from the provided dataset, which represents a typical cold UK day (12.5 hours for radiator based ASHP systems, and 13.5 hours for underfloor systems). This ensures all BESSs can operate for a full typical UK cold day without fully discharging.

$$\mathbf{0}_{n_l,1} \leq \boldsymbol{P}^S \leq \boldsymbol{P}_{\boldsymbol{lim}}^{\boldsymbol{S}} \tag{4.25}$$

The formulation is also subject to constraints that ensure BESSs can only be taken over where BESSs exist (i.e. at selected residences that have been assigned PV systems; this formulation always runs directly after a PV takeover model, so that the same BESS availability pattern can be used), and at residences where ASHP systems are installed. BESSs may not operate for reactive power control. If any discharging is requested of a BESS, the relevant element of the takeover requirement vector $\boldsymbol{X^s}$ is set to 1.

4.2.3 Reconductoring

This category concerns formulations that are used to determine the minimum cost to the DNO/3rd of partially reconductoring any given feeder, whilst ensuring that the reinforcement pattern eliminates the potential for voltage and ampacity violations that would otherwise be caused by the installed PV generation/ ASHP demand.

In all reconductoring formulations, each feeder is simplified into a small set of cable segments - typically 3 - 5 for the main feeder path and 1 per branch, which are denoted 'major line segments'. This method is used because the computational burden of the MILP formulation is too high if every meter of conductor is considered; the number of simulations performed during most later studies is $>10^6$, and so problems must solve rapidly. Furthermore, it would be practically awkward for a DNO to reconductor several very small sections of a feeder. Whist DNOs will ultimately be required to reconductor the entirety of every network (regardless of the presence of PV or BESSs), it is worth considering how partial reconductoring may be used to manage the violations caused by sudden increases in generation capacity on networks where reconductoring is not imminently planned.

4.2.3.1 Reconductoring (PV only)

The reconductoring MILP objective function minimizes the total cost of reconductoring in instances in which only normal domestic loads and PV generators are present on a feeder. The total reconductoring cost is determined by multiplying the cost associated with reconductoring each line segment ($\boldsymbol{c_{Recon}}^T$) by the binary variables that denote whether each major line segment reinforcement exists (these are stored in vector $\boldsymbol{X}^{Recon}$),

$$\min_{(\boldsymbol{X}^{Recon} \in \mathbb{R}^{n_C \times 1})} \boldsymbol{c_{X^{Recon}}}^T \boldsymbol{X}^{Recon} \tag{4.26}$$

Constraint (4.27) predicts how a chosen series of reinforcements will reduce the voltage on each phase of each monitored end point (given by the left hand side of the constraint), and ensures that these reductions are all greater than that required to ensure voltage remains

below 253 V, $\boldsymbol{V}_{max} - \boldsymbol{V}^{End}$. $\boldsymbol{B}_{Recon}$ is a matrix representing expected change in voltage on each phase of every monitored end point to each possible reinforcement e.g. the (7,4)[th] element of $\boldsymbol{B}_{Recon}$, $\frac{\Delta V_{3,1}}{\Delta X_4^c}$, represents the expected change in voltage at end point monitor 3, phase demand exceeds generation 1, when major line segment 4 is reconductored.

$$\boldsymbol{B}_{Recon}\boldsymbol{X}^{Recon} \leq \boldsymbol{V}_{max} - \boldsymbol{V}^{End} \tag{4.27}$$

where,

$$\boldsymbol{B}_{Recon} = \begin{bmatrix} \frac{\Delta V_{1,1}}{\Delta X_1^{Recon}} & \cdots & \frac{\Delta V_{1,1}}{\Delta X_{n_C}^{Recon}} \\ \vdots & \ddots & \vdots \\ \frac{\Delta V_{n_E,n_\emptyset}}{\Delta X_1^{Recon}} & \cdots & \frac{\Delta V_{n_E,n_\emptyset}}{\Delta X_{n_C}^{Recon}} \end{bmatrix}$$

Constraint (4.28) ensures that the current magnitude does not exceed the maximum cable ampacity rating, where $\sqrt{(\boldsymbol{P}^{PV} \oslash \boldsymbol{V}^{PV})^2 + (\boldsymbol{Q}^{PV} \oslash \boldsymbol{V}^{PV})^2}$ denotes the current magnitude along each phase of each major line segment in the PV & ASHP cases respectively. $\boldsymbol{X}^{Recon} \circ \Delta \boldsymbol{I}^{Recon}$ is the increase in ampacity of each major line segment that results from the reconductoring pattern described by $\boldsymbol{X}^{Recon}$.

$$\sqrt{(\boldsymbol{P}^{PV} \oslash \boldsymbol{V}^{PV})^2 + (\boldsymbol{Q}^{PV} \oslash \boldsymbol{V}^{PV})^2} \leq \boldsymbol{I}_{\boldsymbol{max}} + \boldsymbol{X}^{Recon} \circ \Delta \boldsymbol{I}^{Recon} \tag{4.28}$$

4.2.3.2 Reconductoring (PV & ASHP)

The reconductoring model takes the form of a mixed integer linear programming (MILP) problem, with the objective of minimising the reconductoring cost. The existence of reconductoring along each segment is stored in the vector of binary values, $\boldsymbol{X}^{Recon}$.

The objective function is identical to equation 4.18, however, in this formulation, both the violations that the networks PV arrays could cause during summer, and the violations that ASHPs could cause during winter, are considered simultaneously. This ensures that the chosen reconductoring pattern is sufficient to handle stresses caused by both technologies.

Constraint (4.29) ensures that line upgrades are sufficient to reduce peak voltages to 1.09 p.u. at maximum PV generation, and constraint (4.30) ensures that line reinforcement is sufficient to ensure voltages do not fall below 0.94 p.u. at maximum ASHP demand. The terms $\boldsymbol{B}_{Recon}^{PV}\boldsymbol{X}^{Recon}$ and $\boldsymbol{B}_{Recon}^{HP}\boldsymbol{X}^{Recon}$ represent the changes in voltage at the end of each major line segment (arising as a result of the chosen reconductoring pattern) at peak PV generation and ASHP demand respectively, and $\boldsymbol{V}_{max} - \boldsymbol{V}^{\boldsymbol{PV}}$ and $-\left(\boldsymbol{V}^{\boldsymbol{HP}} - \boldsymbol{V}_{min}\right)$ denote

the voltage changes required to bring the network within statutory limits in each instance. $\boldsymbol{B}_{\boldsymbol{Recon}}^{\boldsymbol{PV}}$ is a matrix that contains the expected voltage change at the end of each major line segment on each phase with respect to each reinforcement e.g. the (8,4)th element $\frac{\Delta V_{3,2}^{PV}}{\Delta X_4^{Recon}}$ denotes the expected voltage change at the end of major line segment 3 phase 2 when major line segment 4 is reconductored.

$$\boldsymbol{B}_{Recon}^{PV}\boldsymbol{X}^{Recon} \leq \boldsymbol{V}_{max} - \boldsymbol{V}^{PV} \tag{4.29}$$

$$-(\boldsymbol{V}^{HP} - \boldsymbol{V}_{min}) \leq \boldsymbol{B}_{Recon}^{HP}\boldsymbol{X}^{Recon} \tag{4.30}$$

$$where,$$

$$\boldsymbol{B}_{Recon}^{PV} = \begin{bmatrix} \frac{\Delta V_{1,1}^{PV}}{\Delta X_1^{Recon}} & \cdots & \frac{\Delta V_{1,1}^{PV}}{\Delta X_{n_C}^{Recon}} \\ \vdots & \ddots & \vdots \\ \frac{\Delta V_{n_E,n_\emptyset}^{PV}}{\Delta X_1^{Recon}} & \cdots & \frac{\Delta V_{n_E,n_\emptyset}^{PV}}{\Delta X_{n_C}^{c}} \end{bmatrix} \qquad \boldsymbol{B}_{Recon}^{HP} = \begin{bmatrix} \frac{\Delta V_{1,1}^{HP}}{\Delta X_1^{Recon}} & \cdots & \frac{\Delta V_{1,1}^{HP}}{\Delta X_{n_C}^{Recon}} \\ \vdots & \ddots & \vdots \\ \frac{\Delta V_{n_E,n_\emptyset}^{HP}}{\Delta X_1^{Recon}} & \cdots & \frac{\Delta V_{n_E,n_\emptyset}^{HP}}{\Delta X_{n_C}^{Recon}} \end{bmatrix}$$

Constraints (4.31) and (4.32) ensure that the current magnitude does not exceed the maximum cable ampacity rating, where $\sqrt{(\boldsymbol{P}^{PV} \oslash \boldsymbol{V}^{PV})^{\boldsymbol{2}} + (\boldsymbol{Q}^{PV} \oslash \boldsymbol{V}^{PV})^{\boldsymbol{2}}}$ and $\sqrt{(\boldsymbol{P}^{HP} \oslash \boldsymbol{V}^{HP})^{\boldsymbol{2}} + (\boldsymbol{Q}^{HP} \oslash \boldsymbol{V}^{HP})^{\boldsymbol{2}}}$ denote the current magnitude along each phase of each major line segment in the PV & ASHP cases respectively. $\boldsymbol{X}^{Recon} \circ \Delta \boldsymbol{I}^{Recon}$ is the increase in ampacity of each major line segment that results from the reconductoring pattern described by $\boldsymbol{X}^{Recon}$.

$$\sqrt{(\boldsymbol{P}^{PV} \oslash \boldsymbol{V}^{PV})^{\boldsymbol{2}} + (\boldsymbol{Q}^{PV} \oslash \boldsymbol{V}^{PV})^{\boldsymbol{2}}} \leq \boldsymbol{I}_{\boldsymbol{max}} + \boldsymbol{X}^{Recon} \circ \Delta \boldsymbol{I}^{Recon} \tag{4.31}$$

$$\sqrt{(\boldsymbol{P}^{HP} \oslash \boldsymbol{V}^{HP})^{\boldsymbol{2}} + (\boldsymbol{Q}^{HP} \oslash \boldsymbol{V}^{HP})^{\boldsymbol{2}}} \leq \boldsymbol{I}_{\boldsymbol{max}} + \boldsymbol{X}^{Recon} \circ \Delta \boldsymbol{I}^{Recon} \tag{4.32}$$

4.2.3.3 Parallel partial reconductoring

If the previous reconductoring formulation fails to attain a feasible result, we can consider allowing the head section of the feeder to be replaced with two parallel, equally sized conductors with identical electrical properties. The feeder head line segment is defined as the length of feeder between the secondary substation and the first branch point. The cost of the addition of a parallel conductor is added to the objective function as $\boldsymbol{c}_{X_{Head}^{Recon,P}} X_{Head}^{Recon,P}$.

$$\min_{(\boldsymbol{X}^{Recon} \in \mathbb{R}^{n_C \times 1})} \boldsymbol{c}_{X^{Recon}}{}^{T} \boldsymbol{X}^{Recon} + \boldsymbol{c}_{X_{Head}^{Recon,P}} X_{Head}^{Recon,P} \tag{4.33}$$

The voltage and ampacity constraints from section 4.2.3.2 are adjusted to allow for parallel reconductoring of the feeder head segment. $X_{Head}^{Recon,P}\boldsymbol{B}_{Recon,P}^{PV}$ is the voltage change at the end of each major line segment on each phase if parallel reconductoring on the feeder head segment exists, and zero otherwise. $X_{Head}^{Recon,P}\Delta\boldsymbol{I}_{Head}^{Recon,P}$ handles the change in ampacity of the feeder head segment if it is parallel reconductored, and has no effect otherwise.

$$\boldsymbol{B}_{Recon}^{PV}\boldsymbol{X}^{Recon} + X_{Head}^{Recon,P}\boldsymbol{B}_{Recon,P}^{PV} \leq \boldsymbol{V}_{max} - \boldsymbol{V}^{PV} \tag{4.34}$$

$$-\left(\boldsymbol{V}^{\boldsymbol{HP}} - \boldsymbol{V}_{min}\right) \leq \boldsymbol{B}_{Recon}^{HP}\boldsymbol{X}^{Recon} + X_{Head}^{Recon,P}\boldsymbol{B}_{Recon,P}^{HP} \tag{4.35}$$

$$\sqrt{\left(\frac{\boldsymbol{P}^{PV}}{\boldsymbol{V}^{PV}}\right)^{\boldsymbol{2}} + \left(\frac{\boldsymbol{Q}^{PV}}{\boldsymbol{V}^{PV}}\right)^{\boldsymbol{2}}} \leq \boldsymbol{I}_{\boldsymbol{max}} + \boldsymbol{X}^{Recon} \circ \Delta\boldsymbol{I}^{Recon} + X_{Head}^{Recon,P}\Delta\boldsymbol{I}_{Head}^{Recon,P} \tag{4.36}$$

$$\sqrt{(\boldsymbol{P}^{HP} \oslash \boldsymbol{V}^{HP})^{\boldsymbol{2}} + (\boldsymbol{Q}^{HP} \oslash \boldsymbol{V}^{HP})^{\boldsymbol{2}}} \leq \boldsymbol{I}_{\boldsymbol{max}} + \boldsymbol{X}^{Recon} \circ \Delta\boldsymbol{I}^{Recon} + X_{Head}^{Recon,P}\Delta\boldsymbol{I}_{Head}^{Recon,P} \tag{4.37}$$

Where $\boldsymbol{B}_{Recon,P}^{PV}$ and $\boldsymbol{B}_{Recon,P}^{HP}$ are column vectors that contain the changes in voltage at the end of each major line segment when a parallel conductor is added to the head portion of the feeder.

Furthermore, parallel reconductoring may only occur if the original feeder head segment conductor has already been replaced, and both cables must have identical physical properties.

4.2.4 BESS operational algorithms

This category concerns formulations that are used to determine how any given BESS or set of BESS should be operated.

4.2.4.1 Self-consumption control

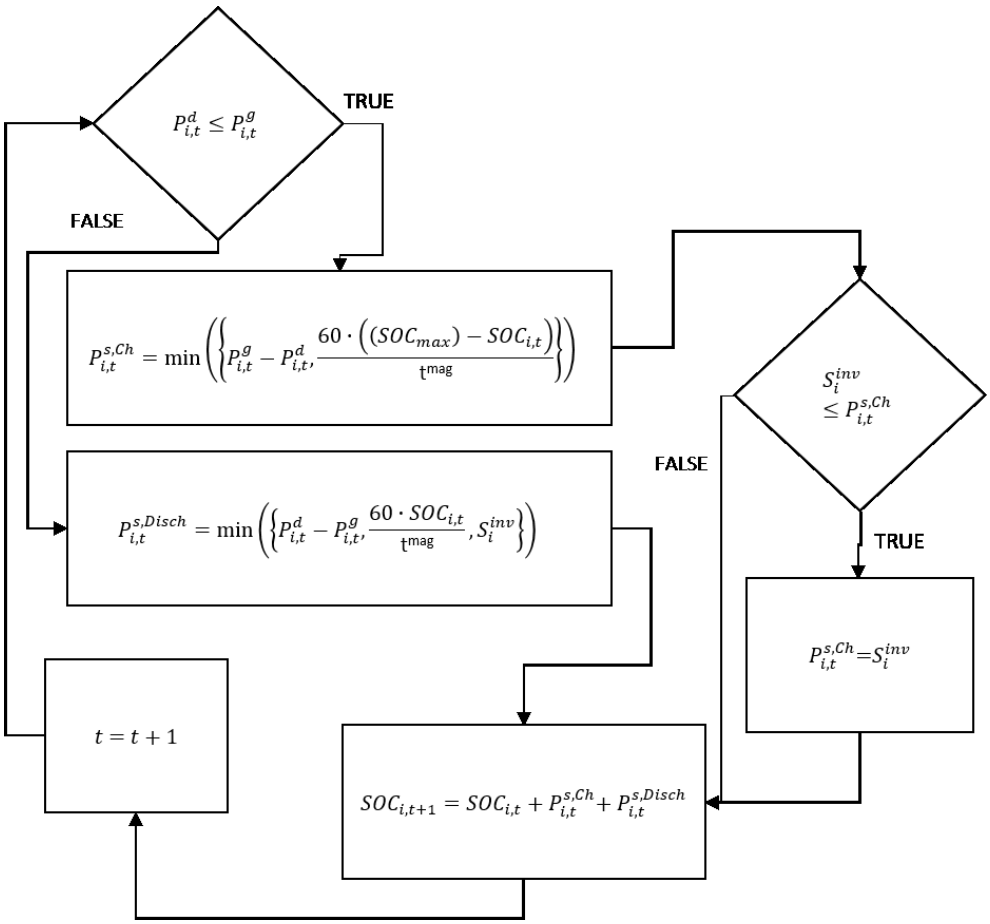

Figure 4.5 – Flow chart mathematical representation of the self-consumption algorithm.

The self-consumption algorithm represents typical current practice in residential PV-BESS system operation (Fig. 4.5). When PV generation exceeds demand, the BESS charges at a rate equal to the excess generation, but is limited by the maximum inverter power and the remaining capacity of the BESS. When demand exceeds generation, the BESS discharges at a rate equal to the excess power demand, but is limited by the maximum inverter power and the quantity of energy remaining in the BESS.

4.2.4.2 FIL Control

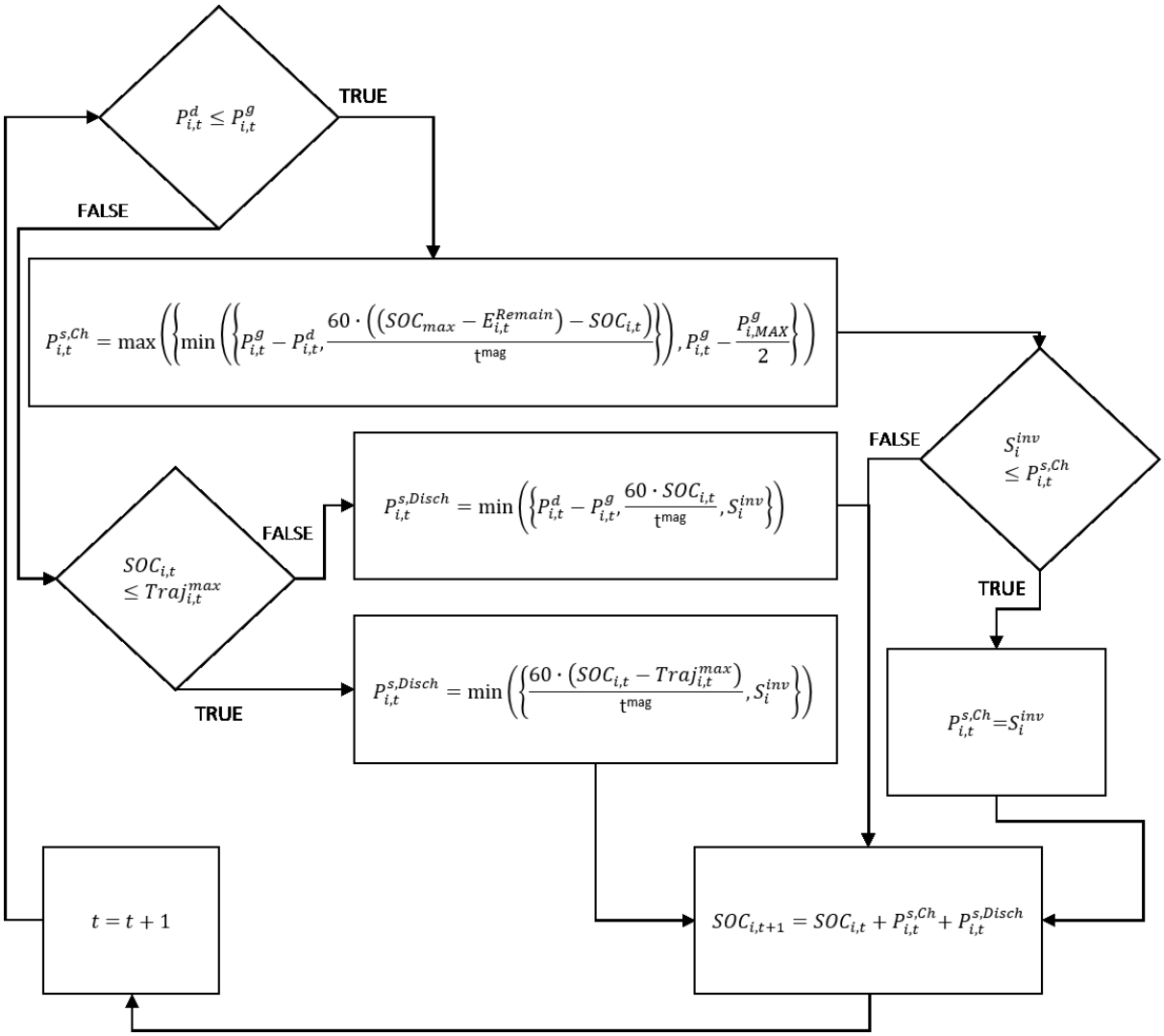

Figure 4.6 – Flow chart mathematical representation of the FIL algorithm.

The FIL algorithm charges the BESS only when generation exceeds demand. Charging is first limited to the minimum of excess generation, or a charging rate that, if exceeded, risks the BESS reaching 100% SOC before the end of the daily generation period. Finally, charging is limited to maximum inverter power, S_i^{inv}, and the BESS will always charge to limit export to ½ of the rated array power. This value of ½ is chosen, as choosing a feed in limit any lower than this results in insufficient BESS capacity on clear sky summer days i.e. the BESS will need to charge more energy than it has capacity for if a feed in limit of 0.49 times the rated array power is chosen.

When demand exceeds generation, the BESS discharges at the minimum of excess demand, maximum inverter power, or the discharge power that would cause the BESS to reach its minimum allowed SOC. If the BESS SOC exceeds the maximum allowed SOC trajectory at time period t, then it discharges at the rate required to bring the SOC below this threshold. The maximum trajectory threshold ensures that BESSs have enough SOC headroom at the start of the next day to fulfil the export limiting duties that may be required. The control algorithm is shown in its mathematical form in fig. 4.6.

4.2.4.3 Centralized control/optimal power flow method

The centralized control algorithm assumes communications infrastructure for data transfer between residences and a central system, and between network monitors and the central system. The central system can process this data to optimize the operation of multiple BESSs for (amongst other factors) voltage and ampacity violation management, maximum self-consumption, and minimum degradation. The model consists of a predictive stage, which determines bounds for BESS SOCs throughout the following 24 h period, and a real time stage, which uses these bounds amongst other available network state information to determine an appropriate operation pattern for BESSs during the next time step (during this thesis, a 1 min time step is used for this formulation).

4.2.4.3.1 Predictive stage

Considering that BESSs are used to maximize customer self-consumption in the real-time dispatch section of the algorithm, and because BESSs must not be at maximum allowed SOC before they are required for network control, predictions of day-ahead generation are required to aid operational decisions. Furthermore, an estimate of future demand is essential, as it is important to determine whether there is likely to be any self-consumption value to charging BESSs. The generation and demand prediction process is carried out at the beginning of each simulated day.

To estimate day ahead PV irradiance, an ARIMA (1,0,0)(1,1,0) prediction model is applied (as suggested and explained in (Reikard, 2009)), with suitable model parameters estimated from 30 days of hourly irradiance data prior to the day being simulated. Two-day ahead generation is also predicted, and is used to determine an end of day goal SOC for the day ahead. The MATLAB ARIMA tool is used for parameter estimation and simulation, and ARIMA+2σ is used as the irradiance prediction; this is cautious, but reduces the risk of irradiance underestimation, and hence reduces the risk of prematurely filling BESSs before they are required for network violation control. Per site generation is estimated using a simple power-

irradiance-temperature regression model (King, Kratochvil and Boyson, 1997, 2004), and the hourly demand prediction is estimated using persistence with consideration of day-type (weekday or weekend); this appears crude, but (Veit *et al.*, 2014) shows that little forecasting improvement is seen with more advanced predictive methods.

A multiperiod LP heuristic is used to approximate the minimum total charging energy required to satisfy voltage and ampacity constraints for the 24h period. Although the operating regions of BESS inverters may be approximated using the hexagonal and power factor constraints (4.3 – 4.9) (Fig. 4.3), the resulting formulation is non-convex in the instance that BESSs are permitted to operate in either charging or discharging mode. It is therefore necessary to use a 2 stage LP optimization heuristic to approximate optimal operation. The results produced using the heuristic are almost no different from those obtained using only hexagonal constraints (as the decision to operate at low power factors is very rarely the optimum), but assure BESS inverters operate only within allowed bounds.

The objective functions for both stages of the formulation are identical, and seek to minimize the total energy charged across all 24 hourly time intervals by all BESSs. This can be expressed mathematically as,

$$\min_{(\boldsymbol{P}^S)\in\mathbb{R}^{n_l\times 24}} \eta_{eff}\boldsymbol{J}_{n_l,1}^T[\boldsymbol{P}_1^S \quad \dots \quad \boldsymbol{P}_t^S \quad \dots \quad \boldsymbol{P}_{24}^S]\boldsymbol{J}_{24,1} \tag{4.38}$$

Because opportunities to discharge may arise during the 24 h period, constraint (4.39) allows BESSs to discharge at a maximum rate equal to the predicted load demands remaining at their respective sites after subtraction of PV generation from the total load demand, which is calculated before the optimization as $max\left(\boldsymbol{P}_t^d - \boldsymbol{P}_t^g, \boldsymbol{0}_{n_l,1}\right)$, where $\boldsymbol{P}_t^d$ and $\boldsymbol{P}_t^g$ here represent predicted demand and PV generation at each load site respectively,

$$\boldsymbol{P}_t^S \leq max\left(\boldsymbol{P}_t^d - \boldsymbol{P}_t^g, \boldsymbol{0}_{n_l,1}\right) \tag{4.39}$$

Constraint (4.40) ensures that the SOC of each BESS at every timestep (expressed as vector $vec\left(\boldsymbol{J}_{\Delta L}[\boldsymbol{P}_1^S \quad \dots \quad \boldsymbol{P}_t^S \quad \dots \quad \boldsymbol{P}_{24}^S]^{\boldsymbol{T}}\right)$), is within the allowed range for the respective BESS. It should be noted that $\boldsymbol{E}^S$ is here a vector of fixed values (decided upon using the placement and sizing formulation) describing the energy capacity of the BESS at each residence, rather than a set of variables.

$$\boldsymbol{0}_{n_l,1}\otimes\boldsymbol{0}_{24,1} \leq vec\left(\boldsymbol{J}_{\Delta L}[\boldsymbol{P}_1^S \quad \dots \quad \boldsymbol{P}_t^S \quad \dots \quad \boldsymbol{P}_{24}^S]^{\boldsymbol{T}}\right) \leq \boldsymbol{E}^S\otimes\boldsymbol{J}_{24,1} \tag{4.40}$$

Stage 1:

In stage 1, BESS inverters are prohibited from supplying leading or lagging reactive power, but BESSs may charge or discharge at the full rated power of their inverters.

Stage 2:

Stage 2 uses the outcome of stage 1 to decide how the real power operation of each BESS should be constrained at each of the 24 hourly time intervals; each BESS is constrained to either 'discharging only' if the BESS was discharging in the stage 1 result, and 'charging only' if the BESS was charging in the stage 1 result. BESSs are allowed to operate at power factors between 0.85 and 1 in stage 2, and this is managed using constraints (4.3 – 4.9). Additionally constraint (4.40) is updated so that BESSs discharging during a given hour, t, experience an SOC change of $\frac{P_{i,t}^{S}}{\eta_{eff}}$, and BESSs that are charging experience an SOC change of $\eta_{eff} P_{i,t}^{S}$.

From the results of step 2, the predicted hourly SOC series are extracted for each BESS - these SOC series represent the predicted SOC evolution of BESSs if used only for violation control. The maximum allowable SOC for each BESS at the end of each hour is determined by adding the difference between the predicted future maximum SOC and the BESS maximum energy capacity to the predicted SOC at the current hour (depicted in fig. 4.7), which creates a maximum allowed SOC trajectory sequence. The 2nd day ahead SOC prediction uses the same maximum trajectory method to determine a suitable SOC to end the day ahead on, which ensures that BESSs do not risk starting the 2nd day ahead without adequate capacity headroom to handle potential voltage and ampacity violations. The maximum trajectory is the modified to account for the need to reduce SOC to the day ahead limit SOC_{DA}. This is done by limiting the BESS SOC to no greater than that determined using equation 4.41,

$$SOC_{DA} + x \cdot (24 - Current\ Hour\ of\ Day) \tag{4.41}$$

Where x is an appropriate maximum hourly discharge rate that must be selected based on specific feeder properties and the number of BESSs on the feeder (see chapter 5 for specific choices).

As an example, if it is 8 am, the BESS has 10 kWh of energy capacity, and it is expected that the BESS will need to increase its SOC by 6 kWh for voltage management over the hours 9 am – 4pm, then it is important that the SOC does not exceed a $(10 - 6)\ kWh = 4\ kWh$ SOC during the time interval 8 – 9 am (i.e. it must have 6kWh of spare capacity). The maximum trajectory for this hour is therefore 4 kWh. If the BESS is at a SOC > 4 kWh, it will try to find

opportunities to discharge such that it reaches the maximum trajectory limit without causing network violations.

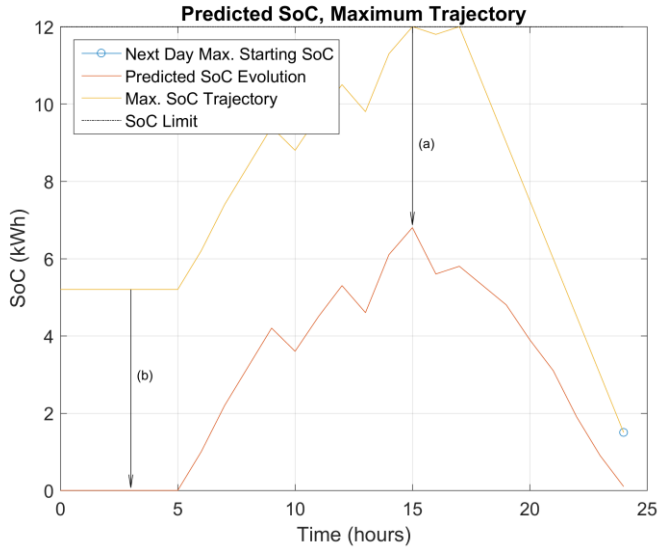

Figure 4.7 – Shows the maximum SOC trajectory and required next day maximum starting SOC for a given hourly predicted SOC evolution. Arrows (a) and (b) are of the same magnitude, as the maximum allowed SOC at hour 3 must equal the SOC headroom at hour 15 plus the predicted SOC at hour 3. In the last 8 hours of the day, the max trajectory progresses towards the desired next day max starting SOC at a rate equal to discharging the BESS at a constant 1.5 kW.

4.2.4.3.2 Real time stage

The OPF cost function takes the form (4.42), which denotes the sum of all residences self-consumption BESS charging benefits $\boldsymbol{A}_{Ch}$, energy import and export penalties $\boldsymbol{A}_{GenDem}$, BESS degradation penalties $\boldsymbol{A}_{Deg}$, deviation of SOC max trajectory penalties, $\boldsymbol{A}_{m}$, BESS efficiency loss penalties $\boldsymbol{A}_{SL}$, and a very small penalty that prevents inverters from injecting reactive power when not required $\boldsymbol{A}_{Q}$. Line loss penalties associated with real power losses along the feeder, $\boldsymbol{A}_{LL,P}$ and $\boldsymbol{A}_{LL,Q}$, are added, along with penalties associated with excessive reactive power demand at the feeder head $\boldsymbol{A}_{PF}$. The formulation and meaning of the penalty terms are discussed throughout this chapter.

$$\min_{\boldsymbol{A}_{Store}\,\boldsymbol{A}_{Line}\in\mathbb{R}} \boldsymbol{A}_{Store,t} + \boldsymbol{A}_{Line,t} \tag{4.42}$$

$$\boldsymbol{A}_{Store,t} = \boldsymbol{J}^{T}_{6n_l,1} \begin{bmatrix} \boldsymbol{A}_{Ch,t} \\ \boldsymbol{A}_{GenDem,t} \\ \boldsymbol{A}_{Deg,t} \\ \boldsymbol{A}_{m,t} \\ \boldsymbol{A}_{SL,t} \\ \boldsymbol{A}_{Q,t} \end{bmatrix} \tag{4.43}$$

$$\boldsymbol{A}_{Line,t} = [\boldsymbol{J}^{T}_{2n_\emptyset n_c,1} \quad \boldsymbol{J}^{T}_{n_\emptyset,1}] \begin{bmatrix} \boldsymbol{A}_{LL,P,t} \\ \boldsymbol{A}_{LL,Q,t} \\ \boldsymbol{A}_{PF,t} \end{bmatrix} \tag{4.44}$$

The optimization process runs as follows

- The state of the line and load powers, losses, and voltages at the timestep that has just occurred (denoted in the subscript as $t-1$), are extracted from the power flow simulator (openDSS).
- The changes in each BESSs real power $\Delta\boldsymbol{P}^{S}_{t}$, and reactive power $\Delta\boldsymbol{Q}^{S}_{t}$ are optimized to find values that would minimize operation costs at $t-1$ - this accounts for the fact that the state of network at time t cannot be known beforehand. The optimization progresses through 2 stages, for the same reason as in formulation (4.38).
- The new time step, t, is reached, and the $\Delta\boldsymbol{P}^{S}_{t}$ and $\Delta\boldsymbol{Q}^{S}_{t}$ values are applied, and the process is repeated until all timesteps have been evaluated.

The input variables to the optimization are $\Delta\boldsymbol{P}^{S}_{t}$ and $\Delta\boldsymbol{Q}^{S}_{t}$. Any other scalars and vectors used are pre-determined constants and coefficients. In the instance that a constraint requires an absolute BESS charging/discharging rate, this is determined using $\boldsymbol{P}^{S}_{t-1} + \Delta\boldsymbol{P}^{S}_{t}$, i.e. the previous BESS setting plus the amendment to the BESS setting for the next time step.

4.2.4.3.2.1 Typical OPF constraints

The real time (RT) OPF constraint (4.45) prevents overvoltage, and is identical to constraint (4.2) aside from absolute BESS powers $\boldsymbol{P}^{S}_{t}$ being replaced by change in BESS powers, $\Delta\boldsymbol{P}^{S}_{t}$. Constraint (4.46) prevents under voltage by ensuring that the predicted change in voltage on each phase at all monitored end points that results from changes in BESS real and reactive powers, $\boldsymbol{B}_{VP}\Delta\boldsymbol{P}^{S}_{t} + \boldsymbol{B}_{VQ}\Delta\boldsymbol{Q}^{S}_{t}$, is greater than that required to bring voltages above the lower limit, $\boldsymbol{V_{min}} - \boldsymbol{V}^{End}_{t-1}$.

$$\boldsymbol{B}_{VP}\Delta\boldsymbol{P}^{S}_{t} + \boldsymbol{B}_{VQ}\Delta\boldsymbol{Q}^{S}_{t} \leq \boldsymbol{V_{max}} - \boldsymbol{V}^{End}_{t-1} \tag{4.45}$$

$$\boldsymbol{B}_{VP}\Delta\boldsymbol{P}^{S}_{t} + \boldsymbol{B}_{VQ}\Delta\boldsymbol{Q}^{S}_{t} \geq \boldsymbol{V_{min}} - \boldsymbol{V}^{End}_{t-1} \tag{4.46}$$

Feeder head ampacity constraints for the RT OPF formulation are identical to those used in the placement and sizing model, except absolute BESS powers are replaced by change in BESS powers,

$$-\alpha \boldsymbol{V}_{t-1}^{Head}\boldsymbol{B}_{HP}\Delta\boldsymbol{P}_t^s + \boldsymbol{V}_{t-1}^{Head}\boldsymbol{B}_{HQ}\Delta\boldsymbol{Q}_t^s \leq \alpha \boldsymbol{V}_{t-1}^{Head} \circ \boldsymbol{P}_{t-1}^{Head} - \boldsymbol{V}_{t-1}^{Head} \circ \boldsymbol{Q}_{t-1}^{Head} + \boldsymbol{I}_{max}^{Head}$$

$$\alpha \boldsymbol{V}_{t-1}^{Head}\boldsymbol{B}_{HP}\Delta\boldsymbol{P}_t^s + \boldsymbol{V}_{t-1}^{Head}\boldsymbol{B}_{HQ}\Delta\boldsymbol{Q}_t^s \leq -\alpha \boldsymbol{V}_{t-1}^{Head} \circ \boldsymbol{P}_{t-1}^{Head} - \boldsymbol{V}_{t-1}^{Head} \circ \boldsymbol{Q}_{t-1}^{Head} + \boldsymbol{I}_{max}^{Head}$$

$$-\alpha \boldsymbol{V}_{t-1}^{Head}\boldsymbol{B}_{HP}\Delta\boldsymbol{P}_t^s + \boldsymbol{V}_{t-1}^{Head}\boldsymbol{B}_{HQ}\Delta\boldsymbol{Q}_t^s \geq \alpha \boldsymbol{V}_{t-1}^{Head} \circ \boldsymbol{P}_{t-1}^{Head} - \boldsymbol{V}_{t-1}^{Head} \circ \boldsymbol{Q}_{t-1}^{Head} - \boldsymbol{I}_{max}^{Head}$$

$$\alpha \boldsymbol{V}_{t-1}^{Head}\boldsymbol{B}_{HP}\Delta\boldsymbol{P}_t^s + \boldsymbol{V}_{t-1}^{Head}\boldsymbol{B}_{HQ}\Delta\boldsymbol{Q}_t^s \geq -\alpha \boldsymbol{V}_{t-1}^{Head} \circ \boldsymbol{P}_{t-1}^{Head} - \boldsymbol{V}_{t-1}^{Head} \circ \boldsymbol{Q}_{t-1}^{Head} - \boldsymbol{I}_{max}^{Head}$$

$$-\beta \boldsymbol{V}_{t-1}^{Head}\boldsymbol{B}_{HP}\Delta\boldsymbol{P}_t^s + \boldsymbol{V}_{t-1}^{Head}\boldsymbol{B}_{HQ}\Delta\boldsymbol{Q}_t^s \leq \beta \boldsymbol{V}_{t-1}^{Head} \circ \boldsymbol{P}_{t-1}^{Head} - \boldsymbol{V}_{t-1}^{Head} \circ \boldsymbol{Q}_{t-1}^{Head} + \beta\boldsymbol{I}_{max}^{Head}$$

$$\beta \boldsymbol{V}_{t-1}^{Head}\boldsymbol{B}_{HP}\Delta\boldsymbol{P}_t^s + \boldsymbol{V}_{t-1}^{Head}\boldsymbol{B}_{HQ}\Delta\boldsymbol{Q}_t^s \leq -\beta \boldsymbol{V}_{t-1}^{Head} \circ \boldsymbol{P}_{t-1}^{Head} - \boldsymbol{V}_{t-1}^{Head} \circ \boldsymbol{Q}_{t-1}^{Head} + \beta\boldsymbol{I}_{max}^{Head}$$

$$-\beta \boldsymbol{V}_{t-1}^{Head}\boldsymbol{B}_{HP}\Delta\boldsymbol{P}_t^s + \boldsymbol{V}_{t-1}^{Head}\boldsymbol{B}_{HQ}\Delta\boldsymbol{Q}_t^s \geq \beta \boldsymbol{V}_{t-1}^{Head} \circ \boldsymbol{P}_{t-1}^{Head} - \boldsymbol{V}_{t-1}^{Head} \circ \boldsymbol{Q}_{t-1}^{Head} - \beta\boldsymbol{I}_{max}^{Head}$$

$$\beta \boldsymbol{V}_{t-1}^{Head}\boldsymbol{B}_{HP}\Delta\boldsymbol{P}_t^s + \boldsymbol{V}_{t-1}^{Head}\boldsymbol{B}_{HQ}\Delta\boldsymbol{Q}_t^s \geq -\beta \boldsymbol{V}_{t-1}^{Head} \circ \boldsymbol{P}_{t-1}^{Head} - \boldsymbol{V}_{t-1}^{Head} \circ \boldsymbol{Q}_{t-1}^{Head} - \beta\boldsymbol{I}_{max}^{Head} \quad (4.47 - 4.54)$$

Stage 1:

Stage 1 is identical to stage 1 in the prediction model in section 4.2.4.3.1, except real powers are expressed as $(\Delta\boldsymbol{P}_t^s + \boldsymbol{P}_{t-1}^s)$ to account for the inverter power at the previous time step.

Stage 2 only:

Stage 2 is identical to stage 2 in the prediction model in section 4.2.4.3.1, except real powers and reactive powers are expressed as $(\Delta\boldsymbol{P}_t^s + \boldsymbol{P}_{t-1}^s)$ and $(\Delta\boldsymbol{Q}_t^s + \boldsymbol{Q}_{t-1}^s)$ respectively to account for the inverter power at the previous time step. Additionally, BESSs are bound so that charging or discharging cannot result in a breach of the SOC limits – BESS efficiency, η_{eff}, is considered in calculation of the bounds.

4.2.4.3.2.2 Predicted Stored Energy Values

Because reclamation of utility bill savings resulting from reduced grid demand (due to BESS operation) may be an effective mechanism for the BESS owner to pay back some system costs, a term is included in the cost function that considers the value of BESS charging at any given point in time for each BESS, $\boldsymbol{A}_{Ch,t}$. The value of any element of the vector $\boldsymbol{A}_{Ch,t}$, $A_{Ch,i,t}$, represents the value of charging BESS i for purposes of self-consumption, and is determined by predicting whether SOC is likely to reach zero whilst load demand still remains ($DNS_{total,i} > 0$) i.e. the formulation predicts whether further charging (that is not necessary for violation control) is likely to reduce the customers future grid demand. From the predicted generation and demand profiles developed in section 4.2.4.3.1, the predicted

charging profiles developed in the same section, and the current SOC, it is possible to determine whether this is likely. $A_{Ch,i,t}$ therefore takes the value,

$$\begin{cases} A_{Ch,i,t} = \left(P^{s}_{i,t-1} + \Delta P^{s}_{i,t}\right) c_{kWh,d,i,t}\,, & if\ DNS_{total,i} > 0 \\ A_{Ch,i,t} = 0\,, & if\ DNS_{total,i} = 0 \end{cases} \tag{4.55}$$

Where $c_{kWh,d,i,t}$ takes the value £0.116/kWh at all times for standard tariff customers, which reflects a typical cost per kWh of electricity to customers in the UK, and results in a negative cost for charging where $DNS_{total,i} > 0$, thus encouraging charging. For example, if a customer with predicted unserved demand were to charge from PV generation at 2 kW, then $A_{Ch,i,t}$ would equate to £0.232, which is the actual cost saving the customer would experience by avoiding future import if this action were continued for a period of 1 hour; it is worth noting that all costs used in the RT OPF formulation are scaled to 1 hour of activity, regardless of the time interval used.

This predicted energy value must be balanced against current import costs, so that energy is not bought at a cost equal to or greater than the cost of the future energy purchase that we are trying to avoid. Current energy import and export costs are managed by constraints (4.56) and (4.57). The constraints form an epigraph which ensures that any element of $\boldsymbol{A}_{GenDem,t}$ (where each element represents the cost penalty/benefit associated with energy import/export at a given residence), is equal to the product of $c_{kWh,d,i,t}$ and the total import (if the residence is operating at a net import), or the product of the respective element of $\boldsymbol{c}_{kWh,ex}$ and the total export (if the residence is operating at a net export). As previously stated $c_{kWh,d,i,t}$ is always £0.116/kWh for standard tariff customers and £0.152/kWh for Economy 7 (E7) customers during peak hours, but the value falls to £0.071/kWh during off peak hours.

$$-\boldsymbol{c}_{kWh,d,t} \circ \left(\boldsymbol{P}^{g}_{t-1} + (\boldsymbol{P}^{s}_{t-1} + \Delta \boldsymbol{P}^{s}_{t}) - \boldsymbol{P}^{d}_{t-1}\right) \leq \boldsymbol{A}_{GenDem,t} \tag{4.56}$$

$$c_{kWh,ex}\left(\boldsymbol{P}^{g}_{t-1} + (\boldsymbol{P}^{s}_{t-1} + \Delta \boldsymbol{P}^{s}_{t}) - \boldsymbol{P}^{d}_{t-1}\right) \leq \boldsymbol{A}_{GenDem,t} \tag{4.57}$$

The result of these additional considerations is a tendency of BESSs to charge only during generation.

4.2.4.3.2.3 Degradation penalties

As BESSs are to be operated over long time periods, the effect of degradation and the way in which this may impact operational costs must be considered. Using the predicted load demand time series and predicted charging profiles from section 4.2.4.3.1, alongside the present BESS SOC, the evolution of SOC over the day is estimated, and an hourly SOC time series is obtained. The magnitude and number of cycles experienced by each BESS over the day in question are extracted using a rainflow counting algorithm (Nieslony, 2010), as is typical in battery degradation modelling studies (Barcellona *et al.*, 2015; Karagiannopoulos *et al.*, 2016). The predicted daily degradation for each BESS is then calculated by feeding the rainflow output into the depth of discharge (DoD)-Capacity fade relationship developed in (Lam and Bauer, 2013), which is coupled with the semi-emperical capacity fade algorithm in (Xu, Oudalov and Ulbig, 2016) that extends the former to include approximations for calendar fading. Such semi-empirical models are readily applicable to BESS planning and operation studies, as they only require inputs that can be readily obtained or approximated, as opposed to physical models that often require information regarding molecular level processes cannot be directly measured in operation. The depth of discharge-capacity fade curve used is derived from a typical curve for li-ion chemistries (Xu, Oudalov and Ulbig, 2016), and is adjusted to represent a cell with a cycle life of 10 years at 70% DOD, which represents the cycle life expectations of typical state of the art residential BESSs such as the Tesla Powerwall (Tesla, 2016) (fig. 4.8).

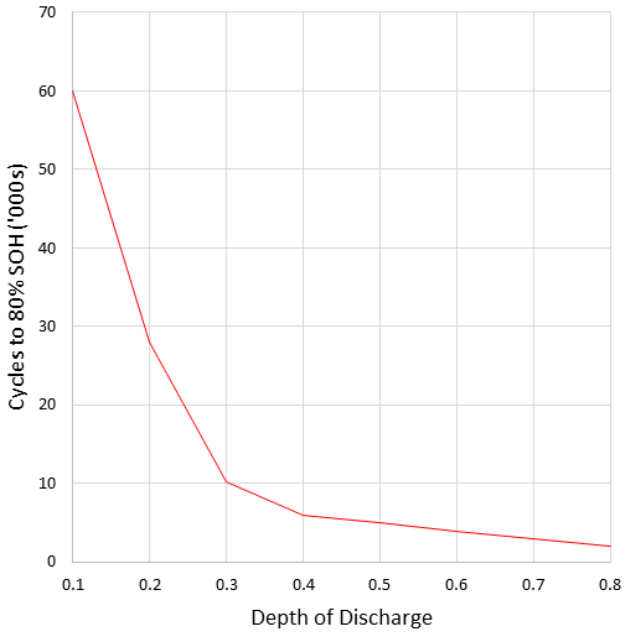

Fig. 4.8 – Shows the cycles to end of life vs. DOD used to calibrate the degradation model.

To approximate the increase in degradation associated with increase in SOC of a given BESS, 1 kWh of charge is added to the BESS, the way in which this will change the SOC hourly time series is predicted (using demand and hourly charging predictions), and the degradation associated with this time series is predicted using the rain flow and capacity fade algorithms discussed previously. The kWh degradation from the base case is then subtracted from the '+1 kWh' case, to give the predicted change in degradation associated with further charging, ΔD_i.

ΔD_i is converted to a cost by dividing ΔD_i by 20% of the system size in kWh (to account for the fact that the BESSs no longer have the capacity to handle violations below 80% state of health and so must be replaced), and multiplying by total capital cost of the BESS,

$$c_{deg,i,t} = \frac{\Delta D_i c_{sys,i}}{0.2(1.25E_i^S)} \tag{4.58}$$

Where the factor 1.25 arises to adjust the maximum usable BESS capacity to total BESS capacity (BESSs are operated within 80% of their maximum SOC range; this range is chosen as it is typical of literature in the field (Bucher, Betcke and Andersson, 2013; Von Appen, Braun and Kneiske, 2013; Fortenbacher, Andersson and Mathieu, 2015; Fortenbacher, Zellner and Andersson, 2016; Fortenbacher, Mathieu and Andersson, 2017)). The costs factors $c_{deg,i,t}$, which represent the £/kW charging penalty for each BESS i at the given time

step, are multiplied by the BESS charging rates in kW (0 if discharging), and stored in the vector $\boldsymbol{A}_{deg,t}$. Additionally, BESSs are allowed to charge with no penalty if they are 'behind schedule' on degradation; for example, if on the final day of year 1 the BESS has not lost 2% of its total energy capacity, it may charge with no penalty unless this limit is met on the day. Preliminary testing of the model without this consideration resulted in under-utilization of BESSs, with BESSs predicted to reach calendar lives after performing very few cycles.

It is worth noting that the value '+1 kWh' is chosen as much smaller and larger values were seen to be misrepresentative of the typical quantities of energy actually charged within a 1 hour period; in this formulation, the cost of charging is linearly scaled to the change in SOC, so the 'cost per kWh SOC change' value determined must be somewhat representative as degradation with change in SOC is actually non-linear. For example, using cost figures derived using '+3 kWh' causes the optimisation formulation to overestimate expected degradation if only 0.5 kWh is charged during a given hour, because the rainflow and degradation models are non-linear with change in SOC.

4.2.4.3.2.4 Other considerations

If BESSs operate at an SOC that exceeds their maximum SOC trajectory at a given time interval, they are penalized using the epigraph formulation programmed into Constraints (4.59, 4.60). The term $(\boldsymbol{P}^{S}_{t-1} + \Delta\boldsymbol{P}^{S}_{t} - \boldsymbol{P}^{S}_{viol})$ determines whether BESSs are charging at too high a rate/discharging at too low a rate to fall below the maximum trajectory at the next time interval, where $\boldsymbol{P}^{S}_{viol}$ denotes the absolute BESS real powers that would be required to fall below the trajectory. If the term is positive for a given BESS, then the BESS is penalized by (4.59) at a rate equal to the product of c_m and the power in kW that the BESS will exceeds the maximum trajectory by. If negative, then the penalty is set equal to zero. The penalties for all BESSs on the network at the given time interval are stored in $\boldsymbol{A}_{m,t}$.

$$-c_m(\boldsymbol{P}^{S}_{t-1} + \Delta\boldsymbol{P}^{S}_{t} - \boldsymbol{P}^{S}_{viol}) \leq \boldsymbol{A}_{m,t} \tag{4.59}$$

$$\boldsymbol{0}_{n_l,1} \leq \boldsymbol{A}_{m,t} \tag{4.60}$$

Constraints (4.61, 4.62) represent an epigraph formulation that penalizes BESS operations when they are expected to result in reactive power demands on a given phase at the feeder head that exceed $\frac{1}{3}$ real power demand i.e. Power factors below 0.95 lagging are penalized. $-\boldsymbol{B}_{HQ}\Delta\boldsymbol{Q}^{S}_{t} - \boldsymbol{Q}^{Head}_{t-1}$ represents reactive power demand, $max\left(\left\{-\frac{1}{3}\boldsymbol{P}^{Head}_{t-1}, \boldsymbol{0}_{n_\emptyset,1}\right\}\right)$

represents real power demand, and c_{PF} is the penalty per kvar excess, and is based on current Electricity North West Limited ENWL charges (ENWL, 2016b). The constraints are effective in reducing the instances in which more reactive than real power is drawn from the wider grid.

$$c_{PF}(-\boldsymbol{B}_{HQ}\Delta\boldsymbol{Q}_t^S - \boldsymbol{Q}_{t-1}^{Head} - max\left(\left\{-\frac{1}{3}\boldsymbol{P}_{t-1}^{Head}, \boldsymbol{0}_{n_\emptyset,1}\right\}\right)) \leq \boldsymbol{A}_{PF,t} \quad (4.61)$$

$$\boldsymbol{0}_{n_\emptyset,1} \leq \boldsymbol{A}_{PF,t} \quad (4.62)$$

As is typical in BESS power flow studies (Bucciarelli *et al.*, 2016; S. W. Alnaser and Ochoa, 2016; Giannitrapani *et al.*, 2017), the modelled Li-ion type BESSs are assumed to have a fixed charging and discharging efficiency of η_{eff} = 0.95, and cost penalties for storage losses at each BESS are approximated by multiplying charging or discharging rate in kW by $\boldsymbol{c}_{kWh,d,t}(1-\eta_{eff})$. The resulting penalties are the stored in $\boldsymbol{A}_{SL,t}$. Though in reality efficiency does vary slightly across charging/discharging rates, it does not vary enough to significantly change the outcome of this work (see section 2.3.4), so a fixed efficiency is deemed adequate for the purpose of this study.

Additionally, line losses resulting from reactive power transfer are penalized using the exact methodology presented and used in the power flow study (Fortenbacher, Mathieu and Andersson, 2017); the authors model line losses that actually vary quadratically with current as a piecewise linear epigraph approximation of the I^2 curve,

$$\varepsilon \circ \boldsymbol{B}_{LP}\boldsymbol{\Delta P}_t^S - \boldsymbol{C}_{LL,P,t} \leq -\varepsilon \circ \boldsymbol{P}_{t-1}$$

$$-\varepsilon \circ \boldsymbol{B}_{LP}\boldsymbol{\Delta P}_t^S - \boldsymbol{C}_{LL,P,t} \leq \varepsilon \circ \boldsymbol{P}_{t-1}$$

$$5\varepsilon \circ \boldsymbol{B}_{LP}\boldsymbol{\Delta P}_t^S - \boldsymbol{C}_{LL,P,t} \leq -5\varepsilon \circ \boldsymbol{P}_{t-1} + \zeta$$

$$-5\varepsilon \circ \boldsymbol{B}_{LP}\boldsymbol{\Delta P}_t^S - \boldsymbol{C}_{LL,P,t} \leq 5\varepsilon \circ \boldsymbol{P}_{t-1} + \zeta$$

$$\rho \circ \boldsymbol{B}_{LQ}\boldsymbol{\Delta Q}_t^S - \boldsymbol{C}_{LL,Q,t} \leq -\rho \circ \boldsymbol{Q}_{t-1}$$

$$-\rho \circ \boldsymbol{B}_{LQ}\boldsymbol{\Delta Q}_t^S - \boldsymbol{C}_{LL,Q,t} \leq \rho \circ \boldsymbol{Q}_{t-1}$$

$$5\rho \circ \boldsymbol{B}_{LQ}\boldsymbol{\Delta Q}_t^S - \boldsymbol{C}_{LL,Q,t} \leq -5\rho \circ \boldsymbol{Q}_{t-1} + \varphi$$

$$-5\rho \circ \boldsymbol{B}_{LQ}\boldsymbol{\Delta Q}_t^S - \boldsymbol{C}_{LL,Q,t} \leq 5\rho \circ \boldsymbol{Q}_{t-1} + \varphi \quad (4.63 – 4.70)$$

Where,

$$\boldsymbol{B}_{LP} = \begin{bmatrix} \frac{\partial P_{1,1}}{\partial P_1^S} & \cdots & \frac{\partial P_{1,1}}{\partial P_i^S} & \cdots & \frac{\partial P_{1,1}}{\partial P_{n_l}^S} \\ \vdots & \ddots & \vdots & & \vdots \\ \frac{\partial P_{L,\emptyset}}{\partial P_1^S} & & \frac{\partial P_{L,\emptyset}}{\partial P_i^S} & & \frac{\partial P_{L,\emptyset}}{\partial P_{n_l}^S} \\ \vdots & & \vdots & \ddots & \vdots \\ \frac{\partial P_{n_C,n_\emptyset}}{\partial P_1^S} & \cdots & \frac{\partial P_{n_C,n_\emptyset}}{\partial P_i^S} & \cdots & \frac{\partial P_{n_C,n_\emptyset}}{\partial P_{n_l}^S} \end{bmatrix} \quad \boldsymbol{B}_{LQ} = \begin{bmatrix} \frac{\partial Q_{1,1}}{\partial Q_1^S} & \cdots & \frac{\partial Q_{1,1}}{\partial Q_i^S} & \cdots & \frac{\partial Q_{1,1}}{\partial Q_{n_l}^S} \\ \vdots & \ddots & \vdots & & \vdots \\ \frac{\partial Q_{L,\emptyset}}{\partial Q_1^S} & & \frac{\partial Q_{L,\emptyset}}{\partial Q_i^S} & & \frac{\partial Q_{L,\emptyset}}{\partial Q_{n_l}^S} \\ \vdots & & \vdots & \ddots & \vdots \\ \frac{\partial Q_{n_C,n_\emptyset}}{\partial Q_1^S} & \cdots & \frac{\partial Q_{n_C,n_\emptyset}}{\partial Q_i^S} & \cdots & \frac{\partial Q_{n_C,n_\emptyset}}{\partial Q_{n_l}^S} \end{bmatrix}$$

$$\varepsilon = \frac{10^6 c_{LL,P}}{4} \boldsymbol{P}_{MAX} \circ \boldsymbol{R} \oslash \left(\boldsymbol{V}_{avg} \circ \boldsymbol{V}_{avg}\right)$$

$$\zeta = \frac{10^6 c_{LL,P}}{4} \boldsymbol{R} \circ \left((\boldsymbol{P}_{MAX} \circ \boldsymbol{P}_{MAX}) \oslash \left(\boldsymbol{V}_{avg} \circ \boldsymbol{V}_{avg}\right)\right)$$

$$\rho = \frac{10^6 c_{LL,P}}{4} \boldsymbol{Q}_{MAX} \circ \boldsymbol{R} \oslash \left(\boldsymbol{V}_{avg} \circ \boldsymbol{V}_{avg}\right)$$

$$\varphi = \frac{10^6 c_{LL,P}}{4} \boldsymbol{R} \circ \left((\boldsymbol{Q}_{MAX} \circ \boldsymbol{Q}_{MAX}) \oslash \left(\boldsymbol{V}_{avg} \circ \boldsymbol{V}_{avg}\right)\right)$$

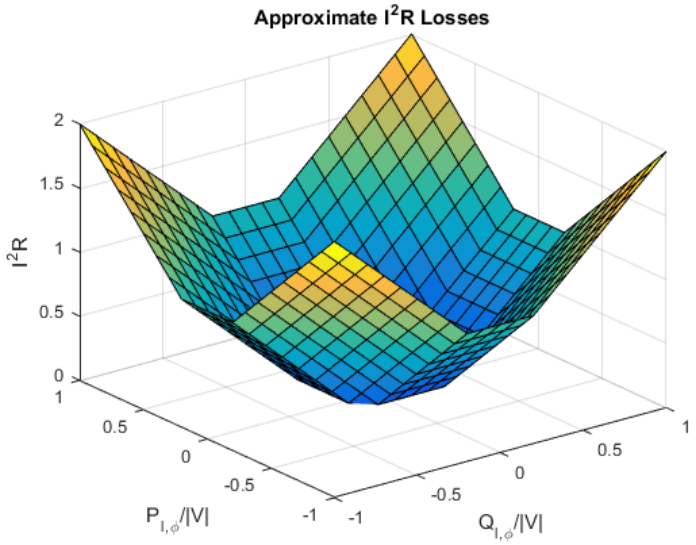

Fig. 4.9 – Shows how losses are approximated in this work.

Consideration of losses for each line segment in any feeder model produces an impractically large problem, so networks are simplified to major line segments for this analysis. Preliminary testing showed that large losses resulting from unnecessary reactive power transfer between buses could be avoided by applying line loss constraints together with a very small cost penalty (£0.0001/kvar) on leading or lagging reactive power injection by BESS

inverters (accounted for in $\boldsymbol{A}_{Q,t}$). The RIIO-ED1 electricity distribution price control document explains the obligation of DNOs to reduce network losses, but does not provide an exact economic incentive for loss reduction (i.e. in £/MWh), so constraints that limit losses due to real power transfer are used only to ensure unnecessarily large line losses are avoided.

5. Optimal placement, sizing, and dispatch of multiple BESSs on UK low voltage networks

5.1 Introduction

In the following chapter, the technical and economic feasibility of using DNO/3rd party owned BESSs violation management on LV residential networks is examined. Whilst Ofgem do not currently permit DNOs to own or operate BESSs (Pratt, 2017), if BESSs were to prove economically viable tools for management of LV network voltage and ampacity violations, an argument to allow DNO ownership may be formed. Furthermore, there is no legislation to prevent a 3rd party from owning and operating a network of BESSs, operating this in a way that is beneficial to the DNO, and selling this service to the DNO. 3rd party ownership of assets located at residences is relatively common for PV in the UK (Solarcentury, 2014), and collaboration between home owners and 3rd party companies for BESS system profitability is being explored in numerous cases (Daniel, 2017). With the increased rollout of smart monitoring equipment, the proposition of utilizing an operational scheme that requires spatially and temporally resolute power and voltage data is becoming more feasible.

In this chapter, the technical and economic effectiveness of DNO/3rd party owned *behind the meter BESSs* for voltage and ampacity management is explored. BESSs are placed and sized using the algorithm presented in section 4.2.1, and BESSs are placed only with customers who also own PV systems. BESS operation is coordinated via a central controller, and relies on the dispatch algorithm presented in section 4.2.4.3. The controller aims to optimize group BESS operation to decrease utility bill costs (via maximization of self- consumption and manipulation of Economy 7 tariffs), whilst ensuring compliance with voltage standards, preventing overutilization of feeder lines, and maintaining adequate control of power factor, line losses, and BESS degradation rates. Simulations are performed using a model of a feeder located in the north west of England, and costs of BESS control are compared to traditional reconductoring costs. Furthermore, the work examines the effect that reclamation of customer bill reductions as a means of repaying capital costs may have on the economic viability of the system. The effects that a change from ESQCR to EN 50160 voltage regulations may have on results are also considered.

The work presented in this chapter gives a preliminary understanding as to whether centrally controlled BESSs for voltage and utilization control on urban residential networks, even under near-ideal placement and dispatch conditions, is likely to prove competitive with traditional means of reinforcement in a 3rd party or DNO owned scheme.

5.2 Methodology

5.2.1 Modelling tools

The BESS sizing and placement formula described in section 4.2.1., and the OPF algorithm described in section 4.2.4.3. are applied to a model of a feeder located in the north west of England (Navarro-Espinosa and Ochoa, 2015). All simulations are carried out at 1 min temporal resolution, with 2 year duration. The topology of the feeder is shown in fig. 5.1. When running the OPF algorithm, a 2 year time series of power demand data is randomly assigned to each residence from a set of profiles generated using the CREST model (McKenna and Thomson, 2016). A comparison of monitored feeder consumption to CREST predicted consumption showed a typical demand over prediction of 7 - 10%, which are acceptable for this study. The number of profiles in the set that represent different occupancies are proportionally scaled to UK national statistics, which suggest 1, 2, 3, and 4 or more occupant residences represent 29%, 35%, 16% and 20% of the UK housing stock respectively. 2 year PV generation profiles are generated using satellite irradiance data measured at the geographic location of the feeder in question with spatial resolution 90m^2 and temporal resolution 1 min, and are converted from irradiance to power using irradiance-power and temperature-power regression models from (King, Kratochvil and Boyson, 1997, 2004).The irradiance for the 2 years in question was chosen because when converted to a generation profile it was found to be reasonably representative of 2 years of typical generation for the area of the country in question (generation is typically 820-880 kWh/kW installed/annum, and the annual average of 2 years in question is 850 kWh/kW installed/year. As of (Navarro-Espinosa and Ochoa, 2016), PV generator sizes are assigned probabilistically based on UK installation size data, that suggests 1%, 8%, 13%, 14%, 14%, 12%, and 37% of all rooftop systems are sized 1.0, 1.5, 2.0, 2.5, 3.0, 3.5 and 4.0 kW respectively. Voltage monitors are positioned at 4 extreme points on the network, and a power meter is placed at the feeder head, as this monitoring scheme was found to be the minimum required to manage network constraints.

Setup, logic, communication, and data analysis are carried out in MATLAB, 3Ø 4-wire unbalanced power flow simulations are performed using openDSS, and the IBM CPLEX optimization suite is used to solve the OPF problem. The OPF can typically be generated and solved within 30 ms for any given time step, and that the placement and sizing problem can be solved in < 1 s.

Optimal reconductoring patterns are determined using the MILP formulation described in section 4.2.3.1. The feeder is integrated into 7 major stretches of feeder cable (denoted 'major line segments'), which are shown in fig. 5.1. This simplifies the problem of modelling every line segment in the model (of which there are 1230), and represents how a DNO may consider reconductoring i.e. replacing stretches of more than a few meters.

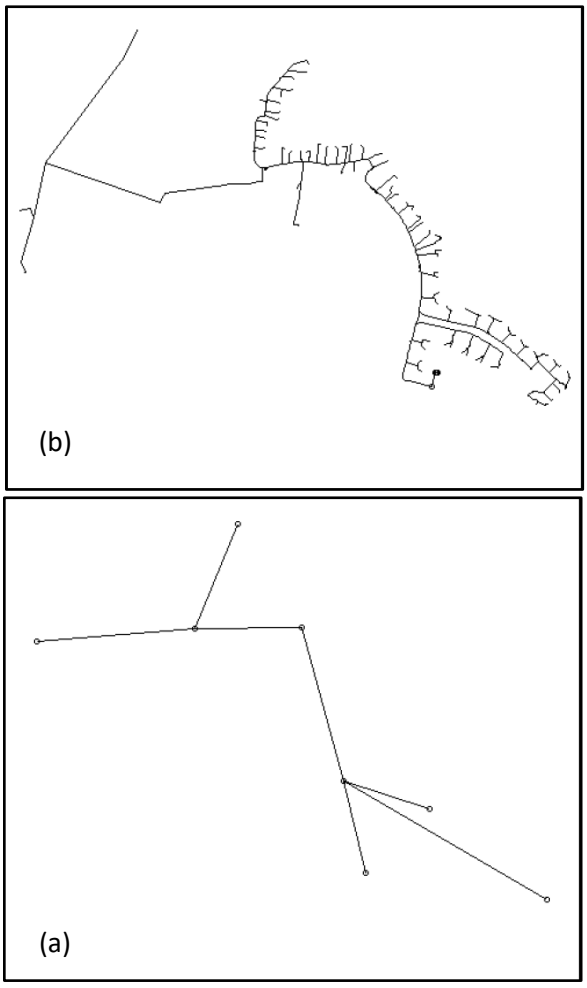

Figure 5.1 – (a) Topology of the feeder used in this case study (b) simplified 7-line segment topology of the network used for line loss approximations, and as the set of 'major line segments' that may be replaced using the reconductoring formulation.

5.2.2 Modelling scenarios and data collection

BESS placement and OPF based control are modelled at PV penetrations of 50%, 70%, and 90%. These particular penetrations are chose because:

- 50% penetration represents the point at which overvoltage violations begin to occur on this network.
- 70% penetration represents the maximum PV penetration possible if only south-facing roofs are assigned PV systems.
- 90% penetration represents a scenario in which even residents of east-west facing houses own PV systems – this may become commonplace if PV array costs fall to the point that such systems are economically viable.

Because a 90% penetration requires that some PV be placed on non-south facing roofs, east-west generation profiles are applied where required. Within each penetration scenario, 3 network reinforcement scenarios are modelled:

- Business as usual – No reinforcement is used.
- Reconductoring – The network is reconductored to the extent that voltage and utilization limits are controlled for 100% of the simulation – requiring use of the reconductoring formulation presented in section 4.2.3.1.
- BESS with E7 - Sufficient BESS capacity is installed on the network to ensure voltage can be controlled on a clear sky summer day (using the placer method described in section 4.2.1), customers with BESSs of usable capacity ≥ 10 kWh are switched to an E7 tariff, and BESSs are centrally controlled using the aforementioned methodology (with the E7 extensions activated for appropriate BESSs). The control model is configured such that BESSs reach cycle life limit after approximately 10 years.

All runs are repeated at tap positions 1.05 p.u. (the current SSS setting) and 1.00 p.u., to assess the effect that a reduction in tap position may have on the required quantity of BESS capacity, and on overall compliance to voltage standards. 1.00 p.u. is chosen as the low tap position because exploratory simulations showed that any tap positions lower than this could cause frequent low voltage violations in winter months. The lowest voltage experienced by the network is shown as a function of tap position in figure 5.2.

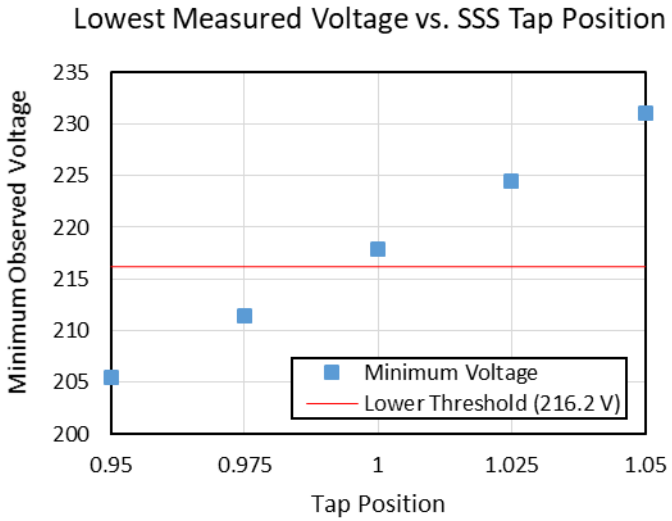

Figure 5.2 – Shows the minimum observed steady state voltage on the network at each of the 5 possible tap positions.

For each model run, the following outputs are recorded;

- Total feeder line loss
- Total customer import from grid
- Total customer export to grid
- Total storage losses
- % voltage control at each load for each day (ESQCR standards)
- % voltage control at each load for each day (EN 50160 standards)
- % utilization control at the feeder head for each day

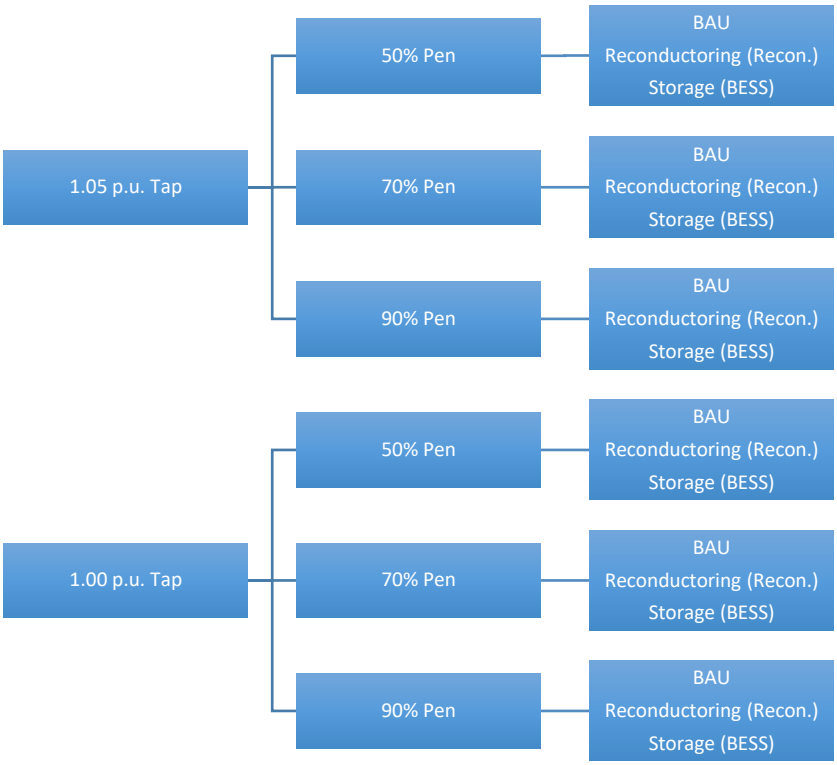

Figure 5.3 – Shows the hierarchy of simulation scenarios.

The hierarchy of scenarios is shown in fig. 5.3. In order to consider how placement of generators may change the results for any given scenario, each scenario is run multiple times with different assignments of demand profiles and generator placements and sizes. Each time, the BESS sizing and placement formula is solved, and the OPF algorithm (described in section 4.2.4.3) is run. Convergence of control and self-consumption statistics typically occurs between 10 - 30 runs, dependent on the scenario.

5.2.3 Other mathematical notes

The polygonal approximation of ampacity constraints presented in chapter 4 is used in both the placement and control models as a compromise between optimality and computational cost, and uses the method presented in (Fortenbacher, Mathieu and Andersson, 2017). For the particular feeder used in this case study, improvements to overall costs are insignificant with respect to increased detail in ampacity limit modelling (as voltage violations always manifest before ampacity violations), and so the polygonal approximation is considered sufficient. Furthermore, the use of such linear approximations increases the optimization rate and therefore increases the temporal resolution at which the dispatch heuristic could theoretically be applied.

During the placement and sizing stage, the usable energy capacity of each BESS is limited between 2.5 kWh and 12 kWh, which represents a BESS of capacity 15 kWh operating within 80% of its SOC range to prolong life. The 15 kWh limit is chosen to prevent BESSs becoming unreasonably large for residential premises, and the 2.5 kWh lower limit prevents impractically small BESSs from being placed.

During the prediction stage, a consideration to ensure that the day ahead initial SOC is low enough to prevent premature BESS filling must be included (see section 4.2.4.3.1). The maximum SOC was calculated using equation (4.41).

In this work, a value of $x = 1.5\ kW$ was used, which ensures that BESSs will never be required to discharge at a rate greater than 1.5 kW to satisfy the trajectory. This value was chosen to prevent BESSs from causing voltage and ampacity violations in the instance that they must all discharge simultaneously.

5.2.4 Analysis methodology

5.2.4.1 Voltage control capabilities

ESQCR regulations require steady state LV network voltage to remain between +10/-6% of 230 V with no specific explanation of how this should be measured, though it is implied that any breach of these bounds can be considered a violation of statute (Electricity North West Ltd, 2015). The European EN 50160 regulations require ±10% of 230 V to be maintained for 95% of 10 min averages across a 7 day period (Electricity North West Ltd, 2015); it is possible that a change to EN50160 regulations may occur, and so the effect that this may have on the % penetration at which reinforcement is required was seen as an interesting consideration in modelling scenarios. Voltage compliance capabilities of each control scheme are therefore judged using the following two methods;

- ESQCR – Compliance is approximated as the % of time periods in which voltage remains within ESQCR limits. Compliance is measured over a typical winter week and a high generation summer week, and is presented in terms of % residences within statute and % time within statute.
- EN 50160 – Compliance is achieved when 100% of 7 day periods remain within EN 50160 limits for 95% of 10 min averaged periods at all loads. Compliance is measured over the entire 2 year period.

5.2.4.2 Utilization control, line losses, and storage losses

Control is simply the % of half-hourly periods within which utilization is below the feeder head capacity. Total line losses and storage losses are calculated internally by openDSS.

5.2.4.3 System costs and adjusted system costs

System costs are equal to initial placement costs plus the cost of monitoring equipment, and results are analysed results using both present and predicted 2035 cost projections. The reinforcement cable sizes are based on future ENWL reinforcement strategies (ENWL, 2015), and LV reconductoring costs are based on figures from consultation with ENWL (Crossland, 2014). These figures are shown in table 5.1. BESS costs are derived from typical present technology costs (Tesla, 2017), (CCL, 2017), suggested costs from academic literature and industrial reports (Crossland, 2014), and on optimistic projections of future system costs (SP Energy, 2015; Hummel *et al.*, 2017), and are shown in table 5.2.

Adjusted system costs are the system costs minus customer utility bill reductions. Adjusted values are calculated by summating grid imports and for each residence in the BESS scenario, assigning the correct costs depending on tariff and time (values from Table 5.3 used), and subtracting the BAU scenario utility bill costs from this. This reduction is then adjusted by a factor of 5 to account for a project lifetime of 10 years i.e. a pro rata increase in utility costs with inflation is assumed. This calculation allows the potential of self-consumption as an additional revenue stream to be determined quantitatively.

Similarly, the system cost in reconductoring scenarios is adjusted by a factor of 0.4, to account for a minimum expected conductor lifetime of 25 years (Bahra Cables Company, 2011). In this work, it is assumed that all customer benefits are recovered by the 3rd party to pay for system installation as an ideal benchmark.

It is important to clarify that the cost analysis assumes that either:

- The DNO are allowed to purchase and install BESSs, and reclaim the entirety of bill savings from customers as a revenue.
- The DNO are paying a 3rd party to operate the set of BESSs, and that the DNO must pay (at least) the total cost of purchasing, installing and operating the system back to the 3rd party for the 3rd party to break even, minus the reduction in customer bills that the 3rd party reclaim as a revenue.

This is an idealistic way of considering the costs in both instances; in reality DNOs would likely have to pay a greater sum than the equipment costs calculated due to operations and maintenance, the need for the 3rd party to profit from their venture, and the very low likelihood that the 3rd party or DNO could actually reclaim much (if any) of the bill reductions from residents. However, the order of magnitude difference in costs between reconductoring and centralized BESS control (presented in section 7.3) suggests that this economic analysis was sufficient to meet the goal of the study, which was to gain a preliminary understanding of whether BESS control could likely compete economically with traditional reconductoring, even under near optimal placement and dispatch conditions.

Property	*Value*
Main conductor size (Typical) (mm^2)	70 - 95
Branch conductor size (Typical) (mm^2)	35
Reinforcement cable size (mm^2)	300
Cost of Reconductoring (Crossland, 2014) (£/m)	80

Table 5.1 – Current conductor and reinforcement conductor properties and costs

Item	*Cost £ (10 years) Current Scenario*	*Cost £ (10 years) Future Scenario*
1 kWh BES Capacity, c_E	385 (Tesla, 2017)	94 (Hummel *et al.*, 2017)
1 kW BES Inverter Capacity, c_S	572 (CCL, 2017)	201 (Hummel *et al.*, 2017)
Install Costs, c_X	400 (Crossland, 2014)	200 (Crossland, 2014)
Network Monitor	1500 (SP Energy, 2015)	800 (SP Energy, 2015)
Monitor install	75 (SP Energy, 2015)	75 (SP Energy, 2015)

Table 5.2 – The capital costs associated with system capacity, installation and monitoring.

Parameter	*Value*	*Parameter*	*Value*
$c_{kWh,ex}$	0.048	c_m	5
$c_{kWh,d}$	0.116	$c_{LL,P}$	0.116
$c_{kWh,hi}$	0.152	$c_{LL,Q}$	0.116
$c_{kWh,lo}$	0.071	$OPF\ Timestep$	1 min
		$Predictor\ Timestep$	60 min

Table 5.3 – Value of model input variables.

5.3 Results

Voltage control is significantly improved by inclusion of BESSs in all 1.00 and 1.05 tap summer scenarios except 1.00 tap 50% pen, in which all loads are under almost 100% control even in the absence of reinforcement. All BESS scenarios and BAU winter scenarios show near 100% control for all loads, though compliance is usually slightly worse in 1.00 tap scenarios due to short voltage dips below 0.94 p.u. that are missed by the algorithm. The control statistics for all ESQCR scenarios except BAU 1.0 and 1.05 summer are shown in table 5.4. Clearly, control cannot be guaranteed 100% of the time for 100% of loads (see table 5.4). This is due to unpredictable but infrequent changes in load that cannot be forecasted correctly, resulting in most loads receiving an acceptable voltage between 99.8-100% of the total simulation time.

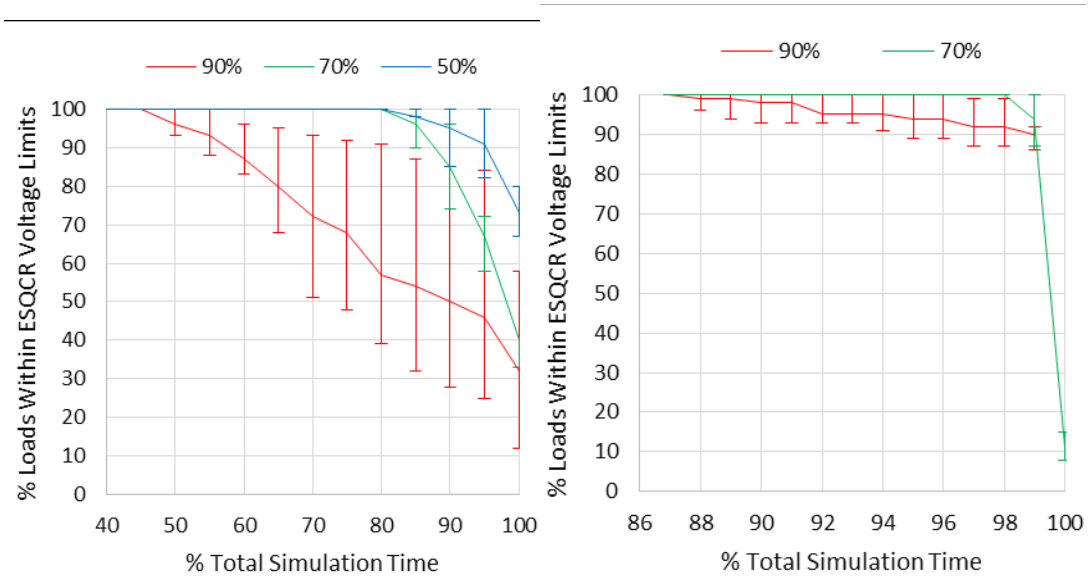

Fig. 5.4 - % loads within ESQCR bounds vs % of simulation time for scenarios BAU 1.05 tap (left) and BAU 1.00 tap (right) during a high irradiance summer week.

		1.05 tap			*1.00 tap*		
		98<x<99	99<x<100	x=100	98<x<99%	99%<x<100	x=100
BESS summer	50% pen.	100%	95%	50%	-	-	-
	70% pen.	100%	95%	55%	99%	96%	18%
	90% pen.	100%	92%	50%	95%	95%	20%
BESS winter	50% pen.	100%	98%	55%	-	-	-
	70% pen.	100%	95%	62%	100%	92%	5%
	90% pen.	100%	92%	58%	100%	88%	14%
BAU winter	50% pen.	100%	100%	100%	-	-	-
	70% pen.	100%	100%	100%	97%	85%	10%
	90% pen.	100%	100%	91%	97%	87%	10%

Table 5.4 - % residential loads controlled (by ESQCR standards) for 98-99%, 99-100%, and 100% of all simulation time - averages for all runs of the same scenario type.

An example of voltage control on a typical summer day at 70% PV penetration is shown in Fig. 5.5. It can be seen that the OPF dispatch algorithm successfully limits the voltage to 1.09 p.u. during periods of high generation, whilst a voltage rise is seen in the evening as a result of BESSs discharging to meet the allowed SOC trajectory.

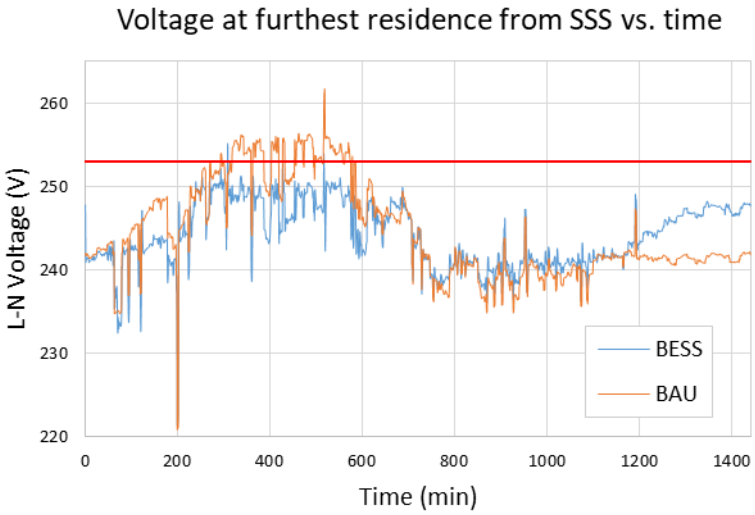

Fig. 5.5 – Voltage (at furthest residence from SSS) vs. time profiles with and without the application of the OPF algorithm for a typical summer day at 70% PV penetration, tap position 1.05 p.u. The red horizontal line denotes the 253 V upper limit.

An analysis of voltage compliance using EN 50160 standards shows that the regulations allow a PV penetration of 70% without any violation of statute (Table 5.5), provided that the tap position is adjusted to 1.00 p.u. Both BESS and reconductoring schemes achieve 100% EN 50160 compliance in all scenarios.

	1.00 Tap	*1.05 Tap*
50 BESS	o	o
70 BESS	o	o
90 BESS	o	o
50 BAU	o	o
70 BAU	o	x
90 BAU	x	x

Table 5.5 – Shows whether 100 % EN 50160 compliance is achieved across all simulations within each scenario, where 'o' denotes 100% control, and 'x' denotes <100% control.

Utilization was below the feeder head ampacity limit for 100% of half-hourly average periods in 100% of simulations for all 50% and 70% penetration scenarios. Infrequent overutilization

is seen in both BAU 90% penetration scenarios, and this improves to near 100% control BESS scenarios (Figure 5.6).

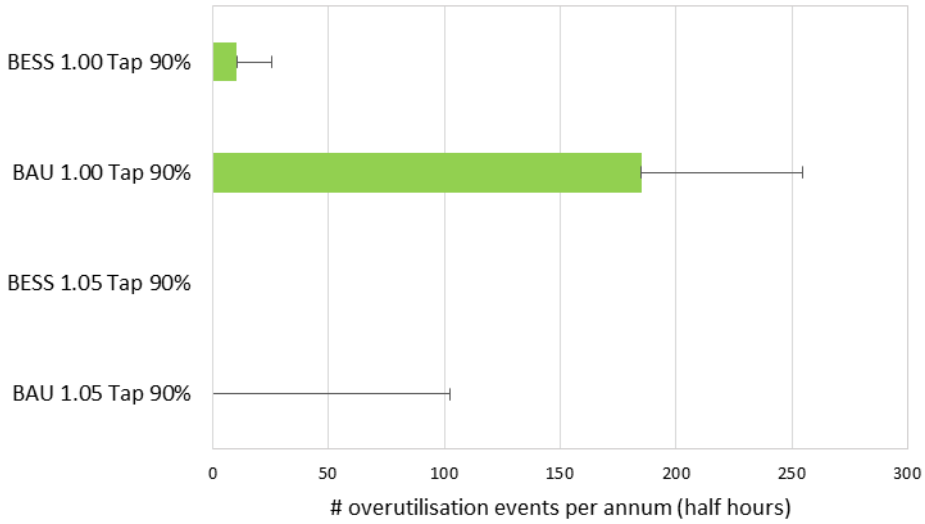

Figure 5.6 – Shows the number of half hourly periods in which the feeder head is over utilized. Error bars show the upper and lower quartiles of results.

Whist BESS scenarios showed lower line losses than BAU scenarios in all cases other than 1.00 Tap 50% (because no BESS control or reconductoring was required in this scenario), the addition of storage efficiency losses resulted in higher total losses in BESS scenarios. Total losses were always lowest in reconductoring scenarios. Annual losses across all scenarios are summarized in figure 5.7, where error bars represent 1 standard deviation around the mean total network loss.

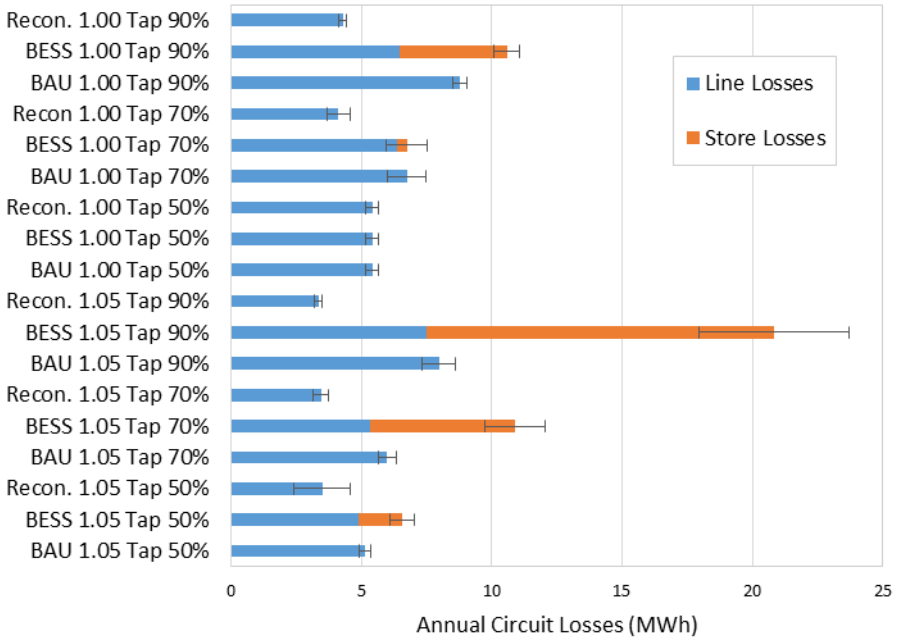

Figure 5.7 - Shows average annual circuit losses associated with each BESS scenario circuit losses. Error bars represent 1σ around the mean total network loss.

The overall reinforcement scenario costs for present and future cost schemes (with potential self-consumption benefit reductions indicated) are summarized in Fig. 5.8 - the total of the stacked bars represents the capital cost of the scenario, and error bars represent 1σ around the cost adjusted for self-consumption recoup. Reconductoring scheme costs are adjusted for their comparatively longer lifetimes than BESS schemes as explained in section 2.4.7.3. Whilst self-consumption benefit recoup may return a significant portion of the capital BESS costs in future cost scenarios, this is still not sufficient to allow BESS systems to compete economically with reconductoring, with the latter typically 9 - 10 times cheaper than the former. At current BESS costs, self-consumption benefit recoup provides insignificant reduction to BESS costs, with reconductoring typically 30 - 40 times cheaper over its lifetime than BESS installation. It should be noted that no significant difference between savings were observed when E7 arbitrage control was included alongside self-consumption of generation. This is simply because generation at most sites is great enough to make E7 arbitrage the less economical option for the majority of the year.

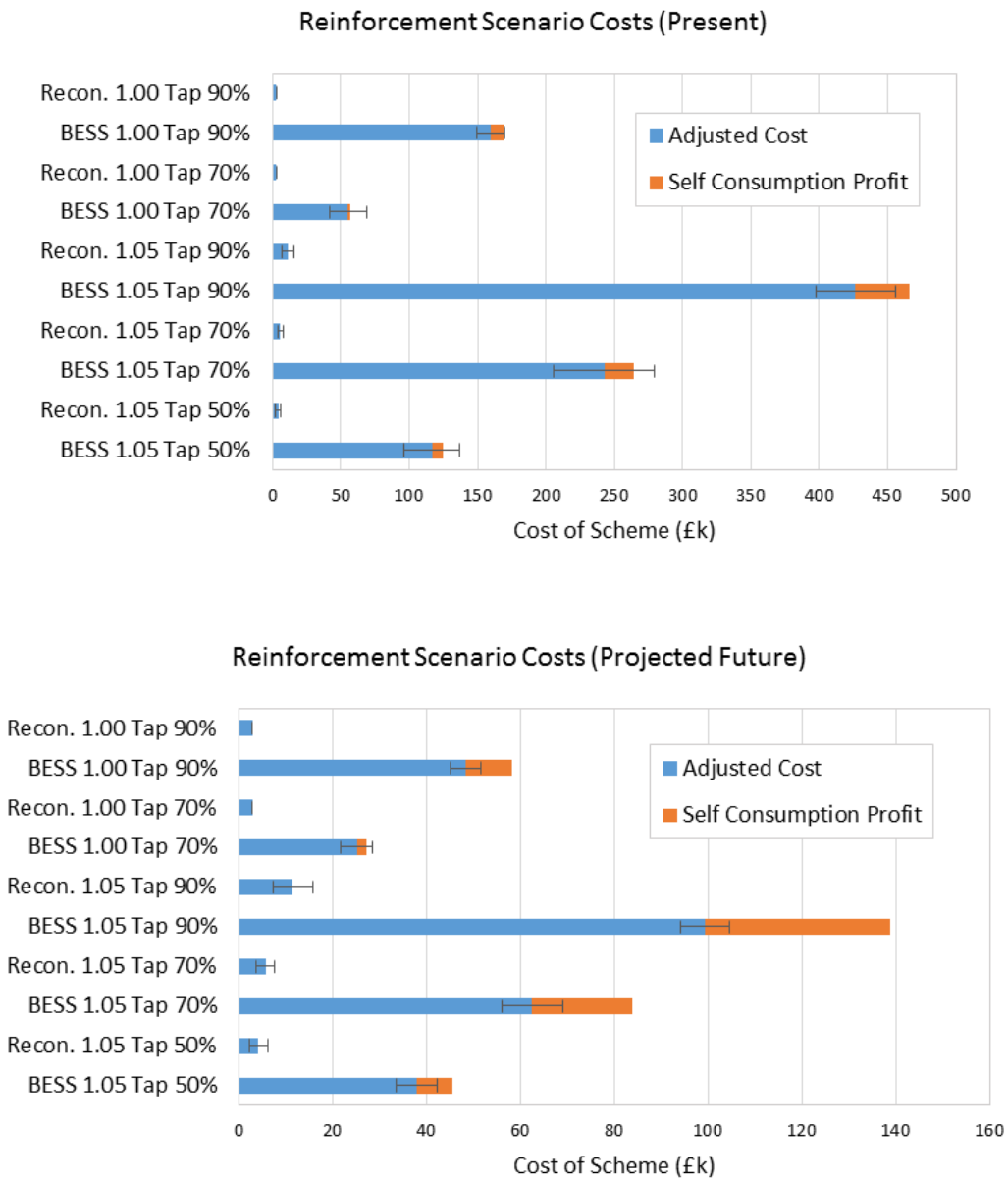

Figure 5.8 – (top) Costs of implementing each reinforcement scenario at current costs. (bottom) for future costs. Error bars represent 1σ around the mean overall cost.

BESS capital cost showed a large sensitivity to PV placement, with a cost range £0.15M-£0.29M for BESS 1.05 Tap 70% and £0.4m-£0.58m for BESS 1.05 Tap 90%. Furthermore, centralized BESS based control was not able to provide a solution in 48% of BESS 1.05 Tap 90% PV placement cases. It is therefore clear that examining only one renewable technology sizing and placement pattern is insufficient for network impact studies, and it is the statistical distribution of results across multiple placement scenarios that should be considered.

5.4 Discussion

The series of BESS placement, sizing and dispatch heuristics presented have been shown to provide an effective strategy with which to manage the operation of behind-the-meter BESSs such that network operational constraints and requirements are satisfied whilst self-consumption is maximized. It is however clear that, for the test feeder in question, reconductoring provides the more cost effective and compliant solution, even when potential self-consumption benefits are considered.

Misprediction in forecasting and minute ahead control results in less than 100% control of load voltages by ESQCR standards. Because some delay between evaluation of the current grid condition and application of new dispatch commands must exist in coordinated control schemes, it is unlikely that a coordinated BESS scheme could ever guarantee 100% control under current statute, making reconductoring the better option for compliance. However, both the reconductoring and BESS scheme would achieve 100% compliance with a statute change to EN 50160.

The reconductoring cost assumption of £80/m was made based on previous work (Crossland, 2014), and it is accepted that this value may vary with the specific nature of the task. However, the results suggest that reconductoring costs would need to increase by at least an order of magnitude to equal BESS costs, before data communication and customer incentive costs are even considered. It is also accepted that adjusting the system lifetime e.g. attempting to coordinate and operate the set of BESSs such that they last for 15 years, may affect results, though there is no way that the overall findings of the study could be altered by this change.

Whilst BESS requirements decrease with change in tap from 1.05 to 1.00, reconductoring requirements also decrease due to the reduction in potential for voltage violations, though this may not be the case for feeders with topologies that result in a higher susceptibility to utilization violations than voltage violations. Furthermore, significant load growth on the feeder (e.g. due to increased penetration of electric heating technologies), or the sharing of a SSS with a more heavily loaded feeder may devalue this strategy, as additional BESSs and reconductoring could be required to maintain steady state voltage above the lower limit. For this reason, the potential for tap position decreases on a series of full networks is examined in chapter 7.

The RIIO-ED1 electricity distribution price control document explains the obligation of DNOs to reduce network losses. Whilst the current mechanism does not provide an exact quantitative value of losses (i.e. in £/MWh), the DNO is required to report on activities conducive to loss reduction in order to be eligible for a losses discretionary reward (Ofgem, 2017). The document does not suggest how storage losses may be handled, making the results of this study somewhat ambiguous; BESS schemes reduced line losses but increased total losses in all scenarios, and It is therefore unclear as to whether BESSs may provide an economically beneficial loss reduction service. Regardless, the lowest line and total losses were always achieved in reconductoring schemes.

The notable cost differences between reinforcement methods suggest it is likely that partial reconductoring will offer a more cost effective route to voltage compliance than the BESS equivalent in the vast majority of short urban and suburban LV feeder cases. This is before non-optimal placement, reclamation of customer benefit, and system performance considerations are investigated, and before desired 3rd party profit margins and communications costs are defined – all of which will impact the cost of the BESS system negatively. Whilst additional revenue streams may arise in future (such as the sale of BESSs that are no longer suitable for the violation control scheme), it is unlikely that such revenue could offset the much greater capital cost of coordinated BESS control when compared to reconductoring. Similarly, an NPV calculation would typically be performed to assess the true cost/benefit of the two methods. However, even in the extreme case that reconductoring is paid for with upfront capital, BESSs capital cost and SC return benefits are split equally over time at a 7% discount rate (representative of current literature values (Balducci *et al.*, 2018; Chen, Wu and Xu, 2018)), and the BESS payback costs are subject to no loan interest, the overall cost of BESSs falls by only 1/3, which is nowhere near significant enough to change the conclusions of the work in this chapter. Therefore, whilst somewhat simplistic, the cost analysis is sufficient to show that coordinated BESS control is likely to remain the most expensive solution to violation issues.

Alternative approaches to centralized voltage control schemes may include fixed payments to customers with BESSs on the proviso that the 3rd party/DNO may take control of such BESSs for violation management when required. and the potential for use of stochastically located customer owned BESSs (see chapters 6 & 7).

5.5 Conclusion

This case study presents placement and sizing, forecasting, and dispatch heuristics for behind the meter BESSs such that violations are managed and self-consumption is maximized. The results of the heuristic are analysed from the perspective of a DNO whom pays for and installs BESSs, or pays a 3rd party to purchase, install and operate BESSs. The remaining system costs are compared to reconductoring costs, and it is clear in the case studied that reconductoring is the cheaper option in all modelled scenarios. The results suggest that a similar outcome is likely for most short urban feeder test cases, but it is unclear whether the same results may be obtained for longer feeders that would potentially require more reconductoring. Further work is therefore required to analyse the sensitivity of results to network topology, and to alternative BESS ownership and control models.

6 Utilization of stochastically located customer owned BESSs for violation management

6.1 Introduction

In the previous chapter, the feasibility of violation management via control of DNO/3rd party owned BESSs was investigated. The strategy was found to be economically ineffective in all tested scenarios, but the feasibility of BESS based violation management from a customer owned perspective was not addressed. To fully understand this situation, the assumption that BESSs may be placed at all residences must be discarded, and control takeover of pre-existing customer BESSs in non-optimal quantity and location must be investigated. Additionally, it is worth considering the potential for control of ASHP caused violations using BESSs, as recent sources suggest deployment of >1 million units by 2035 (National Grid, 2017).

Though studies considering BESS based management of network violations are relatively abundant in literature, only one known previous study has considered how a change in the number of, and location of, customer owned BESSs may affect the technical feasibility of control (Crossland, 2014), and in this case the outcome is assessed for only one PV & BESS configuration at each PV penetration and BESS availability level, and did not consider the issue of varying BESS availability patterns. Furthermore, the author assumes that the BESS may always charge at the full rated power of the array, which is very unlikely to be the case considering the energy capacity limitations of available home BESS systems. As a result, the extent to which customer owned BESS's may be used to mitigate LV network violations, is not yet fully understood. Furthermore, whilst every study considered PV generation, none appear to consider the effect of increased ASHP control on the feasibility of BESS based violation control.

In this chapter, the feasibility of applying centralized and decentralized BESS dispatch algorithms for voltage and line capacity violation control on two urban LV feeders is investigated. The models used represent the situation in which the DNO may optimally select specific BESSs from a set of available customer owned BESSs with the aim of eliminating violations. From the simulations, the effect of the BESS set size on the probability of finding

a feasible BESS solution at various ASHP and PV penetrations is determined. The likelihood of finding a reconductoring solution to violations is also considered, and where possible the cost of reconductoring is compared to the cost of implementing a BESS dispatch scheme.

This chapter reports on work to determine the extent to which BESS based control is feasible on LV networks, specifically where BESSs are static, customer owned systems, and are not necessarily present in the optimum quantity or locations. The secondary objective of the work is to gain a preliminary understanding of whether a customer BESS takeover scheme is likely to be able to compete economically with reconductoring.

6.2 Method

6.2.1 Terminology

To effectively communicate the work presented in this chapter, some additional terminology is required. This full extent of this terminology is described below;

PV Penetration - between 0 and 100%, representing the percentage of residences with a PV array. The array ratings are assigned probabilistically based on UK installation size data, that suggests 1%, 8%, 13%, 14%, 12%, and 37% of systems are sized 1.0, 1.5, 2.0, 2.5, 3.0, 3.5 and 4.0 kWp respectively (Navarro-Espinosa and Mancarella, 2014).

ASHP Penetration - between 0 and 100%, representing the percentage of residences with an ASHP system. ASHPs power ratings are based on physically modelled demand profiles developed in (Good *et al.*, 2013), where ASHPs serving radiator systems are rated at nominal 3 kW_e, and ASHPs serving underfloor heating systems (UHSs) are rated at nominal 2 kW_e.

BESS availability - The percentage of PV owners that also own a BESS that is sufficiently sized and in good enough condition for the takeover scheme, and are willing to allow takeover of their BESS. In this work, it is assumed that PV array owners are the only residents that can own BESSs, that all available BESSs are sized at 13.2 kWh (matching the Tesla Powerwall 2 home BESS (Tesla, 2016)), and that the BESSs are operated only within a SOC deviation range of 70% (in order to limit degradation, recommended by manufacturer).

PV/ASHP/BESS Placement Configuration – the specific location of each of the arrays/ASHPs/available BESS's e.g. at a PV penetration of 20% on a feeder with 75 residences, the entire set of PV placement configurations would represent every possible way to distribute the 15 arrays between 75 residences.

6.2.2 Simulation methodology

The formulations described in section 4.2 are used to assess the technical feasibility of managing PV & ASHP caused violations using both BESS takeover and reconductoring methods. Feasibility is considered at different technology penetrations; PV penetration, ASHP penetration, and BESS availability are varied between 0 and 100%, and coincidence of technologies is permitted (i.e. PV arrays, ASHP systems, and customer owned BESSs may exist on the network at the same time). 50 different PV & ASHP placement configurations are examined at each coinciding PV penetration, ASHP penetration, and BESS availability. 30 different placement configurations of customer BESSs are examined per PV & ASHP placement configuration, where the number of BESSs is dependent on the BESS availability. This is to account for the fact that in a customer owned BESS situation, the pattern of available BESSs may change over time for the following reasons;

- A resident's BESS degrades to the point that it is of no use to the scheme, and it is not replaced.
- A resident who owns an operational BESS opts in/out of the scheme.
- A resident purchases a BESS and opts into the scheme.

Which may affect the implementation costs and technical feasibility of a BESS solution.

For any given PV/ASHP/BESS placement configuration, technical feasibility of violation control is tested using 2 different BESS control algorithms for the PV case – centralized (see section 4.2.4.3) and feed-in-limiting (see section 4.2.4.2). Additionally, 2 different ASHP system types are considered – radiator and underfloor heating; the problem is solved using the formulation presented in section 4.2.2.3 regardless of ASHP system type, but ASHP nominal power is set to 3 kW in the former case and 2 kW in the latter, in accordance with the data provided by the University of Manchester (UoM).

The hierarchy of placement scenarios is show in figure 6.1. The particular penetration and availability levels are chosen so that the entire range of possible scenarios is covered at a granularity appropriate to the computational resources available.

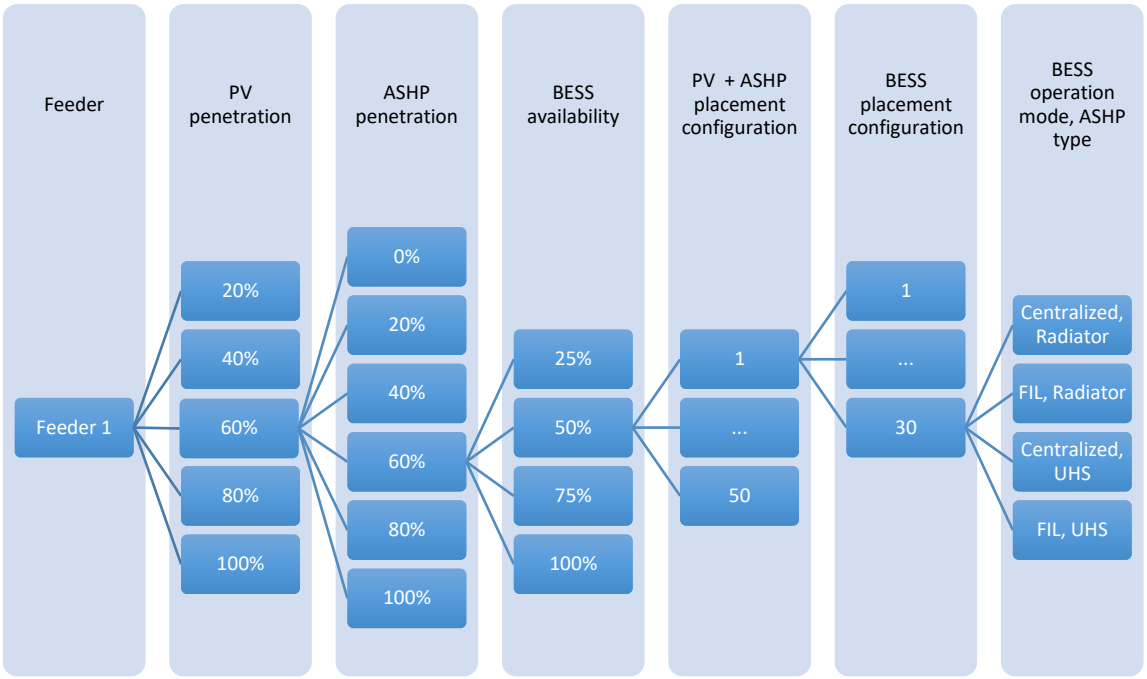

Figure 6.1 – A hierarchal diagram of all simulation scenarios explored during this work.

In the reconductoring case, the formulations described in sections 4.2.4.2 and 4.2.3.3 are used, together with same PV & ASHP placement configurations used in the BESS cases.

The entire process is performed on models of two urban feeders (Figure 6.2). The feeder models were developed during the University of Manchester's Low voltage networks solutions project, and represent real feeders located in the northwest of England. Feeder 1 serves 75 residences at a load density of 600 loads km^{-2}, whereas the much more heavily loaded Feeder 2 serves 186 residences at a load density of 2100 loads km^{-2}. Both feeders experience voltage violations at renewables penetrations < 50%, but feeder 2 is much more vulnerable to thermal congestion than feeder 1.

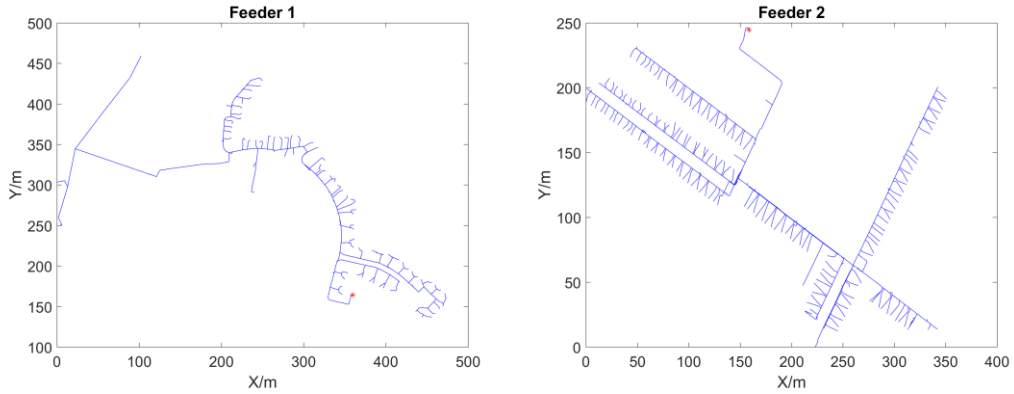

Figure 6.2 – Topology of the 2 feeders examined during this study. The location of the SSS is, in each case, marked with an asterisk.

The assumptions used in the optimization formulations, and cost values used for data analysis, are shown in table 6.1.

Parameter	*Value*	*Parameter*	*Value*
$\boldsymbol{SOC_{max}}$	13.5 kWh (9.45 kWh used)	$Recon.\,cable\ cost$	£100 m^{-1} (ENWL, 2016a; SSE, 2016)
$\boldsymbol{S^{inv}}$	5 kVA (Tesla, 2016)	$Service\ cable\ jointing$	£400 $Joint^{-1}$ (ENWL, 2016a)
$\boldsymbol{c_{Com}}$	£70	$Recon.\,cable\ size$	300mm^2 (ENWL, 2015)
$\boldsymbol{BESS\ CAPEX}$	£6500 (Solarguide, 2017)	$Recon.\,cable\ ampacity$	328 A (each Ø) (Siemens, 2005)
$\boldsymbol{c_{Inc}}$	£25	$Recon.\,cable\ R_1$	0.059 Ω km^{-1} (Navarro-Espinosa and Ochoa, 2015)
$\boldsymbol{Power\ factor}$	±0.85 (Tesla, 2016)	$Recon.\,cable\ X_1$	0.067 Ω km^{-1} (Navarro-Espinosa and Ochoa, 2015)
$\boldsymbol{Conductor\ L}$	25 y (Bahra Cables Company, 2011)	$Recon.\,cable\ R_0$	0.215 Ω km^{-1} (Navarro-Espinosa and Ochoa, 2015)
$\boldsymbol{EOL}$	0.7 (Tesla, 2016)	$Recon.\,cable\ X_0$	0.074 Ω km^{-1} (Navarro-Espinosa and Ochoa, 2015)

Table 6.1 – Shows the input parameters for all simulations performed.

6.2.3 Analysis methodology

If there is no feasible solution to violations for a particular BESS configuration, then the PV & ASHP configuration that it is associated with is considered unsuitable for control using BESSs. A PV & ASHP placement is only considered suitable for BESS control when the violations it produces can be consistently eliminated using BESS takeover strategies, regardless of the exact BESS configuration. It is important to understand that for any given model run, the existence of a solution for violation control in the PV generation case (using the models described in section 4.2.2.1 and section 4.2.2.2) is determined first, then the ASHP demand analogue is run with the same set of available BESSs. This allows determination of whether a network containing both technologies could cope with potential violations during both winter and summer months using a given set of BESSs.

The solution to the reconductoring problem (described in section 4.2.3.2) for every PV & ASHP placement configuration, at every simulated renewables penetration level, is then determined. If there is no standard reconductoring solution for a given configuration, then the parallel reconductoring model presented in section 4.2.3.3 is used. In some situations, even parallel reconductoring cannot provide a solution, and these instances are explored and discussed in sections 6.3.2 and 6.4.7.

Within each PV & ASHP penetration and BESS availability scenario, the number of PV & ASHP placements considered suitable for BESS control are counted, and this figure is reported as '% Success'. The same analysis is performed for reconductoring, though BESS availability is not a consideration in this case. For any PV & ASHP placement configurations suitable for BESS control that require > 0 BESSs, the cost of solving the same placement configuration with reconductoring is calculated, and the difference between the two costs is determined using equation (6.1),

$$\Delta c = \frac{\boldsymbol{c_{XRecon}}^T \boldsymbol{X}^{Recon}}{L^C} - c_{Inc} n_{S,PV} - (c_{Inc} + c_{Com}) n_{S,ASHP} \quad (6.1)$$

Where $n_{S,PV}$ and $n_{S,ASHP}$ are the average numbers of BESS takeovers required for control of PV & ASHP caused violations respectively, and it is assumed that L^C = 25 years. The values of c_{Inc} and c_{Com} are rationalized in section 6.2.4.

The resulting cost differentials are averaged and reported as 'Average Annualized Cost Differential'. A value > 0 suggests that takeover may be less expensive than reconductoring, whereas a value <0 suggests that reconductoring will likely be the cheaper option.

In the base case, FIL is assumed to be the dispatch algorithm, and ASHP compressors are sized at 3 kW_e to serve a radiator system. The sensitivity of the effectiveness of BESS control to a change from the FIL algorithm to the centralized dispatch algorithm in then examined, as is a change from 3 kW_e ASHPs serving radiators to 2 kW_e ASHPs serving underfloor heating systems. The sensitivity of economic feasibility to the changes in customer incentive, BESS system costs, degradation under the ASHP BESS control scheme, and conductor lifetime, is also considered.

6.2.4 Determination of customer incentive and penalty payments

In this chapter, it is assumed that that customers operate their BESSs using the self-consumption algorithm presented in section 4.2.4.1 until they are paid an incentive for takeover, at which point BESSs are operated using either the FIL algorithm (see section 4.2.4.2) the centralized algorithm (see section 4.2.4.3), or ASHP algorithm (discharge on demand during the day at a rate of 0.69 kW for underfloor heating systems and 0.74 kW for radiator systems, the recharge during the night), depending on the time of year and the specifics of the simulation scenario. To determine suitable values for takeover incentives, it is vital to consider whether the algorithms might reduce customer self-consumption or increase BESS degradation.

For the FIL algorithm, the cost of self-consumption decrease was determined by applying each of the self-consumption and FIL algorithms to a series of 180 day, 5 min resolution generation and demand time series. The self-consumption cost difference was then calculated using equation 6.2,

$$\Delta C_{SC} = -c_{kWh}\left[\sum_{t=1}^{n_t} \max\left(\{min\left(\{P_t^g + P_t^{s,FIL}, P_t^d\}\right), 0\}\right) - \sum_{t=1}^{n_t} \max\left(\{min\left(\{P_t^g + P_t^{s,SC}, P_t^d\}\right), 0\}\right)\right] \quad (6.2)$$

The BESS degradation associated with each algorithm was determined by applying the SOC series generated during the previous step to the degradation estimation model presented by Xu (Xu, Oudalov and Ulbig, 2016), with rain flow-counting tasks performed using (Nieslony, 2010). The cost to the customer associated with change in generation was then calculated using equation 6.3,

$$\Delta C_{DEG} = -c_{DEG}(D_{FIL} - D_{SC}) \quad (6.3)$$

Where c_{DEG} is the cost of 1 kWh of degradation,

$$c_{DEG} = \frac{c_{sys}}{\boldsymbol{SOC_{max}} \cdot (1 - EOL)} \quad (6.4)$$

The calculation was applied for PV array sizes between 1 kW_p and 4 kW_p. Results showed either a marginal increase or decrease in self-consumption (depending on array rating) (figure 6.3), and a significant decrease in degradation in all cases, which can be attributed to the lower average SOC experienced by each BESS in the FIL case. For this reason the assumption that switching from SC to FIL over months of high generation has no negative economic implications for the customer is made, and so the cost of takeover is assumed to be £25 per half annum (which is competitive with the annual takeover payment currently offered by MOIXA (Moixa, 2017b)).

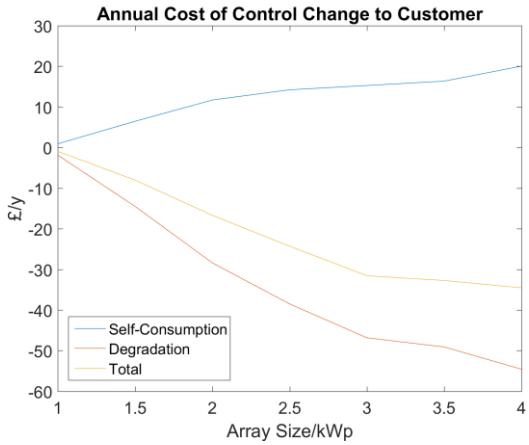

Figure 6.3 – Shows the effective cost to the customer resulting from reduced self-consumption and increased cell degradation with a change from the SC to FIL algorithm.

A comparison of the SC algorithm output to the output data from the optimal dispatch algorithm used in chapter 5 showed that the centralized algorithm generally decreases self-consumption by £6 - 10 per annum, but also reduces degradation at a value of £30 - 50 per annum. This results from both the lower average SOC and the more conservative charging behaviour the algorithm tends to exhibit. It is therefore assumed that a switch from the SC to centralized algorithm carries no negative financial implications to the customer.

A payment of £70 + £25 is made to any customer whom allows control takeover of their BESS's for ASHP demand limiting; this is equal to the additional degradation predicted for 3 months of cycling over the winter period (predicted using (Xu, Oudalov and Ulbig, 2016)), plus the half annum incentive.

Although the payments for takeover and the penalty payment for increased degradation in the ASHP case are reasoned, a lack of anecdotal real world data on the effectiveness of the cost incentive, and limited ASHP profile data means that both may vary from the chosen

values, and so the effects of a higher than expected incentive payment and a lower than expected BESS degradation on the economics of a BESS based control system are investigated section 6.4.

6.3 Results

6.3.1 Feeder 1

The BESS takeover algorithm provides a possibility of solution to violations at up to 80% PV penetration and 40% ASHP penetration, provided that every PV owner allows use of an adequate BESS. The maximum solvable PV penetration drops to 40% at 75% BESS availability (figure 6.4); this is because the likelihood of an effectively located BESS being available is lower, and the total number of BESSs is much lower. Below 50% BESS availability, solutions only exist where the solution requires no BESSs, and therefore the BESS takeover method is useless unless the majority of PV system owners offer access to an adequate BESS. The % success does not change between 0 → 20% ASHP penetration, and this is because BESSs are not required for management of ASHPs at these low penetrations. It is possible to solve one PV & ASHP configuration at 80% PV penetration. Inspecting this solvable configuration showed that PV systems were spread very evenly across phases (reducing thermal issues on unequally loaded phases), and concentrated at residences closer to the SSS (reducing voltage rise).

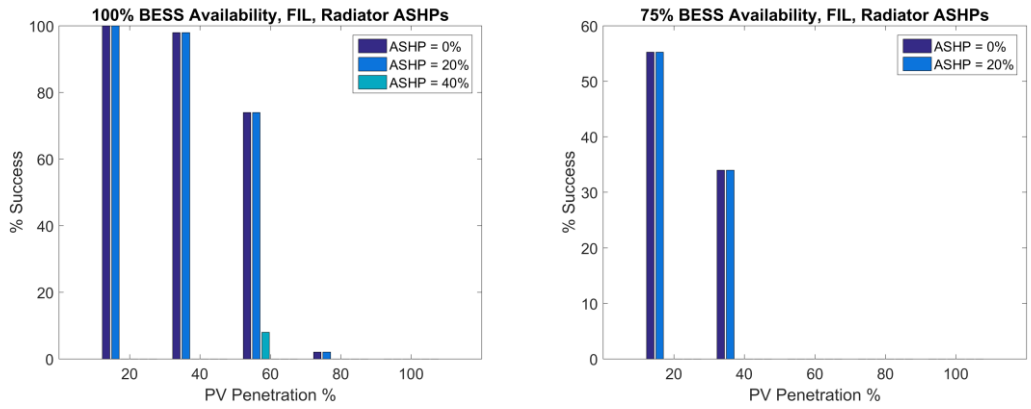

Figure 6.4 - Average % success of the FIL BESS solution on feeder 1, where ASHPs are sized 3 kW for radiator systems.

Considering the costs (Table 6.1), it appears that the takeover scheme is cheaper than the reconductoring alternative at low PV & ASHP penetrations (0 - 40%), suggesting that in a small set of circumstances the takeover scheme may provide an economically acceptable means to delay reconductoring figure 6.5. If a BESS solution is technically infeasible for all of

the placements tested within a given PV & ASHP penetration, the bar representing this penetration is absent.

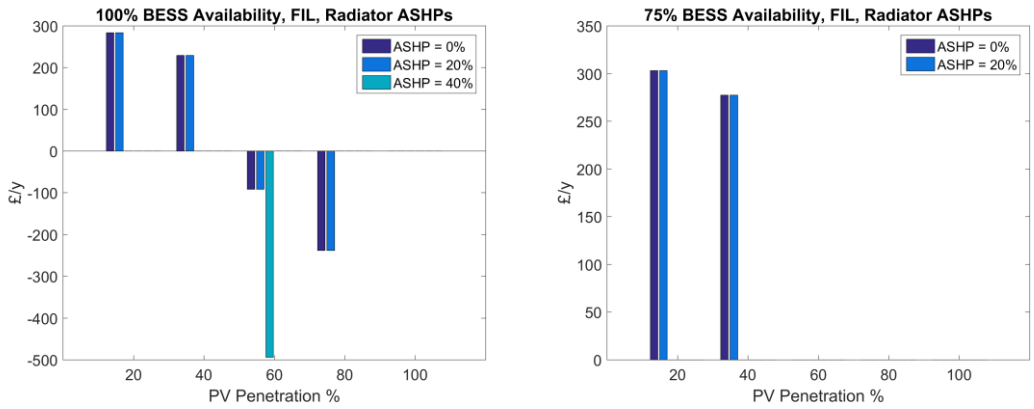

Figure 6.5 - Average annualized cost differential for feeder 1.

It is observed that reconductoring adequately mitigates voltage and ampacity violations at all PV & ASHP penetrations for 100% of simulations, and therefore parallel reconductoring never needs to be considered for this network.

Adopting a centralized BESS control approach increases the likelihood of finding a feasible BESSs solution at all BESS availabilities except 25% (Fig. 6.6). BESS control cannot solve violation problems at high renewable penetrations unless BESS availability exceeds 50%, suggesting that the BESS takeover method has limited scope with regards to this feeder. It should be noted that in the 100% availability case, and in various other scenarios presented in this study, the % success for ASHPs increases with increasing PV penetration, which may appear counterintuitive. This is because the number of available BESSs increases with PV penetration in any given % availability scenario, so the likelihood of these BESSs being located at the same site as an ASHP does also. Consequently, ASHP hosting capacity increases. Where BESS availability = 100%, it becomes possible to incorporate an 80% PV penetration in some cases.

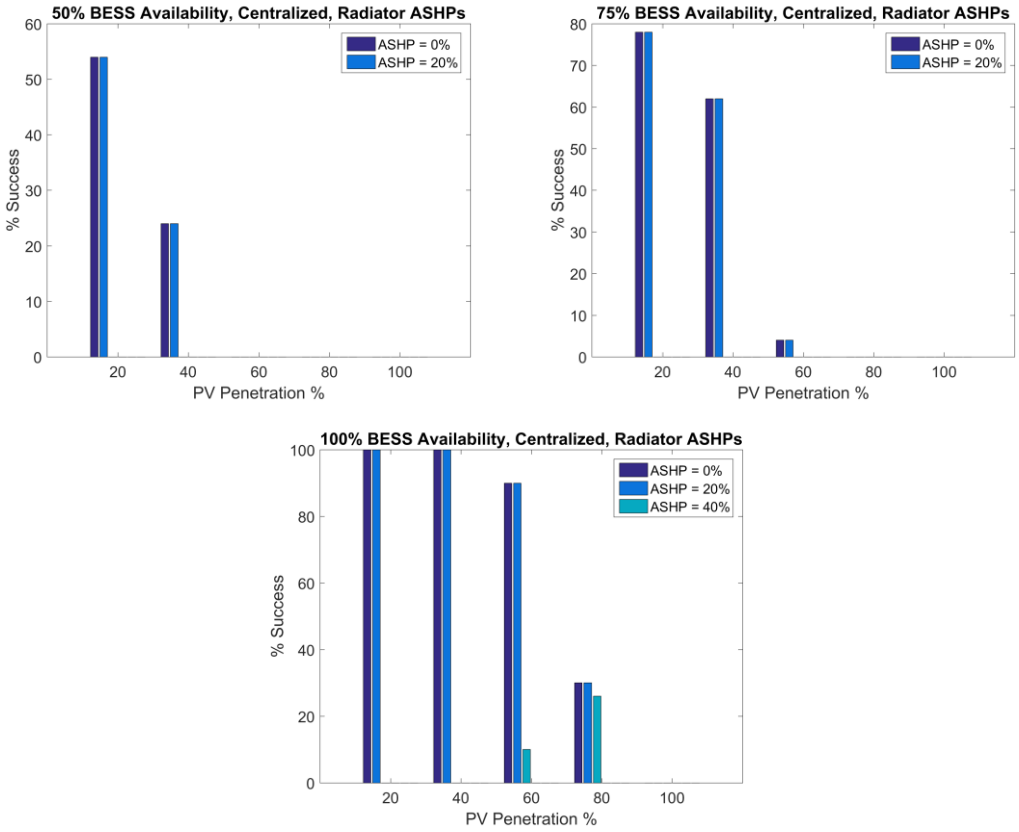

Figure 6.6 - Average % success of the Centralized BESS solution where ASHPs are sized at 3 kW for radiator systems on Feeder 1

Furthermore, the additional cost of monitoring equipment results in average annualized costs that exceed those from the reconductoring and the FIL operation method (Figure 6.7). This is before the costs of data communication and processing are considered, which may present a substantial additional cost. The economic viability of BESSs falls most notably in the PV Penetration = 20 & 40% scenarios when changing from FIL to Centralized control – this reduction is enough to cause reconductoring to become the more economically viable option in both cases.

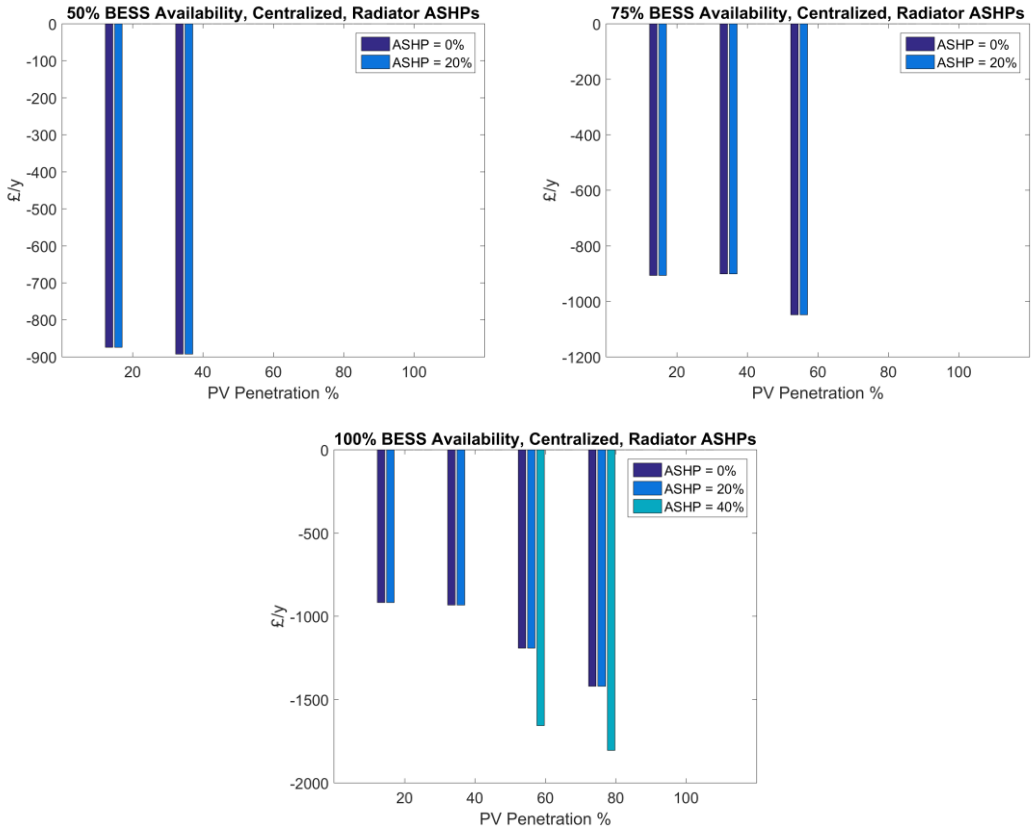

Figure 6.7 - Average annualized cost differential for PV & ASHP configurations in which the centralized BESS and ASHP BESS models are able to provide a solution to violations on Feeder 1. ASHPS are sized at 3 kW for radiators.

It can be seen from the fig. 6.7, that there is very no cost change between 0 → 20% ASHP penetration in all scenarios. This is because ASHP-caused violations do not emerge until 40% ASHP penetration, and so no reinforcement is required at lower penetrations. The cost change between 20 → 40% PV penetration is very small at all BESS availabilities – this is simply because the costs of BESS control and reconductoring are very similar in solvable 20% and 40% PV penetration scenarios.

6.3.2 Feeder 2

BESS FIL control was completely ineffective on the 186 residence feeder; the probability of the existence of a successful BESS takeover pattern exceeding 0 in only 5 scenarios (table 6.2), with control of ASHP violations failing above 20% penetration. Further investigation of the output data showed that a BESS takeover solution only exists in situations where the required BESS capacity equals zero, and fails wherever any violation is present. If control is

switched to centralized, the results are unchanging from the FIL case, which further highlights the limited scope for the BESS takeover method.

		BESS availability			
		25%	**50%**	**75%**	**100%**
PV penetration	**20%**	100	100	100	100
	40%	0	0	0	74

Table 6.2 - Shows the % likelihood that a PV placement scenario can be solved with a given BESS availability.

Reconductoring is always able to provide a solution to violations provided that the PV penetration ≤ 80%, and the ASHP penetration ≤ 60%, beyond this range reconductoring becomes less effective. This is entirely due to thermal congestion; even with parallel 300 mm^2 conductors, the maximum currents at PV penetration = 100% and ASHP penetration ≤ 80% can exceed the cable ratings (table 6.3).

		ASHP penetration					
		0%	**20%**	**40%**	**60%**	**80%**	**100%**
PV penetration	**20%**	100	100	100	100	32	0
	40%	100	100	100	100	32	0
	60%	100	100	100	100	32	0
	80%	100	100	100	100	32	0
	100%	36	36	36	36	12	0

Table 6.3 - Shows % success of reconductoring across all placement configurations at all tested PV & ASHP penetrations.

6.4 Sensitivity analysis

In this section, the sensitivity of the base case scenario (the scenario that uses parameters - FIL BESS control, 3kW ASHP, radiator systems, 25 year conductor lifetime, £6500 BESS cost, £25 incentive for takeover, £70 compensation for BESS degradation associated with operation for ASHP-caused violation management) to various system changes is investigated. Changes are made individually i.e. only one parameter (e.g. size of ASHP) is altered, and all other parameters remain the same as in the base case. The parameter changes, and justification for these changes (and their magnitudes), are summarised in table 6.4.

Parameter	*Change*	*Justification*
Heating Type/ASHP sizing	Radiators → UFH/3kW →2kW	Installing UFH systems allows a lower flow temperature, therefore a higher ASHP COP and the opportunity to reduce ASHP power capacity. Researchers at UoM deduced that a typical 3 kW ASHP serving a radiator system could be downsized to 2 kW if radiators were replaced with underfloor heating (Good, 2015). It is therefore important to examine how such a change could affect network functioning.
Conductor Lifetime	25y → 40y	Cable datasheets typically specify an expected lifetime. Warranty is usually 25 years, but it is noted in some literature that such cables can actually remain in service for 40 years (Bahra Cables Company, 2011; AEI, 2014).
BESS degradation	Full → Half	The data used to estimate the additional BESS degradation associated with ASHP demand limiting operation assumes a consistent fairly low temperature (≈0^{o}C). In reality, it is often not as cold as this for the entirety of a UK winter, and so the estimate is likely to be on the high side. Half degradation is chosen to see whether a rather extreme change actually affects the economics. This change could also be thought of as a halving of BESS cost, as the same amount of degradation will have half the economic impact.
Incentive Payment	£25 → £40	The £25 payment is based on the lower end of Moixa's Gridshare annual battery takeover fee (£50) (Moixa, 2017b). In this study the customer is paid £25 per 6 month period, so can earn the full £50 for a full year takeover. The upper limit on the fee is £80, and so the incentive increase in the sensitivity study has been adjusted to reflect this.

Table 6.4 – Justification for sensitivity study parameter changes.

6.4.1 Change to underfloor heating systems

The change to a lower power heating system allows an increase in maximum controllable ASHP penetration to 40% at 25% BESS availability, and 60% in some cases for higher BESS availabilities. In all cases of ASHP penetration ≤ 40%, the % success does not change between penetration levels, and this is because ASHP systems require no control at penetrations ≤ 40%, and require at least one BESSs for control at 60% penetration. There is never a feasible BESS control solution where ASHP penetration reaches 80%. Where PV is no greater than 40%, BESSs takeover is typically cheaper than reconductoring where feasible (figure 6.9), though a BESS solution is never guaranteed below 100% BESS availability.

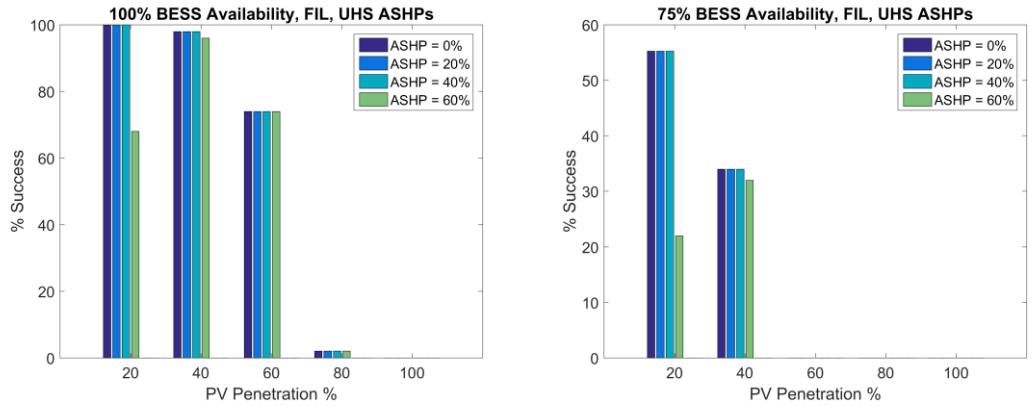

Figure 6.8 - Average % success of the FIL BESS solution where ASHPs are sized at 2 kW for UHSs on feeder 1.

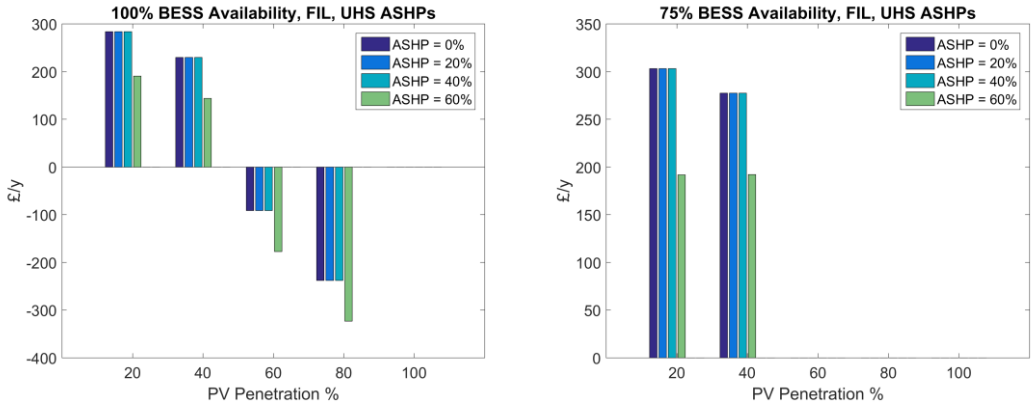

Figure 6.9 - Average annualized cost differential for PV & ASHP configurations in which the FIL BESS and ASHP BESS models are able to provide a solution to violations on network 1, where the ASHPS are sized at 2 kW for UHSs.

6.4.2 40 year reconductoring lifetime

The 25 year conductor lifetime assumption is fairly conservative, and so it is important to consider how the average annualized cost differentials may change if conductors are assumed to last for a longer period of time. Whist the economic advantages of the BESS solution become more marginal, the BESS solution still proves cheaper than the reconductoring solution at PV & ASHP penetrations ≤ 20%, provided that BESS availability is very high (figure 6.10).

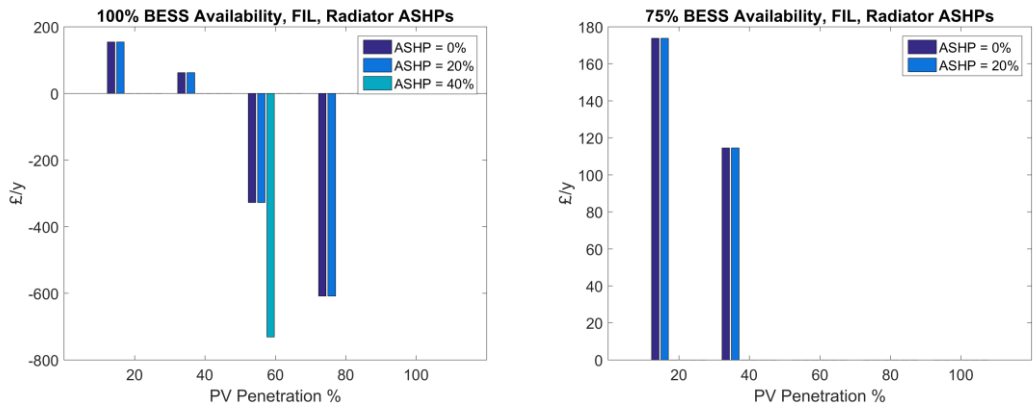

Figure 6.10 - Average annualized cost differentials for Feeder 1. A conductor lifetime of 40 years is assumed.

6.4.3 Half expected BESS degradation/half BESS system cost

A halved system cost or ½ BESS degradation rate (and therefore ½ the penalty payment) has a small negative effect on differential costs at PV penetration = 60% and ASHP penetration = 20%, with average cost reduction of £150 per annum. This small reduction results from a reduced compensation payment to an average of 4 customers. At any other PV penetration, ASHP penetration, or BESS availability below 100%, BESS control of ASHP-caused violations is either unrequired or impossible, so this change has no effect.

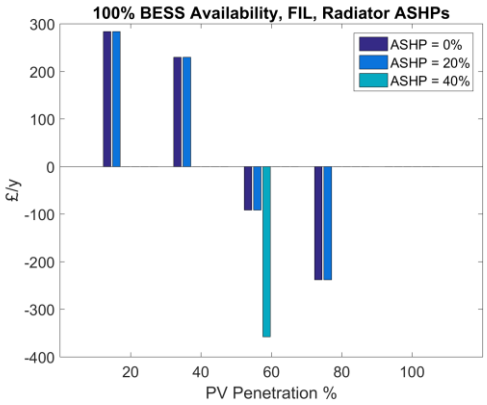

Figure 6.11 - Average annualized cost differentials for PV & ASHP configurations in which the FIL BESS and ASHP BESS models are able to provide a solution to violations on network 1, and half the expected BESS degradation under ASHP demand limiting operation is assumed.

6.4.4 Increase in customer incentive payment

If a higher incentive of £40 is assumed (which reflects the higher end of Moixas proposed takeover incentive (Moixa, 2017b)), the cost effectiveness of BESSs takeover falls to become only slightly more cost effective than reconductoring at PV penetration = 40%, BESS takeover is still the most cost effective option at PV penetration = 20% (figure 6.12), though violations only occurred in 4% of simulations at this penetration level.

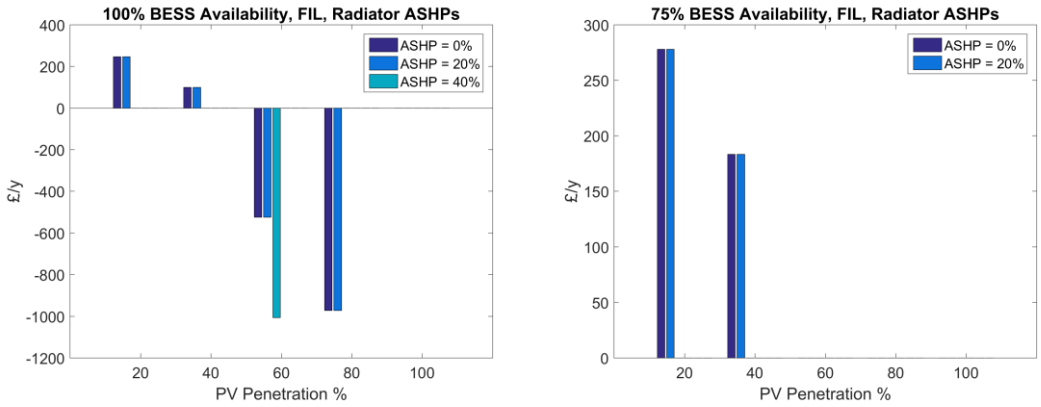

Figure 6.12 - Average annualized cost differentials for PV & ASHP configurations in which the FIL BESS and ASHP BESS models are able to provide a solution to violations on Network 1, and an incentive cost increase from £25 - £40 is assumed.

6.4.5 Change in ASHP sizing requirements

The work presented so far has used ASHP compressor demand profiles from UoM datasets, which were developed under assumptions about house insulation levels and age based on their knowledge of their outward appearance. If properties are indeed older/less well insulated than expected, larger ASHPs may be required. Data from BRE and Clearly Heat Pump Systems (BRE, 2018) suggests pre 1970's properties could require ASHPs > 4 kW_e, and so it is important to consider the sensitivity of the networks to higher heating requirements. An investigation into how the need for ASHPs with kW_e ratings between 4 → 6 increases solution costs/reduces success % has therefore been performed (where 6 kW_e represents the requirements of a pre 1900s terrace house served by a pump operating at COP ≈ 2, $T_{in\text{-}out}$ = 24 °C).

If parallel reconductoring is allowed only along the feeder head segment, reconductoring is unreliable for feeder 1 where 6 kW_e ASHPs are required, though the technique is robust enough to eliminate violations when ASHP electrical demand ≤ 5 kW_e (fig. 6.13). Furthermore, BESS control fails wherever reinforcement is required to manage violations if ASHP compressor demand ≥ 4 kW_e, and this always occurs at ASHP penetration ≤ 20%.

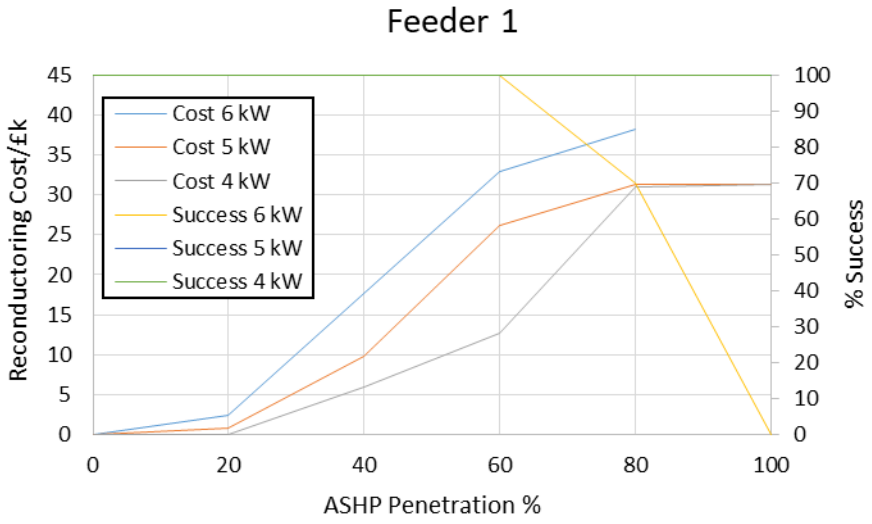

Figure 6.13 – Shows average reconductoring cost and probability of violation elimination at different ASHP penetrations for feeder 1. Parallel reconductoring is allowed along the head stretch of the feeder only (≈ the first 80 – 100 m).

Where ASHP compressor demand = 6 kW_e, and parallel reconductoring is allowed along the entire main stretch of the feeder, reconductoring provides a solution on feeder 1 at all ASHP penetrations ≤ 80%, though is not sufficient for control at 100% penetration.

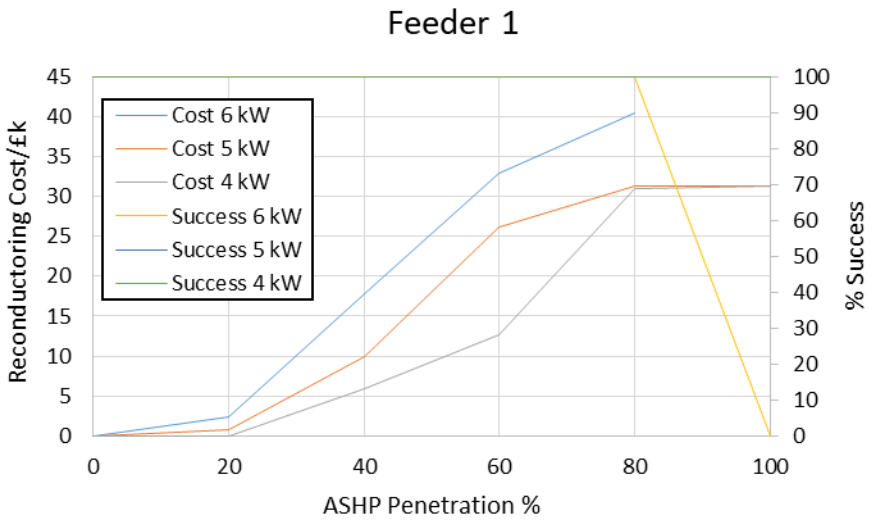

Figure 6.14 – Shows average reconductoring cost and probability of violation elimination at different ASHP penetrations for feeder 1, where parallel reconductoring is allowed.

The observation that reconductoring cannot always eliminate violations under the stresses caused by large ASHP systems suggests that

1. Building age and extent of retrofit may determine the extent to which ASHP systems can be integrated into electricity distribution systems.
2. The extent to which thermal energy storage, hybrid ASHP/Boiler systems, and existing storage heaters may aid in integration of ASHPs requires further investigation.

6.4.6 Feeder 2 sensitivity

If it is assumed that all ASHPs are 2 kW_e and serve underfloor heating, results are unchanging from the base scenario. It is not possible to assess sensitivity of results to cost on this network, because no solutions to violations involve BESS control. However, the reduced ASHP nominal power results in approximately $\frac{1}{3}$ current flow reduction on the main portion of the feeder, and the congestion problem can now be solved at ASHP penetration = 100% (table 6.5).

		ASHP penetration					
		0%	**20%**	**40%**	**60%**	**80%**	**100%**
PV penetration	**20%**	100	100	100	100	100	100
	40%	100	100	100	100	100	100
	60%	100	100	100	100	100	100
	80%	100	100	100	100	100	100
	100%	36	36	36	36	36	36

Table 6.5 - Shows % success of reconductoring across all placement configurations at all tested PV & ASHP penetrations in the case of underfloor, 2 kW ASHP systems

Where larger ASHP sizes are considered, If parallel reconductoring is allowed only along the feeder head segment, reconductoring fails above ASHP penetration = 20% at all compressor powers (fig. 6.15).

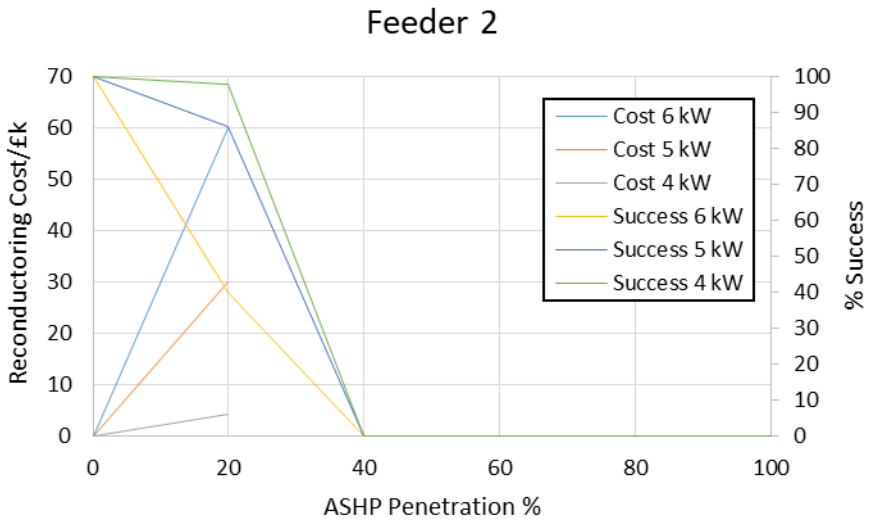

Figure 6.15 – Shows average reconductoring cost and probability of violation elimination at different ASHP penetrations for feeder 2. Parallel reconductoring is allowed along the head stretch of the feeder only (≈ the first 80 – 100 m).

Where parallel reconductoring is allowed across the entire run of the main feeder, the maximum ASHP hosting capacity varies with compressor demand, and reconductoring in never a reliable reinforcement strategy at any ASHP penetration > 40% (fig. 6.16)

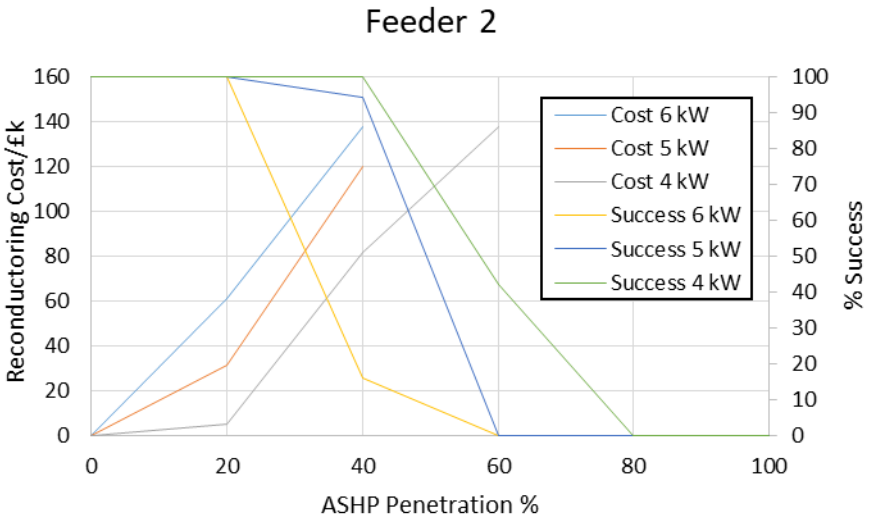

Figure 6.16 – Shows average reconductoring cost and probability of violation elimination at different ASHP penetrations for feeder 2, where parallel reconductoring is allowed.

Whilst static home BESS systems alone are of limited use in customer takeover schemes for network 2, it is possible that electric vehicles batteries may provide greater feasibility as a result of their larger energy and power capacities. To demonstrate, the BESS takeover model was applied to network 2, and the energy and charging capacities of all BESSs were altered to 30 kWh/7 kW (representative of the charging capacity and the energy capacity of a Nissan Leaf, or around half the energy capacity of a tesla model S (Battery University, 2018). Results are shown in table 6.6.

ASHP Penetration (UHS)

		20%	**40%**	**60%**	**80%**	**100%**
BESS availability	**25%**	100	100	0	0	0
	50%	100	100	0	0	0
	75%	100	100	100	0	0
	100%	100	100	100	100	100

ASHP Penetration (Radiator)

		20%	**40%**	**60%**	**80%**	**100%**
BESS availability	**25%**	100	0	0	0	0
	50%	100	0	0	0	0
	75%	100	0	0	0	0
	100%	100	100	0	0	0

Table 6.6 – Shows the % success of BESS takeover on the 186 resident feeders examined in chapter 6, when BESS specs are adjusted to those of a typical modern EV. (top) shows % success when it is assumed that the ASHP serves a UHS system, and (bottom) shows % success when it is assumed that the ASHP serves a radiator system.

Clearly, in the ideal situations that vehicles remain entirely static, some improvements could be achieved, however, the above results are flawed due to BESS availability issues, which are discussed in section 6.5.

6.4.7 NPV Calculations

The results presented in this chapter so far have assumed pro rata inflation and discount rates, and thus no discount is applied to BESS takeover payments in any given year. However, it is common to apply a rate of 7% to BESS projects (Balducci *et al.*, 2018; Chen, Wu and Xu, 2018). Applying this to all scenarios resulted in a significant change in only 3. These were:

- Base case, 100% BESS availability
- Half expected BESS degradation, 100% BESS availability
- Increase in customer incentive payment, 100% BESS availability

In the base case, at 100% BESS availability, BESSs become the most economically feasible at all PV penetrations, including those ≥ 60% (which was not the case without the NPV discount) (fig. 6.17).

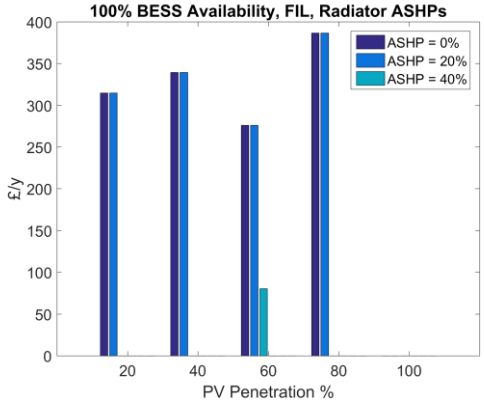

Figure 6.17 - *Average annualized cost differential for feeder 1 in the base case, at 100% BESS Availability, and with a 7% discount rates on BESS payments.*

The same change is seen in the 'Half expected BESS degradation/half BESS cost' scenario (fig. 6.18).

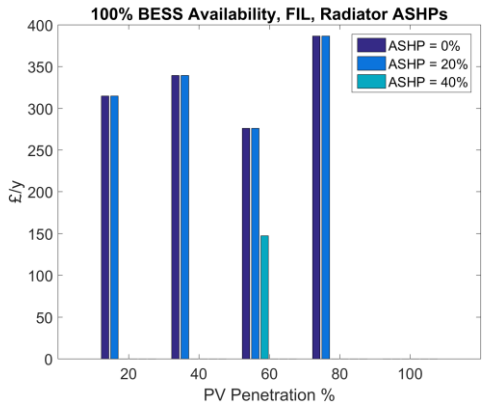

Figure 6.18 - *Average annualized cost differential for feeder 1 in the half expected BESS degradation/half BESS cost case, at 100% BESS Availability, and with a 7% discount rates on BESS payments.*

In the 'increase in customer incentive' case, BESSs become the least expensive way to manage violations wherever ASHP penetration ≤ 20% (fig. 6.19). Without the NPV, reconductoring was the least expensive at all PV penetrations ≤ 60%.

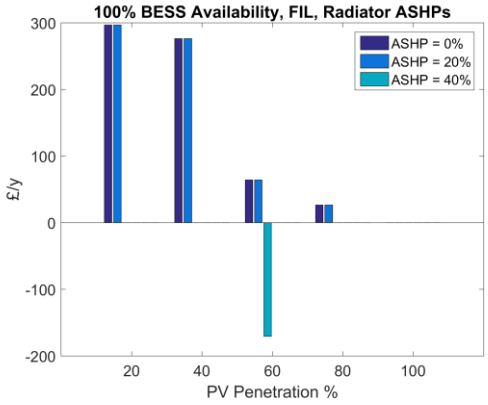

Figure 6.19 - *Average annualized cost differential for feeder 1 in the increase in customer incentive case, at 100% BESS Availability, and with a 7% discount rates on BESS payments.*

6.5 Discussion

The relative ineffectiveness of BESS control in the ASHP case (when compared to PV generation case) can be rationalized by considering required operating times; BESS's may only need to operate for 2 hours to limit export during peak generation, whereas a cold day may require BESS operation for over 12 hours to limit ASHP demand. To ensure the BESS does not prematurely reach minimum SOC, it must discharge at a much lower power than it charges in the PV case, thus limiting the efficacy of BESS control. Additionally, where BESS availability is below 100%, it is often seen that the existence of a BESS and ASHP at the same residence does not coincide, and therefore the demand of a fraction of the ASHPs cannot be reduced.

As mentioned previously, in the ideal situation that vehicles remain static, some improvements is the ASHP management case could be achieved. However, the EV BESS results are an overestimation of the technologies suitability to LV network management because:

- To manage violations of any kind, the BESS must be present. It is obvious that a customers EV will sometimes be elsewhere whilst a renewable technology is operating (this is particularly true in the case of PV, as generation occurs during most homeowners working hours). It is therefore possible that such a scheme would fail technically as a result of low BESS availability, or require the DNO to pay for much more capacity than would ideally be required. The presence or absence of a BESS during any given time period would probably have to be approximated using agent based modelling.
- For an EV battery to be of use in a PV management scheme, the battery would be required to begin any generation period at a lower than ideal SOC, which could cause transportation issues for some customers. The prospect of increasing the risk of reaching 0% SOC may be sufficient to put off those that would otherwise wish to be involved in such a scheme.
- The additional cycling wear on the EV battery could significantly shorten its life, at a high cost to the customer. This would need to be considered, and may impact the economic feasibility of such a scheme.

Furthermore, only marginal improvements are seen when ASHPs have a power capacity of 3 kW_e or greater, and so it appears that the effectiveness of EV battery storage for violation management on LV networks is likely to be very limited.

Though the results suggest that long term control using customer owned BESSs is not likely to be possible in any realistic scenario (and therefore it would be unwise to plan for this), if violations were occurring on an LV network, the DNO may be able to implement a BESS takeover scheme temporarily (provided that the configuration of PV, ASHPs, and available BESS's allows a BESS solution) to delay the need to reinforce– though this would require a very high incidence of available BESSs and a suitable network topology.

A change from the FIL to centralized algorithm increases the likelihood of a feasible solution at BESS availability percentages of 50% upwards, though no positive effect is observed at 25% availability. It is therefore clear that a high BESSs availability is required for any a benefit to emerge from an increase in algorithm complexity on feeder 1. On feeder 2, neither the FIL or centralized algorithms successfully increase the renewable hosting capacity of the network. This is a result of the low ampacity headroom at the feeder head in relation to the number of loads it serves; feeder 2 must serve 2.4 times the loads that feeder 1 must, with only 1.2 times the feeder head ampacity, and thus suffers thermal congestion issues at much lower renewables penetrations.

The current work considers the control of violations caused only by typical on-off cycle heat pump systems. However, there is a strong possibility that inverter driven variable capacity ASHPs will become the dominant technology in future. Because there is no available demand data for variable speed domestic ASHP, their inclusion is considered beyond the scope this thesis. However, it is unlikely that this will change the outcome more than slightly, as variable ASHP systems still consume considerable power for the majority of heating periods during cold days (such systems are still only 10 - 15% more efficient than fixed speed systems during heating periods (Adhikari *et al.*, 2012; Son, 2017)).

6.6 Conclusion

The work presented in this chapter has explored the feasibility of optimal customer owned BESS takeover for the prevention of voltage and line ampacity violations. The formulations expand on previous work in the field by allowing low BESS uptake and non-ideal location of technologies i.e. the approach better approximates the non-optimal ownership conditions that may occur on future LV networks.

It has been shown that, assuming a competitive customer incentive payment, the BESS solution could be less expensive than the reconductoring alternative in some low PV & ASHP penetration situations. However, violations could never be prevented on the 186 load network using BESSs, a BESS solution could not be guaranteed at any particular renewable penetration level on the 75 load network, and the reliability of BESS control fell substantially in all instances that BESS availability fell below 100%.

The results of this work suggest it is reasonable to conclude that BESSs are unsuited to managing ASHP caused network violations. Although it does not appear that behind-the-meter BESS control can be consistently relied upon to delay reconductoring requirements in the PV case, the presented analysis considers only 2 feeders. It is therefore important to consider the possibility that BESS control viability may vary with network topology, and this is addressed in chapter 7.

7. BESSs for management of LV network operational violations: A multi-feeder analysis

7.1. Introduction

While previous chapters focussed on specific feeders, it is important to examine how the feasibility of BESS based violation control and traditional reconductoring violation control extends to LV networks in general. By doing so, the extent to which reconductoring may be delayed using BESSs can be predicted, the utility of both reinforcement methods can be quantitatively compared. Therefore, in this chapter 29 different feeders (making up 6 networks) are analysed using the same centralized and decentralized takeover models used in chapter 6 (but from the perspective of PV-caused violation management only). The work then involves analysing their suitability to BESS and reconductoring violation control methods, and the extent of asset takeover/replacement required to sufficiently reduce violations on each network. The trends between the violation control capability of each method and a set of feeder topology metrics are then examined, to determine whether the suitability of networks to violation management strategies may be predicted from easy to obtain metrics, rather than extensive power flow modelling.

7.2 Method

7.2.1 Generation of raw output data

Using the BESS optimal takeover models (presented in 4.2.2.1 and 4.2.2.2), and the reconductoring models (presented in 4.2.3.2 and 4.2.3.3), the % of PV/BESS placement configurations at which each method is capable of eliminating network violations at PV penetrations of 0%, 20%, 40%, 60%, 80%, 100% and BESS availability of 25%, 50% , 75%, and 100% is determined. The number of BESS takeovers required for violation elimination for each solvable PV/BESS placement configuration (if the placement configuration has a solution) is also recorded, as is the reconductoring cost for violation elimination (for solvable configurations). As in chapter 6, 50 different PV placement configurations are assessed at each PV penetration. Within each PV placement configuration, 30 BESS placement configurations are tested, to account for the fact that in a customer owned BESS situation, the pattern of available BESSs may change over time.

The models are applied to 29 feeders across 7 UK LV networks located in the northwest of England, which were chosen for their range of different topological properties (shown in fig. 7.1). Feeder models were obtained from the UoM dataset (Navarro-Espinosa and Ochoa, 2015). Power flow simulations are performed using openDSS, the optimization uses the MIQCP and MILP functionality of IBM CPLEX, and data communications and processing tasks are performed in MATLAB. As stated in chapter 6, because the optimization stage utilizes linear approximations of non-linear sensitivities, the problem is solved iteratively until there is no change in the value of optimization output variables. It is assumed that any BESS owner owns a BESS with properties identical to those of the Tesla Powerwall 2 system (Solarguide, 2017), and that PV array systems are limited to 50% peak output by BESSs in the FIL control situation, for the reasons discussed in section 4.2.4.2.

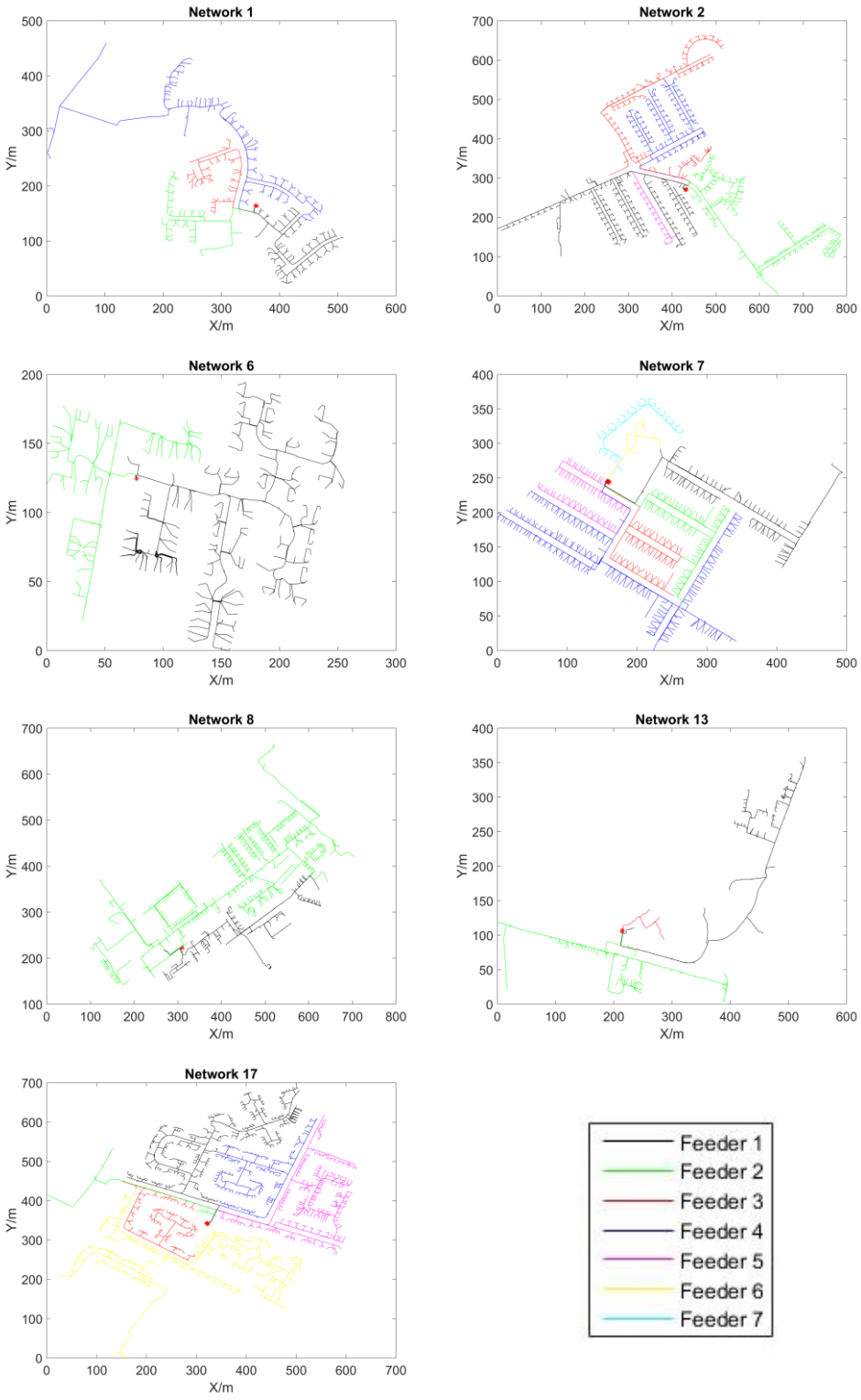

Fig. 7.1 – Topology of each of the 7 networks examined (feeders 1-7 shown in colour order black, green, red, blue, magenta, yellow, cyan).

7.2.2 Data processing & nomenclature

The following terms are used as shorthand throughout this chapter,

- PV penetration – percentage of residences who have a PV array installed on the rooftop of their property.
- BESS availability - percentage of PV array owners who also own BESS systems.
- PV/BESS configuration – the specific location of each of the PV arrays/available BESSs
- FIL – Feed-in-limiting control – BESSs charges when PV generation exceeds a threshold (details in chapter 4.2.4.2).
- Centralized - the set of BESSs are controlled as an ensemble, based on network voltages, line ampacities, present BESS SOCs and predicted BESS SOCs, with the aim of minimising total charging power (details in 4.2.4.3).
- Solvable – Implies that a solution exists to the violation elimination problem (e.g. 'solvable placement configuration' means that the violations caused by this specific PV configuration are technically solvable by either takeover of BESSs or reconductoring, dependent on which technology is being considered).

The following output metrics are defined, and are used to assess success of violation control and the extent of required reinforcement.

- Specific feeder BESS control % (SFBC%) - The percentage of simulated PV placement configurations that are solvable using BESS takeover methods, at a given PV penetration and BESS availability.
- Full set BESS control % (FSBC%) - The percentage of simulated feeders that achieve a SFBC% ≥ 95% at a given PV penetration and BESS availability.
- Specific feeder reconductoring elimination % (SFRE%) - The percentage of simulated PV placement configurations that are solvable using reconductoring, at a given PV penetration and BESS availability.
- Full set reconductoring elimination % (FSRE%)- The percentage of simulated feeders that achieve a SFRE% ≥ 95% at a given PV penetration and BESS availability.
- Specific feeder reconductoring cost (SFRC) – estimated average cost of reconductoring a specific feeder at any given PV penetration, calculated by determining the cost of reconductoring in each solvable PV placement configuration,

and taking an average of the results. This considers only solvable placement configurations, and so it is possible for a feeder to have a low SFRC but also have a low SFRE% (i.e. only be solvable for a few PV/BESS placement configurations), so it is important to consider both metrics.

- Specific feeder BESS takeover number (SFBTN) – estimated average number of BESSs that would need to be taken over (either using FIL or centralized control) to control violations on a specific feeder at any given PV penetration and BESS availability. Calculated by determining the number of required BESS takeovers at each tested PV and BESS configuration, and taking the average of the results. This considers only solvable placement configurations, and so it is possible for a feeder to have a low SFBTN but only be solvable in 1 PV/BESS placement configuration (i.e. SFBC% is low), so it is important to consider both metrics.
- Full set incremental reconductoring cost (FSIRC) – The average cost of reconductoring per weighted percentage of feeders at any given PV penetration and BESS availability. This is calculated by dividing the total cost of reconductoring all solvable feeders in a given set of 29 placement configurations (one for each feeder) by the weighted percentage of solvable feeders (feeders are weighted based on their load count). This is repeated for 50 sets of placement configurations and the average is taken.
- Full set incremental BESS takeover cost (FSIBTC) – The average cost of applying the BESS takeover method per weighted percentage of feeders at any given PV penetration and BESS availability. This is calculated by dividing the total cost of reconductoring all solvable feeders in a given set of 29 placement configurations (one for each feeder) by the weighted percentage of solvable feeders (feeders are weighted based on their load count). This is repeated for 50 sets of placement configurations and the average is taken.

Full set BESS control %, FSRE%, FSIRC, and FSIBTC are determined at all PV penetrations and BESS availabilities. The correlation between the output metrics SFBC%, SFRE%, SFRC, and SFBTN, and a set of topological metrics, are examined. This allows determination of whether the technical feasibility and cost of BESS or reconductoring based violation management may be adequately approximated without the need for detailed simulation. Furthermore, all BESS takeover output metrics are evaluated from both the

centralized and FIL based control perspectives. The following topological metrics are considered:

- Load count – The total number of residences served by the feeder
- Convex area – Total area of the feeders' convex hull (km^2)
- Convex load density – Ratio of load count to convex area
- Feeder head loading – The ratio of number of loads to the feeder head capacity (in kVA).
- Mean path resistance – Average resistance between residence and the SSS.
- Total resistance – Sum of resistances of the entire feeder (i.e. laterals and service cables included).
- Main path resistance – Resistance of the main length of the feeder (i.e. laterals excluded)
- Mean path length – Average cable length between residence and the SSS.
- Total length – Total length of the entire feeder (i.e. laterals and service cables included).
- Main path length – Length of the main length of the feeder (i.e. laterals and service cables excluded)

The values of these metrics are shown in table 7.1.

	Load Count (loads)	*Convex Load Density (loads/km²)*	*Convex Area (km²)*	*Feeder Load (loads/kW)*	*Mean Path Length (m)*	*Total length (km)*	*Main Path Length (m)*	*Mean path R (Ω)*	*Total R (Ω)*	*Main Path R (Ω)*
1F1	55	4070	0.013	1.61	171	1.43	296	0.077	1.12	0.11
1F2	31	1929	0.016	0.91	197	0.94	274	0.090	0.71	0.16
1F3	39	3618	0.010	1.14	194	0.91	291	0.095	1.17	0.13
1F4	75	905	0.082	1.38	249	2.56	551	0.11	2.00	0.19
2F1	175	2585	0.067	1.94	285	5.20	488	0.069	3.62	0.08
2F2	142	2276	0.062	2.63	361	3.61	390	0.09	2.53	0.06
2F3	112	1504	0.074	1.13	398	2.76	495	0.088	1.86	0.11
2F4	115	3414	0.033	1.21	491	2.66	493	0.139	1.81	0.11
2F5	23	1593	0.014	0.24	268	0.73	358	0.051	0.29	0.07
6F1	117	4348	0.026	1.23	167	3.15	205	0.05	2.63	0.06
6F2	54	4356	0.012	0.57	117	1.26	136	0.034	0.98	0.02
7F1	71	2071	0.034	1.69	283	1.71	501	0.1	1.48	0.28
7F2	58	3802	0.015	0.93	203	1.42	321	0.049	0.66	0.07
7F3	50	5055	0.0098	0.81	181	1.10	263	0.04	0.40	0.05
7F4	186	3279	0.056	2.06	305	4.19	456	0.058	1.90	0.09
7F5	61	8468	0.0072	0.64	117	1.06	242	0.029	0.56	0.05
7F6	23	7453	0.0030	0.33	113	0.40	118	0.037	0.35	0.03
7F7	22	2699	0.0081	0.31	155	0.55	224	0.049	0.46	0.05
8F1	52	1142	0.0454	0.55	266	2.28	405	0.057	1.84	0.06
8F2	302	1878	0.1607	3.18	395	10.23	791	0.07	6.84	0.010
13F1	46	1060	0.0433	0.48	451	1.52	473	0.077	1.44	0.08
13F2	37	1158	0.0319	0.59	168	1.59	249	0.041	1.10	0.05
13F3	2	1121	0.0017	0.02	88	0.15	112	0.02	0.03	0.02
17F1	188	2865	0.0656	1.98	393	4.36	584	0.075	3.30	0.07
17F2	8	247	0.0323	0.08	115	1.43	453	0.028	0.31	0.09
17F3	78	3431	0.0227	0.82	429	1.84	504	0.081	0.99	0.06
17F4	106	3177	0.0333	1.12	374	2.30	417	0.079	1.59	0.05
17F5	159	2781	0.0571	1.67	342	4.05	457	0.067	2.53	0.08
17F6	223	1746	0.1276	2.35	285	5.65	419	0.069	3.54	0.08

Table 7.1 – Values of topological metrics for each of the studied feeders.

7.3 Results

7.3.1 FSBC%/FSRE% and costs

In the centralized control context, BESS control is feasible for 80% of networks at PV penetrations ≤ 40%. However, at BESS availability = 50%, control % is only slightly higher than the no reinforcement case (i.e. BESS takeover is of little use in the majority of situations), and at BESS availability = 25%, control % is nearly equal to the no reinforcement case (i.e. BESS takeover is never useful for violation control). No BESS availability < 75% results in a significant control % improvement at PV penetrations ≥ 80% (figure 7.2). When considering control in the FIL context, results are almost identical to those seen in the centralized case at BESS availability = 50%, and 25%. However, technical feasibility falls at all PV penetrations where BESS availability = 75% if the control strategy is switched from centralized to FIL. When BESS availability < 100% and PV penetrations ≥ 80%, no control % improvement is seen over the base case (BESS availability = 0%) at BESS availabilitys = 75%, 50% and 25% (figure 7.2).

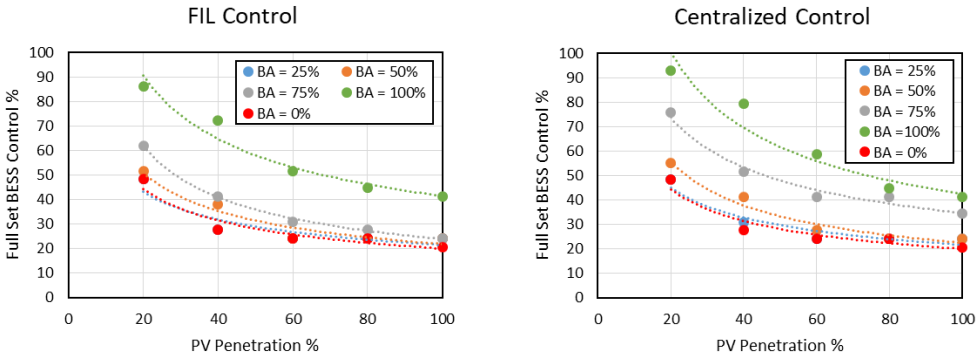

Figure 7.2 – (left) shows FSBC % at every tested BESS availability and PV penetration *in the FIL control case (right) the same for the centralized control case.*

FSRE% is much greater than FSBC% at all PV penetrations (figure 7.3), achieving violation elimination in >95% of placement configurations on almost 100% of networks up to PV penetration = 60%. It is also worth noting that there was no placement configuration on any network whose violations could be controlled exclusively using BESS's (i.e. if a BESS solution existed, a reconductoring solution existed too).

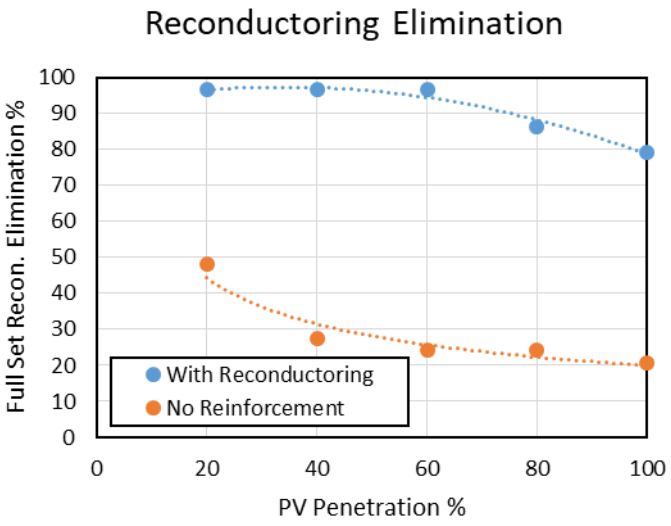

Fig. 7.3 – Shows full set reconductoring elimination % and the no reinforcement case.

FSIRC increases slightly from 0 to £0.4k/% between PV penetrations 0% → 20%; this is because networks never require any reinforcement when no PV is present, but some of the larger feeders (namely n1f4, n2f2, n2f3, n2f4, n7f1, n8f2) require slight reconductoring (figure 7.4). The FSIRC values then increase linearly. This is because as PV penetration increases each solvable network requires a greater amount of reconductoring to prevent violations.

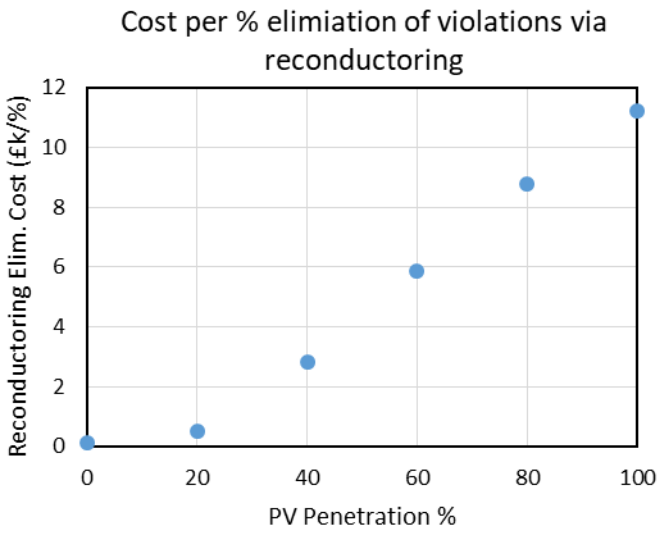

Figure 7.4 – FSIRC as a function of PV penetration.

While the above plot provides an expression for the cost of reconductoring, it cannot be directly compared to a similar plot for BESS costs; BESS's can only be used to eliminate

violations on shorter, smaller networks, or networks with oversized conductors (i.e. networks where the ratio of total cost of reconductoring for violation elimination to number of loads is low). Conversely, reconductoring can be used to handle expensive to eliminate violations (i.e. eliminate violations on networks where the ratio of total cost of reconductoring to number of loads is high). The result is a falsely reduced FSIBTC relative to FSIRC.

To allow a fair comparison, the FSIBTC and FSIRC are presented only for the feeders that can be solved using either technologies (figure 7.5). This means that when BESS availability = 100% and PV penetration = 100%, the violation elimination costs per % of customers are considered for only 42% of all residences (see figure 7.2). The £25/customer payments suggested in table 6.1 for BESS takeover over the 6 month period April - September (violations are rarely seen on these networks at any PV penetration during winter months) are assumed, and reconductoring costs are adjusted to reflect a conductor lifetime of 25 years (Bahra Cables Company, 2011), so that cost can be compared from an annualized perspective. It is also important to note that the same discount rate of 7% (used in chapter 6) is applied here.

The annualized cost of reconductoring in the base case (25 year conductor lifetime, £25 per customer cost for 6 months BESS takeover) is clearly greater than the cost of BESS alternatives (fig. 7.5).

In the centralized case, the annualized reconductoring cost is again greater than the annualized BESS takeover cost (fig. 7.5). However this does not consider any monitoring, data communications, or processing costs, and the addition of 1 voltage monitor priced at current monitoring costs and lifetimes (SP Energy, 2015), would be sufficient to make reconductoring the most economically effective long term measure.

FSIBTC and FSIRC increase with increasing BESS availability in both cases because the number of networks with high violation elimination costs per customer that fall into the solvable set of networks increases.

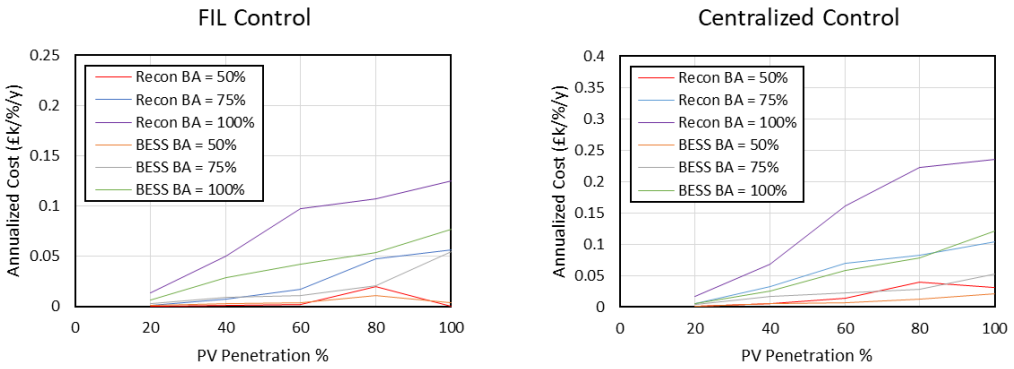

Figure 7.5 – Annualized FSIRC and FSIBTC as a function of PV penetration and BESS availability, considering only the feeders that (left) are solvable using FIL control (right) are solvable using centralized control. Takeover payment = £25, reconductoring lifetime = 25 years.

The sensitivity of the results to higher customer payments (£40 per half annum) and longer conductor lifetimes (40 years) is also considered. This represents a possible realistic scenario in which the economics are less favourable towards BESS management strategies. In this case, the cost difference between options becomes negligible at the majority of PV penetrations and BESS availabilities, regardless of the BESS control strategy, and regardless of the presence or absence of monitoring and data communications and processing costs (figure 7.6).

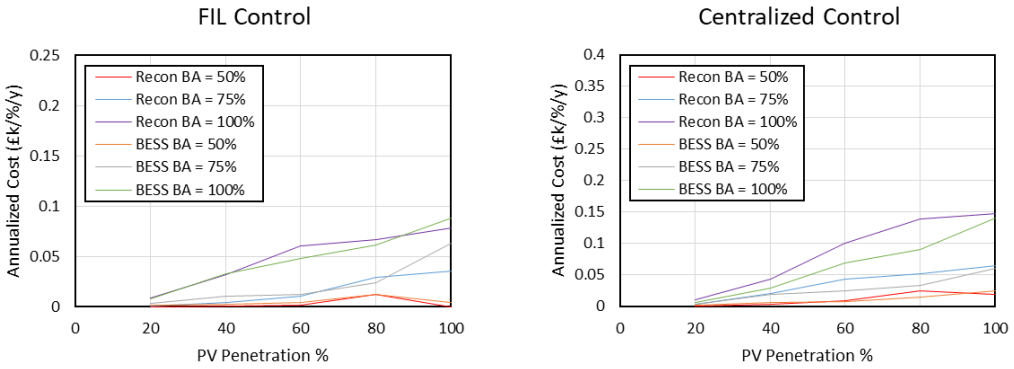

Figure 7.6 – Annualized FSIRC and FSIBTC as a function of PV penetration and BESS availability, considering only the feeders that (left) are solvable using FIL control (right) are solvable using centralized control. Takeover payment = £40, reconductoring lifetime = 40 years.

As many of the networks experience voltage violations before ampacity violations, it was seen as necessary to consider the effect of reducing the tap position at SSSs from 1.05 p.u.

to either 1.025 p.u. or 1.0 p.u. where possible. Of the 29 feeders examined, only 9 could host any reduction in tap position; most violated the lower voltage limit during high demand periods in this instance. FSBC% was improved in all decreased tap scenarios, though the presence of BESSs at an availability level <50% resulted in no rise of FSBC% above the base case (figure 7.7).

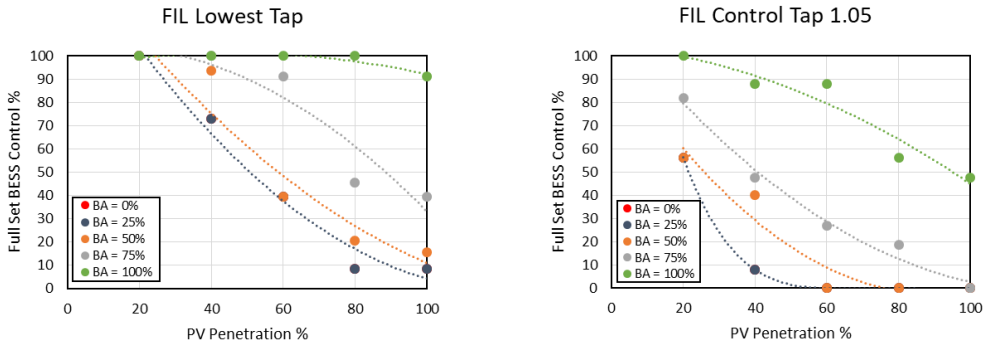

Figure 7.7 – (left) FSBC% vs PV penetration for the 9 feeders that can operate at lower tap positions, in their lower tap positions (left), and results for the same feeders in tap position 1.05 p.u. (right).

7.3.2 Specific Feeder Control/Elimination %, Takeover Counts, and Costs

Unfortunately, no correlation strong enough to be represented by regression could be found between SFBC% and any of the metrics listed in table 7.1 (e.g. figure 7.8). The same was true when comparing SFRE% to all metrics, though it was noticed that reconductoring could almost always eliminate violations for networks with Load Count < 50 (figure 7.8). This phenomena can be explained by the binary nature of SFBC% and SFRE%; both the BESS control and reconductoring solutions have a tendency to be able to solve either almost all placement configurations of a given network, PV penetration and BESS availability, or almost none (in fact only 16% of points on figure 7.8 fall between 5% - 95% success).

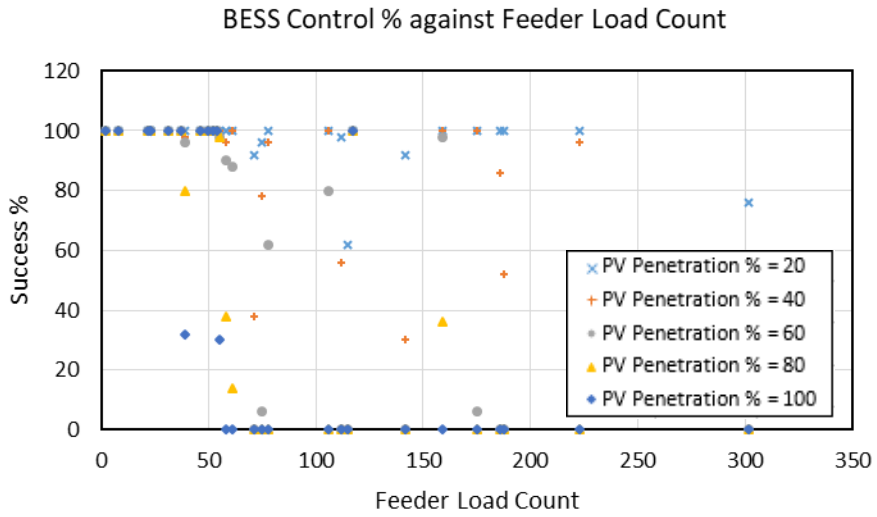

Figure 7.8 example of specific feeder control % vs topological metric

However, it was clear from the results that the analysis in section 7.3.1 (FSBC% at different PV penetrations/BESS availabilities) could be performed across different bands of topology metrics to give different distributions (e.g. 0 - 100m mean path, 101 - 200m mean path). Though this cannot be analysed reliably with only 29 feeders, it may be worth further investigation.

To calculate the corellation between SFBTN and any given topological metric, SFBTN is plotted against the topological metric at each PV penetration and BESS availability scenario, the R^2 for each scenario is extracted, and the average is determined. This is repeated for all topological metrics discussed in section 7.2.1 , and the results are shown in table 7.2. The

correlation between SFRC and any given metric is calculated in much the same way, though different BESS availability scenarios do not need to be considered.

Whilst some topolgical metrics result in little or no correlation, load count, feeder loading ratio, total length, and total resistance all show a fair positive correlation. Perhaps surprisingly, the topological metric that results in the greatest correlation is load count, which is also the easiest of the examined metrics to obtain. This is most likely due to the fact that a high load count usually suggests a long network with high peak ampacity (therefore greatest potential for feeder head overload and voltage rise at the end of feeder branches). A negative R^2 is seen between the output metrics and convex load density, which suggests that the load density has no implications for network operation.

Topological metric	*Average R^2 (recon)*	*Average R^2 (FIL)*	*Average R^2 (centralized)*
Load count	0.58	0.56	0.58
Convex load density	-0.18	-0.02	-0.16
Convex area	0.47	0.38	0.44
Feeder loading ratio	0.45	0.49	0.46
Mean path length	0.26	0.16	0.23
Total length	0.55	0.46	0.53
Main path length	0.28	0.17	0.27
Mean path resistance	0.12	0.14	0.15
Total resistance	0.47	0.43	0.46
Main path resistance	-0.04	0.03	0

Table 7.2 – The average R^2 value for SFBTN (centralized), SFBTN (FIL) and SFRC, when plotted against each of the topological input metrics.

When the R^2 values for SFRC vs. load count are examined separately, rather than as an average over all PV penetrations, it can be seen that the correlation is stronger at higher PV penetrations (figure 7.9), which is likely due to the fact that many networks require no reinforcement at low PV penetrations, and thus costs remain at zero, rather than progressing along a trend. A similar effect is seen for both the centralized (figure 7.10) and FIL (figure 7.11) contexts of SFBTN vs load count, and this trend persists at lower BESS availabilities.

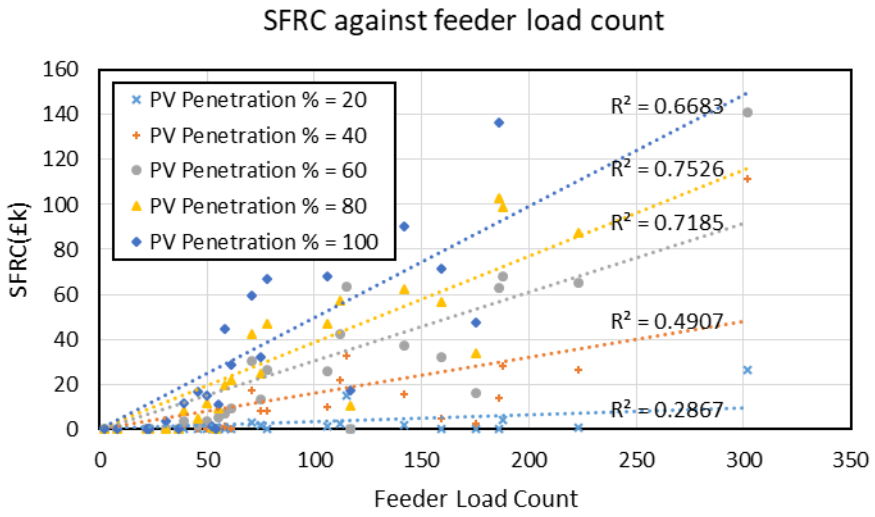

Figure 7.9 – SFRC against load count.

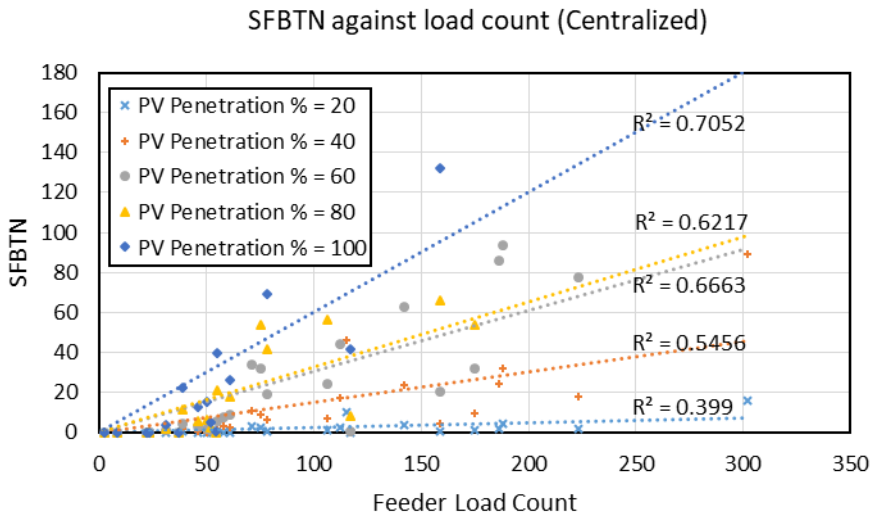

Figure 7.10 – SFBTN (Centralized) against load count. Shown at BESS availability = 100%.

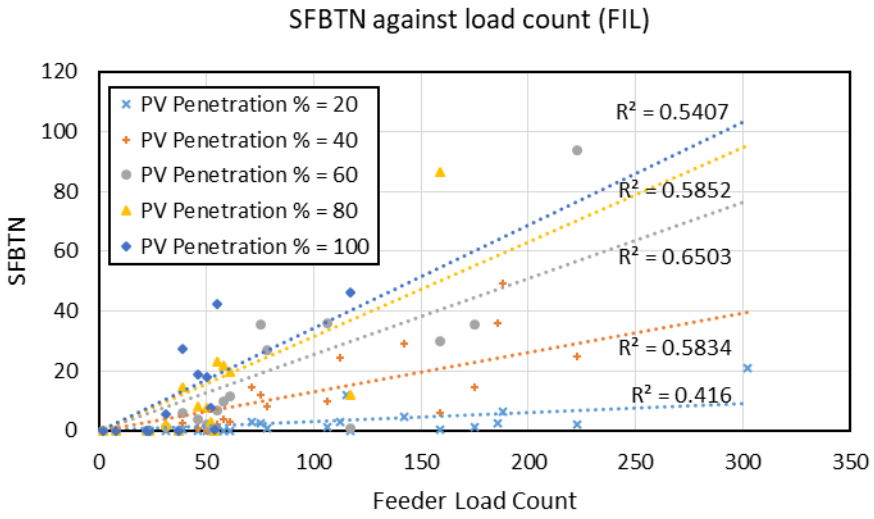

Figure 7.11 – SFBTN (FIL) against load count. Shown at BESS availability = 100%.

7.4 Discussion

The FSBC% analysis provides an insight into the fraction of LV networks that could benefit from the use of BESSs to defer traditional reinforcement, as a function of PV penetration and availability of behind-the-meter BESS systems. However, due to the extensive resources required to run the simulations it has only been possible to analyse a small number of feeders. It is hoped that in future a wider scale analysis will be possible, so that the reproducibility and generality of the observed trends can be confirmed.

The full set cost analysis showed that the annualized cost of reconductoring was greater than that required for BESS takeover using FIL control in the 25 year conductor lifetime, £25/BESS takeover case, and that there was little difference in the 40 year conductor lifetime, £40/BESS takeover scenario. It is therefore likely the FIL method would ultimately be cheaper than early partial reconductoring in many cases, and it would likely be faster to implement, require a smaller workforce (if any), and carry a much lower initial CAPEX. However, the full set control % analysis showed that instances in which FIL based BESS takeover can provide a solution to violations are rare when BESS availability = 0 - 50%, even at low PV penetrations. This supports the observation from chapter 5, that a high incidence of customer BESSs would need to be available to make a takeover scheme viable. Furthermore, even at higher BESS availabilities, slight changes in PV and BESS placement configuration were seen to alter the technical feasibility of BESS control on many feeders, and so in these cases it may not be

possible to rely on BESSs for long term control due to possible changes in PV penetration and BESS ownership and availability patterns.

In the centralized case, the likelihood of finding a feeder that can be solved consistently across PV placement configurations is slightly higher than in the FIL case. However, with monitoring and data processing taken into account, the cost will always exceed reconductoring costs. Furthermore, purchase and installation of monitoring and data communications equipment is likely to require significant capital and skilled labour, so may not provide the short term reinforcement CAPEX benefits that a decentralized control approach may.

Though analysis of a larger set of networks would be required to fully confirm the trends observed between SFBTN and load count, or SFRC and load count, it is unlikely that any single topological measure could provide an adequate predictor of reinforcement costs at lower PV penetrations (as very low correlations are seen at PV penetration < 40%), though correlations at high PV penetrations could be adequate for estimation of potential future reinforcement costs on specific feeders and networks.

This work assumes that all feeder are individual instances of high PV penetration i.e. all other feeders in the LV network have low or zero PV penetration. If the work were extended to include all networks, effects of SSS overloading would need to be considered. Furthermore the work could be extended to model an entire 11 kV feeder of 400V secondary networks with high PV penetrations, in which case voltage rises and ampacity along the 11 kV feeder would come into importance. Whilst these changes would affect results, it is overwhelmingly likely that they would further reduce the technical feasibility of both reconductoring and BESS control. Therefore, it is felt that the work presented in this chapter adequately shows that technical limitations will significantly affect the feasibility of BESS takeover type control on LV networks.

7.5 Conclusion

In this chapter, the technical feasibility of BESS based and reconductoring based violation control and elimination has been analysed across 29 feeders, for the purpose of assessing the feasibility of utilizing customer owned BESSs for violation management and reconductoring delay. Though results suggest that a BESS takeover scheme may be economically feasible in some cases, the technical feasibility of such a scheme is rarely guaranteed, requiring BESS availabilities > 50% for solvability to become common. Therefore, it appears that whist BESS control may be useful on certain networks for short term deferral of reconductoring, BESSs should not be relied on to provide long term control of violations.

8. Conclusions

8.1 Economic Viability of BESS control

A major aim of the work presented to answer the following research questions:

- Are the costs associated with deploying behind-the-meter BESSs for the purpose of violation control enough to the cost of reconductoring, such that BESS control could be considered as a means to delay reconductoring if necessary? How does cost vary when switching between a DNO/3rd party owned perspective and a customer owned perspective?
- Is increased self-consumption a potential additional revenue in the instance that BESSs are controlling for violation control?
- Are BESS systems technically and economically suited to control of violations caused by ASHP systems?

In chapter 5, the costs associated with DNO/3rd party BESS installation and control were explored. The results were analysed from the perspective of both present day and future system costs, varied PV penetration between 50% – 90%, and assumed control via the centralized algorithm presented in section 4.2.4.3. BESS cost results were then compared to reconductoring costs. Whilst it is undeniable that uncertainties exist in the costs and lifetime estimates (e.g. cost per meter of reconductoring, BESS lifetime, conductor lifetime), the order of magnitude cost difference between reconductoring solutions and BESS solutions seen in all future cost scenarios shows conclusively that 3rd party owned BESS systems cannot provide an economically feasible LV network management solution. This conclusion is further supported by the omission of data communication and processing costs in the results – whilst these could not be estimated, they could only possibly have a negative effect on the affordability of the BESS solution.

Whilst the self-consumption benefit was not insignificant, it did not prove to be a large enough revenue stream to overcome the capital costs of BESS systems to the DNO. Furthermore, the work assumed 100% DNO/3rd party reclaim of any self-consumption benefits to the customer, which in reality would provide no incentive for the customer to

allow installation of a DNO/3rd party owned BESS on their property, and thus reclaim would have to be lower than this.

In chapter 6, the costing problem was examined from the perspective of DNO takeover of customer owned BESSs, for control of both PV and ASHP-caused violation. In the case of decentralized FIL based BESS operation, the difference between reconductoring and BESS control could not be defined conclusively (i.e. neither technology appeared substantially more expensive than the other in most scenarios), though the result was somewhat sensitive to predicted conductor lifetime and takeover cost (assuming a 40 year conductor lifetime or an increased takeover cost resulted in reconductoring being the most cost effective solution), and in some instances the choice of discount rate has a significant enough effect to alter which technology is the most cost effective. Therefore, if planning such a project, the choice of discount rate should be carefully considered. In the case of centralized control, reconductoring always provided the cheaper solution, as the cost savings resulting from the reduced number of BESSs were outweighed by monitor costs. This was without the additional costs of data communication hardware, communication service costs, data processing hardware and software, and system maintenance – all of which will add to expenses When repeated for 29 feeders in chapter 7, results were similar, suggesting that FIL BESS control costs are generally the lowest, and centralized BESS control costs are usually the highest.

It is therefore reasonable to conclude that DNO/3rd party owned BESS schemes for LV violation management are economically infeasible, but that takeover schemes (utilizing FIL type control) can be economically feasible in many instances.

8.2 Technical Viability of BESS control

The work presented addresses the gaps in our understanding of the technical barriers that limit the effectiveness of BESSs as violation control devices. These gaps were addressed using following research questions:

- Are there technical barriers to the use of BESSs for violation control, when ideal and non-ideal BESS ownership and availability patterns occur?
- Are BESS systems technically suited to control of violations caused by ASHP systems?
- How does technical feasibility of BESS based violation control vary with feeder topology?

- Does control algorithm complexity affect the technical suitability of BESSs to management of voltage and thermal violations on LV feeders?

In chapter 5, DNO/3rd party ownership, placement, and control of BESSs was assumed, and whilst BESS control was always technically feasible at PV penetrations of 50% and 70% for the network examined, feasibility could not be guaranteed at 90% penetration and tap position = 1.05. Conversely, technical feasibility could be guaranteed in all scenarios where reconductoring was used as the violation control method.

Chapters 6 and 7 showed that customer BESS takeover schemes were technically unreliable across a range of feeder topologies; the existence of a technically feasible BESS solution to PV-caused violations was rarely guaranteed for any network at any PV penetration exceeding 40%, even in the instance that all PV array owners provided access to a BESS. Furthermore, the incidence of feasible solutions dropped substantially when BESS availabilities were reduced to values below 100%. Modest technical reliability gains were achieved by switching to the centralized scheme from the FIL scheme, but in no instances were these significant enough to make BESS based management reliable if it was already unreliable under the FIL scheme.

Is it therefore concluded that unless the DNO is able to access or place BESSs at any residence desired, the likelihood of finding a static BESS based solution to violations under high PV penetration is far too low for this type of reinforcement to be considered as a serious option in future network planning. This contradicts the findings in the majority of current literature, and the reasons for this are as follows,

- Studies that assume a balanced network are not able to account for single phase PV penetrations that are greater in magnitude that the overall penetration (Giannitrapani *et al.*, 2015, 2017; Bucciarelli *et al.*, 2016; Fortenbacher, Zellner and Andersson, 2016) e.g. if each phase hosts 25 residences, and the overall feeder PV penetration is 20% (i.e. 15 PV systems) it is technically possible that all systems are on one phase, and thus that phase experiences voltage rises that would require a 60% penetration in the balanced scenario. In practice, none of the PV placement configurations explored in this thesis were imbalanced to this extent, but were imbalanced enough for this phenomena to be significant.
- The work in this thesis considered the effect of BESS location changes over time, which may occur due to customers adding/removing BESSs, or entering/leaving a

takeover scheme. This consideration was enough to notably alter results, but other studies that considered multiple placements did not account for this (Crossland, 2014; Procopiou, 2017). In addition, some studies only considered one placement (Ranaweera and Midtgard, 2016; Hilton, Cruden and Kent, 2017).

- Some studies only considered (relatively) low PV penetrations that would not usually cause significant violations on UK LV feeders (Marra, Fawzy and Bulo, 2012; Marra *et al.*, 2014; Ranaweera and Midtgard, 2016; Hilton, Cruden and Kent, 2017), and thus overestimated the applicability of BESS based violation management.
- Certain studies assumed infinite BESS capacity, or at least unrealistically high energy and power characteristics for a domestic BESS (Crossland, 2014; Fortenbacher, Zellner and Andersson, 2016), and therefore overestimated the capabilities of BESSs.
- Studies often assumed that all PV systems had an associated BESS, which is likely an overestimate of BESS availability (Fortenbacher, Andersson and Mathieu, 2015; Lamberti *et al.*, 2015, 2017). The work in this thesis showed that removal of this assumption could drastically alter the technical feasibility of BESS based violation management.
- The networks chosen in some studies were to short and of service to too few loads (and therefore too resilient to violations) to show significant voltage and thermal violations (Marra *et al.*, 2014; Fortenbacher, Zellner and Andersson, 2016; Ranaweera and Midtgard, 2016; Fortenbacher, Mathieu and Andersson, 2017; Giannitrapani *et al.*, 2017). In the UK, feeders can often be 5-10 larger (from a length and load count perspective) than those presented in these studies.

Furthermore, BESS takeover was ineffective for control of ASHP-caused violations.

Whilst the reconductoring method could not always provide a solution, it was significantly more reliable for all networks at most PV & ASHP penetrations.

8.3 Topology

The work documented in chapter 7 aimed to address the research question:

- How does technical and economic feasibility of BESS based violation control vary with feeder topology?

Unfortunately no correlation could be found between any feeder topology metrics and the likelihood of that either reinforcement strategy could provide a solution to PV-caused violations. Moderate correlations were found between the output metrics reconductoring cost and SFBTN, and the input metrics load count, feeder loading ratio, and total length. It was noticed that technical feasibility metric may exhibit some trend with input metrics if the output were arranged in statistical bins, though it was not possible to process enough data to confirm the existence of such trends; performing the BESS and reconductoring study on any given feeder typically took >250 times longer than a renewables impact study, and it was therefore not possible to examine every feeder available to us. Future work may therefore aim to examine a larger set of feeders and determine whether such a trend does indeed exist. Furthermore, topological metrics were examined individually (e.g. SFBTN was compared to total path length, then to total path resistance *etc.*), but a linear combination of topological metrics (e.g. compare SFBTN to 0.5 x total path length + 0.5 x total path resistance) may result in a much stronger trends. This study would require a linear/non-linear least squares optimisation function, and analysis of a significantly greater number of feeders. Therefore it was not possible to perform with the time and computational resources available.

8.4 Future Work

Whilst BESS takeover was proven unreliable as a standalone technique, it has not yet been determined whether a combination of reconductoring, tap changing, and BESS control could provide a more economically feasible solution to network management than redesign – particularly in cases where reconductoring alone could not provide a solution. Furthermore, it is entirely possible that in future, grid operations may rely on a much greater quantity of storage to supply sufficient balancing and ancillary services – in such instances, the exact location of storage may not matter from a technical perspective, but the aggregation of customer owned BESSs into virtual power plants (VPPs) may allow provision of such services. In this case, it may be possible to operate BESSs in a mode that also reduces network stresses and barely affects potential P2P schemes. In this instance, it may become sensible for BESS subsidies to be offered to PV array owners on certain heavily loaded feeders that cannot be solved by reconductoring alone. At the present time, such work would be very speculative, and therefore investigation should be postponed until (or if) such scheme are seriously considered. However, in future work, simultaneous BESS takeover, reconductoring, tap changing, curtailment, and reactive power control should be examined, as it is possible that the economic optimum LV reinforcement strategy is not reconductoring/BESS control alone. Furthermore, future work will examine the effect of different BESS control schemes on technical and economic feasibility of network violation management; the current work compares a very simple, and very complex dispatch algorithm, but does not account for 'in-between' strategies that may offer the technical feasibility benefits of the centralized algorithm with little more control complexity than the FIL algorithm.

The work presented in this thesis examines the cost and technical feasibility of BESS control strategies relative to 230 V network reconductoring, but assumes that the LV network being examined in any given instance is the only LV feeder on its respective 11 kV network with an increased PV/ASHP penetration. It is therefore unclear as to how the outcome of this thesis could be affected if this were not the case. For example, if a number of the 230 V networks associated with a given 11 kV feeder experienced an increase in PV penetration, this may in turn stress the 11 kV feeder to the point that reinforcement of the 11 kV network becomes necessary. In this instance, the use of BESSs may save capital investment in reconductoring of both LV and MV networks. However, this has been investigated in (Crossland, 2014) - a single 11 kV feeder was examined, and it was found that reconductoring still provided the cheapest solution. It is likely that this trend holds across all 11 kV feeders, though the

generality of this result may still be worth examining. Additionally, the model should be expanded to include an entire 11 kV feeder, with associated LV networks. This will allow a more realistic voltage profile to be assigned at the SSS point, provided that a representative primary substation tap scheme is employed. Again, the effect of this alteration is likely to be quite minor, but is certainly worth incorporating into future models.

Whilst the work presents the technical an economic feasibility of BESS control for violation management on LV power networks, it does not consider the environmental effect (e.g. CO_2 intensity) associated with producing copper and aluminium conductors, or Li ion BESSs. Reliable data in this field is scarce, and reports are often contradictory (McManus, 2011; Barnhart and Benson, 2013; Pellow *et al.*, 2015). Should reliable data become available in future, it may be possible to work material constraints, and environmental metrics into the optimization formulations.

Results presented in chapter 6 show that reconductoring alone will likely be inadequate for most feeders in the ASHP case. As there are no plans to remove renewable heating tariffs, we must look for affordable, tractable ways in which to solve the problem that such systems present to the network. Therefore future work will examine the effectiveness of retrofit, thermal storage, and storage heaters, together with reconductoring, to solve this problem. Future work will also address the increasing popularity of variable speed compressor ASHPs, and how, or whether, these change the resilience of the feeder set to increasing ASHP ownership.

As mentioned in section 8.4, a linear combination study for topological metrics will be carried out, once voltage and thermal constraint data is available for a greater number of feeders.

8.5 Concluding remarks

The use of BESS systems alone for the management of LV network violations may be technically possible in ideal scenarios, but the concept is economically infeasible in the DNO/3rd part owned case (and in some cases technically infeasible), and technically infeasible in the majority of customer owned cases, particularly where sub-optimal location of customer owned BESSs is considered. This finding is in contradiction with studies that consider more idealistic BESS availability and placement patterns. Future work will address the potential for BESSs to be used in violation management and reinforcement deferral schemes that take into account multiple coincident reinforcement technologies simultaneously, and the spatial boundary of the model will be extended to encompass entire primary feeders/networks.

References

Adhikari, R. S. *et al.* (2012) 'Energy Savings through Variable Speed Compressor Heat Pump Systems', in *2nd International Conference on Advances in Energy Engineering 2011 Energy*. Bangkok: Elsevier Procedia, pp. 1337–1342. doi: 10.1016/j.egypro.2011.12.1098.

AEI (2014) *Current Ratings*. Durham: AEI Cables. Available at: http://www.aeicables.co.uk/literature/CurrentRatings.pdf.

Ai, W. L. *et al.* (2014) 'Optimal battery placement in photovoltaic based distributed generation using binary firefly algorithm for voltage rise mitigation', *Conference Proceeding - 2014 IEEE International Conference on Power and Energy, PECon 2014*, 2014, pp. 155–158. doi: 10.1109/PECON.2014.7062432.

Akhil, A. A. *et al.* (2015) *SANDIA REPORT DOE / EPRI Electricity Storage Handbook in Collaboration with NRECA*. NM: SANDIA.

Alam, M. J. E., Muttaqi, K. M. and Sutanto, D. (2012) 'Distributed energy storage for mitigation of voltage-rise impact caused by rooftop solar PV', in *IEEE Power and Energy Society General Meeting 2012*. San Diego, CA: IEEE, pp. 1–8. doi: 10.1109/PESGM.2012.6345726.

Alam, M. J. E., Muttaqi, K. M. and Sutanto, D. (2015) 'Community Energy Storage for Neutral Voltage Rise Mitigation in Four-Wire Multigrounded LV Feeders with Unbalanced Solar PV Allocation', *IEEE Transactions on Smart Grid*, 6(6), pp. 2845–2855. doi: 10.1109/TSG.2015.2427872.

Ali, M. H. *et al.* (2010) 'An Overview of SMES Applications in Power and Energy Systems', in *IEEE Transactions on Sustainable Energy*, pp. 38–47.

Alnaser, S. and Ochoa, L. F. (2016) 'Optimial sizing and control of energy storage in wind power-right distribution networks', *IEEE Transactions on Power Systems*, 31(3), pp. 2004–2013. doi: 10.1109/TPWRS.2015.2465181.

Alnaser, S. W. and Ochoa, L. F. (2016) 'Optimal Sizing and Control of Energy Storage in Wind Power-Rich Distribution Networks', *IEEE Transactions on Power Systems*, 31(3), pp. 2004–2013. doi: 10.1109/TPWRS.2015.2465181.

Anusha, G. (2015) 'Coordinated Control of Grid-Connected Photovoltaic Reactive Power and Battery Energy Storage Systems to Improve the Voltage Profile of a Residential Distribution Feeder', *International Journal of Scientific Engineering and Technology Research*, 4(16), pp. 3014–3019. doi: 10.1109/TII.2014.2299336.

Von Appen, J. *et al.* (2014) 'Local voltage control strategies for PV storage systems in distribution grids', *IEEE Transactions on Smart Grid*, 5(2), pp. 1002–1009. doi: 10.1109/TSG.2013.2291116.

Von Appen, J., Braun, M. and Kneiske, T. (2013) 'Voltage control using pv storage systems in distribution systems', *22nd Int. Conf. Exhibition Electricity Distribution*, (1396), pp. 10–13. doi: 10.1049/cp.2013.1217.

Ardani, K. *et al.* (2018) *Cost-Reduction Roadmap for Residential Solar Photovoltaics (PV), 2017 – 2030 Cost-Reduction Roadmap for Residential Solar Photovoltaics (PV), 2017 – 2030*. CO: National Renewable Energy Laboratory. Available at:

https://www.nrel.gov/docs/fy18osti/70748.pdf.

Bahra Cables Company (2011) *Low Voltage Power Cables*. Bahra: Bahra Cables Company. Available at: http://www.bahra-cables.com/downloads/low_voltage.pdf.

Balducci, P. J. *et al.* (2018) 'Assigning value to energy storage systems at multiple points in an electrical grid', *Energy and Environmental Science*, 11(8), pp. 1926–1944. doi: 10.1039/c8ee00569a.

Ballanti, A. (2015) 'On the Integrated PV Hosting Capacity of MV and LV Distribution Networks', in *IEEE/PES Innovative Smart Grid Technologies ISGT Latin America 2015*. Montevideo: IEEE, pp. 366–370. doi: 10.1109/ISGT-LA.2015.7381183.

Ballanti, A. and Ochoa, L. F. (2016) 'On the integrated PV hosting capacity of MV and LV distribution networks', *2015 IEEE PES Innovative Smart Grid Technologies Latin America, ISGT LATAM 2015*, pp. 366–370. doi: 10.1109/ISGT-LA.2015.7381183.

Baqari, F. and Vahidi, B. (2013) 'Small-compressed air energy storage system integrated with induction generator for metropolises: A case study', *Renewable and Sustainable Energy Reviews*. Elsevier, 21, pp. 365–370. doi: 10.1016/j.rser.2012.12.040.

Barcellona, S. *et al.* (2015) 'Analysis of Ageing Effect on Li-Polymer Batteries', *Scientific World Journal*, 2015. doi: 10.1155/2015/979321.

Barnhart, C. J. and Benson, S. M. (2013) 'On the importance of reducing the energetic and material demands of electrical energy storage', *Energy Environ. Sci.*, 6, pp. 1083–1092. doi: 10.1039/C3EE24040A.

Battery University (2018) *Electric Vehicle (EV)*. Available at: http://batteryuniversity.com/learn/article/electric_vehicle_ev (Accessed: 6 June 2018).

Bennett, C. J., Stewart, R. A. and Lu, J. W. (2015) 'Development of a three-phase battery energy storage scheduling and operation system for low voltage distribution networks', *Applied Energy*. Elsevier Ltd, 146, pp. 122–134. doi: 10.1016/j.apenergy.2015.02.012.

Besenhard, J. O. and Eichinger, G. (1976) 'HIGH ENERGY DENSITY LITHIUM CELLS', *J. Electroanal. Chem.*, 68.

BRE (2018) *Dwelling Heat Losses*. Available at: https://www.bre.co.uk/heatpumpefficiency/dwelling-heat-loss (Accessed: 10 July 2018).

Broderick, R. (2013) *Interconnection of High Penetration PV on Distribution Circuits*. NM: SANDIA.

Bucciarelli, M. *et al.* (2016) 'Energy storage sizing for voltage control in LV networks under uncertainty on PV generation', in *2016 IEEE 2nd International Forum on Research and Technologies for Society and Industry Leveraging a Better Tomorrow*. Bologna, Italy: IEEE. doi: 10.1109/RTSI.2016.7740580.

Bucher, C. (2014) *Analysis and simulation of distribution grids with photovoltaics*. ETH Zurich.

Bucher, C., Betcke, J. and Andersson, G. (2013) 'Effects of variation of temporal resolution on domestic power and solar irradiance measurements', in *2013 IEEE Grenoble Conference PowerTech*. Grenoble, France: Powertech. doi: 10.1109/PTC.2013.6652217.

Butcher, M. (2018) *Power Ledger deploys first blockchain-based P2P energy trading system in Chicago*. Available at: https://techcrunch.com/2018/05/03/power-ledger-deploys-first-blockchain-based-p2p-energy-trading-system-in-chicago/?guccounter=1 (Accessed: 27 July 2018).

CCL (2017) *Fronius Symo Hybrid 4kW Solar Inverter - Three Phase - 1 MPPT with Communication*. Available at: https://www.cclcomponents.com/fronius-symo-hybrid-4kw-solar-inverter-three-phase-1-mppt-with-communication?gclid=EAIaIQobChMIp9r-8e_b1QIVATPTCh1yrQqxEAQYAiABEgJ0xfD_BwE (Accessed: 18 September 2017).

Chen, H. *et al.* (2009) 'Progress in electrical energy storage system: A critical review', *Progress in Natural Science*. National Natural Science Foundation of China and Chinese Academy of Sciences, 19(3), pp. 291–312. doi: 10.1016/j.pnsc.2008.07.014.

Chen, L., Wu, T. and Xu, X. (2018) 'Optimal Configuration of Different Energy Storage Batteries for Providing Auxiliary Service and Economic Revenue', *Applied Sciences*, 8(12), p. 2633. doi: 10.3390/app8122633.

Chua, K. H. *et al.* (2012) 'Energy storage system for mitigating voltage unbalance on low-voltage networks with photovoltaic systems', *IEEE Transactions on Power Delivery*, 27(4), pp. 1783–1790. doi: 10.1109/TPWRD.2012.2195035.

Chua, K. H. *et al.* (2012) 'Voltage Unbalance Mitigation in Low Voltage Distribution Networks with Photovoltaic Systems', *Journal of Electronic Science and Technology*, 10(1), pp. 1–6.

Crossland, A. F. (2014) *Application of stochastic and evolutionary methods to plan for the installation of energy storage in voltage constrained LV networks*. Durham University. Available at: http://etheses.dur.ac.uk/10819/.

Crossland, A. F., Jones, D. and Wade, N. S. (2014) 'Planning the location and rating of distributed energy storage in LV networks using a genetic algorithm with simulated annealing', *International Journal of Electrical Power and Energy Systems*. Elsevier Ltd, 59, pp. 103–110. doi: 10.1016/j.ijepes.2014.02.001.

Daniel, S. (2017) *Energy Storage A Major Growth Sector*. London: Moixa. Available at: https://masterinvestor.co.uk/wp-content/uploads/2017/04/MI_2017_Simon_Daniel_-_Moixa.pdf.

Danila, E. (2010) 'HISTORY OF THE FIRST ENERGY STORAGE SYSTEMS', in *3RD INTERNATIONAL SYMPOSIUM ON THE HISTORY OF ELECTRICAL ENGINEERING AND OF TERTIARY-LEVEL ENGINEERING EDUCATION*, pp. 1–4. doi: 10.13140/2.1.1564.7040.

Daud, M. Z. *et al.* (2014) 'An Optimal Control Strategy for DC Bus Voltage Regulation in Photovoltaic System with Battery Energy Storage', *The Scientific World Journal*, 2014, pp. 1–16. doi: 10.1155/2014/271087.

DECC (2016) *Solar Photovoltaics Deployment in the UK December 2018*. Available at: https://www.gov.uk/government/statistics/solar-photovoltaics-deployment.

Delille, G. *et al.* (2012) 'Dynamic Frequency Control Support by Energy Storage to Reduce the Impact of Wind and Solar Generation on Isolated Power System ' s Inertia', 3(4), pp. 931–939.

Denholm, P. *et al.* (2010) *The Role of Energy Storage with Renewable Electricity Generation*.

CO: National Renewable Energy Laboratory. doi: 69.

Dept. of BEIS (2016) *Digest of UK Energy Statistics (DUKES)*. London: GOV UK. Available at: https://assets.publishing.service.gov.uk/government/uploads/system/uploads/attachment_data/file/736148/DUKES_2018.pdf.

Dept. of BEIS (2017) *Solar Photovoltaics Deployment in the UK December 2017*. Gov. UK. Available at: https://www.gov.uk/government/statistics/solar-photovoltaics-deployment (Accessed: 8 January 2018).

Dinorwig (no date). Available at: http.www.electricmountain.co.uk (Accessed: 1 April 2018).

Dugan, R. C. (2012) 'The Open Distribution System Simulator (OpenDSS) Reference Guide'.

Eckroad, S. (2007) 'Vanadium Redox-Flow Battery', *Large.Stanford.Edu*, 3(3), p. 102. doi: 10.1149/1.3589916.

Electricity North West Ltd (2015) *Customer Voltage & Power Quality Limits 'Changing Standards', closedown report*. Manchester: ENWL. Available at: http://www.enwl.co.uk/docs/default-source/class-documents/changing-standards-closedown-report.pdf?sfvrsn=4.

Elsinga, B. and Sark, W. Van (2014) 'Spatial power fluctuation correlations in urban rooftop photovoltaic systems', *Progress in Photovoltaics Research and Applications*, 23(10), pp. 1390–1397. doi: 10.1002/pip.

Enernex (2010) *Eastern Wind Integration and Transmission Study*, *Energy*. CO: National Renewable Energy Laboratory. doi: CP-550-46505.

ENWL (2014) *Low Voltage Network Solutions A First Tier Low Carbon Networks Fund Project Closedown Report*. Manchester: ENWL.

ENWL (2015) *Losses Strategy*. Manchester: ENWL.

ENWL (2016a) *Statement of methodology and charges for connection to electricicty north west limited's electricity distribution system*. Manchester: ENWL.

ENWL (2016b) *Uses of System Charging Statement*. Manchester: ENWL. Available at: www.enwl.co.uk/docs/default-source/system-charges/enwl-overview-statement-to-suite-of-charging-statements---april-2016-and-april-2017.pdf?sfvrsn=0.

EWEA (2016) *Wind in power - 2015 European statistics*, *2015 European statistics.* Available at: http://www.ewea.org/fileadmin/ewea_documents/documents/publications/statistics/Stats_2011.pdf.

Foggia, G. *et al.* (2015) 'Coordinated control of dispersed battery energy storage systems for services to network operators', in *23rd International Conference on Electricity Distribution*. Lyon. Available at: https://hal-mines-paristech.archives-ouvertes.fr/hal-01168569/.

Fortenbacher, P. (2016) 'Distributed Battery Storage : Operation and Integration Power Systems Laboratory (PSL)'.

Fortenbacher, P., Andersson, G. and Mathieu, J. L. (2015) 'Optimal real-time control of

multiple battery sets for power system applications', in *2015 IEEE Eindhoven PowerTech*. Eindhoven, Netherlands, pp. 1–6. doi: 10.1109/PTC.2015.7232763.

Fortenbacher, P., Mathieu, J. L. and Andersson, G. (2017) 'Modeling and Optimal Operation of Distributed Battery Storage in Low Voltage Grids', *IEEE Transactions on Power Systems*, 32(6), pp. 4340–4350. doi: 10.1109/TPWRS.2017.2682339.

Fortenbacher, P., Zellner, M. and Andersson, G. (2016) 'Optimal Sizing and Placement of Distributed Storage in Low Voltage Networks', in *2016 Power Systems Computation Conference*. Genoa, Italy: IEEE, pp. 1–7. Available at: http://arxiv.org/abs/1512.01218.

Gayathri, N. S., Senroy, N. and Kar, I. N. (2016) 'Smoothing of wind power using flywheel energy storage system', *IET Renewable Power Generation*, 11(3), pp. 289–298. doi: 10.1049/iet-rpg.2016.0076.

GE Energy (2008) *Analysis of Wind Generation Impact on ERCOT Ancillary Services Requirements Electric Reliability Council of Texas*, *GE Report for Electric Reliability Council of Texas*. NY: GE.

General Electric (2011) 'FlexEfficiency* 50 combined cycle power plant'. Available at: www.ge-energy.com/content/multimedia/_files/downloads/FlexEfficiency 50 Plant eBrochure.pdf.

Ghoniem, A. F. (2011) 'Needs, resources and climate change: Clean and efficient conversion technologies', *Progress in Energy and Combustion Science*. Elsevier Ltd, 37(1), pp. 15–51. doi: 10.1016/j.pecs.2010.02.006.

Giannitrapani, A. *et al.* (2015) 'Algorithms for placement and sizing of energy storage systems in low voltage networks', in *2015 54th IEEE Conference on Decision and Control (CDC)*. Osaka, Japan: IEEE, pp. 3945–3950. doi: 10.1109/CDC.2015.7402832.

Giannitrapani, A. *et al.* (2016) 'Optimal allocation of energy storage systems for voltage control in LV distribution networks', in *IEEE Transactions on Smart Grid*. doi: 10.1109/TSG.2016.2602480.

Giannitrapani, A. *et al.* (2017) 'Optimal allocation of energy storage systems for voltage control in LV distribution networks', in *IEEE Transactions on Smart Grid*. doi: 10.1109/TSG.2016.2602480.

Godshall, N. A. and Huggins, R. A. (1980) 'THERMODYNAMIC INVESTIGATIONS OF TERNARY LITHIUM-TRANSITION METAL-OXYGEN CATHODE MATERIALS N.', *Materials Research Bulletin*, 15, pp. 561–570.

Gonzalez-longatt, F. M. (2016) 'Enabling Inertial Response in Utility-Scale Battery Energy Storage System'.

Good, N. *et al.* (2013) 'Physical modeling of electro-thermal domestic heating systems with quantification of economic and environmental costs', in *IEEE EuroCon 2013*. Zagreb, Croatia: IEEE, pp. 1164–1171. doi: 10.1109/EUROCON.2013.6625128.

Good, N. (2015) 'Physically Modelled ASHP Data'. Manchester.

Greenwood, D. M. *et al.* (2017) 'Frequency response services designed for energy storage', *Applied Energy*. The Authors, 203, pp. 115–127. doi: 10.1016/j.apenergy.2017.06.046.

Grünewald, P., McKenna, E. and Thomson, M. (2015) 'Going with the wind: temporal

characteristics of potential wind curtailment in Ireland in 2020 and opportunities for demand response', *IET Renewable Power Generation*, 9(1), pp. 66–77. doi: 10.1049/iet-rpg.2013.0320.

Guan, Y., Vasquez, J. C. and Guerrero, J. M. (2016) 'Coordinated Secondary Control for Balanced Discharge Rate of Energy Storage System in Islanded AC Microgrids', *IEEE Transactions on Industry Applications*, 52(6), pp. 5019–5028. doi: 10.1109/TIA.2016.2598724.

Haque, A. N. M. M., Nguyen, P. H. and Kling, W. L. (2014) 'Congestion Management in Smart Distribution Network', in *2014 49th International Universities Power Engineering Conference (UPEC)*. Cluj-Napoca, Romania: IEEE. doi: 10.1109/UPEC.2014.6934751.

Hay, R. and Macwhinnie, N. (2015) 'Making the electricity system more flexible and delivering the benefits for consumers'.

Hell, J. (no date) 'High flexible Hydropower Generation concepts for future grids'. doi: 10.1088/1742-6596/755/1/011001.

Hilton, G. (2015) *Distributed v Centralised : A Question of Energy Storage*. Southampton: ESA CDT.

Hilton, G., Cruden, A. and Kent, J. (2017) 'Comparative analysis of domestic and feeder connected batteries for low voltage networks with high photovoltaic penetration', *Journal of Energy Storage*. Elsevier Ltd, 13, pp. 334–343. doi: 10.1016/j.est.2017.07.019.

HSE (2003) *The Electricity Safety , Quality and Continuity Regulations 2002*. Bootle: HSE.

Hummel, P. *et al.* (2017) *UBS Evidence Lab Electric Car Teardown – Disruption Ahead? 1*. Basel: UBS.

International Energy Agency (2014) *Technology Roadmap*. Paris: International Energy Agency.

Ippolito, M. G. *et al.* (2013) 'A New Device for the Control and the Connection to the Grid of Combined RES-based Generators and Electric Storage Systems', in *4th International Conference on Clean Electrical Power: Renewable Energy Resources Impact*. Piscataway, NJ: IEEE: IEEE, pp. 262–267.

IRENA (2017a) *ELECTRICITY STORAGE AND RENEWABLES : COSTS AND MARKETS TO 2030*. Abu Dhabi: IRENA: Inernational Renewable Energy Agency.

IRENA (2017b) *Renewable Power : Sharply Falling Generation Costs*. Abu Dhabi: IRENA.

Isono, E. *et al.* (2013) 'Battery SCADA Demonstration System in YSCP', in *22nd International Conference on Electricity Distribution*. Stockholm, Sweeden: IET, pp. 1–4.

Jabir, M. *et al.* (2017) 'Intermittent Smoothing Approaches for Wind Power Output : A Review', *Energies*, 10. doi: 10.3390/en10101572.

Jamieson, P. (2011) *Innovation in Wind Turbine Design*. 1st edn. Sussex: John Wiley & Sons.

Jana, S., Gangopadhyay, U. and Das, S. (2013) 'State of the Art of Solar Photovoltaic Technology', *Conference Papers in Energy*, 2013. doi: 10.1155/2013/764132.

Karagiannopoulos, S. *et al.* (2016) 'Battery energy storage capacity fading and control strategies for deterministic and stochastic power profiles', in *19th Power Systems*

Computation Conference, PSCC 2016. Genoa, Italy: PSCC, pp. 1–7. doi: 10.1109/PSCC.2016.7540956.

Kashem, M. A. and Ledwich, G. (2007) 'Energy requirement for distributed energy resources with battery energy storage for voltage support in three-phase distribution lines', *Electric Power Systems Research*, 77(1), pp. 10–23. doi: 10.1016/j.epsr.2006.01.008.

King, D. L., Kratochvil, J. A. and Boyson, W. E. (1997) *Temperature coefficients for pv modules and arrays: measurement methods, difficulties, and results*. NM: SANDIA.

King, D. L., Kratochvil, J. a and Boyson, W. E. (2004) *Photovoltaic array performance model*, *Online*. NM: SANDIA. doi: 10.2172/919131.

de la Parra, I. *et al.* (2015) 'Storage requirements for PV power ramp-rate control in a PV fleet', *Solar Energy*, 118, pp. 426–440. doi: 10.1016/j.solener.2015.05.046.

Lam, L. and Bauer, P. (2013) 'Practical capacity fading model for Li-ion battery cells in electric vehicles', *IEEE Transactions on Power Electronics*, 28(12), pp. 5910–5918. doi: 10.1109/TPEL.2012.2235083.

Lamberti, F. *et al.* (2015) 'Impact analysis of distributed PV and energy storage systems in unbalanced LV networks', in *2015 IEEE Eindhoven PowerTech*. Eindhoven, Netherlands: IEEE, pp. 1–6. doi: 10.1109/PTC.2015.7232717.

Lamberti, F. *et al.* (2017) 'Massive data analysis to assess PV / ESS integration in residential unbalanced LV networks to support voltage profiles', *Electric Power Systems Research*. Elsevier B.V., 143, pp. 206–214. doi: 10.1016/j.epsr.2016.10.037.

Lamberti, F. and Calderaro, V. (2013) 'Estimating the Load Response to Voltage Changes at UK Primary Substations', in *4th IEEE PES Innovative Smart Grid Technologies Europe*. Lyngby, Denmark: IEEE, pp. 1–5. doi: 10.1109/ISGTEurope.2013.6695466.

Lave, M. (2011) *Ota City : Characterizing Output Variability from 553 Homes with Residential PV Systems on a Distribution Feeder Ota City : Characterizing Output Variability from 553 Homes with Residential PV Systems on a Distribution Feeder*. NM: SANDIA. doi: 10.2172/1035324.

Lave, M., Reno, M. J. and Broderick, R. J. (2015) 'Characterizing local high-frequency solar variability and its impact to distribution studies', *Solar Energy*. Elsevier Ltd, 118, pp. 327–337. doi: 10.1016/j.solener.2015.05.028.

Lin, B. (2015) *Top Ten Facts about Tesla's $350/kWh (DC) PowerWall battery*. Available at: http://www.catalyticengineering.com/top-ten-facts-about-teslas-350kwh-powerwall-battery/ (Accessed: 4 July 2016).

Liu, X. *et al.* (2012) 'Coordinated control of distributed energy storage system with tap changer transformers for voltage rise mitigation under high photovoltaic penetration', *IEEE Transactions on Smart Grid*, 3(2), pp. 897–906. doi: 10.1109/TSG.2011.2177501.

Long, C., Ochoa, L. F. and Member, S. (2016) 'Voltage Control of PV-Rich LV Networks : OLTC-Fitted Transformer and Capacitor Banks', *IEEE Transactions on Power Systems*, 31(5), pp. 4016–4025. doi: 10.1109/TPWRS.2015.2494627.

Lott, M. C. and Kim, S.-I. (2014) *Technology Roadmap: Energy storage*, *Energy Technology Perspectives*. Paris: International Energy Agency. doi: 10.1007/SpringerReference_7300.

Lu, C. *et al.* (2014) 'Optimal Sizing and Control of Battery Energy Storage System for Peak Load Shaving', *Energies*, 7(12), pp. 8396–8410. doi: 10.3390/en7128396.

MacKay, D. (2008) *Sustainable Energy-without the hot air*, *Sustainable Energy-without the hot air*. Cambridge: Cambridge Univ. Press. doi: 10.1109/PES.2004.1373296.

Marra, F. *et al.* (2013) 'EV charging facilities and their application in LV feeders with photovoltaics', *IEEE Transactions on Smart Grid*, 4(3), pp. 1533–1540. doi: 10.1109/TSG.2013.2271489.

Marra, F. *et al.* (2014) 'A decentralized storage strategy for residential feeders with photovoltaics', *IEEE Transactions on Smart Grid*, 5(2), pp. 974–981. doi: 10.1109/TSG.2013.2281175.

Marra, F., Fawzy, Y. T. and Bulo, T. (2012) 'Energy storage options for voltage support in low-voltage grids with high penetration of photovoltaic', in *IEEE PES Innovative Smart Grid Technologies Conference Europe*. Berlin, Germany: IEEE, pp. 1–7. doi: 10.1109/ISGTEurope.2012.6465690.

Marsh, G. *et al.* (2016) 'Review and application of Rainflow residue processing techniques for accurate fatigue damage estimation', *International Journal of Fatigue*. Elsevier Ltd, 82, pp. 757–765. doi: 10.1016/j.ijfatigue.2015.10.007.

McKenna, E. and Thomson, M. (2016) 'High-resolution stochastic integrated thermal-electrical domestic demand model', *Applied Energy*, 165, pp. 445–461.

McManus, M. C. (2011) 'Environmental Consequences of the Use of Batteries in Sustainable Systems : Battery Production.', in *2nd International Conference on Microgeneration and Related Technologies*. Glasgow, Scotland: University of Strathclyde. doi: http://dx.doi.org/10.1016/j.apenergy.2011.12.062.

Mégel, O., Mathieu, J. L. and Andersson, G. (2015) 'Scheduling distributed energy storage units to provide multiple services under forecast error', *International Journal of Electrical Power and Energy Systems*, 72, pp. 48–57. doi: 10.1016/j.ijepes.2015.02.010.

Meghasai *et al.* (2015) 'Simulation of smart functionalities of photovoltaic inverters by interfacing OpenDSS and Matlab', in *2015 IEEE 16th Workshop on Control and Modeling for Power Electronics, COMPEL 2015*. Vancouver, pp. 1–5. doi: 10.1109/COMPEL.2015.7236443.

Mercedes (2014) *Mercedes-Benz Energiespeicher Home*. Kamenz: Mercedes-Benz. Available at: http://www.off-grid-europe.com/downloads/dl/file/id/587/mercedes_benz_db_sb_mb_2_5_20_0_datasheet_de.pdf.

Millner, A. (2010) 'Modeling Lithium Ion Battery Degradation in Electric Vehicles', in *2010 IEEE Conference on Innovative Technologies for an Efficient and Reliable Electricity Supply*. MA, USA: IEEE, pp. 349–356. doi: 10.1109/CITRES.2010.5619782.

Mizushima, K. *et al.* (1980) 'A NEW CATHODE MATERIAL FOR BATTERIES OF HIGH ENERGY DENSITY', *Materials Research Bulletin*, 15, pp. 783–789.

Moixa (2017a) *Home battery trial aims to increase electricity network capacity to enable more solar homes and save £millions for customers*. Available at: http://www.moixa.com/press-release/home-battery-trial-aims-increase-electricity-

network-capacity-enable-solar-homes-save-millions-customers/ (Accessed: 19 December 2017).

Moixa (2017b) *Moixa GridShare*. Available at: http://www.moixa.com/products/ (Accessed: 19 December 2017).

Mokhtari, G. *et al.* (2013) 'Smart robust resources control in lv network to deal with voltage rise issue', *IEEE Transactions on Sustainable Energy*, 4(4), pp. 1043–1050. doi: 10.1109/TSTE.2013.2265100.

Mokhtari, G., Nourbakhsh, G. and Gosh, A. (2013) 'Optimal Sizing of Combined PV-Energy Storagefor a Grid-connected Residential Building', *Advances in Energy Engineering*, 1(3), pp. 53–65.

National Grid (2009) *Ancillary Service Settlement Guide*. Warwick: National Grid plc.

National Grid (2014) *Outlook Report*. Warwick: National Grid plc.

National Grid (2015) *Future Energy Scenarios*. Warwick: National Grid plc.

National Grid (2016a) 'Derived from Data Obtained from the National Grid Dashboard'. Available at: http://www.gridwatch.templar.co.uk/download.php.

National Grid (2016b) 'Enhanced Frequency Response Market Information Report', pp. 1–3.

National Grid (2017) *Future Energy Scenarios*. Warwick: National Grid plc. Available at: http://fes.nationalgrid.com/media/1253/final-fes-2017-updated-interactive-pdf-44-amended.pdf.

National Grid (2018) *Short term operating reserve (STOR)*. Available at: https://www.nationalgrid.com/uk/electricity/balancing-services/reserve-services/short-term-operating-reserve-stor (Accessed: 30 May 2018).

Navarro-Espinosa, A. (no date) 'LV Network Models (Dataset)'. Available at: https://www.researchgate.net/publication/283569605_Low_Voltage_Network_Models.

Navarro-Espinosa, A. and Mancarella, P. (2014) 'Probabilistic modeling and assessment of the impact of electric heat pumps on low voltage distribution networks', *Applied Energy*. Elsevier Ltd, 127, pp. 249–266. doi: 10.1016/j.apenergy.2014.04.026.

Navarro-Espinosa, A. and Ochoa, L. F. (2015) 'Low Voltage Network Models'. Available at: https://www.researchgate.net/publication/283569605_Low_Voltage_Network_Models.

Navarro-Espinosa, A. and Ochoa, L. F. (2016) 'Probabilistic Impact Assessment of Low Carbon Technologies in LV Distribution Systems', *IEEE Transactions on Power Systems*, 31(3), pp. 2192–2203. doi: 10.1109/TPWRS.2015.2448663.

Nieslony, A. (2010) 'Rainflow Counting Algorithm'. Mathworks. Available at: https://uk.mathworks.com/matlabcentral/fileexchange/3026-rainflow-counting-algorithm?requestedDomain=www.mathworks.com.

Ochoa, L. F., Dent, C. J. and Harrison, G. P. (2010) 'Distribution Network Capacity Assessment: Variable DG and Active Networks', *IEEE Transactions on Power Systems*, 25(1), pp. 87–95. doi: 10.1109/TPWRS.2009.2031223.

Ofgem (2017) *Guide to the RIIO-ED1 electricity distribution price control*. London: Ofgem.

Ofgem (2018) *Feed-In Tariff (FIT) rates*. Available at: https://www.ofgem.gov.uk/publications-and-updates/feed-tariff-fit-tariff-table-1-april-2018 (Accessed: 17 January 2018).

Olinsky-paul, T. and Mullendore, S. (2018) *Energy Storage Basics for State Policymakers : Technology , Policy , Economics , and the State of the Industry*.

Omar, N. *et al.* (2013) 'Peukert revisited-critical appraisal and need for modification for lithium-ion batteries', *Energies*, 6(11), pp. 5625–5641. doi: 10.3390/en6115625.

Padhi, A. K. and Goodenough, J. B. (1997) 'Phospho-olivines as Positive-Electrode Materials for Rechargeable Lithium Batteries', *J. Elecrochem. Soc.*, 144(4).

Pellow, M. a *et al.* (2015) 'Hydrogen or batteries for grid storage? A net energy analysis', *Energy Environ. Sci.* Royal Society of Chemistry, 8(7), pp. 1938–1952. doi: 10.1039/C4EE04041D.

Petinrin, J. O. and Shaaban, M. (2016) 'Integration of Energy Storage for Voltage Support in Smart Distribution Systems', *Journal of Electrical Engineering and Technology*, 11(5), pp. 1921–1927. Available at: 10.5370/JEET.2016.11.5.1077.

Poulios, V. (2015) 'Optimal placement and sizing of battery storage to increase the PV hosting capacity of low voltage grids', in *International ETG Congress 2015; Die Energiewende - Blueprints for the new energy age*. Bonn, Germany: VDE, pp. 85–92.

Pratt, D. (2017) *Ofgem moves to limit DNO participation wth storage as Northen Powergrid reveals battery ambitions*, *Clean Energy News*. Available at: https://cleanenergynews.co.uk/news/storage/ofgem-moves-to-limit-dno-participation-with-storage-as-northern-powergrid-r (Accessed: 14 November 2017).

Procopiou, A. T. (2017) *Active Management of PV-Rich Low Voltage Networks*. University of Manchester.

Procopiou, A. T., Long, C. and Ochoa, L. F. (2014) 'Voltage control in LV networks: An initial investigation', in *IEEE PES Innovative Smart Grid Technologies, Europe*. Istanbul, pp. 1–6. doi: 10.1109/ISGTEurope.2014.7028971.

Procopiou, A. T. and Ochoa, L. F. (2017) 'Voltage Control in PV-Rich LV Networks Without Remote Monitoring', *IEEE Transactions on Power Systems*, 32(2), pp. 1224–1236. doi: 10.1109/TPWRS.2016.2591063.

Procopiou, A. T., Quiros-Tortos, J. and Ochoa, L. F. (2017) 'HPC-Based Probabilistic Analysis of LV Networks With EVs: Impacts and Control', *IEEE Transactions on Smart Grid*, 8(3), pp. 1479–1487. doi: 10.1109/TSG.2016.2604245.

Rainflow-Counting Algorithm (no date). Available at: https://en.wikipedia.org/wiki/Rainflow-counting_algorithm#/media/File:Rainflow_fig4.PNG (Accessed: 29 May 2018).

Ranaweera, I. and Midtgard, O. M. (2016) 'Centralized control of energy storages for voltage support in low-voltage distribution grids', in *EEEIC 2016 - International Conference on Environment and Electrical Engineering*. Florence, Italy. doi: 10.1109/EEEIC.2016.7555488.

REA (2015) *UK solar beyond subsidy : the transition*. London: Renewable Energy Agency.

Available at: http://www.r-e-a.net/upload/uk-solar-beyond-subsidy-the-transition.pdf.

Reed, A. (2018) *P2P Energy Trading on the Blockchain*. Available at: https://medium.com/wolverineblockchain/p2p-energy-trading-on-the-blockchain-db61fa2c8caf (Accessed: 27 July 2018).

Reikard, G. (2009) 'Predicting solar radiation at high resolutions: A comparison of time series forecasts', *Solar Energy*. Elsevier Ltd, 83(3), pp. 342–349. doi: 10.1016/j.solener.2008.08.007.

Remund, J. *et al.* (2015) *Characterization of the spatio-temporal variations and ramp rates of solar radiation and Characterization of the spatio-temporal variations and ramp rates of solar*. Paris: IEA.

RenewableUK (2018) *renewableUK Wind Energy Statistics*. Available at: http://www.renewableuk.com/page/UKWEDhome (Accessed: 31 January 2018).

Richardson, I. and Thomson, M. (2009) 'One-Minute Resolution Domestic Electricity Use Data'. Available at: https://beta.ukdataservice.ac.uk/datacatalogue/studies/study?id=6583.

Rigoni, V. *et al.* (2016) 'Representative residential LV feeders: A case study for the North West of England', *IEEE Transactions on Power Systems*, 31(1), pp. 348–360. doi: 10.1109/TPWRS.2015.2403252.

Ruben, B. *et al.* (2011) 'Meshing radial networks at 11kV', in *IEEE PES Innovative Smart Grid Technologies Conference Europe*. Manchester: IEEE, pp. 1–8. doi: 10.1109/ISGTEurope.2011.6162691.

Ruf, H. *et al.* (2016) 'Quantifying residential PV feed-in power in low voltage grids based on satellite-derived irradiance data with application to power flow calculations', *Solar Energy*. The Authors, 135, pp. 692–702. doi: 10.1016/j.solener.2016.06.001.

Santos-Martin, D. *et al.* (2015) 'Impact of solar photovoltaics on the low-voltage distribution network in New Zealand', *IET Generation, Transmission & Distribution*, 10(1), pp. 1–9. doi: 10.1049/iet-gtd.2014.1076.

Shibata, T. *et al.* (2013) 'Redox flow batteries for the stable supply of renewable energy', *SEI Technical Review*, (76), pp. 14–22.

Siemens (2005) *Thermal Overload Protection of Cables*. Munich: Siemens.

SMA (no date) 'Sunny Boy Storage 2.5'.

Solarcentury (2014) *Solar PV : Shedding light on the opportunities*. IL: Jones Lang LaSalle.

SolarEdge (2017) *SolarEdge Export Limitation Application Note*. Herzliya: SolarEdge.

Solarguide (2017) *Tesla Powerwall 2.0 Cost, Specs, and Reviews*. Available at: https://www.solarguide.co.uk/tesla-energy/powerwall-2 (Accessed: 19 December 2017).

Somma, M. Di *et al.* (2018) 'Stochastic optimal scheduling of distributed energy resources with renewables considering economic and environmental aspects', *Renewable Energy*, 116, pp. 272–287. doi: 10.1016/j.renene.2017.09.074.

Son, F. J. (2017) 'Performance Testing of a Unitary Split-System Variable-Speed Heat Pump', *Journal of Purdue Undergraduate Research*, 7, pp. 83–84. doi: 10.5703/1288284316413.

SP Energy (2015) *Future Network Monitoring Strategy*. Middlewich: SP Energy.

SSE (2016) *Statement of methodology and charges for connection to southern electric power distribution plc.s electricity distribution system*. Perth: SSE.

Tesla (2016) *Powerwall 2 AC Specifications*. CA: Tesla.

Tesla (2017) *Powerwall*. Available at: https://www.tesla.com/en_GB/powerwall (Accessed: 18 September 2017).

Tester, J. (2012) *Sustainable Energy: Choosing Among Options*. 2nd edn. MA: MIT Press.

The Carbon Trust (2011) 'Micro-CHP Accelerator'.

Tielens, P. and van Hertem, D. (2012) *Grid Inertia and Frequency Control in Power Systems with High Penetration of Renewables*. Available at: https://lirias.kuleuven.be/handle/123456789/345286.

Tonkoski, R., Turcotte, D. and El-Fouly, T. H. M. (2012) 'Impact of high PV penetration on voltage profiles in residential neighborhoods', *IEEE Transactions on Sustainable Energy*, 3(3), pp. 518–527. doi: 10.1109/TSTE.2012.2191425.

Veit, A. *et al.* (2014) *Household Electricity Demand Forecasting -- Benchmarking State-of-the-Art Methods*, *e-Energy*. doi: 10.1145/2602044.2602082.

Wang, L. *et al.* (2015) 'Coordination of Multiple Energy Storage Units in a Low-Voltage Distribution Network', *IEEE Transactions on Smart Grid*, 6(6), pp. 2906–2918. doi: 10.1109/TSG.2015.2452579.

Wang, P. *et al.* (2014) 'Integrating Electrical Energy Storage Into Coordinated Voltage Control Schemes for Distribution Networks', *IEEE Transactions on Smart Grid*, 5(2), pp. 1018–1032. doi: 10.1109/TSG.2013.2292530.

Wang, Y. *et al.* (2015) 'Coordinated Control of Distributed Energy Storage Systems for Voltage Regulation in Distribution Networks', *IEEE Transactions on Power Delivery*, 31(3), pp. 1132–1141. doi: 10.1109/TPWRD.2015.2462723.

Wang, Z. *et al.* (2015) 'Distributed Storage Capacity Reservations for LV Network Operation', in *2015 IEEE Power & Energy Society General Meeting*. CO: IEEE, pp. 1–5. doi: 10.1109/PESGM.2015.7286114.

Weniger, J., Tjaden, T. and Quaschning, V. (2013) 'Sizing and grid integration of residential PV battery systems', *8th International Renewable Energy Storage Conference and Exhibition (IRES 2013)*, 8, pp. 1–15. doi: 10.1016/j.egypro.2014.01.160.

White, L. (1975) 'Medieval Engineering and the Sociology of Knowledge', *Pacific Historical Review*, 44(1), pp. 1–21. Available at: http://www.jstor.org/stable/3637895.

Whittingham, B. M. S. (2012) 'History , Evolution , and Future Status of Energy Storage', *Proceedings of the IEEE*, 100.

Xing, Y. *et al.* (2015) 'A review of concentrator silicon solar cells', *Renewable and Sustainable Energy Reviews*. Elsevier, 51, pp. 1697–1708. doi: 10.1016/j.rser.2015.07.035.

Xu, B., Oudalov, A. and Ulbig, A. (2016) 'Modeling of Lithium-Ion Battery Degradation for Cell Life Assessment', *IEEE Transactions on Smart Grid*, 9(2), pp. 1131–1140. doi: 10.1109/TSG.2016.2578950.

Yang, H., Lu, L. and Zhou, W. (2007) ‘A novel optimization sizing model for hybrid solar-wind power generation system’, *Solar Energy*, 81(1), pp. 76–84. doi: 10.1016/j.solener.2006.06.010.

Zhang, C. *et al.* (2016) ‘Using CPE Function to Size Capacitor Storage for Electric Vehicles and Quantifying Battery Degradation during Different Driving Cycles’, *Energies*, 9. doi: 10.3390/en9110903.